LONG TERM OCULAR DRUG DELIVERY WITH NOVEL PENTABLOCK COPOLYMERS

PART I: COMPOSITE NANOFORMULATION OF MACROMOLECULES FOR BACK OF THE EYE DISEASES

PART II: DEXAMETHASONE NANOPARTICLE TO DEVELOP AN *IN VITRO* MODEL FOR GLAUCOMA

A DISSERTATION IN

Pharmaceutical Sciences

and

Chemistry

Presented to the Faculty of the University
of Missouri-Kansas City in partial fulfillment of
the requirements for the degree

DOCTOR OF PHILOSOPHY

By

Vibhuti Agrahari

M. Pharm, Medicinal & Pharmaceutical Chemistry, 2008

Rajiv Gandhi Proudyogiki Vishwavidyalaya, India

Kansas City, Missouri

2017

LONG TERM OCULAR DRUG DELIVERY WITH NOVEL PENTABLOCK COPOLYMERS

PART I: COMPOSITE NANOFORMULATION OF MACROMOLECULES FOR BACK OF THE EYE DISEASES

PART II: DEXAMETHASONE NANOPARTICLE TO DEVELOP AN *IN VITRO* MODEL FOR GLAUCOMA

Vibhuti Agrahari, Candidate for the Doctor of Philosophy Degree

University of Missouri-Kansas City, 2017

ABSTRACT

PART I: COMPOSITE NANOFORMULATION OF MACROMOLECULES FOR BACK OF THE EYE DISEASES

Pentablock (PB) copolymers have been successfully synthesized for long term delivery in the treatment of posterior segment ocular diseases. PB copolymers are comprised of FDA approved biodegradable polymer such as polyethylene glycol (PEG), polycaprolactone (PCL), polylactic acid (PLA) and polyglycolic acid (PGA). PB copolymers of different composition, molecular weights and block arrangements were synthesized by ring opening bulk copolymerization method and analyzed by NMR, GPC FT-IR and XRD analyses. Further, these PB copolymers have been utilized to develop the macromolecule-embedded thermosensitive gels or nanoparticles (NPs) or composite nanoformulation (NPs suspended in gel) for a sustained drug delivery. PBG (PLA-PCL-PEG-PCL-PLA; PBG-1 and PEG-PCL-PLA-PCL-PEG; PBG-2) gelling copolymers were evaluated for

their utility as injectable *in situ* hydrogel forming depot for controlled ocular delivery of macromolecules (proteins, peptides and Fab fragments). A wide variety of macromolecules (Octreotide, IgG-Fab, IgG-Fab' and IgG) with molecular weights ranging from 1 - 150 kDa have been used for this purpose. The kinematic viscosity of the copolymer solution was studied at different polymer concentration with different block arrangment. It was observed that viscosity of hydrophobic polymer (PBG-1) was considerably higher relative to PBG-2 copolymer. Sol-gel transition curves for PBG-1 and PBG-2 copolymer was compared to understand the effect of hydrophobicity and effect of block arrangement on the sol-gel behavior of block copolymers. Sol-gel transition and rheology revealed that PBG block arrangements were easy to handle at room temperature and easy to administer through small gauge needle. Cell viability and cytotoxicity studies confirmed that PBG copolymers are superior biomaterials for ocular delivery. It was observed that the *in vitro* release pattern was depended on the molecular weight of the macromolecules and amphiphilic nature of the PBG copolymers. It is anticipated that much longer release can be obtained by altering block composition or change in hydrophobicity and/or hydrophilicity of the gelling polymer. The *in vitro* release pattern was in conjunction with the facts that amorphous and hydrophilic polymer degrades fast. CD spectroscopy results revealed no changes in the secondary structure of macromoelcules (studied for IgG as a model macromoelcule). The *in vitro* degradation study for PBG-2 copolymer was performed under four different conditions; (i) in pH 7.4 PBS at 37°C, (ii) in presence of enzymes acetylcholinesterase (14.7 mU/mL) and butyrylcholinesterase (5.9 mU/mL), (iii) in pH 9.0 borate buffer at 37°C and (iv) in pH 7.4 PBS at 40°C. The samples were analyzed by XRD and GPC to determine the weight

loss of the PBG-2 copolymer. It was observed that accelerated conditions such as pH 9.0 (37°C) and high temperature (40°C) exhibited weight loss of ~45% and ~40%, respectively which were significantly higher than weight loss observed under normal condition (pH - 7.4, 37°C) i.e., ~35%. No significant effect of enzymes was observed on polymer degradation. Besides, *in vivo* assessment of PBG-2 copolymer provided a safe environment and was well tolerated in the rabbit eyes analyzed up to 33 weeks.

Further, PB-NPs were formulated with different molecular weights of PB copolymer (PCL-PLA-PEG-PLA-PCL) to study the release pattern of macromolecules (lysozyme, IgG-Fab, ranibizumab and IgG). The macromolecules encapsulated in PB-NPs were prepared by $W_1/O/W_2$ double emulsion solvent evaporation method. The macromolecules were optimized to achieve a high drug loading (~17%) and entrapment efficiency (~66%) in the NPs. PB-NPs alone exhibited significant burst release in the first few days however, the dual approach i.e., composite nanoformulations (macromolecules-encapsulated PB-NPs dispersed in thermosensitive gel) eliminated the burst release effect and exhibited nearly zero-order protein release for significantly longer durations (~3-6 months). In order to compare the duration of *in vitro* release, PB copolymers with different molecular weight have been studied. The enzymatic activity of lysozyme with its respective enzymatic assays was used to investigate the activity of released macromolecule. Anti-VEGF activity of ranibizumab released from composite nanoformulation was analyzed by indirect ELISA. It was observed that macromolecules maintained their structural integrity and bioactivity during the preparation of the nanoformulation and also during the drug release process. The mean particle size distribution of NPs in PBS was found in the range of ~150 nm and was consistent

throughout the study in different media analyzed up to 10 days. The results confirmed the higher stability of NPs in different cell culture media. *In vitro* cell viability, cytotoxicity and biocompatibility studies performed on various ocular cells, confirmed the safety of PB copolymers for ocular applications.

PART II: DEXAMETHASONE NANOPARTICLE TO DEVELOP AN *IN VITRO* MODEL FOR GLAUCOMA

The aim of the present study was to examine the elevation of myocillin (MYOC); one of the extra cellular matrix related proteins whose expression is altered in presence of long-term treatment of Glucocorticoids. In this study, dexamethasone (DEX) was selected as model drug. The different strains of primary cultures of human trabecular meshwork (HTM) cell line (HTM120, 136, 126, 134 and 141) were used to develop the *in vitro* cell culture model of glaucoma. To obtain a long-term delivery of DEX, pentablock (PB) copolymer was synthesize using the ring opening bulk copolymerization method and characterized by NMR, GPC and XRD analyses. PB copolymer was used to formulate the DEX encapsulated nanoparticles (NPs) with entrapment efficiency of ~63% and drug loading of ~11% w/w. The mean particle size distribution of NPs was analyzed by NTA in PBS was found in the range of ~109 nm. The biomaterial was further studied for *in vitro* cytotoxicity and cell viability. Results showed that neither cell viability nor cytotoxicity was affected up to 12 weeks of treatment. DEX-PB-NPs or control NPs treatments were given to the HTM cells and cell culture supernatant was collected/replaced with fresh 1% DMEM once/week for 12 weeks. DEX or vehicle was used as controls to compare MYOC secretion levels by Western blot (WB). Four HTM

cell strains tested showed similar MYOC secretion patterns, having robust responses for the entire monitoring period. In contrast, one cell strain responded only for a few weeks. Quantitation of WB data from five HTM cell strains showed that MYOC increased by 5.2 ± 1.3, 7.4 ± 4.3, and 2.8 ± 1.1 fold at 4, 8, and 12 weeks in the presence of DEX-PB-NPs compared to 9.2 ± 3.8, 2.2 ± 0.5, and 1.5 ± 0.3 fold at 4, 8, and 12 weeks in control DEX treatment group. Based on the decline in MYOC levels after withdrawal of DEX from control wells, results indicate that DEX-PB-NPs released biologically active DEX for at least 10 weeks. By comparison, MYOC levels in vehicle treated control wells remained unchanged. Moreover, PB copolymers were biocompatible and didn't modifying the cellular functions of HTM cells. Although the PB copolymers did not show any sign of cytotoxicity to HTM cells in this long-term study, they did modify HTM cell morphology. HTM cell elongation was present in all cell strains after both Con-NPs and DEX-PB-NPs treatment. Morphological modification of HTM cells by the polymers may accompany functional changes those were not measured in the present study, but needs further investigations. Meanwhile, this study provides the evidence that our *in vitro* system developed in this study is a valuable tool for analyzing the safety of the polymers and biological effects of steroids released from the polymers. In addition, histological observations in the C57BL/6 mice showed normal phenomenon in ocular tissue morphology.

APPROVAL PAGE

The faculty listed below, appointed by the Dean of the School of Graduate Studies, have examined the dissertation titled "Long Term Ocular Drug Delivery with Novel Pentablock Copolymers; Part I: Composite Nanoformulation of Macromolecules For Back of the Eye Diseases, Part II: Dexamethasone Nanoparticle to Develop an *In Vitro* Model for Glaucoma, presented by Vibhuti Agrahari, candidate for the Doctor of Philosophy Degree, and certify that in their opinion it is worthy of acceptance.

Supervisory Committee

Ashim K. Mitra, Ph.D., Committee Chair
Department of Pharmaceutical Sciences

Kun Cheng, Ph.D.
Department of Pharmaceutical Sciences

Zhoungha Peng, Ph.D.
Department of Chemistry

Russell B. Melchert, Ph.D., R.Ph
Department of Pharmacology and Toxicology

Karen B. Williams, Ph.D.
Department of Biomedical and Health Informatics

TABLE OF CONTENTS

LIST OF ILLUSTRATIONS

Figure Page

LIST OF TABLES

Table Page

ACKNOWLEDGMENTS

My wholehearted gratitude goes to my advisor, **Dr. Ashim K. Mitra,** Chair and Professor of the Division of Pharmaceutical Sciences, UMKC, whose mentorship and guidance has not only made this dissertation possible but has proven to be invaluable in this project. His constructive feedback and critics in commenting the drafts helped me to develop my writing skills. I sincerely dedicate all my scientific understanding and passion to him.

I am grateful to my Ph.D. committee members, **Dr. Kun Cheng, Dr. Zhoungha Peng, Dr. Karen Williams** and **Dr. Russell B. Melchert** for their invaluable time serving in my Ph.D. supervisory committee and genuinely applaud their compassionate gesture. Their unlimited enthusiasm and zeal to the exploration of science have been the major driving force throughout my graduate career.

I am thankful to **Dr. Jennifer Friend,** Associate Dean School of Graduate Studies, UMKC and Director, Preparing Future Faculty (PFF) Program for providing me mentorship and often times, stands with me in my tough time with all sorts of advice or help she could have provided to me. I owe my sincere thanks to **Dean Russell B. Melchert**, School of Pharmacy, UMKC, for lighting up my path through constant guidance, advocacy and encouragement towards building my long term career goal. My sincere thanks to **Dean Denis M. Medeiros,** School of Graduate Studies, UMKC, for providing me a great deal of leadership skills, and suggestions to become a good scientist and professional. I would like to extend my appreciation to **Mrs. Ranjana Mitra** for her constant support and encouragement during my stay at UMKC. I am also thankful to **Dr.**

Thomas Johnston and **Dr. David Van Horn** for their valuable time and suggestion whenever I needed.

I am thankful to **Dr. Dhananjay Pal** for teaching me cell culture techniques and valuable scientific discussions which helped me in my research project. I express my sincere & heartfelt gratitude to the professors of Division of Pharmaceutical Sciences, UMKC, **Dr. Simon Friedman, Dr. Chi Lee, Dr. William Gutheil and Dr. Bi-Botti Celestine Youan** for helping me in building up my concepts and developing the ethics of my profession. I am thankful to **Dr. Patricia Hovis-French,** retired PFF Director and **Dr. Michelle Maher,** School of Education, UMKC for their insight in the PFF course-work to develop my teaching skills. I would like to extend my appreciation to the professors of division of pharmaceutical sciences and division of pharmacy practice and administration to make my teaching assistantship a great learning experience for me.

I am earnestly thankful to **Joyce Johnson** and **Sharon Self** for their endless support. I extend my sincere thanks to the administrative staff members of School of Pharmacy, UMKC, **Nancy Bahner, Shana Eisentrager, Jane Poe** and **Tamica Lige** for their invaluable unwavering support and timely help. I am thankful to the administrative staff members of the School of Graduate Studies, UMKC, **Michelle Heiman, Alphia Curry, Nancy Hoover,** and **Quincy Benette** for their kind support to me.

Over the years, I am fortunate to work with a team of brilliant scientists in my lab. I owe thanks to **Drs. Sulabh Patel** and **Ravi Vaishya** for their guidance and key learnings to enhance my understanding on this project. I would like to express my thanks to **Drs. Varun Khurana, Mitan Gokulgandhi, Ashaben Patel, Xiaoyang Yang** and **Carol** for helping me in learning several techniques, and scientific discussion. I also owe

my thanks to **Abhirup Mandal, Nitish Mishra, Parteek Patel, Mary Joseph** and **Drs. Shreeram Gunda, Kishore Cholkar, Megha Barot, Animikh Ray** and other lab mates for their support in the lab and friendship.

I am thankful to **Dr. James Murowchick** (Department of Geosciences, UMKC) for helping me in XRD experiments. I am thankful to several investigators and collaborator who supported in my experiments; **Dr. Brian Gilger** from North Carolina State University for performing animal studies of PB copolymer based formulations at their facility and **Drs. Poonam R. Velagaleti, Ulrich M. Grau, Sidney L. Weiss**, i-Novion for their valuable suggestions to this project. I am deeply thankful **to Drs. Lane K. Christenson** and **Wei-Ting Hung** of the University of Kansas Medical Center for their kind helps in nanoparticle tracking analysis. I am thankful to **Drs. Daniel Stamer** and **Guorong Li** of the Department of ophthalmology, Duke University for helping in the development glaucoma model. I would like to extend my sincere thanks to **Dr. Ibrahim Youm** for his valuable time and support. I am thankful to high school summer intern **Ryan Conley** and **Zach Aulgar, Nikhil Dhall, Siddhant Thukral** from School of Medicine, UMKC for assisting in my experiments.

My sincere thanks to the several people, I came across at UMKC and UM System while taking several inter-collaboration projects alongside of my scientific career. I would like to mention, **Colleen Kelly, Jana Boschert, Janasz Shelly, Dr. Greg Holiday, Dr. Robin G. Walker, Kevin Sansburry, Kara Bollinger,** and **Richard Monroe** to help me in learning several things at different platforms at UMKC.

My gratitude goes to my friends **Drs. Ravi Shukla**, **Satyakam Singh, Rubi Mahato,** and **Hao Liu, Bhagyesh Sarode, Ashutosh Barve, Nidhi Jain, Nitin Jain,**

Amardeep Sharma, Pratibha Sharma, they brought me through a time where I have been everything from enthusiastic, challenged, and stressed about my work. I feel short of words to express my thanks to them for being a great company.

I am thankful to the funding institutions, the **National Institutes of Health (NIH)** for providing the financial supports (NIH R01 EY09171-14) in this project and the travel supports/scholarships provided by **School of Graduate Studies, Women's Council, Pharmacy Foundation,** and **Student Activity Fee Committee** at UMKC. I owe sincere thanks to School of Pharmacy, UMKC for providing teaching assistantship funds to support my finances during my PhD program. I am deeply thankful to **School of Graduate Studies, Women's Council, Student Government Association, Graduate Student Council** and **Office of Student Involvement** at UMKC for providing a great platform to me to take responsibility and value to give back to the place I belong. I also want to thanks to professional organization; American Association of Pharmaceutical Scientists and Controlled Release Society to provide several opportunities to me.

My very special and heartfelt thanks to **my family members** whom I owe everything I am today. My Parents, **Dr. Vishnukant Kabra and Mrs. Sadhana Kabra**, who have given me great upbringing to take responsibilities and instilled strength to face any challenges of life with unconditional faith, love and support over the years. I am grateful to my sister **Swati Kabra**, brother in law **Naveen Mantri** and nephew **Navansh Mantri** for their love, friendship, and encouragements in my studies. The strength and sacrifice of my beloved sister make my journey come through from all the way. I would like to express my gratitude to my in-laws family members **Munna Lal Gupta**, **Meena**

Gupta, Vikas Agrahari, Vishal Agrahari, Vinay Agrahari, **Shraddha Agrahari**, **Pragya Agrahari** and **Aashvi Agrahari** for their unconditional love to me.

My heartfelt thanks to my loving husband **Vivek Agrahari**, who has been my enduring source of strength and helped me from my day one journey to the PhD program along with the research in numerous ways. This list is not comprehensive and there were many others who have contributed to my journey of these last several years. I am greatly thankful to them for their inspiring interactions and care devoted towards my success. Thanks to all of them! At last I would like to thanks almighty for showering blessings to me and make my life purposeful and full of happiness.

Dedicated to My Family

CHAPTER 1

LITERATURE REVIEW [1], [2]

Introduction

Ocular diseases pose a major problem and affect quality of life. It is estimated that 285 million people worldwide are visually impaired, and 39 million are blind (http://www.who.int/mediacentre/factsheets/fs282/en/). In the United States itself, about 3.4 million people over the age of 40 are blind or have significant visual impairment (https://www.cdc.gov/visionhealth/data/national.htm). Normal aging of the eye is characterized by a continuous loss of Photoreceptor (PRs), Bruch's membrane (BM) thickening, choroidal thinning, scleral stiffening, vitreous degradation and accumulation of debris. Among these, age-related macular degeneration (AMD), diabetic retinopathy (DR), macular edema (ME), diabetic macular edema (DME), and glaucoma are the leading causes of vision loss.

Age-related macular degeneration (AMD)

Macular degeneration occurs when the small area in the retina (macula) deteriorates, and develops as person ages, hence referred to as AMD. It is a degenerative disease that damages the retinal pigment epithelium (RPE) and PRs. A total of 8.7% of the world population has AMD, and it is projected that the number of people with the disease will be at about 196 million in 2020, and 288 million in 2040 (3). About 1.75 million Americans are affected by AMD, and this number is expected to increase about 3 million by 2020 (3). As the disease progresses, AMD can be classified into dry and wet

forms. Based on the absence or presence of blood vessel growth progressing from the choroidal side towards the retina, the disease is broadly subdivided into non-neovascular (NNV) and neovascular (NV) AMD (wet AMD). In wet AMD, new blood vessels from the choroid may leak, resulting in ME and hemorrhage. Wet AMD accounts for about 20% of patients, but 90% of AMD patients suffer from severe visual loss. The risk of getting advanced AMD increases from 2% for those ages 50-59 years, to nearly 30% for those over the age of 75 years (4). Multiple factors such as oxidative stress, lipid metabolism, immune system activation, and angiogenesis (5) play a key role in AMD pathogenesis. The protein aggregation and immunologic processes are also involved, including the inflammatory molecules in BM, recruitment of macrophages/dendritic cells, and complement system components in the macula area. In addition, smoking is a major oxidative stress factor in the progress of AMD (6). The detailed effects of these factors can be explored elsewhere (7, 8).

RPE performs a variety of complex processes that are essential for proper visual functions. RPE plays crucial roles in the retina including formation of blood retinal barrier (BRB) by tight junctions, transportation of nutrients from blood to PRs, light absorption, secretion of cytokines/growth factors and phagocytosis of outer segments of PRs (6, 9). AMD starts with the deposit of drusen between RPE and basal membrane (BM) and progresses with the death of RPE and PRs degeneration and eventually loss of central vision (6). BM is a thin (2–4 μm) connective tissue located between the RPE and the choriocapillaris. It functions as a physical as well as biochemical barrier for normal physiological and pathological processes. The primary functions of BM include regulating the diffusion of biomolecules, minerals, antioxidants, etc., between the choroid

and RPE. BM also provides physical support for migration and differentiation of RPE for RPE cell adhesion.

In case of dry AMD, the gradual deterioration of RPE leads to subsequent PR loss at the macula. The vascular endothelial growth factor (VEGF) produced by the basal side of the RPE cells is essential to the health of the choriocapillaris. In wet AMD, RPE produces excessive amounts of VEGF, and this contributes to the breakdown of the BRB and sprouting of fragile blood vessels from the choroid through BM into retina in a process called NV. Leakage of blood from these abnormal vessels causes an acute loss of vision. Additionally, pigment epithelium-derived factor (PEDF) and transforming growth factor-beta (TGF-β), secreted by the apical side of RPE cells provide an immunosuppressive microenvironment in the sub-retinal space (6, 10).

Over the past decade, interesting progress has been made in the treatment of AMD owing to an increased understanding of the mechanisms of ocular angiogenesis and factors affecting (11). There are several factors involved in angiogenesis in the eye, with VEGF playing a central role (12). VEGF-A is a 46 kDa glycoprotein produced by ocular cells in response to oxidative stress and has multiple functions in the eye. It stimulates endothelial cell growth, promotes vascular permeability and induces dissociation of tight junction components. Out of various isoforms of VEGF in humans, VEGF165 is primarily responsible for angiogenesis. Currently, no therapy exists for dry AMD and only dietary modifications such as increase in intake of antioxidants, cessation of smoking, and control of blood pressure slow down disease progression. The approved treatment for dry AMD is the use of the Age-Related Eye Disease Study (AREDS)-based vitamin supplements that lowers the risk of developing advanced stages of AMD (13).

In wet AMD, VEGF has been reported to be present below the RPE cell layer and around PRs. VEGF-A is the most potent mediator of both retinal and choroidal angiogenesis, and its inhibition via intraocular anti-VEGF treatments to prevent the formation of new blood vessels represents the cornerstone of wet AMD therapies. However, the primary atrophic component of AMD still progresses despite anti-VEGF therapy (6). Recombinant humanized anti-VEGF antibody fragments or soluble receptor decoys (e.g., ranibizumab (Lucentis; Genentech/Roche), bevacizumab (off label drug: Avastin; Genentech/Roche), pegatanib (Macugen®), and aflibercept (Eylea; Regeneron Pharmaceuticals) are current FDA approved therapies for wet AMD. The physicochemical and pharmacokinetics parameters of anti-VEGF therapeutics for the treatment of wet AMD are summarized in Table 1.1. The development of new agents for wet AMD has been focused on both improving efficacy and extending the duration of action. Other available treatments for wet AMD include photodynamic therapy (PDT) with intravenous verteporfin (14). Studies suggested that the combination of PDT with angiogenic inhibitors may reduce the frequency of Intravitreal (IVT) injections and the risks associated with long-term IVT therapy (15).

Challenges with current intravitreal anti-VEGF treatments

IVT injections are associated with multiple adverse events including subconjunctival hemorrhage, retinal tears, retinal detachments, vitreous hemorrhage, intraocular inflammation, tachyphylaxis, retinal vascular occlusion, cataract, and endophthalmitis. Furthermore, an increase in IOP has also been observed. Despite the facts that effective, IVT anti-VEGF therapies have several drawbacks.

- VEGF plays a protective role in the retinal tissue. The knockout of VEGF in retina can lead to severe side effects such as defects in the RPE choroid complex or the loss of interaction between the RPE and PRs outer segments.
- Prolonged suppression of the plasma VEGF due to anti-VEGF therapy may lead to an increased risk of cardiovascular diseases.
- The short intraocular retention of anti-VEGF drugs is a major issue due to the high clearance rate from the posterior eye, thus requiring frequent administration.
- Patients suffering from recurrent NV AMD may develop mechanisms of resistance to anti-VEGF therapy, which can result in a diminished therapeutic effect(16).
- An effective and safe anti-VEGF therapy should not damage the normal blood vessels; preserve the physiologic functions of the retinal neurons and other cells.
- IVT injections require a high degree of sterility to prevent infection.
- The long-term anti-VEGF treatment carries a high financial burden to the patients.

To improve the safety, cost-effectiveness and impact on patients receiving IVT anti-VEGF treatments, a reduction in the drug administration frequency is required. Thus, there remains a need for the development of novel strategies for sustained and efficient anti-VEGF delivery. Newer agents may offer longer duration and minimize treatment burden thus, the overall cost of the therapy (17, 18). However, conventional ocular dosage formulations cannot overcome several barriers to ocular delivery and reduce the frequency of IVT injections. The uses of nanotechnology based approaches are a possible way to overcome these limitations. Thus, there has been considerable effort in the development of novel delivery approaches to selectively target and maintain the therapeutic drug concentration in the back of the eye for prolonged periods (19, 20).

Table 1.1 Characteristics of different anti-VEGF agents used in the clinical management of AMD

Anti-VEGF agents	**Structure**	**Biological target and mechanism**	**K_D, IC_{50} for VEGF**	**Mol wt.**	**Approvals**	**Vitreous half-life**	**Intravitreal dose**	**Regimen**	**Cost (Approx.)**	**Ref.**
Pegaptanib sodium (Macugen®)	Pegylated RNA aptamer (28 base)	VEGF-A_{165}	200 pM,	50 kDa	FDA (2004) EMA(2005)	10 days (human)	0.30 mg	every 6 weeks	US$995	(16, 21),(22, 23)
Bevacizumab (Avastin®)	Recombinant humanized mAb lgG1	All isoforms of VEGF-A	58 pM, 423 pM	149 kDa	FDA (2004) EMA(2005) CFDA(2010)	6.7 days (human), 4.32–6.61 days (in rabbits)	1.25 mg	every 4 weeks	US$50	(16, 21, 23)
Ranibizumab (Lucentis®)	Recombinant humanized lgG1-κ isotypemAb fragment	All isoforms of VEGF-A	46 pM, 343	48 kDa	FDA (2006) EMA (2007) CFDA (2012)	9 days (human), 2.88-2.89 days (in rabbits	0.50 mg	every 4 weeks	US$2000	(16, 21, 23)
Aflibercept (Eylea®)	Fusion protein: domain 2 of VEGFR-1 and domain 3 of VEGFR-2 fused with lgG1 Fc	All isoforms of VEGF-A, VEGF-B, and PIGF	0.50 pM, 8 pM	115 kDa	FDA (2011) EMA (2012)	7 days	2.0 mg	every 4 weeks for 3 months and then once every 8 weeks	US$1850	(16, 21, 23)

Anti-VEGF agents	Structure	Biological target and mechanism	K_D, IC_{50} for VEGF	Mol wt.	Approvals	Vitreous half-life	Intravitreal dose	Regimen	Cost (Approx.)	Ref.
Conbercept	Fusion protein: domain 2 of VEGFR-1 and domains 3 & 4 of VEGFR-2 fused with lgG1 Fc	All isoforms of VEGF-A, VEGF-B, VEGF-C, and PIGF	0.50 pM, 10 pM	143 kDa	CFDA (2013)	4.2 days (in rabbits)	0.50 or 2.0 mg	every 4 weeks	*	(23)
Brolucizumab	Immunoglobulin Fv fragments; mAb. Humanized, single-chain Ab fragment inhibitor of VEGF-A.	binds all isoforms of VEGF-A	*	26 kDa	Phase III	4.9 days	1.25 mg	every 4 weeks	*	(17, 24)
Abicipar	Small molecule: (DARPins)	inhibits all subtypes of VEGF-A	*	34 kDa	Phase II	6 days	1 or 2.0 mg	every 4 weeks	*	(17, 25)
Tanibirumab	hlgG from a fully human naive single-chain phage library	VEGFR-2 receptor Ab	*	*	Preclinical	*	*	*	*	(26, 27)

- No information could be found.

Diabetic retinopathy (DR)

Patients with diabetes (whether Type 1 or Type 2 diabetes) develop 'macrovascular' complications which affect the kidneys (nephropathy), eyes (retinopathy) and peripheral nerves (neuropathy) (28). Among people with diabetes, the overall prevalence of DR worldwide is about one third, with increasing risk associated with longer disease duration, and presence of hypertension. It is the leading cause of vision loss in adults aged 20–64 years in developed countries. Recent estimates suggest that the number of people with DR will increase from 127 million in 2010 to 191 million by 2030 (29). Primary cause of DR is diabetes—a condition in which the levels of glucose (sugar) in the blood are too high. Elevated sugar levels from diabetes can damage the small blood vessels that nourish the retina and in some cases, block them completely. When damaged blood vessels leak fluid into the retina it results in a condition known as diabetic macular edema which causes swelling in the center part of the eye (macula) that provides the sharp vision needed for reading and recognizing faces (30). Prolonged damage to the small blood vessels in the retina results in poor circulation to it and macula. This leads to the development of growth factors that cause generation of new abnormal blood vessels (neovascularization) and scar tissue to grow on the surface of the retina. This stage of the disease is known as proliferative diabetic retinopathy (PDR) (31). New vessels may bleed into the middle of the eye, cause scar tissue formation, pull on the retina, cause retinal detachment, or may cause high pressure and pain if the blood vessels grow on the iris, clogging the drainage system of the eye leads to vision loss (30).

DR can be very broadly classified into two stages based on the level of microvascular degeneration and related ischemic damage: non-proliferative DR and advanced, proliferative DR (32). The progression of DR is related to abnormalities of the vasculature including permeability

of the BRB, progressive microvascular damage with vascular endothelial cell and pericyte loss, subsequent occlusion of capillaries, thickening of vascular BM, and retinal neuronal and glial abnormalities (29). The alteration of the BRB is the hallmark of the pathogenesis of diabetic retinopathy. In diabetes, three changes happen at the BRB: (i) loss of endothelial cell–cell junctions; (ii) thickening of the basement membrane; and (iii) selective loss of pericytes. The breakdown of the BRB leads to intraretinal haemorrhages, hard exudates and macular oedema (33). At present there are few measures available to prevent DR beyond regulating hyperglycaemia, preventing dyslipidemia, controlling hypertension and cessation of tobacco smoking. The laser photocoagulation therapy has been the mainstay of management therapy in addition to the use of IVT anti-VEGF agents & steroids (34, 35).

Diabetic macular edema (DME)

Diabetic macular edema is the common cause of vision loss from diabetic retinopathy, typically presenting as a varying degree of central blurring. DME is defined as a thickening and cystoid edema of the macula, often with exudate deposition, attributable to DR (36). Pathology in the retinal microvasculature is an early indicator of the vasculopathy: microaneurysms, capillary dropout, and blood–retinal barrier dysfunction leads to DME (37). The resultant anatomical alterations (loss of retinal capillary pericytes and endothelial cells, dilated capillaries, and retinal microaneurysms) and chemical induction of hyperpermeability (via cytokines, including VEGF) leads to breakdown of the blood–retinal barrier, resulting in fluid leakage into the extracellular space: in the macular region, leading to DME (36) (38). Diabetes and hyperglycaemia have obvious effects on intraocular vascular endothelial cell permeability, adhesion to leukocytes, as well as angiogenesis. These alterations result in increased vascular

leakage (increased permeability), vascular occlusions, ischemia, and angiogenesis (39). The pathogenesis of DME is believed to be secondary chronic hyperglycemia. Chronic hyperglycemia causes systemic small vessel vasculopathy (capillary endothelial damage) related to factors that lead to retinal capillary hyperpermeability: hyperglycemic toxicity, inflammation, oxidative stress, and angiogenesis (39) (40). Chronically elevated serum glucose leads to a breakdown of the inner and outer retinal blood barrier. Hypoxia, oxygen-free radical accumulation, and inflammatory mediators result in VEGF-A expression (41).

VEGF plays a critical role in DME development. VEGF is implicated in NV and increased vascular permeability (42). VEGF levels in both the anterior and vitreous chambers correlate with DME severity. These observations made VEGF a distinct target in the treatment of DME (39). IVT pharmacologic agents have demonstrated superior efficacy in clinical trials compared to laser for treatment of DME. However, laser photocoagulation has largely been replaced by IVT pharmacologic injections over the past decade as a principal therapy for DME (43).

Glaucoma

Glaucoma is the second leading cause of irreversible vision loss and blindness worldwide. Approximately 60 million people worldwide are afflicted with glaucoma. This number is expected to increase to 80 million in 2020 because of both demographic expansion and population aging (44). Glaucoma is a group of progressive optic neuropathies characterized by degeneration of retinal ganglion cells and resulting changes in the optic nerve head. Loss of ganglion cells is related to the level of intraocular pressure, but other factors may also play a role. The death of retinal ganglion cells is accompanied by morphologic changes of the retina.

These are central nervous system neurons that have their cell bodies in the inner retina and axons in the optic nerve. Degeneration of these nerves results in cupping, a characteristic appearance of the optic disc and visual loss (45) (44). The biological basis of glaucoma is poorly understood and the factors contributing to its progression have not been fully characterized. The two main types of glaucoma are open-angle and angle-closure. These are marked by an increase in intraocular pressure. Well-marked symptoms are observed only in acute angle-closure glaucoma. All other forms of chronic glaucoma are largely asymptomatic. Normal-tension glaucoma is a form of glaucoma in which damage occurs to the optic nerve without eye pressure exceeding the normal range (12-22 mm Hg). Secondary glaucoma refers to any form of glaucoma in which there is an identifiable cause of increased eye pressure (traumatic glaucoma, uveitis glaucoma, drug induced glaucoma, advanced cases of cataract or diabetes, and others) (46). The only signs are gradually progressive visual field loss and optic nerve changes. Unfortunately, because of the asymptomatic nature of chronic glaucoma, upto 50% of people are unaware of their diagnosis and not receiving treatment. Management of glaucoma focuses on lowering intraocular pressure, which remains the principal proven method of treatment initiated with ocular hypotensive drops, laser trabeculoplasty or surgery may also be used to slow disease progression (47).

Ocular drug delivery to back of the eye

The major diseases that significantly impact vision problems are AMD, DR, ME, DME, uveitis, and glaucoma. The treatment of these diseases, especially those associated with the retina requires a direct and local application of the therapeutic molecules since there are several anatomical and physiological barriers present in the eye (48). Due to these barriers, the drug delivery to the intraocular tissues especially to the posterior of the eye is significantly limited,

especially via the topical and systemic routes (19, 20). However, with a better understanding of the anatomy of the eye, and pathophysiology of these diseases, several effective treatment options are now being offered. In addition, the uses of nanotechnology based delivery systems and availability of different routes of drug administration have been shown to overcome several ocular barriers and target specific tissues, including the retina (49). Current treatments for posterior eye diseases suffer from significant disadvantages including frequent intraocular injections and related adverse events, in addition to the high cost of the treatment (17).

Barriers and various routes of drug delivery to the posterior segment of the eye

The interior of the human eye is subdivided into anterior and posterior segments. The anterior segment is filled with aqueous humor which provides nourishment to the lens and cornea and removes degradation products. The iris (colored part of the eye), separates the anterior segment from the posterior segment. The ciliary body, located behind the iris, produces the aqueous humor, which fills the two chambers. The posterior segment consists of the vitreous humor, retina, choroid, and sclera (50). The retina is consist of the inner limiting membrane, nerve fiber layer, ganglion cell layer, inner and outer plexiform layers, inner and outer nuclear layers, external limiting membrane; PR layer; and RPE. The choroid is the vascular cover of the eye lying between the retina and the sclera, which provide nourishment to the PRs.

The regular routes to target back of the eye are topical (51), systemic, intraocular (suprachoroidal, IVT), and periocular (subconjunctival, subtenon, retrobulbar). These routes are briefly discussed along with their advantages and limitations in **Table 1.2** and a schematic representation is provided in **Figure 1.1**. The drug bioavailability in the eye is limited by several anatomical/static (conjunctiva, cornea, sclera, blood aqueous and retinal barriers) and

physiological/dynamic (choroidal blood flow, efflux transporters, tear washing, nasolacrimal drainage) barriers (48). These barriers effectively limit the drug access to the back of the eye as shown in schematic representation in **Figure 1.2.**

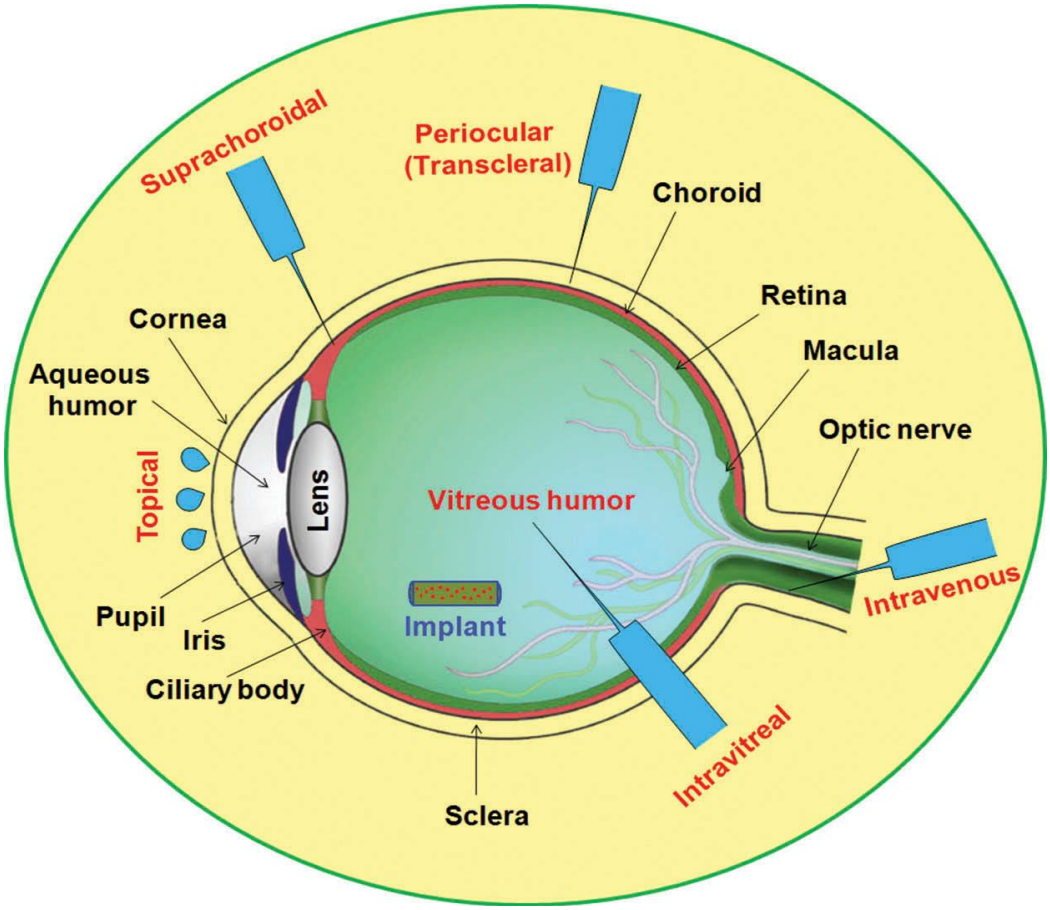

Figure 1.1 Schematic representation of routes of administration (Reproduced from permission (1)

Table 1.2 Characteristics of various routes of administration for posterior eye delivery

Route	Comments
Topical	
Drug entry pathways	Corneal, conjunctival, and scleral pathways.
Delivery barriers	Membrane barriers and elimination pathways on the eye surface, cornea, BRB, and tight junctions.
Elimination pathway	Tear wash out, nasolacrimal drainage, choroid, conjunctiva blood flow, and lachrymation, blinking.
Advantages	• High patient compliance. • Less systemic side effects. • Relatively easy to administer.
Limitations	• Small retention time of drug or dosage forms. • Blurring of vision, irritation. • Precorneal drug losses, drainage through the nasolacrimal duct. • Low bioavailability. • Limited volume of administration (approx. 30 μL). • Fast clearance from ocular surface. • Metabolism by tear enzymes. • Nonproductive uptake into systemic circulation via highly vascularized conjunctiva, choroid, uveal tract and inner retina. • Aqueous humor outflow gradient.
Approaches for improvement in therapeutic efficacy	• Bioadhesive formulations may be employed to reduce precorneal clearance and increase corneal surface contact time. • Positive charge of formulations may enhance the contact time with cornea to interact with negatively charged mucosa. • Nanowafers approach may be beneficial for long-term and sustained drug release.
Systemic	
Drug entry pathways	Choroid, conjunctiva
Delivery barriers	Choroid; efflux transporters, BRB (selectively permeable to highly lipophilic molecules).
Elimination pathway	Hepatic clearance, conjunctival and choroid capillaries, phagocytic clearance.
Advantages	• Better patient compliant than intraocular injection. • Comparatively safer to eye since not a direct administration.
Limitations	• Low bioavailability due to the BRB, hence high doses required which produce systemic side effects.
Approaches for improvement in therapeutic efficacy	Large molecules and/or hydrophilic drugs are able to penetrate the choroid from the systemic circulation, but are unable to cross the inner BRB into the retina. Thus, drugs must exit the choroidal circulation and permeate the outer BRB.

Routes	Comments
Intravitreal	
Drug entry pathways	Directly to the vitreous chamber
Delivery barriers	Diffusion through the vitreous chamber, neural retina, and BRB.
Elimination pathway	• Movement to aqueous chamber and retina. • Dynamic clearance mechanisms, such as anterior bulk aqueous flow or posterior vitreoretinal-choroidal flow, eliminate drugs from the site of deposition.
Advantages	• Local and direct delivery. • High therapeutic concentration. • No barrier to reaching macula.
Limitations	• It is necessary to administer the drug frequently to maintain adequate intraocular concentrations. Frequent injections have been associated with adverse events especially retinal detachment, vitreous hemorrhage and endophthalmitis. • Linked to degeneration of PRs and cataracts. • Only about 50–100 μl being administrable in human via IVT route • High cost of administration and drugs (anti-VEGF).
Approaches for improvement in therapeutic efficacy	Changes in the drug's formulation to release the drug for longer duration or modify specific properties of the drug, such as size, charge, and lipophilicity. Stimuli-responsive approach may be beneficial to release the drug when required.
Periocular	
Drug entry pathways	Majorly via the transscleral pathway to effectively deliver drugs next to the choroid.
Delivery barriers	Scleral thickness, choroidal blood circulation and BRBs [21].
Elimination pathway	• Conjunctival and choroidal blood and lymphatic flow. • Losses from the periocular space, BRB, choroidal circulation. • Binding of drugs to tissue proteins; efflux transporters.
Advantages	• Less invasive. • High therapeutic drug levels. • Repetitive periocular administration under local anesthesia is possible without direct interference with the vision. • High volumes of drug solution can be administered in humans. • Can bypass the BRB without intraocular penetration.
Limitations	• Low retinal bioavailability compared to IVT injections. • The injected drug still has to traverse the sclera, which is less permeable to larger molecules. • The drug has to pass through several layers-including the episclera, sclera, choroid, BM, and RPE-while overcoming choroid circulatory clearance, delivery is not as effective as intraocular injections in targeting retinal targeting. • Rapid drug clearance, systemic side effects, tissue hemorrhage.

Routes	Comments
Approaches for improvement in therapeutic efficacy	Improvements to formulations that either increase residence time or promote diffusion from the middle coat may be effective ways to overcome the barriers to periocular delivery. Nano-size formulations with small size may provide superior diffusion. Negative charge or positive charge of formulations depends if interaction or diffusion required.
Suprachoroidal	
Drug entry pathways	Across the sclera to flow quickly along the inner surface of the eye and subsequently into the posterior chamber.
Delivery barriers	Choroid-BM.
Elimination pathway	High blood flow in the choriocapillaries washes away therapeutic molecules deposited in the suprachoroidal (SCS).
Advantages	• Preferred site for drug delivery to the posterior tissues such as choroid, RPE and macula, due to its non-interference with the optical pathways and improved diffusional access to the choroid. • Allow for larger volumes of drugs with a safer procedure. • Drugs injected into the SCS are less likely to reach the RPE, interact with the rods and cones of the PR cells and ultimately to trigger immunologic responses. • SCS can accommodate up to 1 mL of fluid, which rapidly diffused into the posterior segment. • Injections of 10–50 µL into the SCS have been demonstrated to be well tolerated with a low risk of ocular complications.
Limitations	• Injection of a drug solution into the SCS can result in rapid drug diffusion to cover the entire SC surface; this could potentially induce drug-related toxicities of the surrounding tissues. • Rapid clearance of macromolecules following suprachoroidal route. • Postoperative inflammation and choroidal hemorrhage remain a concern and needs to be overcome when injecting into the SCS.
Approaches for improvement in therapeutic efficacy	• Diffusion kinetics from the SCS could be optimized using sustained release formulations such as nanoparticles and microparticles. • Drug delivery systems that can provide controlled and continuous drug release are likely to minimize such side-effects. • Microneedles appear to offer a viable option to deliver drugs to the back of the eye, especially through the SCS route. These needles help to deposit drug or carrier system into sclera or into the SCS which may facilitate diffusion of drug into deeper ocular tissues, choroid and neural retina.

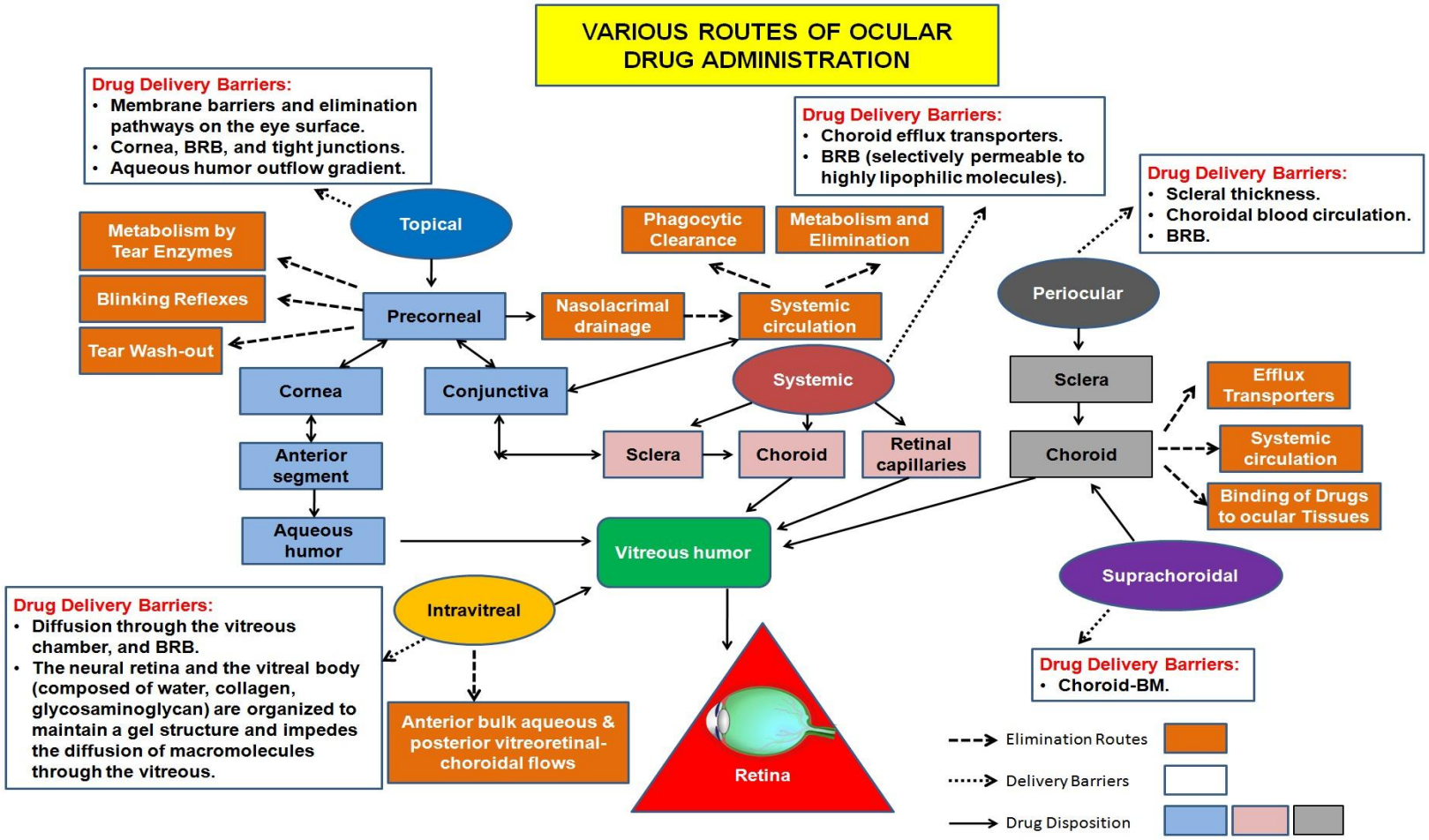

Figure 1.2: Schematic representation of drug disposition in eye following various routes of ocular administration. (Reproduced with permission from (1)

Biodegradable polymers for ocular drug delivery

Many approaches have been evaluated to improve ophthalmic drug delivery. Applications of controlled drug delivery systems have been anticipated as an effective approach to circumvent all these limitations. Controlled drug delivery systems release the drug in a sustained and controlled manner by which the therapeutic concentration is maintained for the prolonged period of time (52). These systems provide many practical advantages such as avoid frequent administration, which is a major non-compliance with many chronic eye disorders. The delivery of emerging therapeutic macromolecule therapeutics having short biological half-lives could be possible with polymeric delivery (53). These systems protect the protein drugs *in situ* and have an ability to deliver them at desire rate by overcoming anatomical and biochemical barriers (54). For such purpose, biodegradable polymers are of enormous importance. Biodegradable polymers are generally divided into two groups, natural and synthetic based on their origin. Natural biodegradable polymers such as gelatin, albumin, chitosan, hyaluronic acid and synthetic biodegradable polymers such as polyethylene glycol (PEG), polyglycolic acid (PGA) and polylactic acid (PLA), polyvinyl alcohol (PVP) have been thoroughly explored for ocular delivery systems. These polymers are approved by FDA for human applications (55). Synthetic origin polymers offer advantages over natural polymers by being versatile with a wide spectrum of applications, having a capability to tailor mechanical properties and altering the rate of degradation according to the need.

In the past two decades the development and application of synthetic biodegradable polymers for ocular drug delivery have gained significant momentum. (52). Polymeric delivery approaches such as micro and nanoparticles (NPs),

microspheres, liposomes, hydrogels and ocular implants have been designed to deliver the therapeutic agents in the controlled manner for long duration (56). The release rate of the drug molecules from these polymeric system depends on many factors such as, molecular weight (MW) and degradation mechanisms, physicochemical properties of the drug, interaction between the drug and polymer (1).

The natural and synthetic biodegradable polymers have many favorable properties such as biocompatibility with ocular tissues, biodegradability and mechanical strength (57). They provide negligible toxicity and also their degradation products are non-toxic in terms of both local and systemic response. In addition, the inability of a single biodegradable polymer to meet all the requirements leads to the development of the block copolymers strategy.

PLA, PGA and their copolymers polylactide-co- glycolide (PLGA) (58, 59) are the most promising biodegradable polymers. PLGA copolymers of different MWs widely used for opthalmic applications. PGA alone is highly prone to hydrolysis and remains insoluble in common organic solvents therefore it is not widely acceptable for the fabrication of controlled drug delivery systems (60). PLA offers unique features of biodegradability, biocompatibility, thermoplastic processability and eco-friendliness that offer potential and being a bioresorbable polymer that play an increasingly important role in biomedical applications due to their unique ability to be completely resorbed in pre-designed time frames ranging from months to a few years (61). PLA alone and in combination with PGA with different ratios are mostly utilized in the formulations. These polymers upon non-enzymatic or enzymatic hydrolysis produce water soluble metabolic products, which are not harmful to living tissues. These polymers belong to polyester

class and degrade mainly through bulk erosion (61). *In vitro* degradation of polyesters primarily occurs through hydrolytic cleavage. However, *in vivo*, enzymes play an important role to initiate the degradation process (62). The degradation products lactic acid and glycolic acid are nontoxic and eliminate in the form of CO2 and water via Krebs cycle (63). (64). PLA and PLGA are widely utilized in ocular drug delivery systems such as implants, injectable microspheres and NPs (65).

Poly- ε-caprolactone (PCL) is an aliphatic polyester synthesized form monomer ε-caprolactone through ring opening polymerization. It is a tough semi crystalline polymer having the melting point in the range of 59 and 64 °C (66). Permeability and crystallinity of the PCL can be modified by copolymerization with PLA or PGA. PCL is utilized for sustained drug delivery due to its higher permeability to various drug molecules and slower degradation in comparison to other polymers (67). Degradation rate of PCL can be improved by copolymerizing with other fast degrading polymers (68).

Nanotechnology based delivery systems for the posterior segment of eye diseases

There are several novel delivery technologies that are designed to serve as drug delivery systems in ocular and other applications (19, 20, 48, 69, 70). Among these, nanocarrier (NC)-based delivery systems are extensively studied (19, 20, 71). NCs are colloidal systems in the nano-scale size range and capable of loading the lipophilic and hydrophilic as well as small and macromolecule drugs. Because of the small size and use of biodegradable materials in the formulation development, NCs offer various significant advantages such as, small size avoids irritation considering the highly sensitive nature of ocular tissue (20, 72), improved drug bioavailability and ocular tissues biocompatibility,

provide stability to drug from *in vivo/in vitro* degradation, reduction of drug clearance and increase of the *in vivo* half-life, sustain or controlled drug release profile, site-specific delivery by targeting ligand, and potential to combine diagnosis and therapy. In the following sub-sections, several types of NCs systems, their advantages and limitations are discussed. The therapeutic potential of these carriers in the posterior segment eye diseases is summarized in **Table 1.3**.

Liposomes

Liposomes are lipid vesicles in the size range from 0.1 to 10μm. They are made of amphiphilic phospholipids bilayers (to encapsulate hydrophobic drugs) surrounding an aqueous core (to encapsulate hydrophilic drugs) (48, 73). Liposomes have been comprehensively used in ocular therapeutics due to several advantages such as high versatility of surface chemical modification, specific targeting, drug release can be controlled depending on the number of bilayers number and composition, and potential of stimuli-sensitive delivery system (73). Also, the physiochemical properties of liposomes (size, surface charge, and functional chemistry) can be modified by mixing different lipids during their formulation development. However, liposomes present certain limitations, such as low reproducibility, instability of macromolecules during the formulation process, manufacturing cost and scale up issues, difficulties in sterilization, immunotoxicity, variable size distribution, and instability in biological environment (74).

Polymeric nanoparticles (NPs) and microparticles (MPs)

Polymeric NPs are biodegradable and biocompatible colloidal systems in the size range of 10-1000nm (48). MPs are delivery systems having the micrometer size range of about 1 to 1000μm (75). In addition the above advantages as of liposomes, NPs and MPs

provide flexibility in various routes of administration, stimuli-responsive system, encapsulation and delivery of multiple drugs in a single particle, and flexibility in modifying size, shape, and surface functionality in ocular drug delivery (20, 76). They can also achieve cellular drug delivery either via endocytosis or phagocytosis. However, these particles have several drawbacks, such as burst release which may lead to drug toxicity, rapid phagocytic clearance in systemic circulation, immunogenicity, scale-up issues, particle aggregation due to large surface area, and non-uniformity in size distribution.

Nanomicelles

Nanomicelles are self-assembled systems from biodegradable and biocompatible amphiphilic block polymers in the size range of ~10-100nm. They can encapsulate poorly or highly-water soluble drugs in the core or outer hydrophilic shell, respectively (77, 78). Nanomicelles have wide advantages in ocular and other drug delivery applications, such as easy and reproducible formulation, easy sterilization by filtration, ability to enhance solubility of hydrophobic drugs, prevention or minimization of drug degradation, possibilities of changing polymer block arrangements as needed, and improved drug permeation through ocular epithelia with minimal or no irritation, ultimately leading to enhanced ocular bioavailability (20, 79). Drawbacks of nanomicelles include instability in biological/physiological environment, immunogenicity and toxicity, premature drug release, and lack of formulation scale-up methods.

Dendrimers

Dendrimers are branched polymeric systems in the size range of 10-100nm. Drugs can be either entrapped in the dendrimers network through hydrogen bonds, hydrophobic

and ionic interactions or conjugated through covalent bonds (80, 81). These systems have terminal end groups of amine/hydroxyl/carboxyl functionality which may be utilized to conjugate targeting ligand or therapeutic molecules. Due to their unique structure, dendrimers exhibit improved physicochemical properties, uniform size distribution, and higher biocompatibility. However, the complexity and multistep in formulation process and, toxicity issues limit their applicability.

Nanowafers

Nanowafers are tiny disc-like or rectangular membrane that contains drug loaded nano-reservoirs. Nanowafers can be readily applied on the eye and release the drug for a longer duration, thus improving the overall therapeutic efficacy. During the course of the drug release, nanowafer slowly dissolves and fades away. Recently, topically applied nanowafers with extended drug release attributes and enhanced efficacy has been developed to treat dry eye diseases (82, 83). The slow drug release from the nanowafer increases the ocular surface drug residence time and subsequent absorption into the surrounding tissue. Although, nanowafers are in early development phases, they have the potential for treating posterior eye diseases.

Nanocrystals

Nanocrystals are drug particles stabilized by the surfactant or polymeric stabilizers and have a size range between 10 and 1000 nm. Nanocrystals possess outstanding features enabling to overcome the solubility problems of poorly soluble drugs and provide an enhanced bioavailability, high drug load, low side effects, fast onset of action and an overall improved efficiency and safety (84). Nanocrystals have been explored for the delivery of antiglaucoma drugs forskolin (85) and brinzolamide (86).

Thus, it can be postulated as future choice for the treatment of various posterior ocular diseases.

Hydrogels

Hydrogels have several potential applications in ophthalmology and delivery systems (87). Porous, soft nature and high water content of hydrogels are suitable for higher encapsulation of water soluble drugs including proteins and peptides. The processing of hydrogels usually occurs at ambient temperatures and organic solvents are rarely used, thus, they are excellent for encapsulating biomacromolecules (87, 88). Hydrogels can be made from natural or synthetic polymers. Natural polymers provide biocompatibility, and biodegradability however, may suffer from weak mechanical strength, high batch-to-batch variability, and immunogenicity. Synthetic polymers provide tunable mechanical properties and prolonged stability. Hydrogels permit various mechanisms (diffusion/swelling/chemically controlled and stimuli-responsive) of drug release. However, the high water content and soft nature of hydrogels may result in relatively rapid release of biomolecules from the gel matrix. The low mechanical strength represents a major limitation and the degradation of the polymers during the sterilization processes may affect the gel properties of the hydrogel (48, 87, 88). Moreover, the rapidly gelling formulations may clog the needle and affect the injectability of the hydrogel (88).

Composite nanosystems

Composite nanosystems (NPs suspended in a gel matrix) are made of biodegradable, FDA approved block copolymers and emerging as a versatile platform in ocular drug delivery applications (89, 90). The suspended NPs in the thermo-responsive

gel matrix encounter an additional diffusion barrier which in turn provides the long-term release especially for macromolecules. Similarly, it minimizes burst effect, and follows long-term zero order kinetics. In addition, composite nanosystems provide stability to macromolecules from enzymatic degradation and helps in improving the biological half-life. The physicochemical characteristic of composite nanosystems can be modified by varying the chemistry, MW, and block arrangements of the polymers. However, premature drug release from the NPs and drug accumulation in the gel matrix could give burst effect and needs further evaluation.

Ocular implants

Intraocular implants are designed to provide localized controlled drug release over an extended period of time. Implants are placed intravitreally by making an incision through minor surgery located posterior to the lens and anterior to the retina (87, 91). Though implantation is invasive, these devices are gaining interest due to their several advantages such as sustained and local drug release to diseased ocular tissues at therapeutic levels, reduced side effects and ability to circumvent BRB (50, 92). Ocular implants are available as biodegradable and non-biodegradable devices. Biodegradable implants of PLA, polyglycolic acid PGA, PLGA, and PCL are gaining attention due to their biocompatibility and sustained drug release properties (92, 93). Drug release can vary depending on the surface area, rate of polymer degradation, polymer swelling, MW and nature of the encapsulated drug molecule (91).

Non-biodegradable implants using the polymers such as polyvinyl alcohol (PVA), ethylene vinyl acetate (EVA), and polysulfone capillary fiber (PCF) offer long-lasting release by achieving near zero order release kinetics (92). However, these devices have to

be surgery implanted and removed after drug depletion, which makes the treatment expensive and patient non-compliance. Also, adverse events such as endophthalmitis, pseudoendophthalmitis, vitreous haze, hemorrhage, cataract development and retinal detachment limit their applications. In general, non-biodegradable polymers are preferred for implant fabrication to release the drug in a more controlled manner over long-time, while they can be easily removed in case of adverse reactions.

Stimuli-responsive nanosystems for the posterior segment of eye diseases

Developing a stimuli-responsive NC system is an attractive area for drug delivery to the posterior segment of the eye diseases since variable drug concentrations may be required at various time points depending on the individual's and the disease state (91, 94, 95). These novel systems are able to enhance/trigger the release of therapeutic molecules within a particular site in response to a number of intrinsic (pH, temperature, enzymes, oxidative stress) (96-98) and external (magnetic field, light, and heat) stimuli to control the release of therapeutic molecules in a spatial and temporal manner. In the following sub-sections several stimuli-responsive delivery approaches are briefly discussed.

Light-activated systems

The transparent nature of the cornea and the lens makes the eye an organ of choice for light activated drug delivery system (91, 99). These systems have incorporated light sensitive materials into the formulation which respond to a specific wavelength. However, UV irradiation will likely raise the safety issue as UV light causes adverse effects in the cornea, lens and retina. The NPs drug delivery depot formulated for on-demand light-triggered release of drugs post-implantation has been developed (100).

These NPs rapidly release encapsulated small molecules upon exposure to 365 nm light. One implant system has been developed by On Demand Therapeutics (ODTx), which contains several drug reservoirs that can be activated individually by laser light (91). This implantable light activated system provides a platform for controlled delivery of many types of drugs in the treatment of posterior eye diseases. Recently, suprachoroidal delivery of bevacizumab was demonstrated using a light-activated in situ gel (101).

Thermo-responsive systems

Thermosensitive polymers undergo abrupt change in their solubility in response to a small change in temperature (102). This can cause conformational changes in the polymer material that triggers the drug release. An injectable PLGA-PEG-PLGA-based thermo-responsive hydrogel for IVT sustained release of bevacizumab has been designed (103). Results entail an initial burst release of bevacizumab followed by a sustained release of hydrogel. The hydrogel showed higher intraocular biocompatibility and extended drug release.

Ultrasound-responsive systems

Recent advances demonstrate the significant potential of ultrasound mediated drug release for ocular applications (104, 105). Ultrasound is an exogenous stimulus which employs pressure waves with frequency of ≥20 kHz. Ocular formulations have the potential be combined with ultrasound method to increase the drug permeability of the ocular barriers (106). Ultrasound-responsive drug delivery systems have been used with several NCs formulations (104, 107). Ultrasound application has shown to enhance the delivery of dexamethasone sodium phosphate, through the cornea *in vivo* (108). However, the physical effect of ultrasound on the stability of the NCs formulations is yet

to be evaluated in addition to risk of sonication side effects, patient's compliance and cost issues.

Micro Electro Mechanical (MEM) systems

MEM systems consist of one or more drug reservoirs and actuators which are responsible to push the drug out of the reservoir by mechanical means in response to the stimulus including temperature, electrical stimulus, magnetic field, and osmotic pressure (91). A MEM based ocular implant has been studies for phenylephrine delivery (109). The approach has been later modified using a mini drug pump (hydrolysis based actuation) (110) to provide a precise control over the amount of drug released in response to the stimulus, exhibiting more accurate drug delivery. Another MEMS based magnetic responsive drug release ocular implant is investigated to provide a precise control over docetaxel release intended for the treatment of PVR (111).

Table 1.3 Nanocarriers (NCs) drug delivery systems in posterior segment of eye diseases

Delivery system/Stimuli	Therapeutics	Polymer	Route of administration	Target disease	Ref.
Liposomes	pDNA, and bevacizumab	PEI Annexin A5-associated Liposomes	Topical Topical	AMD Posterior eye diseases	(112) (113)
	SU5416: angigenesis inhibitor	Ala-Pro-Arg-Pro-Gly-modified liposomes	Intravitreal	CNV	(114)
	Bevacizumab	Phospholipid (egg phosphatidylcholine or 1,2-dipalmitoyl-sn-glycero-3-phosphocholine) and cholesterol	Intravitreal	Posterior eye diseases	(115)
Nanoparticles					
UV light	Nintedanib	Light-sensitive polymer	Intravitreal	Macular degeneration and DR	(100)
	Ranibizumab	PLGA MPs entrapping chitosan NPs	Intravitreal	AMD	(116)
Temperature	Triamcinolone acetonide	PEGylated PLGA NPs incorporated into PLGA-PEG-PLGA thermo-reversible gel	Intravitreal	AMD	(117)
	Triamcinolone acetonide	Folate-PEG-b-PCL		AMD	(118)
	Bevacizumab	PLGA	Intravitreal	AMD	(119)
	Brimonidine tartrate	Alkoxylphenacyl-based polycarbonates copolymer with PCL	Intravitreal	glaucoma	(120)
Ultrasound	FITC-BSA	Silk fibroin	Transscleral	Posterior eye diseases	(104)

Delivery system/Stimuli	Therapeutics	Polymer	Route of administration	Target disease	Ref.
	Coumairn-6	Chitosan and poloxamer 407	Topical	Posterior eye diseases	(121)
Microparticles/ Microspheres	Ranibizumab	PLGA	Intravitreal	AMD	(122)
	Bevacizumab	PLA NPs encapsulated into PLGA MPs	Intravitreal	Posterior eye diseases	(123)
	Bevacizumab	PLGA	Intravitreal	Posterior eye diseases	(124)
Temperature	Ovalbumin	PLGA MPs suspended in poly (N-isopropyl acrylamide)-based hydrogel	Intravitreal	Posterior eye diseases	(125)
Nanomicelles	Dexamethasone	Polyoxyl 40 stearate and polysorbate 80	Topical	Posterior uveitis	(126)
	Cidofovir	Hexadecyloxypropyl-cidofovir	Intravitreal	Chronic retinal diseases	(127)
Dendrimers	Dexamethasone	Poly (amidoamine)	Topical and Subconjunctival	DR	(128)
	Brimonidine and timolol maleate	Polyamidoamine			(129)
Light	5-Aminosalicylic acid	G2 lysine dendrimers with a silsesquioxane core	Intraperitoneal	Retinal degeneration	(130)
Nanowafers	Dexamethasone	Carboxymethyl cellulose polymer	Topical	Dry eye	(82)
	Axitinib	PVA, polyvinylpyrrolidone, (hydroxypropyl) methyl cellulose, and carboxymethyl cellulose		CNV	(83)
Nanocrystals	Brinzolamide	Different polymer stabilizers	Topical	Prolonged reduction of IOP	(86)
Temperature	Forskolin	Poloxamer 407 and polycarbophil	Topical	Glaucoma	(85)

Delivery system/Stimuli	Therapeutics	Polymer	Route of administration	Target disease	Ref.
Hydrogels	Bevacizumab	Oxidized alginate and glycol chitosan	Intravitreal	AMD	(131)
UV light	Bevacizumab	PCL dimethacrylate and hydroxyethyl methacrylate	Suprachoroidal	CNV	(101)
Temperature	Bevacizumab	PEG-poly-(serinolhexamethylene urethane)	Intravitreal	Posterior eye diseases	(132)
Temperature	Bevacizumab	poly(2-ethyl-2-oxazoline)-b-poly(ε-caprolactone)-b-poly(2-ethyl-2-oxazoline)	Intraocular	Posterior eye diseases	(133)
	Bevacizumab	Vinyl sulfone functionalized hyaluronic acid and thiolated dextran	Intravitreal	Posterior eye diseases	(134)
	Bevacizumab	PLGA-PEG-PLGA	Intravitreal	Posterior eye diseases	(103)
Composite Nanosystems					
Temperature	IgG-Fab	PCL-PLA-PEG-PLA-PCL) based NPs suspended in a thermo-sensitive gelling copolymer (mPEG-PCL-PLA-PCL-PEGm)	Intravitreal	Posterior eye diseases	(89)
Temperature	Octreotide, insulin, lysozyme, IgG-Fab, IgG, and catalase		Intravitreal	Posterior eye diseases	(90)

Macromolecule drug delivery nanocarrier fabrication

Macromolecule drugs have shown great promise as a novel therapeutics in the treatment of ocular diseases. These large molecule drugs offer many advantages compared to small molecule drugs with respect to high potency, activity, low unspecific binding, less toxicity, minimization of drug-drug interaction, biological and chemical diversity. The chemical structure of macromolecules enables them to perform several specific functions in the body. However, these macromolecules are subjected to the physical and chemical degradation, short *in vivo* circulation half-life and biodistribution, lack of an efficient, safe, and specific delivery. In addition, clearance by the mononuclear phagocytes of the reticuloendothelial system, risk of immunogenic effect, solubility challenges, high MW, structural complexity, and failure to permeate cell membranes further reduce their therapeutic efficacy. In general, systemically delivered formulations either for small or macromolecule drugs faces several barriers before reaching the target cell/organs. Hence, there is a requirement to develop new methods and formulation strategies to deliver these highly potent macromolecule drugs for ocular treatment. However, due to several physiochemical instability and enzymatic barriers of macromolecules delivery, it is very difficult to develop a suitable formulation for these drugs. Several novel delivery technologies have been designed for ocular applications. The ideal characteristics and therapeutic potential of these carriers are summarized in **Table 1.4 and Table 1.5** respectively.

Table 1.4 Ideal characteristics of an ocular drug delivery formulation for macromolecules

Property	Description
Features of drug delivery system	• Should allow a high drug loading to reduce the instilled volume. • Appropriate size to facilitate corneal uptake and passage. • Isotonic and close to physiological pH with physiological fluids to avoid irritation and lacrimation. • Product should provide a controlled, sustained or stimuli-sensitive drug release as required. • High specificity to the ocular tissues. • Possess more local activity than systemic effects. • Dosage forms should allow the active drug to distribute through the target site for adequate time. • Proper syringeability and injectability to assure the administration of the prescribed dose of therapeutics. • The physical properties (size, shape and the charge), of the delivery system are among the key attributes that can influence the performance of a formulation of ocular drug delivery system. • It is essential that the product is not inducing any drug resistance. • In general, for vision to be unaffected, ocular delivery systems should be smaller than 50 μm in order to decrease the light-scattering effects associated with larger particles.
Active agents attributes	• Preferentially lipophilic since non-ionizable lipophilic compounds will concentrate into the corneal epithelium, while ionizable lipophilic ones will partition into the aqueous humor. • Should provide a long-term efficacy. • Drugs should have an amphipathic nature in order to pass through these different layers of cornea. • Compatibility with other drugs having different physicochemical properties.
Stability concern and adverse-effects	• Limited side effects associated with systemic, topical administration and frequent intraocular injections. • Products should be safe, with no localized/systemic toxicity. • Must be inert towards the ocular tissues. • The products should be stable under diverse environmental conditions, possess adequate shelf-life and proper storage stability.
Process parameters, manufacturing and cost effectiveness	• Formulation and manufacturing of dosage forms must be feasible. • Allowing for the production in the amounts needed to meet the projected needs. • Product must be economically feasible, cost benefits to the patients as well as easy to use.
Patient Acceptance	• Products should be simple, acceptable, easy to self-administer, and have a convenient dosage regimen. • Products must be non-irritating, with a long-lasting action. • Minimal number of surgical interventions is required.

Table 1.5 Macromolecules Delivery Systems: Advantages and Limitations

Delivery systems	Advantages	Limitations
Micro and Nanoparticle	• Controlled and long-term drug release is possible using various routes of administration • Small size allows enhanced permeation in to various organs • Greater flexibility of surface modification ligands molecule • High adjuvancy for vaccine • Encapsulation and delivery of various drugs on one nanocarrier. • Adjustable physicochemical properties (size, shape, surface functionality). • Higher possibility of stimuli sensitive delivery. • Targeted delivery system	• Burst release of drug can produce potential toxicity. • Non-specific uptake in RES system and phagocytic clearance • Challenges include the biocompatibility, toxicity, safety, stability, and immunotoxicity. • Polymer has strong influence on drug release and stability. • Various factors (size, shape, surface properties of carriers) affect their release behavior, stability and targeting efficiency. • Scale-up of nanoformulations. • Small size and large surface area can leads to particle aggregation. • Non-uniformity of particle size distribution. • Polymers hydrophobicity and acidic microenvironment by degradation leads to protein denaturation/aggregation. • Chemical reactions between macromolecules and polymers.
Solid Lipid NPs (135-137)	• Large scale and effective production. • Small size, large surface area, high drug loading. • Improved drug stability. • Avoidance of organic solvents in the production can avoid the stability problems of macromolecules. • Potential of carrying both lipophilic and hydrophilic drugs.	• Complexity of the physical state of the lipid. • Phagocytic uptake and clearance. • Lipid particle growth and tendency to gelation. • Sometimes low drug loading capacity due to the formation of a lipid crystal matrix.

Delivery systems	Advantages	Limitations
Liposomes	• Versatility of surface chemical modification and specific targeting. • Delivery to CNS through blood-brain barrier due to their lipophilic nature of liposomes. • Entrapment of hydrophilic and hydrophobic drugs to aqueous and lipid phases, respectively. • Can provide a sustained and controlled release. • Drug release can be controlled, depending on the bilayers number and composition. • Possibility of stimuli sensitive delivery system. • Higher biocompatibility and non-immunogenicity.	• Instability in biological media. • Phagocytic uptake. • Process of the formation of liposomes has stability issues on macromolecules. • Manufacturing cost, scale up, batch-to-batch reproducibility. • The production of sterile liposomes is expensive which reduces their applicability. • Interactions of phospholipids with protein drugs. • Heterogeneous particle size distribution.
Hydrogels	• The porous nature of hydrogels can be finely tuned to allow for drug loading. • Pharmacokinetic properties for release of the loaded therapeutic molecule can be easily adjusted to the requirements of individual molecule. • Biocompatible materials because their high water content and soft nature. • Unlike other delivery systems, organic solvents and protein denaturing processes are not used in hydrogel preparation procedures. This is beneficial in preserving protein stability, as very mild conditions (aqueous environment, room temperature) are normally used. • Proteins have a limited mobility or are immobilized in the hydrogel network, which is favorable for preservation of their fragile 3D structure.	• High water content and soft nature of hydrogels typically results in relatively rapid release of proteins from the gel matrix. • Burst release, low mechanical strength, and short durability. • Protein damage due to encapsulation. • Stability of hydrogels is poor in most cases and represents a major limitation. • The low tensile strength of many hydrogels limits their use in load-bearing applications and can result in the premature dissolution or flow away of the hydrogel from a targeted local site. • The quantity and homogeneity of drug loading into hydrogels may be limited, particularly in the case of hydrophobic drugs.

Delivery systems	Advantages	Limitations
	• Hydrogel's soft and hydrophilic nature and mild preparation methods are well-suited to enhance efficacy, reduce dosing interval, and provide a more convenient dosage route of large and labile protein • Stimuli sensitive hydrogel delivery is feasible.	• Sometimes, hydrogels are not sufficiently deformable to be injectable, necessitating surgical implantation. • Each of the above issues significantly restricts the practical use of hydrogel-based drug delivery therapies in the clinic.
Micelles	• High diversity of polymers. • Suitable for intravenous administration. • Easy of sterilization by simple filtration process for safe administration. • High biocompatibility, biodegradability, and the multiplicity of functional groups. • Possibilities of different polymer block arrangements based on the requirements. • The hydrophobic core serves as a solubilization depot for drugs with poor aqueous solubility. • Hydrophilic shell limits the opsonin adsorption, contributes towards longer blood circulation • The small size of polymeric micelles contributes towards longer blood circulation time by evading scavenging by the MPS system in the liver and bypassing the filtration of inter-endothelial cells in the spleen. • Longer circulation time leads to improved accumulation at tissue sites with vascular abnormalities.	• Toxicity and immunogenicity concern. • Lack of suitable formulation methods for scale-up. • Formulation instability. • Low cellular uptake and tissue accumulation. • Self-assembled polymeric micelles are not stable and may dissociate upon dilution however, lipid-core micelles demonstrate high stability, biocompatibility, and prolonged blood circulation time. • Potential use in gene delivery is small and not well evaluated. • Instability in the physiological environment. • Micelles are liable to dissociate, especially upon administration when they are diluted to a concentration below the CMC. • Limitations in entrapping hydrophilic small as well as macromolecule drugs.
Dendrimers	• Can be tailored by manipulating the structure/composition or number of surface functional groups.	• Toxicological issues are major limitations of the dendrimers in their clinical application.

Delivery systems	Advantages	Limitations
	• Thermodynamically stable system. • Uniform size distribution • Drug molecules can be loaded both in the interior as well as attached to the surface groups. • High transfection efficiency not only due to their well-defined shape, but may also be caused by the amine functionality.	• Complexity of formulation methods • Core of structure is difficult to access as the complexity of the system increases with multiple generation structures.
Composite formulations (NPs-in-gel)	• Minimizes the burst effect (dose dumping) effect of nanoformulations which may result in severe dose related toxicity. • Exhibit nearly zero order release for longer period of time. • This novel system provides stable environment for macromolecules against catalytic enzyme.	• NPs can be suspended to the gel at the time of delivery only otherwise drug will be released from the NPs and accumulate in the gel which could give burst effect. Therefore, this novel approach require dual chamber mixing device. • Storage at cool temperature.

PART I: COMPOSITE NANOFORMULATIONS OF MACROMOLECULE FOR BACK OF THE EYE DISEASES

CHAPTER 2

INTRODUCTION

Overview

Ever since the emergence of the first US Food and Drug Administration (FDA)-approved recombinant protein, human insulin, in 1982, there has been a tremendous surge in the development of commercial protein therapeutics for applications in various fields of medicine (138). Ophthalmology is one such field that has benefited greatly from the advent of commercial therapeutic proteins. The role of therapeutic proteins used in the eye ranges from the neutralization of biomolecules, such as cytokines and growth factors, to protection of photoreceptors and prevention of angiogenesis (139). Among these, many proteins are used for the treatment of diseases affecting the back of the eye diseases such as age-related macular degeneration (AMD), retinal vein occlusion with cystoid macular edema (CME), posterior uveitis, glaucoma, diabetic retinopathy (DR), and retinitis pigmentosa (1). Of these, the most common ones are AMD, glaucoma, and DR, which accounts for nearly 26% of the cases of blindness worldwide and a staggering 85% of all cases of blindness in the developed world (139). Hence, a huge amount of research time and money has been spent on the development of drugs and treatment modalities in this area. The disease progression in DR involves neovascularization of the retina and choroidal neovascularization (CNV) in the case of AMD, which is responsible for the loss of vision.

The gold-standard treatment for retinal/ choroidal neovascularization involves ablation of CNV or laser-assisted thermal photocoagulation to make the retina anoxic

(140). However, these approaches are gradually being replaced by intravitreal injections of anti-vascular endothelial growth factor (anti-VEGF) agents (141). Anti-VEGF agents are essentially antibodies or fragments thereof that can bind to and block VEGF, thereby inhibiting neovascularization (142). In a land-mark study conducted in 2006, it was shown that repeated injections of ranibizumab (Lucentis^{TM}), a recombinant antibody fragment developed by Genentech and Novartis, prevented vision loss in nearly 95% of patients, and significantly improved vision in 40%. Ranibizumab was designed such that it contained only the Fab portion of the anti-VEGF antibody bevacizumab (Avastin^{TM}), which is used off label to treat AMD/DR (143), (144). Compared with bevacizumab, ranibizumab is one-third the size, has higher binding affinity for VEGF, is cleared from the circulatory system 100-fold faster, and is expected to be able to penetrate better into the retina because of its small size (145). Biological advantages of aflibercept include its greater binding affinity for VEGF, a longer intravitreal half-life relative to other anti-VEGF agents, and the capacity to antagonize growth factors other than VEGF (146). Currently, recombinant humanized anti-VEGF antibody fragments or soluble receptor decoys (e.g., ranibizumab (Lucentis; Genentech/Roche), bevacizumab (off label drug: Avastin; Genentech/Roche), pegatanib (Macugen®), and aflibercept (Eylea; Regeneron Pharmaceuticals) are current FDA approved therapies for wet AMD (1).

Conventional drugs failed to achieve required therapeutic levels of drugs in the posterior eye segment owing to the presence of several ocular barriers. Intravitreal injection is currently the only approved mode of administration, although it is suboptimal because of repeated injection every 1–2 months due to high protein clearance rates from the vitreous humor (147), (148). In addition, the associated side effects includes the

blurred vision, increase in intraocular pressure, cataract and risk of retinal detachment (149). Moreover, current intravitreal therapies are available at high cost and brand drugs like Avastin™ and Lucentis™ have the treatment cost of around $590 and $23,400 per month, respectively (http://www.allaboutvision.com/conditions/lucentis-vs-avastin.htm). Therefore, development of a cost effective, long term efficient therapy which can also reduce the frequency of intra-vitreal injection is needed. In this regard, the full clinical potential of many novel therapeutic proteins designed for posterior segment of the eye diseases has often been limited because of their inherent instability and difficulty in overcoming various ocular barriers.

To reduce the need for repeated intraocular injections and to maintain a constant and safer level of therapeutic proteins, different drug delivery systems have been designed (93). However, one of the major problems when designing such technologies is to maintain the therapeutic compounds without their degradation during the preparation, sterilization, and drug release processes. Optimally, the drug delivery system should be injectable and biodegradable to limit the potential side effects. To make them injectable, proteins, peptides or vaccines are encapsulated in particulate systems, mostly composed of poly-lactic acid (PLA), poly-glycolic acid (PGA) and poly (D, L-lactide-co-glycolide) (PLGA) (65), (150), (151). However, these polymers produce a high molar mass of lactic acid and glycolic acid upon degradation under physiological conditions in the body, which causes the tissue irritation and toxicity. Moreover, degradation products of PLGA drastically reduces the pH in the microenvironment which directly affects the stability of protein drugs (152) (153). Thus, there is a need to develop a polymer and its delivery system which ensure the stability and sustain release of large molecules, often called

macromolecule or biologics (protein, peptide and antibodies) for longer duration of time, thus eliminating the repeated injections.

Recent years have seen the emergence of protein delivery systems specifically developed for applications to the back of the eye. These systems can be broadly classified as injectable colloidal particles and injectable hydrogels. Injectable colloidal particles such as nanoparticles (NPs) may offer an advantage of providing long term release and higher residence time for large molecules. In this regard, the formulation of NP encapsulated with drug can be achieved by using FDA approved biodegradable and biocompatible polymers such as PCL (polycaprolactone), PLA, PGA and PEG (polyethylene glycol).

Rationale for investigation

The rationale behind developing novel biodegradable and biocompatible PB based biomaterial is to achieve controlled drug delivery over a period of several weeks from a single IVT injection that can provide a cost effective, long term and efficient therapy. Therefore, pentablock (PB) copolymers are introduced to fabricate such delivery system. PB copolymers are composed of FDA approved polymer blocks such as PEG, PCL, and PLA /PGA with different block ratios. The focus of this work is to utilize the polymeric biomaterials to design the constructs which can modulate the release for longer duration by using their inherent properties. PB copolymers have been utilized for the preparation of NPs and thermosensitive gel. Each block plays an important role such as the presence of PEG helps to improve stability of NPs to escape phagocytosis by

macrophages resulting in improved circulation half-life. PCL is a slow degrading highly crystalline polymer which improves macromolecule encapsulation of NPs and also sustains drug release for longer duration of time (90), (154). Moreover, these tailor-made polymers are designed in a manner which releases lower amount of lactic and glycolic acid comparison to PLGA (155). Based on previous studies, existing PCL or PLA based block polymers primarily showed diffusion mediated drug release due to their extremely slow degradation (156). Therefore, tailor-made PB copolymers are designed to overcome the aforementioned problems. It is anticipated that reduction of the PLA molar mass in PB copolymers will improve the stability of encapsulated protein molecules, in addition to reduction in possible tissue irritation and toxicity. This novel approach will provide the entire range of polymers with different hydrophilicity-hydrophobicity index. This enormous advantage will allow us to select a unique composition of the polymer which is suitable for a respective therapeutic agent. Furthermore, reduction in the MW and/or change in the polymer block arrangement allow us to prepare PB copolymer with different physicochemical property. Besides, PB copolymers may be utilized to prepare thermosensitive gel and NPs both.

The thermosensitive gelling polymer will remain in liquid aqueous state at room temperature (25 °C) and form a thin transparent film upon contact with eye temperature i.e. 34 °C. It has been reported in earlier studies that NPs alone causes burst effect (157), (158). Therefore, the dual approach of NPs suspended in a thermogelling system could minimize burst release due to longer diffusion pathway of entrapped molecules from the system. This technology is termed as composite nanoformulation (**Fig 2.1)** which in turn results into a prolonged duration of action. The purpose of this study is to prepare

injectable composite nanoformulations comprised of macromolecule encapsulated NPs suspended in thermosensitive gel that can act as depots for sustained release without disturbing the stability.

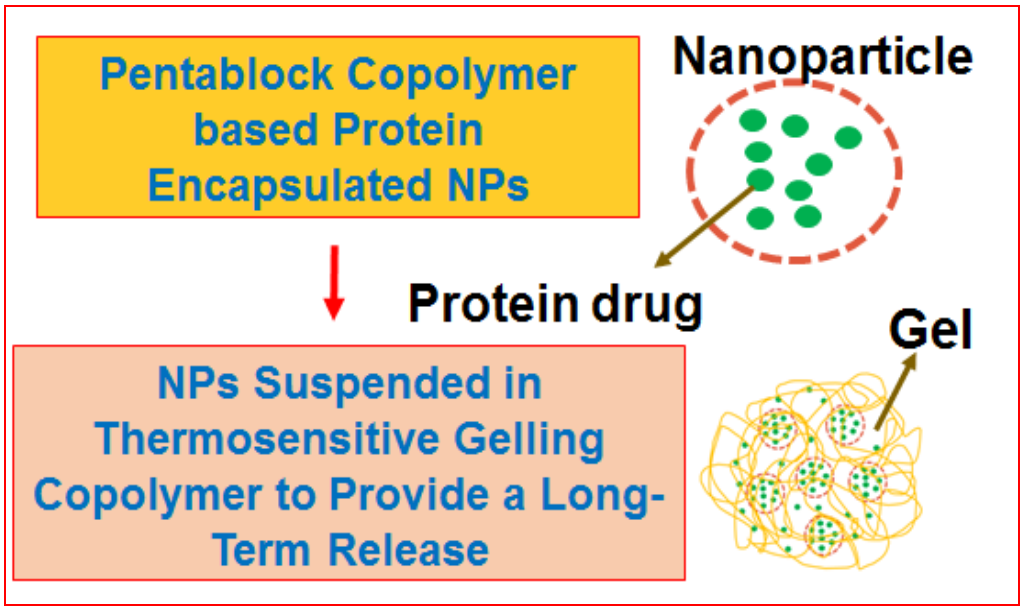

Figure 2.1 Composite nanoformulation approach acts as depots for sustained release

Subconjunctival/IVT administration of such a novel formulation may result in a prolong duration of action (~3-6 months) and thereby eliminate the need for repeated administration. It is anticipated that this formulation may provide higher patient compliance with reduced side effects. This approach may act as a platform for ocular delivery of other macromolecules such as siRNA, aptamers, peptides and large proteins. Therefore, the broad objective of this work is to develop novel PB copolymer based sustained delivery systems of macromolecules for posterior eye diseases.

Objectives

In this study, macromolecules such as IgG, IgG-Fab', IgG-Fab, lysozyme, ranibizumab, and octreotide were loaded in PB copolymers based thermosensitive gels and/or NPs. The macromolecule encapsulated NPs were suspended in a thermosensitive gel to formulate the composite nanoformulations. The composite nanoformulation was investigated to study the effect of new polymeric compositions from low to high MWs. A major focus was given to optimize the formulation parameters to achieve a higher drug loading and to examine the effect of different MW of PB copolymer on drug release profile. In addition, the effect of hydrodynamic behavior of different MW macromolecules on *in vitro* release was studied. To test this, following specific aims are proposed.

Aim 1: Synthesis of PB thermosensitive gelling (PBG) copolymers and comparative *in vitro* release study of different MW of macromolecules: PBG copolymers with various MW ratios and block arrangement were synthesized by ring opening polymerization method. The effects of block arrangement on sol-gel transition, viscosity and *in vitro* drug release of different MW of macromolecules (IgG, IgG-Fab', IgG-Fab, octreotide) was investigated. The aim 1 is subdivided into the following sections;

(A) Characterization of PBG copolymers: The synthesized copolymers were characterized for their structure, purity, MW, PDI and crystallinity, using various analytical methods such as nuclear magnetic resonance (NMR), X-ray diffraction analysis (XRD) and gel permeation chromatography (GPC).

(B) Rheology study of PBG copolymers: Viscosity measurement by Ubbelohde viscometer and sol-gel transition curve by tube inverting method.

(C) Cytotoxicity evaluation of PBG copolymers: *In vitro* cytotoxicity (LDH assay) and cell viability (MTS assay) was performed on ocular cells.

(D) Biocompatibility evaluation of PBG copolymers: *In vitro* biocompatibility study was performed on macrophage (RAW 264.7) cells. The release of various inflammatory mediators such as TNFα, IL-6 and IL-1β was evaluated.

***(E) In vitro* release study and kinetic mechanisms PBG copolymers:** *In vitro* drug release from hydrophilic and hydrophobic thermosensitive gels was quantified by the Bradford assay. The release kinetic model was applied to study the release mechanism.

(F) Stability studies of macromolecule: The stability of released protein was investigated by circular dichroism (CD) spectroscopy.

(G) *In vitro* degradation of PBG copolymer: The study was performed under four conditions; (i) in pH 7.4 PBS at 37°C, (ii) in presence of enzymes acetylcholinesterase (14.7 mU/mL) and butyrylcholinesterase (5.9 mU/mL), (iii) in pH 9.0 borate buffer at 37°C and (iv) in pH 7.4 PBS at 40°C. The samples were analyzed by XRD and GPC.

(H) *In vivo* histology of PBG copolymer: Histology study was performed in New Zealand White Rabbit to examine the changes in the tissue morphology of the eye.

Aim 2: Synthesis of PB copolymers for NP preparation and comparative *in vitro* release study of different MW of macromolecules from composite nanoformulations: The synthesis of PB copolymers with various MW ratios was carried out by the ring opening bulk polymerization method. The effects of *in vitro* drug release of different MW of macromolecules were investigated.

(A) Characterization of PB copolymers: The synthesized copolymers were characterized for their structure, purity, MW, PDI, and crystallinity using various analytical methods such as NMR, XRD and GPC.

(B) Biocompatibility evaluation of PB copolymers: *In vitro* biocompatibility study was performed on macrophage (RAW 264.7) cells. The release of various inflammatory mediators such as TNFα, IL-6 and IL-1β was evaluated.

(D) NP preparation, optimization and characterization: The PB copolymers were utilized to encapsulate macromolecules (IgG, IgG-Fab, lysozyme) in NPs using Water-in-oil-in-water ($W_1/O/W_2$) double emulsion solvent evaporation method. The NPs were characterized for Particle mean diameter (PMD), Size distribution and PDI using dynamic light scattering (DLS) method with Zetasizer Nano ZS. The drug encapsulation and loading efficiency of NPs was assessed by Micro-BCA^{TM} assay.

(C) *In vitro* release study and kinetic mechanisms: *In vitro* drug release from composite nanoformulation (NPs suspended in a thermosensitive gel) was quantified by Micro-BCA^{TM}. The release kinetic models were applied to study the release mechanism.

(D) Enzymatic activity of released macromolecule: Lysozyme released from composite nanoformulation was analyzed by enzyme assay.

Aim 3: Development, optimization and evaluation of PB copolymer based IgG-Fab and Ranibizumab-encapsulated composite nanoformulation: To synthesize and characterize PB copolymers for the preparation of IgG-Fab and ranibizumab-encapsulated NPs. Composite nanoformulations (NP suspended in a thermosensitive gel) were investigated to achieve zero order drug release. In addition, formulation parameters were optimized to achieve higher drug loading.

(A) Characterization of PB copolymers: The synthesized copolymers were characterized for their structure, purity, MW, PDI and crystallinity, using NMR, XRD GPC and Fourier-transform infrared spectroscopy (FT-IR).

(B) Cytotoxicity evaluation of PB copolymers: *In vitro* cytotoxicity (LDH assay) and cell viability (MTS assay) was performed on ocular cells.

(C) Biocompatibility evaluation of PB copolymers: *In vitro* biocompatibility study was performed on macrophage (RAW 264.7) cells. The release of various inflammatory mediators such as TNFα, IL-6 and IL-1β was evaluated.

(D) NP preparation, optimization and characterization: IgG-Fab and ranibizumab were used as therapeutic drug for the optimization of NP formulation. Water-in-oil-in-water ($W_1/O/W_2$) double emulsion solvent evaporation method was used to formulate the NPs. In order to improve drug loading, encapsulation efficiency and sustained release profile of NPs, various process parameters such *as drug: polymer ratio, amount of emulsifier and stabilizer, types of PB copolymer and its polymer blend ratio, aqueous: non-aqueous phase ratio,* and *sonication time* were optimized. The NPs were characterized for Size distribution and PDI by DLS method. The drug encapsulation and loading efficiency of NPs was assessed by Micro-BCA^{TM} assay.

(E) *In vitro* release study and release kinetic mechanisms: *In vitro* drug release from composite nanoformulation (NPs suspended in a thermosensitive gel) was quantified by Micro-BCA^{TM} assay. The kinetic models were applied to study the release mechanisms.

(F) Stability studies of released macromolecule: Indirect ELISA was performed to determine the activity of released drugs from the composite nanoformulations.

CHAPTER 3

BIODEGRADABLE AND BIOCOMPATIBLE THERMOSENSITIVE GELLING PENTABLOCK COPOLYMERS FOR LONG TERM OCULAR DELIVERY OF MACROMOLECULES

Rationale

Increase in the use of macromolecules, often called biologics has occurred over the past decade for the treatment, prevention, or cure of a variety of ocular diseases (159). Biological products include vaccines, immunoglobulins, cells or microorganisms, other proteins and peptides (160). Among several biologics, anti-Vascular Endothelial Growth Factor (VEGF) agents are administered for back of the eye diseases, usually by monthly intravitreal injection (161). A controlled, sustained release therapeutic would decrease the frequency of injections, leading to increased patient compliance and therapeutic efficacy especially for the sensitive organ like eye.

FDA approved biodegradable polymers such as polycaprolactone (PCL), polylactic acid (PLA), polyglycolic acid (PGA) and polyethylene glycol (PEG) have been comprehensively studied for the sustained delivery of the macromolecules (152). These polymers are widely explored to prepare various diblock, triblock and PB copolymers in drug delivery approaches. Recently, many investigators have applied various block copolymers combinations such as poly lactide-co-glycolide (PLGA) (119), PLGA-PEG-PLGA (162), PEG-PCL-PEG (163), (164), and PEG-PLA (165) for the development of sustained release formulations. PLGA based hydrogels exhibit better biodegradability, higher gelation temperatures and longer periods of sustained drug release compared to

poloxamer systems (166). However, degradation of copolymers produces lactic acid and glycolic acid, which reduces local pH substantially and may degrade macromolecules. Furthermore, local tissue reaction to the PLGA may reduce tolerability and biocompatibility (152). Other types of multiblock amphiphilic polymer (i.e., with both hydrophilic and hydrophobic domains) have been synthesized using a wide range of gelling polymers. Some of these gelling polymers are sufficiently deformable to be injectable, but many are not, necessitating surgical implantation for drug delivery (103). In either case, a high initial burst and lack of sustained drug release limit the clinical utility of these gels. Hydrogels provide a deformable drug depot that slowly elutes a high concentration of drug to surrounding tissue for an extended period of time (167), (168). However, because most hydrogels only physically incorporate to the drugs, a rapid drug release occurs over a few hours to days, limiting their value for sustained drug delivery. Therefore, an injectable and biocompatible hydrogel that provides a sustained release of biologically active protein therapeutic remains to be developed.

Considering these facts, comparative studies have been done to develop PB thermosensitive gelling (PBG) copolymer to achieve long term delivery. PBG copolymers are composed of biodegradable or biocompatible polymer blocks of PEG, PCL, PGA, and PLA. The *in vitro* drug release profile of macromolecules can be optimized by adjusting the block length, arrangement and ratio of the PCL/PLA/PGA with PEG. The arrangements may be further optimized by changing the MW of each polymeric block. PBG copolymers have different MW, ratios and arrangement, which can influence the drug release profile.

The relative block arrangement and MW of PBG copolymers affect the solution-gelation (sol-gel) transition behavior, viscosity, degradation, and *in vitro* release characteristics of the macromolecule. PBG can be injected through a small-gauge needle to form a firm, *in situ*, hydrogel depot. Therefore, the potential advantages of PBG as carriers for sustained delivery of macromolecule/biologic therapeutics include biodegradation, biocompatibility, long-term release, ease of injectability, and stability of the therapeutic being delivered.

Biodegradable polymers generally undergo homogenous or heterogeneous erosion (169). Homogenous erosion, commonly referred as bulk erosion, involves hydrolytic cleavage of the complete cross-section of polymer matrix. The degradation rate of bulk eroding polymers is slower and varies from several weeks to years (170). Heterogeneous degradation generally referred as surface erosion. Heterogeneous degradation take place at faster rate compared to homogeneous degradation because slower diffusion of water molecules inside the polymer matrix (171). Drug release from a bulk eroding polymer matrix depends upon swelling, diffusion, and hydrolytic degradation in contrast to surface eroding polymers, where it primarily depends on hydrolytic degradation (170), (169). The hydrolytic degradation rate of polyesters depends on their MW and crystallinity. Low MW PLGA degrades faster than high MW PLGA (65) (172).

In the present study, we have synthesized and evaluated various novel thermosensitive hydrogels composed of FDA approved polymer. This study has addressed five important aspects; (i) synthesis and characterization of PBG copolymers; (ii) effect of hydrophilic and hydrophobic block copolymers on sol-gel transition behavior; (iii) *in vitro* cytotoxicity/biocompatibility; (iv) *in vitro* release study and

hydrodynamic behavior of different MW of the macromolecule drugs (IgG, 150 kD; IgG Fab', 110 kD; IgG-Fab, 50 kD; and Octreotide 1 kD); (v) release kinetic mechanism (vi) *in vitro* degradation studies of hydrophilic gelling polymer (vii) *in vivo* ocular histology.

Materials and methods

Materials

Poly (ethylene glycol), monomethoxy PEG, poly (vinyl alcohol) (PVA), stannous octoacte were obtained from Sigma Aldrich, USA. ε-caprolactone, and L-lactide were obtained from Acros organics, USA. Lactate dehydrogenase estimation kit and CellTiter 96® AQ_{ueous} non-radioactive cell proliferation assay (MTS) kit were obtained from Takara Bio Inc. and Promega Corp., respectively. All other reagents utilized in this study were of analytical grade.

Methods

Synthesis of PB copolymers

Synthesis of hydrophobic PBG-1 copolymer (PLA-PCL-PEG-PCL-PLA)

PCL-PEG-PCL; TB copolymer was synthesized by ring-opening bulk copolymerization of ε-caprolactone. PEG was utilized as macro-initiator whereas stannous octoate as a catalyst. Briefly, PEG was vacuum dried for 4 h before polymerization. Predetermined amount of PEG and ε-caprolactone were added in the round bottom flask. Polymer melt was degassed under vacuum for 30 min at 130°C followed by addition of stannous octoate (0.5 wt%) and purged with nitrogen gas. Reaction was carried out for 24 h at 130°C. The resulting polymer was then dissolved in

dichloromethane and precipitated by addition of cold diethyl ether. Precipitates were centrifuged and sediments were vacuum-dried to remove any residual solvents. Purified polymers were stored at -20°C. To synthesize PBG-1, predetermined amount of TB and L-lactide were added in a round bottom flask and degassed under vacuum for 30 min at 130°C. Flask was then purged with nitrogen gas and followed by addition of stannous octoate (0.5 wt%). Reaction was carried out at 130°C for 24 h. The resulting polymers were purified and stored at -20 °C. A schematic synthesis raection of PBG-1 is represented in **Figure 3.1**.

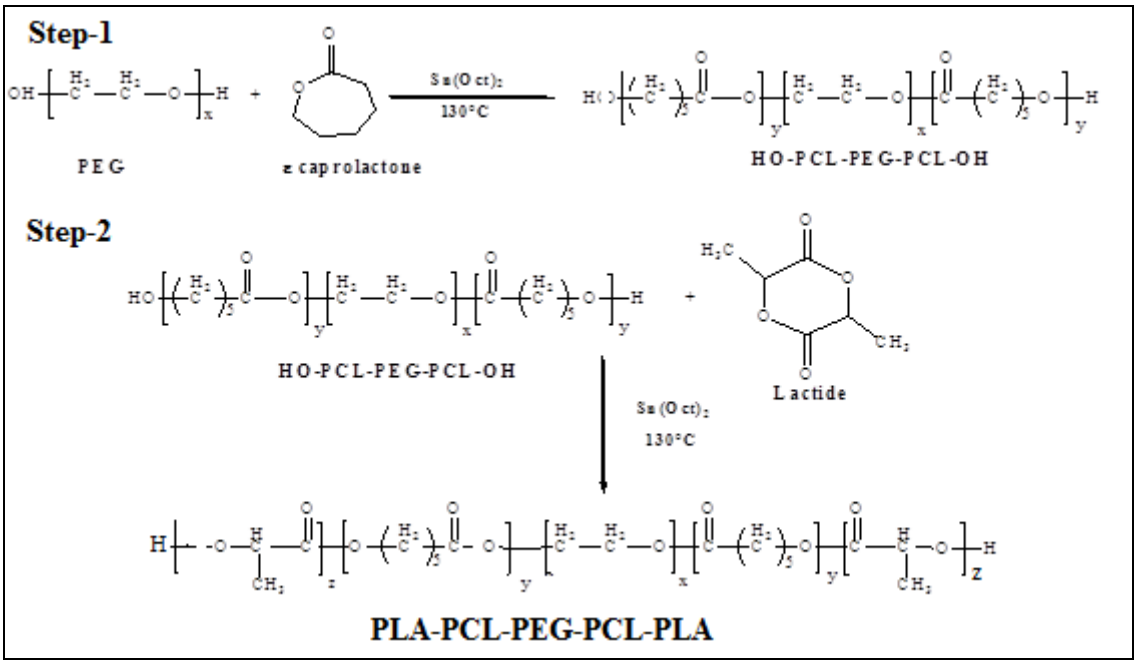

Figure 3.1 Synthesis of hydrophobic PBG-1 copolymers (PLA-PCL-PEG-PCL-PLA)

Synthesis of hydrophilic PBG-2 copolymer (PEG-PCL-PLA-PCL-PEG)

To synthesize the thermosensitive gelling copolymer (PBG-2; PEG-PCL-PLA-PCL-PEG), intermediate copolymer (mPEG-PCL-PLA) was synthesized by ring-opening bulk copolymerization. ε-caprolactone was polymerized at the hydroxyl terminal of mPEG (550 Da) followed by second polymerization with L-lactide. The resulting intermediate copolymer was coupled using HMDI as a linker. The coupling reaction was continued for 8 h at 70°C. The synthesized PBG-2 copolymers was purified by cold ether precipitation followed by drying under vacuum and stored at -20°C until further uses. A schematic synthesis reaction of PBG-2 is depicted in **Figure 3.2**.

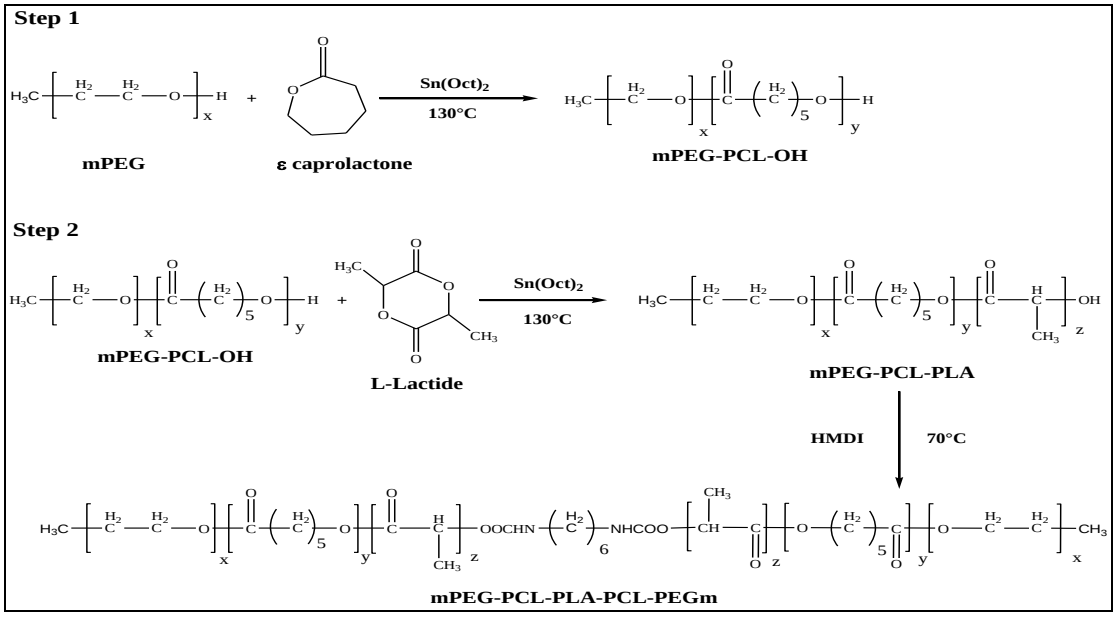

Figure 3.2 Synthesis of hydrophilic PBG-2 copolymers (PEG-PCL-PLA-PCL-PEG)

Characterization of PBG copolymers

PBG-1 and PBG-2 copolymers were characterized for their MWs and purity by (^{1}H) nuclear magnetic resonance (^{1}H-NMR) spectroscopy, gel permeation chromatography (GPC), X-ray diffraction (XRD). The structures and MWs of PBG-1 and PBG-2 copolymers are described based on ^{1}H-NMR and GPC.

Proton (^{1}H) nuclear magnetic resonance (NMR) spectroscopy

The ^{1}H-NMR spectra of PBG-1 and PBG-2 copolymers were acquired on a 400 MHz NMR instrument (Varian Inc., Palo Alto, CA). The chemical shift values were reported as δ in parts per million (ppm). The NMR samples were prepared by dissolving each copolymer in deuterated chloroform as solvent in a 5-mm outer diameter NMR tubes (Wilmad-LabGlass, Vineland, NJ).

Gel permeation chromatography (GPC) analysis

The purity, MWs and PDI of PBG-1 and PBG-2 copolymers were further confirmed by GPC analysis. Polymeric samples were analyzed with Waters 410 refractive index detector (Waters, Milford, MA). Briefly, samples were prepared by dissolving 5 mg of polymeric material in tetrahydrofuran (THF) whereas THF was utilized as eluting agent at the flow rate of 1 mL/min. Separation was carried out on Styragel HR-3 column (Waters, Milford, MA). Polystyrene samples with narrow MW distribution were considered as standards.

X-ray diffraction (XRD) analysis

To analyze the crystallinity of copolymers, XRD analysis was performed using Rigaku MiniFlex automated X-ray diffractometer (Rigaku, The Woodland, TX) equipped

with Ni-filtered Cu-Kα radiation (30 kV and 15 mA). The analysis was performed at room temperature at the scanning rate of 5°/min.

Thermosensitive PB copolymer characterization

Sol-gel transition

The sol (flow)-gel (no flow) transition of block copolymers was examined by following a previously published protocol with minor modifications. Briefly, block copolymers ranging from 15-30 wt% were dissolved in distilled deionized water followed by 12 h of incubation at 4°C. After equilibration, 1 mL of aqueous polymeric solution was transferred in 4 mL glass vial and placed in water bath. The temperature of the water bath was raised gradually from 10°C to 50°C at an increment of 1°C. Vials were kept for 5 min at each temperature. Gel formation was observed visually by inverting the tubes. A physical state with no fluidity for 1 min was considered as gel phase. The temperature at which the solution transforms to gel phase was considered as critical gelling temperature (CGT) and the temperature where polymer starts to precipitate (phase separation) was described as critical precipitation temperature (CPT).

Viscosity measurements

The change in the viscosity of the PBG-1 and PBG-2 copolymer solution as a function of temperature may also be employed to gain an understanding of the phase transitions. A viscosity change may suggest the formation or destruction of a structured network, implying a sol or gel state. Rheological properties of 20 wt% aqueous solution of PBG-1 and PBG-2 copolymers were estimated with an Ubbelohde capillary viscometer at temperatures ranging from 5±1°C to 25±1°C. Temperature of the

viscometer was maintained with a temperature controlled water bath. Viscosity values are represented as an average of triplicates (kinematic viscosity, cP± standard deviation).

In Vitro cytotoxicity of gelling polymers

To analyze the cytotoxic effects of PBG-1 and PBG-2 gelling copolymers *Lactate Dehydrogenase (*LDH) assay (Takara Bio Inc.) and cell viability (MTT) assay Promega Corp) were performed according to the supplier's instructions. Retinal Pigment Epithelium (D407) cells are immortalized and can be sub-cultured many times, while maintaining their physiological properties. Cells were cultured at 37°C, humidified 5% CO_2/95% air atmosphere in a culture medium containing DMEM/F-12 supplemented with 15% (*v*/*v*) FBS (heat inactivated), 15 mM HEPES, 22 mM $NaHCO_3$, 100 mg of penicillin and streptomycin each, 5 μg/mL insulin, and 10 ng/mL of human epidermal growth factor. Cells of passage numbers between 62 and 65 were utilized for all the experiments. The growth medium was changed every other day. A D407 cell was cultured in flasks, harvested at 80–90% confluency with TrypLE™ Express (a superior replacement for trypsin).

Lactate dehydrogenase (LDH) assay

LDH assay was performed using previously published protocol with minor modifications to evaluate the cytotoxicity of both PBG copolymers. Briefly, 5, 25 and 50 mg/mL of PBG-1 and PBG-2 copolymers were dissolved in acetonitrile (ACN) and hundred microliter solutions were aliquoted in each of the 96-well. Plates were exposed overnight under UV light (laminar flow) for polymer sterilization as well as evaporation of ACN. D407 cells at the density of 1.0×10^4 were seeded in each well and incubated at

37°C, 5% CO_2 in humidified atmosphere for 48 h. After completion of incubation period, cell supernatants were analyzed for quantification of LDH using LDH assay kit. Absorbance of each well was measured at 450 nm using a DTX 800 multimode microplate reader (Beckman Coulter, Brea, CA). More than 10% of LDH release was considered as cytotoxic. The LDH release (%) was calculated according to Eq. 3.1,

$$LDH\ release(\%) = \frac{Abs.of Sample - Abs.of negative control}{Abs.of positive control - Abs.of negative control} * 100 \quad \ldots \text{Eq. 3.1}$$

MTS assay

The safety and biocompatibility of PBG copolymers was further established by performing an *in vitro* cell viability assay (MTS; (3-(4, 5-dimethylthiazol-2-yl)-2, 5-diphenyltetrazolium bromide) tetrazolium reduction). MTS assay was performed according to previously reported protocol with minor modifications (89). As described earlier, PBG-1 and PBG-2 copolymer solutions at the concentration of 5, 25 and 50 mg/mL were prepared, aliquoted and sterilized. After sterilization, D407 cells were seeded in each well of 96-well plate at a cell density of 1.0 x 10^4, and incubated at 37°C and 5% CO_2 in humidified atmosphere for 48 h. At the end of incubation period, cell culture medium was aspirated and cells were incubated for 4 h (37°C and 5% CO_2) in presence of hundred microliter of serum free medium containing twenty microliter of MTS solution. The fluorescence was measured at the excitation and emission wavelengths of 560 nm and 590 nm, respectively, using the above microplate reader. Percent cell viability was calculated according to Eq. 3. 2. In this study, PBG copolymers exhibiting more than 90% of cell viability were considered non-toxic and suitable for ocular applications.

$$Cell\ viability(\%) = \frac{Abs.of\ Sample - Abs.of\ negative\ control}{Abs.of\ positive control - Abs.of\ negative control} * 100 \qquad \text{Eq. 3.2}$$

In vitro drug release studies of macromolecule drug

For the *in vitro* release experiments, one hundred µL of 20 wt% aqueous block copolymer solutions were added to 1 mL Eppendorf tubes. Solutions were gently mixed (~30 sec) at 4°C until drugs (Octreotide, IgG Fab, IgG-Fab' and IgG) was dissolved in respective vials. Eppendorf tubes were incubated at 37°C for 5 min followed by addition of 1 mL phosphate buffer saline (PBS, pH 7.4). Throughout the release period, Eppendorf tubes were kept in a water bath maintained at 37°C. At predetermined time intervals, two hundred µL of release samples were collected and replaced with fresh PBS (pre-incubated at 37°C). The amount of released macromolecule drugs was estimated by Bradford assay (Thermo Fischer Scientific, USA).

Release kinetics

In order to investigate release mechanisms, release data were fitted to various kinetic models i.e., Zero-order ($C = K_0t$), First-order ($LogC = LogC_0 - Kt/2.303$), Higuchi ($Q_t = Kt^{1/2}$), and Korsmeyer-Peppas ($M_t/M_\infty = kt^n$). Based on the R^2 value, best fit model was identified. Diffusion exponent (n) of Korsmeyer-Peppas equation was utilized to understand the mechanism of release.

Stability analysis of IgG by ultraviolet circular dichroism spectroscopy

Circular dichroism (CD) spectroscopy was performed to evaluate effect on secondary structure of IgG from the released sample. Consequently, released sample was diluted using 10 mM phosphate buffer. IgG freshly prepared standard solution was used

as control. Concentration was adjusted to 0.05mg/mL for both sample and control. CD spectra was collected over a range of 200-250 nm using Jasco 720 spectropolarimeter at room temperature at a scan speed of 20 nm/min. Cuvette of 0.01 cm path length was employed for all measurement. An average of three signals was recorded and measurements were reported as ellipticity (θ, mdeg).

In vitro degradation study of PBG-2 copolymer

In Vitro degradation studies were performed by taking approximately 20 wt% gelling solution (100 µL, n=3) in phosphate buffered saline (PBS), pH 7.4. PBG-2 copolymer was incubated under various conditions. These conditions are; (i) gel in pH 7.4 PBS at 37°C, (ii) gel in presence of enzymes acetylcholinesterase (14.7 mU/mL) and butyrylcholinesterase (5.9 mU/mL), (iii) gel in pH 9.0 borate buffer at 37°C and (iv) gel incubated in pH 7.4 PBS at 40°C. Buffer volume was kept constant at 4mL under all four conditions. Solutions were replaced every 5 day. Samples were withdrawn after 0, 5, 15, 30, and 45 days, centrifuged to collect sediment and freeze-dried further subjected to GPC and XRD analyses.

In vivo safety assessment

Use of animals in this study adhered to the ARVO Statement for the Use of Animals in Ophthalmic and Vision Research. It was approved and monitored by the North Carolina State University Institutional Animal Care and Use Committee. *In vivo* ocular histology studies were performed in New Zealand White Rabbits to evaluate intravitreal toxicity after injecting 100µl of filter sterilized low endotoxin thermosensitive

gel. Rabbits from each group were euthanized at 1, 4, 16 and 33 weeks after injection. Euthanasia was performed by intravenous injection of a barbiturate based agent. Immediately after euthanasia, eyes were enucleated and placed in Davidson's solution for 24 hours, followed by alcohol. Central sections of each globe, including the optic nerve, were stained with H&E and examined using light microscopy.

Result and discussion

Synthesis and characterization

PBG-1 and PBG-2 copolymers were synthesized successfully by ring opening bulk copolymerization method. The process of block copolymerization of ε-caprolactone initiated by dihydroxyl PEG involved two steps. In the first step, ring-opening polymerization of ε-caprolactone initiated by dihydroxyl PEG formed a TB copolymer with a central PEG block and two lateral PCL blocks. The TB copolymer served as macroinitiator and opened the ring of L-lactide in the second step. The resulting polymer presented a chain structure of PLA-PCL-PEG-PCL-PLA. On the other hand, copolymerization initiated by PEG propagated at one end only.

Proton NMR showed all the characteristic peaks for the polycaprolactone, polylactide and mPEG residues. ^{1}H NMR spectrum of PBG-1 and PBG-2 copolymer in deuterated chloroform was observed in **Figure 3.3 A and Figure 3.3 B** respectively. Typical signals of PLA, PCL and PEG components were observed; Signals at 1.5 (–CH3;g) and 5.1 ppm (–CH;f) were assigned to PLA blocks, 1.3 (a), 1.6 (b), 2.3 (c) and 4.0 (d) ppm to the different methylene protons (–CH2–) of PCL blocks, and 3.6 ppm (–

CH2–) to PEG blocks, respectively. A peak at 3.38 δ ppm was denoted to terminal methyl of (-OCH_3-; e) of PEG.

Molecular weights (Mw and Mn) and PDI of PBG copolymers were determined by GPC. A unimodal distribution of MW was observed (not shown here). The MWs of block copolymers were very close to feed ratio. PDI was also below 2.0 describing narrow distribution of MWs. ^{1}H-NMR and GPC were applied to calculate the MW of block copolymers. As summarized in **Table 3.1**, experimental values were consistent with theoretical values derived from feed ratio. Hence for simplicity, theoretical values are mentioned in the following text.

Table 3.1 Characterization of PBG Copolymers

Name	**Structure**	**Total Mn[a] (theoretical)**	**Total Mn[b] (calculated)**	**Total Mn[c] (calculated)**	**Mw[c] (GPC)**
PBG-1	PLA_{250}-PCL_{850}-PEG_{1050}-PCL_{850}-PLA_{250}	3250	2890	3085	3108
PBG-2	PEG_{550}-PCL_{825}-PLA_{500}-PCL_{825}-PEG_{550}	3300	2910	3020	3120

a: Theoretical value, calculated according to the feed ratio.
b: Calculated from ^{1}H-NMR.
c: Determined by GPC analysis.

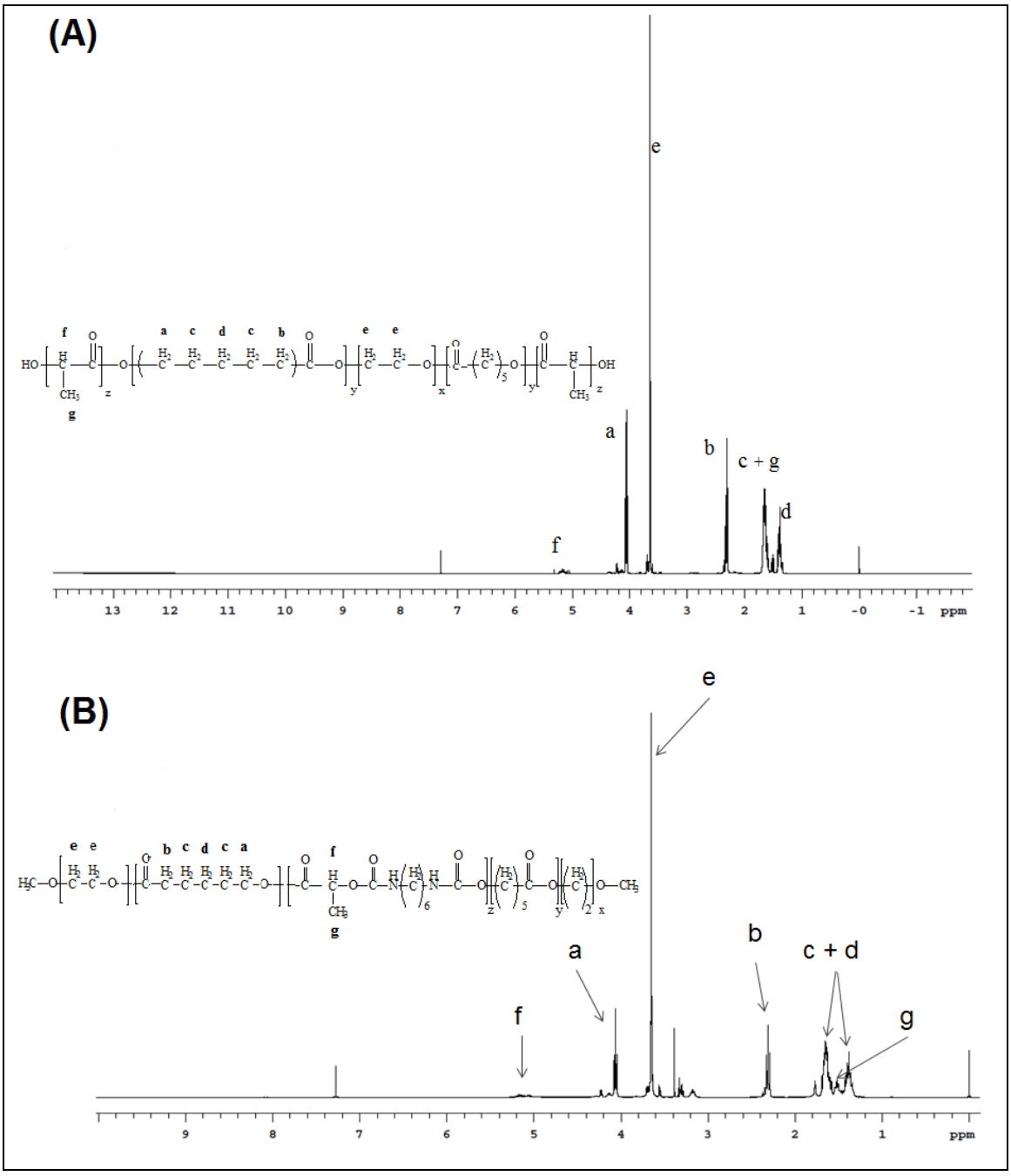

Figure 3.3 Proton (^{1}H) Nuclear magnetic resonance (NMR) spectroscopy (A) PLA-PCL-PEG-PCL-PLA (PBG-1); (B) PEG-PCL-PLA-PCL-PEG (PBG-2)

In order to evaluate crystallinity, PBG-1 and PBG-2 copolymers were analyzed for XRD patterns **(Figure 3.4A and 3.4B)**. Interestingly, PBG-1 exhibited crystalline peaks of PCL at 2θ = 21.5° and 23.9°, whereas PBG-2 was devoid of any such peaks.

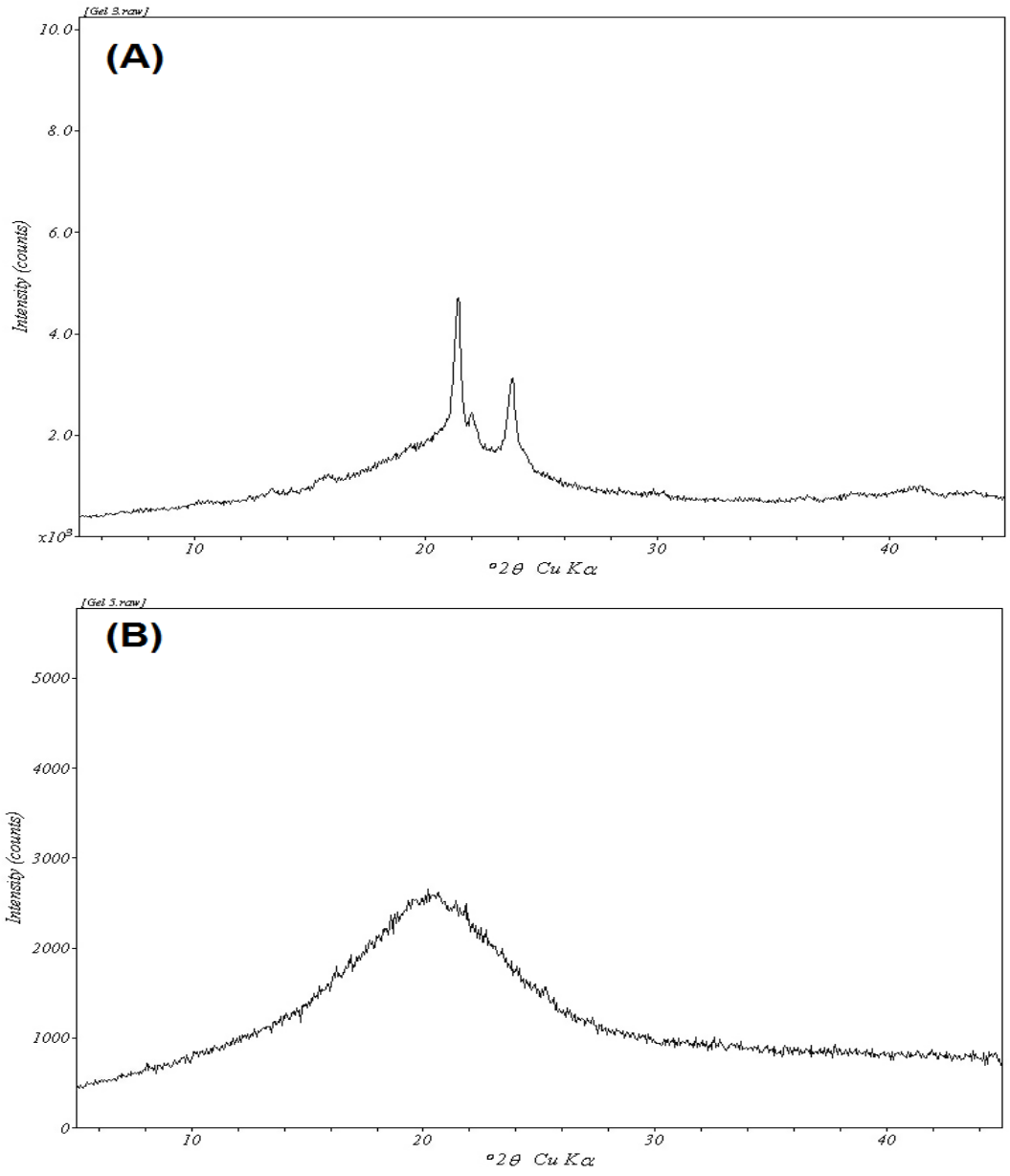

Figure 3.4 X-ray diffraction (XRD) analysis (A) PLA-PCL-PEG-PCL-PLA (PBG-1); (B) PEG-PCL-PLA-PCL-PEG (PBG-2)

Sol-gel transition

PBG copolymers reported in this study are amphiphilic in nature containing hydrophilic block (PEG) and hydrophobic block(s) (PCL and/or PLA). Synthesized PBG copolymers exhibited a temperature-dependent reversible sol-to-gel transition in water: a sol-to-gel transition (at the lower transition temperature) and a gel-to-precipitate transition (at the upper transition temperature). PBG-1 and PBG-2 copolymers (approximately similar MW but different arrangement) did not significantly alter the thermosensitive behavior. Change in block arrangement may enhance intermolecular and intramolecular hydrophobic interactions of the polymers. Both PBG copolymers are soluble in water and exhibit sol-gel transition behavior. However, PEG at the terminal (PB) exhibited good aqueous solubility. For both copolymers, rise in aqueous polymer concentration from 15 to 30 wt% significantly shifted CGT to lower and CPT to higher values. The polymer solutions formed translucent sol at room temperature.

Sol-gel transition curves for PBG-1 and PBG-2 **(Figure 3.5)**, was compared to understand the effect of hydrophobicity on the sol-gel behavior of block copolymers. Increased hydrophobicity of PBG-1 has reduced the CGT and shifted the value of CPT at higher temperature. Higher hydrophobicity of polymers may enhance the intramolecular and intermolecular hydrophobic interactions even at lower temperature compared to the hydrophilic copolymers which lead to lower CGT. Additionally, these hydrophobic interactions allow more rigid gel matrix and hence delay polymer precipitation at higher temperature (CPT).

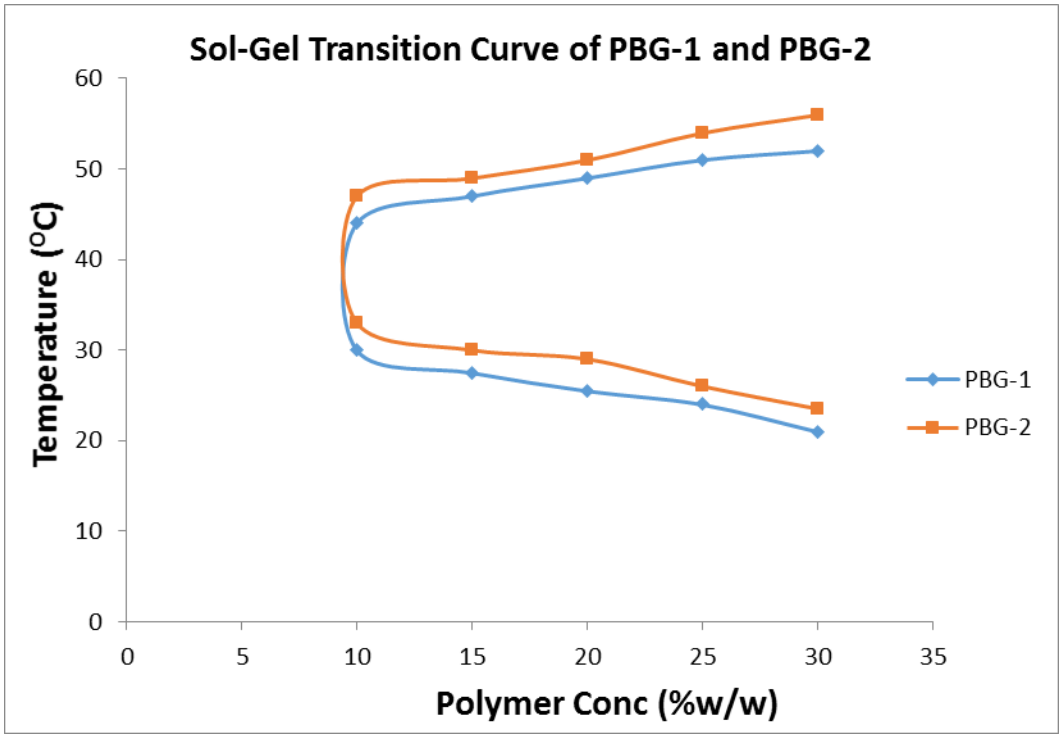

Figure 3.5 Sol-Gel transition of (A) PLA-PCL-PEG-PCL-PLA (PBG-1); (B) PEG-PCL-PLA-PCL-PEG (PBG-2)

In order to understand the effect of block arrangement on thermogelling behavior, sol-gel transition curves of PBG-1 and PBG-2 was compared. Interestingly, CGT and CPT for PBG-1 copolymer were significantly lower than PBG-2 copolymer at any respective concentration. This behavior may be attributed to the different mechanism of gelation of these block copolymers. Effects of arrangement of blocks and hydrophobicity of PBG on sol-gel transition behavior are in agreement with previously published reports of PLGA-PEG-PLGA (173) and PEG-PLGA-PEG (174) copolymer hydrogels.

Both types of copolymers (i) hydrophobic segments at the terminals PBG-1 and (ii) hydrophilic segments at the terminals PBG-2 can be dissolved via micellization where the core is composed of hydrophobic segments and shell is made up of hydrophilic

segment. Therefore, interaction of PEG with water molecules was dominated at low temperature (4°C) allowing polymer to solubilize. In contrast, elevation in temperature may cause polymer aggregation and initiate the process of micellization. PBG-1 copolymers possess hydrophobic terminals and hence may possibly behave differently in aqueous solution relative to PBG-2 copolymers. It might be due to strong hydrophobic interactions between PCL or PCL-PLA chains which can significantly overcome weak hydrophilic interactions (hydrogen bonds) between PEG and water molecules.

Viscosity measurement

Table 3.2 describes the kinematic viscosity of 15 wt% aqueous gelling solutions of different block copolymers at various temperatures ranging from 5°C to 25°C. Kinematic viscosities of PBG copolymer solutions accelerated with rise in temperature. Interestingly, at any given temperature, increase in MW of block copolymers exhibited higher viscosity. Also, viscosity of hydrophobic polymer was considerably higher relative to PBG-2 as shown in **Figure 3.6**. It is speculated that hydrophobic interactions exerted by PCL or PCL-PLA blocks (hydrophobic copolymers) are significantly stronger at any given temperature relative to hydrophilic copolymers, irrespective of approximately similar MW. In addition, as temperature of the solution rises, these hydrophobic interactions also begin to dominate which eventually improve the viscosity of aqueous polymer solution. Interestingly, polymer arrangement also exhibited noticeable effect on viscosity. Hence, kinematic viscosity of PBG-2 solution was significantly lower compared to PBG-1 aqueous solution.

Table 3.2 Viscosity of thermosensitive gelling solutions (20 wt %) at various temperatures

Block copolymers	Viscosity (cp) at various temperature					
	5ºC	10ºC	15ºC	20ºC	25ºC	30ºC
PBG-1	3.06 ± 0.05	3.32 ± 0.11	3.62 ± 0.07	4.15 ± 0.12	4.87± 0.11	-
PBG-2	2.18 ± 0.11	2.37 ± 0.09	2.63 ± 0.06	3.02 ± 0.08	3.39± 0.14	4.08

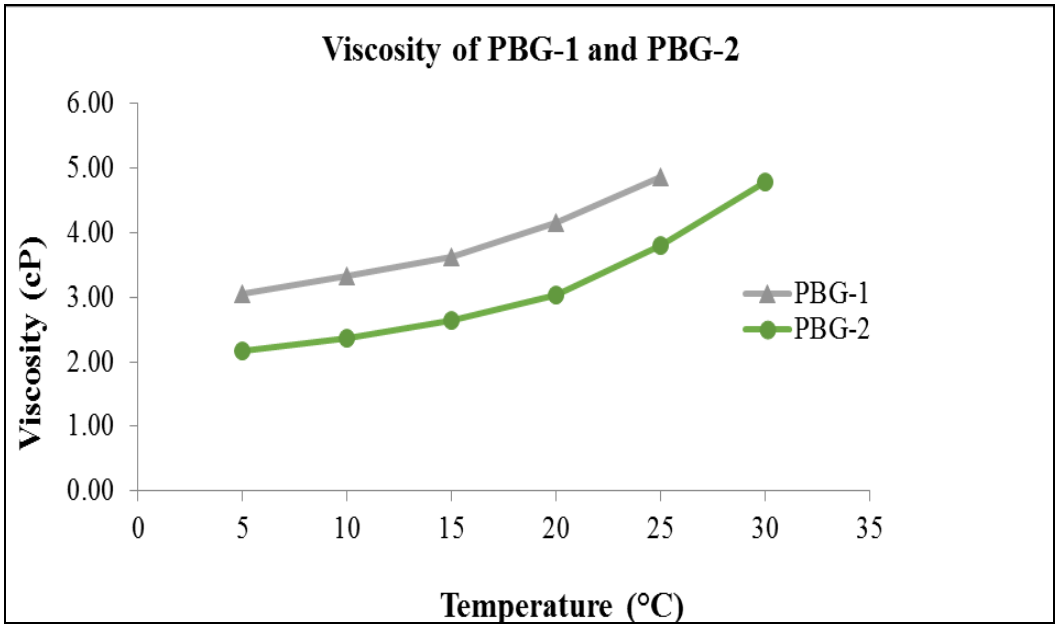

Figure 3.6 Kinematic viscosity of (A) PLA-PCL-PEG-PCL-PLA (PBG-1); (B) PEG-PCL-PLA-PCL-PEG (PBG-2)

At low temperature, the viscosity of the PBG copolymers solution remains close to that of water. This fluid-like zone corresponds to a homogeneous solution in which the block copolymers could be completely dissolved in water. At intermediate temperatures, the solution viscosity increases as the system enters a gel-like zone. On further increase of the temperature, the viscosity goes through a sharp maximum and then drops rapidly.

At higher temperatures, the viscosity returns to a value close to that of water, and then increases on entering a fluid-gel transition zone or precipitation zone. This last effect is presumably associated with phase separation of the solution. The transition from the sol state to a structured network gel caused a viscosity change because of the aggregation of the PCL hydrophobic segments. The maximum viscosity of the copolymer solution increased with increasing hydrophobicity of the copolymer and with increasing copolymer concentration.

In vitro cytotoxicity and cell culture study

I*n vitro* cell culture model has been utilized to study the compatibility between the PBG copolymer and biological system. PBG-1 and PBG-2 copolymers at various concentrations were exposed to D407 cells for 48 h. LDH is the cytosolic enzyme, which is secreted into the cell supernatant following membrane damage. Concentration of released LDH provides a direct estimation of polymer toxicity. Results **(Figures 3.7)** indicate less than 10% of LDH release at any given concentration for both the cell types. The results were not significantly different than negative controls i.e., cells without treatment.

Results observed in LDH assay were further confirmed by employing MTS cell viability study. In order to study metabolic response, D407 cells were incubated with PBG-1 and PBG-2 block copolymers at various concentrations. Results indicated in **Figure 3.8** demonstrate that more than 90% of cells are viable even after 48 h of polymer exposure. No significant difference in cell viability is observed relative to negative

control. Results obtained from LDH and MTS assay indicated negligible toxicity suggesting excellent safety profile of block copolymers for back of the eye applications.

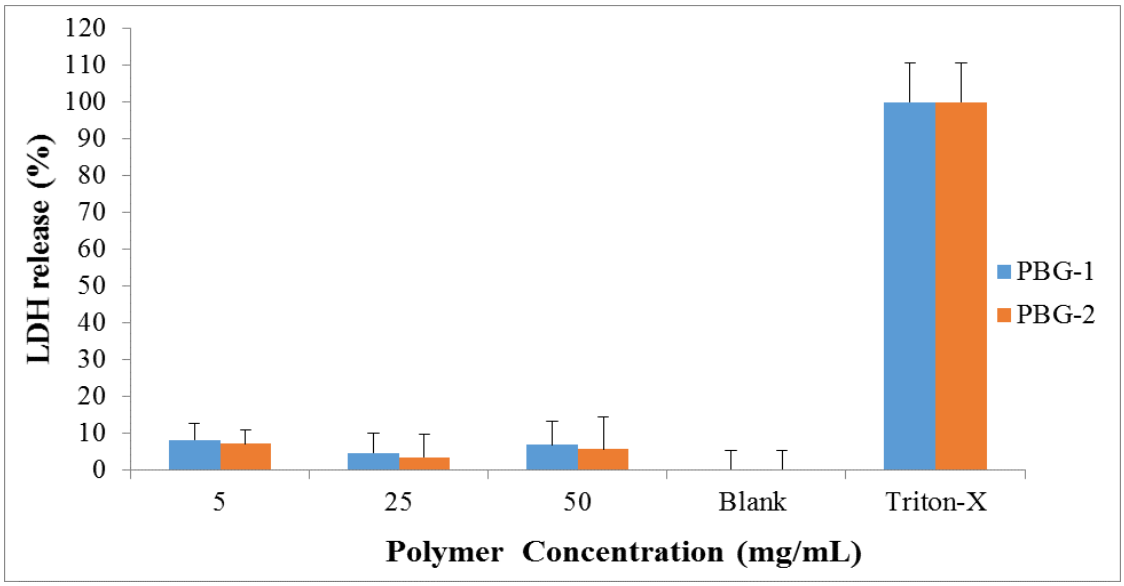

Figure 3.7 LDH assay of (A) PLA-PCL-PEG-PCL-PLA (PBG-1); (B) PEG-PCL-PLA-PCL-PEG (PBG-2). Results are given as mean ± SD, n = 5.

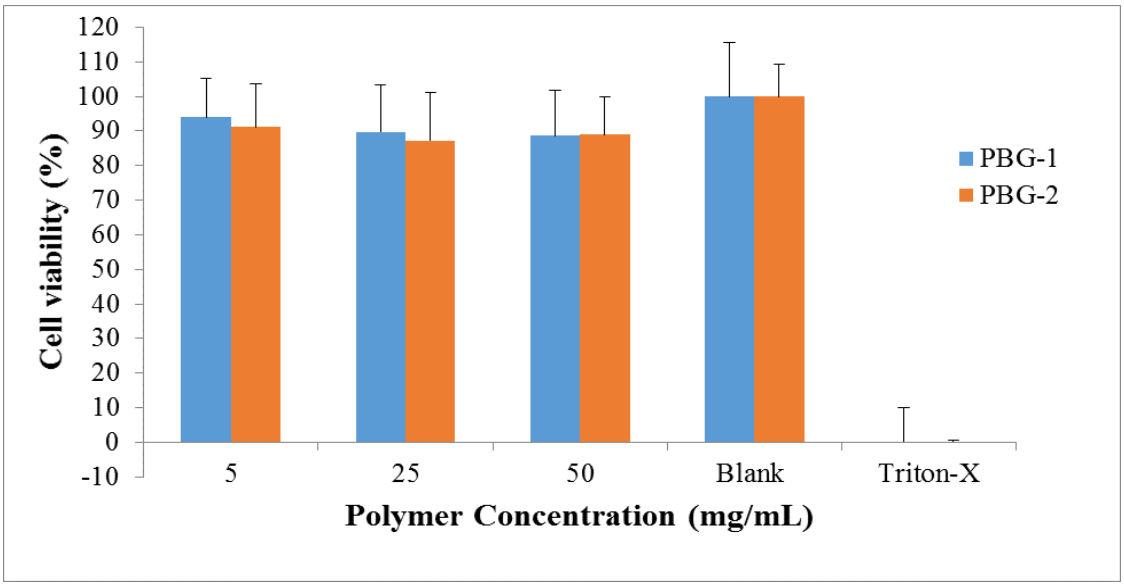

Figure 3.8 MTT assay of (A) PLA-PCL-PEG-PCL-PLA (PBG-1); (B) PEG-PCL-PLA-PCL-PEG (PBG-2). Results are given as mean ± SD, n = 5.

***In vitro* release study of macromolecules**

The model macromolecule [(IgG, 150 kD), (IgG Fab', 110 kD), (IgG-Fab 50 kD) and (Octreotide, 1 kD)] drugs were utilized to evaluate the suitability of PBG copolymers as controlled release delivery systems. *In vitro* release studies were performed by adding the above mentioned model drugs in 20 wt% aqueous solution of respective PBG-1 and PBG-2 copolymers. To estimate the concentration of all model drugs, release samples were analyzed by Bradford Assay (Thermo Fisher scientific).

In vitro release behavior of different MW of model drugs from PBG-1 and PBG-2 thermosensitive gels was compared and represented in **Figures 3.9 and 3.10**. Release of these model drugs was noticeably affected by the block arrangements of the copolymers. Hydrophilic gelling polymer (PBG-2) exhibited faster release relative to hydrophobic gelling polymer (PBG-1) noticed in all macromolecule model drugs. Therefore, *in vitro* release profile of these drugs was sustained for longer duration in case of PBG-1 compared to PBG-2. It is anticipated that PLA block at the terminal may have prolonged the release of macromolecule drugs due to hydrophobic nature relative to PBG-2 copolymers. PBG-1 gelling polymer may form compact structure with smaller porosity of gel matrix relative to PBG-2 polymer. This structural difference may lower the diffusion of the macromolecule drugs across gel matrix resulting in prolong duration of release. This study also supports that decrease in crystallinity increase the drug release. According to XRD spectra, amorphous nature of PBG-2 gelling polymer exhibit faster drug release.

In vitro release of lowest MW octreotide showed burst release of 35% and 30% with PBG-2 and PBG-1 respectively. Approximately, 90% cumulative release released

was observed in three days with PBG-2 and four days in case of PBG-1. Similarly, due to loose matrix of the thermosensitive gelling copolymer burst release was observed in all model drugs with both PBG-1 and PBG-2. Approximately, 90% cumulative drug release of IgG, IgG Fab', IgG-Fab was observed 19 days, 16 days, 10 days, in case of PBG-1 and 14 days, 9 days, 7 days in case of PBG-2, respectively.

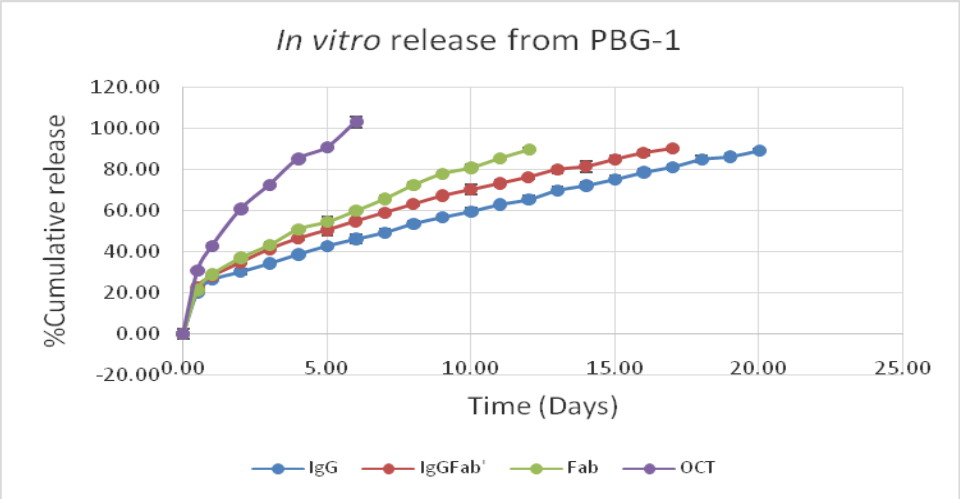

Figures 3.9 *In vitro* drug release studies from PBG-1 copolymer. Results are given as mean ± SD, n = 3

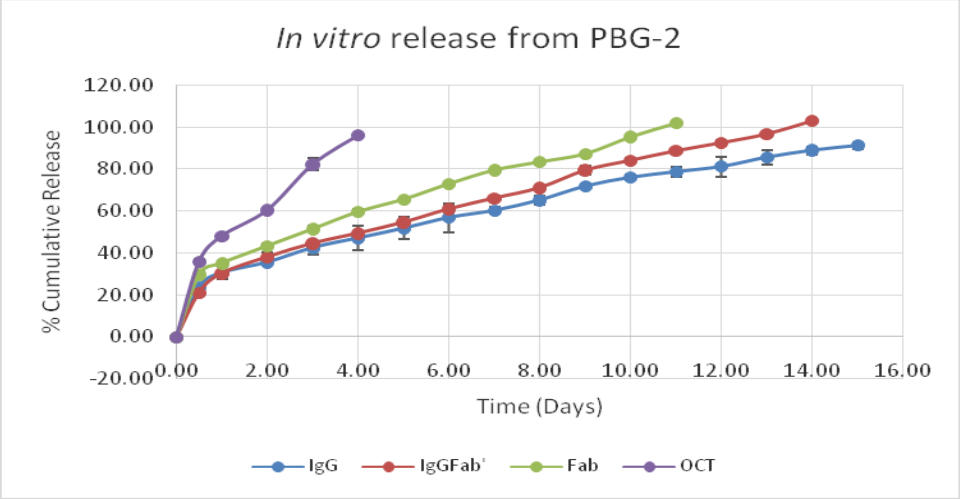

Figures 3.10 *In vitro* drug release studies from PBG-2 copolymer. Results are given as mean ± SD, n = 3

In vitro release kinetics

Table 3.3 Coefficient of determination (R^2) for various kinetic models for *in vitro* release of octreotide, IgG Fab, IgG Fab' and IgG from PBG-1

Block copolymers	**Korsmeyer-Peppas**		**Higuchi**	**First-Order**	**Zero-Order**	**Best fit model**
	R^2	n	R^2	R^2	R^2	
Octreotide	0.993	0.301	0.964	0.982	0.866	Korsmeyer-Peppas
IgG-Fab	0.995	0.318	0.984	0.964	0.933	Korsmeyer-Peppas
IgG-Fab'	0.997	0.360	0.994	0.979	0.951	Korsmeyer-Peppas
IgG	0.991	0.414	0.993	0.980	0.971	Korsmeyer-Peppas

Table 3.4 Coefficient of determination (R^2) for various kinetic models for *in vitro* release of octreotide, IgG Fab, IgG Fab' and IgG from PBG-2

Block copolymers	**Korsmeyer-Peppas**		**Higuchi**	**First-Order**	**Zero-Order**	**Best fit model**
	R^2	n	R^2	R^2	R^2	
Octreotide	0.997	0.346	0.979	0.985	0.873	Korsmeyer-Peppas
IgG-Fab	0.995	0.293	0.976	0.954	0.922	Korsmeyer-Peppas
IgG-Fab'	0.990	0.347	0.987	0.961	0.950	Korsmeyer-Peppas
IgG	0.994	0.367	0.992	0.977	0.957	Korsmeyer-Peppas

Stability analysis of IgG by ultraviolet circular dichroism spectroscopy

In CD spectra, negative band near 218 nm that corresponds to presence of β-sheets in IgG structure have been observed. There was no difference in peak maxima observed between standard and sample (**Figure 3.11)**. Results indicated that secondary structure of IgG was not destabilized by PBG-2 polymer.

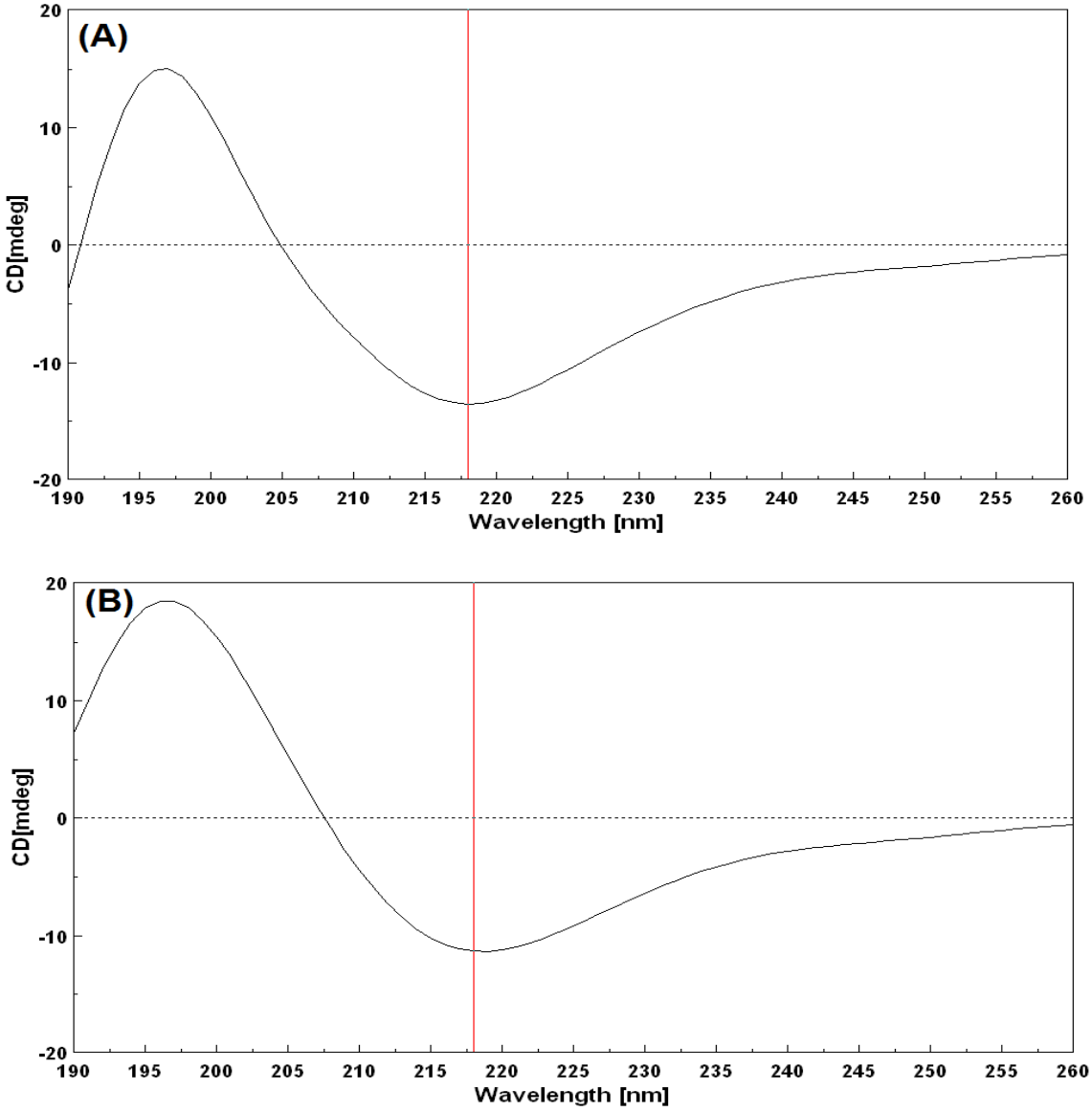

Figure 3.11 Circular dichroism spectroscopy of IgG from PBG-2 copolymer (A) Standard IgG; (B) Sample IgG

***In vitro* degradation studies**

Weight loss of PBG-2 copolymer: Similar degradation pattern was observed under all four conditions as shown in **Figure 3.12**. Total weight loss after 45 day was 31% with PBS pH 7.4 and 34% with PBS pH 7.4 with acetylcholinesterase and butylcholinesterase at 37^{o}C. In addition, higher weight loss was observed at accelerated conditions, 44%, borate buffer pH 9.0 at 37 ^{o}C and 39% with PBS pH 7.4 at 40^{o}C. The rate of degradation was most rapid in borate buffer (pH 9.0) incubated at 37°C. Accelerated conditions such as pH 9.0 (37°C) and high temperature (40°C) exhibited weight loss of ~45% and ~40%, respectively which were significantly higher than weight loss observed under normal condition (pH - 7.4, 37°C) i.e., ~35%. No significant effect of enzymes was observed on polymer degradation relative to other conditions without using enzyme.

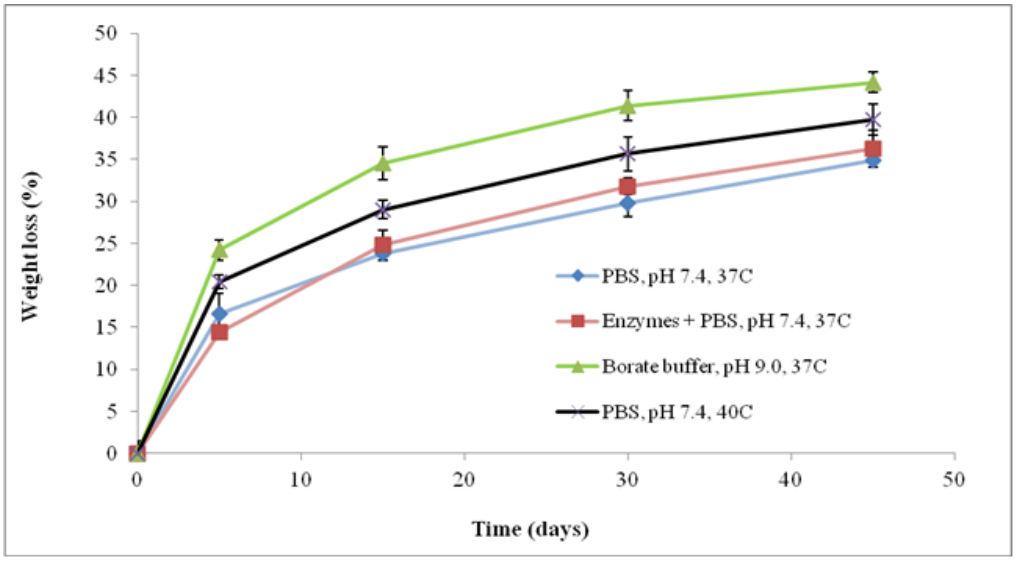

Figure 3.12 Degradation of PBG-2 (PEG-PCL-PLA-PCL-PEG) gelling polymer at different conditions (Weight loss Vs time). Results are given as mean ± SD, n = 3.

GPC analysis of PBG-2 copolymer: The gelling polymer was degraded at a faster rate due to its amorphous and hydrophilic nature (**Figure 3.13)**. Approximately 50% MW loss was noticed in 5 days. Similar pattern of degradation was observed under all four conditions. After hydrolytic degradation of PEG, PCL was present at the terminal. Therefore, degradation is slow and MW was fairly constant till 45 days.

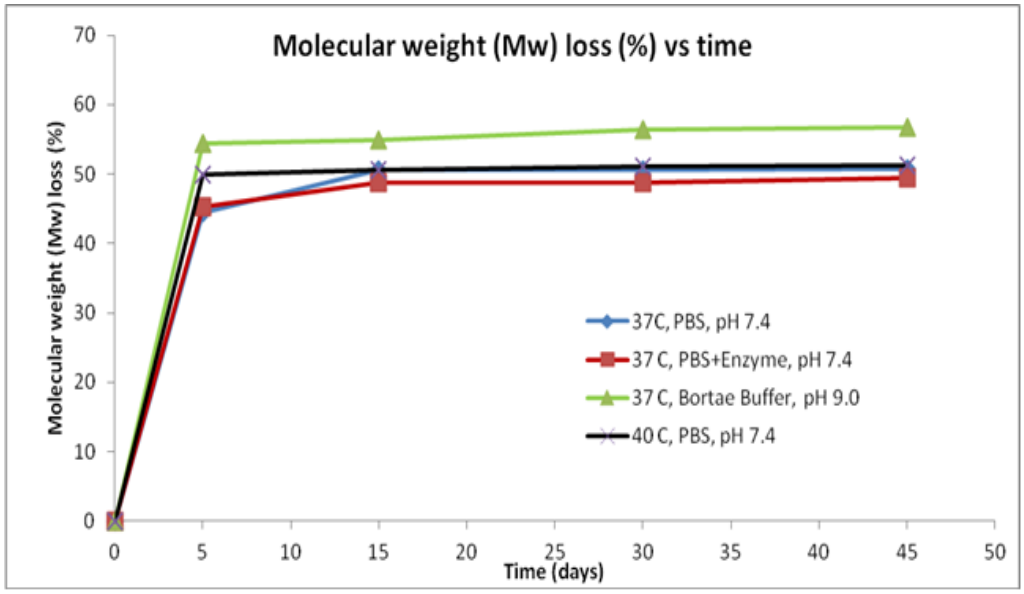

Figure 3.13 Molecular weight (MW) loss estimated by GPC of PBG-2 (PEG-PCL-PLA-PCL-PEG) gelling polymer. Results are given as mean ± SD, n = 3.

XRD analyses of PBG-2 copolymer: In order to evaluate crystallinity of gelling polymer, X-ray diffraction studies were conducted. **Figures 3.14, 3.15, 3.16, and 3.17** illustrate XRD patterns of gelling polymer at 0, 5, 15, 30, and 45 days incubated under four different conditions. Gelling polymer exhibited three characteristic crystalline peaks of PCL blocks at diffraction angles (2θ) of 21.5°, 24°, and 28°. In case of group A (Fig.3.14) and group B (Fig.3.15) crystallinity was observed after 30 days. However, crystallinity was observed at 5 day onwards for group C (Fig.3.16) and 15 days onwards with group D (Fig. 3.17). The rate of degradation was more rapid under accelerated condition relative to normal condition. Rapid degradation of gelling polymer may be due to amorphous nature and hydrophilicity of PEG at the terminal. The degradation is primarily caused by ester hydrolysis. No significant effect of enzymes was observed on degradation.

The fast degradation of gelling polymer was found more due to amorphous and hydrophilic nature of gelling polymer. However, degradation rate was reduced after 5 days as observed by MW loss analyzed by GPC. It could be due to exposure of PCL flank after the degradation of PEG flank presented at the terminal end. However, at accelerated condition the rate of degradation of polymer was found more as compare to normal condition. Conversely, no significant effect of enzyme degradation was observed. Further, XRD results indicate increase of crystallinity with progress of degradation time. This could be due to increase of PCL component after degradation of PEG.

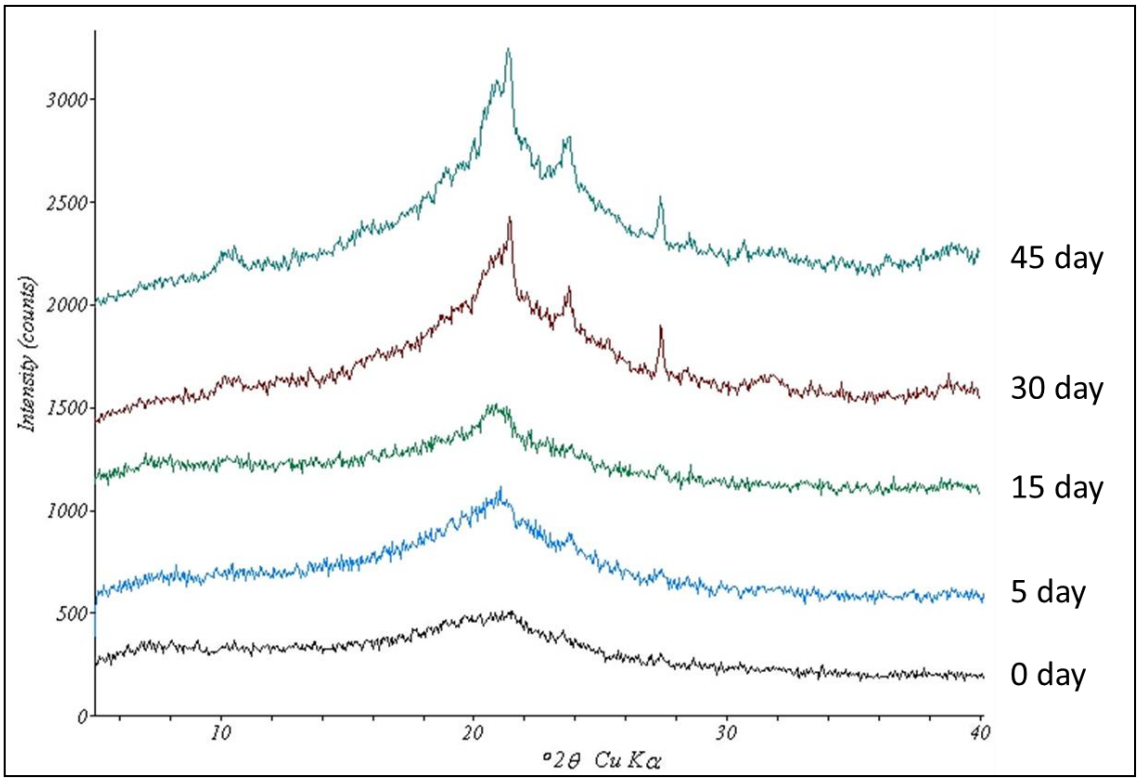

Figures 3.14 XRD patterns for Group - A (PBS pH – 7.4, 37^0 C)

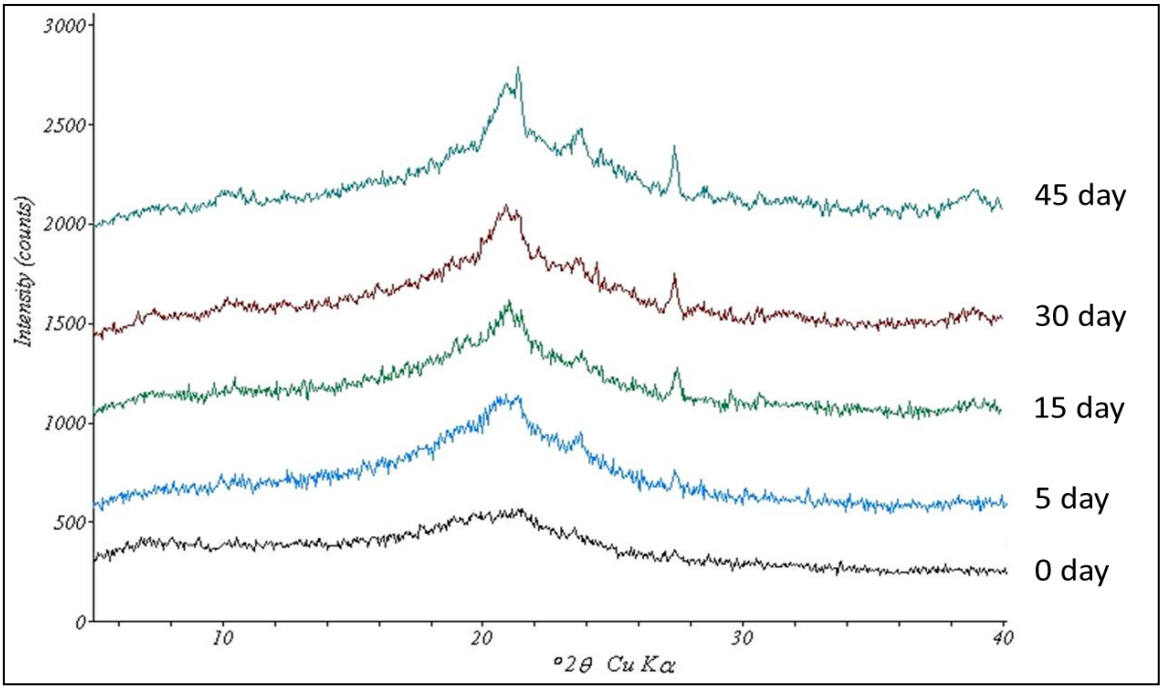

Figures 3.15 XRD patterns for Group - B (Enzymes, PBS pH – 7.4, 37^0 C)

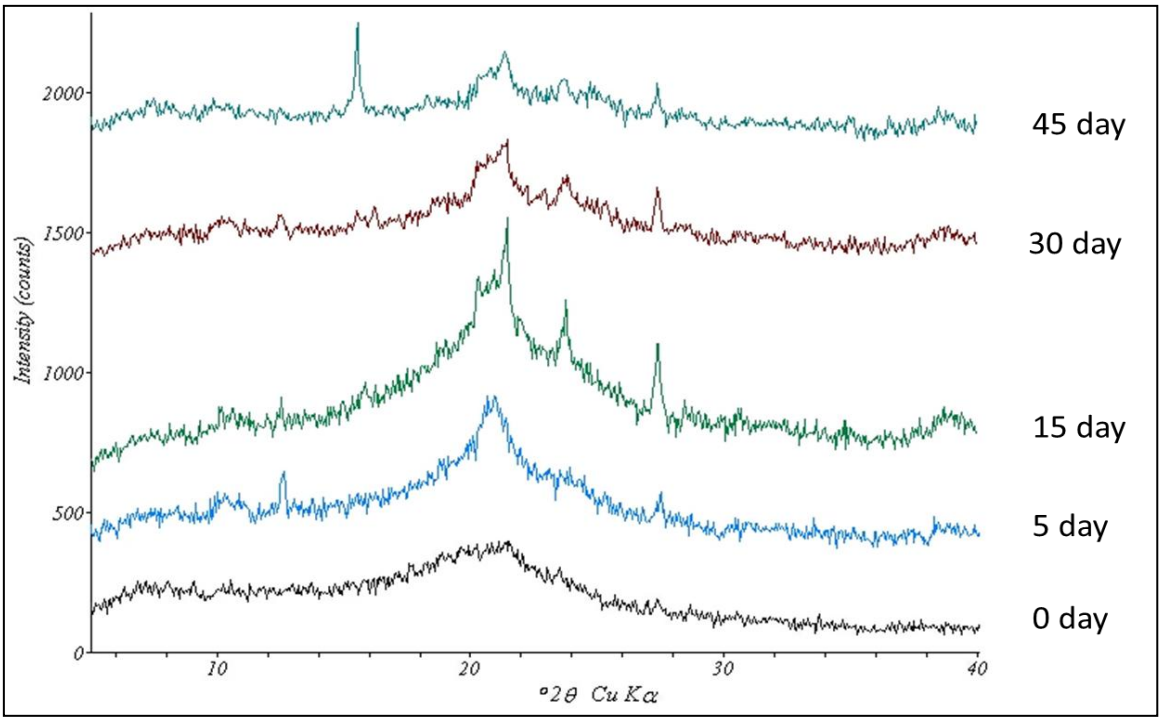

Figures 3.16 XRD patterns for Group - C (Borate buffer, pH – 9.0, 37^0 C)

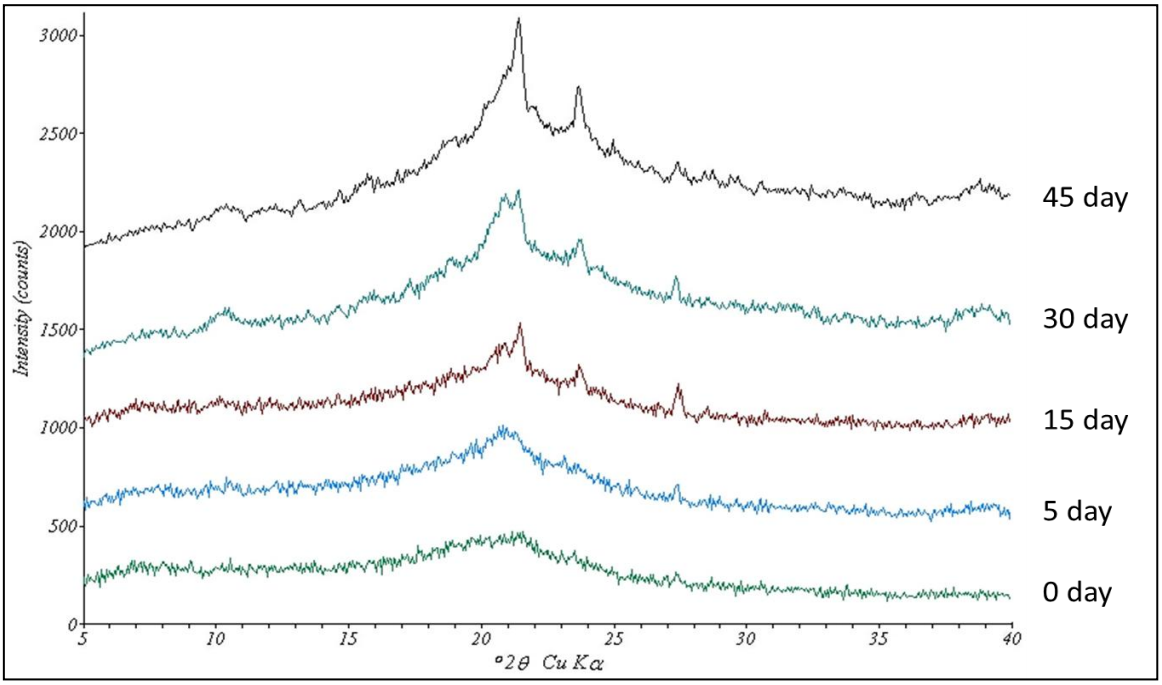

Figures 3.17 XRD patterns for Group – D (PBS, pH – 7.4, 40^0 C)

***In vivo* safety assessment**

Ocular histopathology was performed at weeks 1, 4, 16 and 33 after intravitreal injection to New Zealand white Rabbit **(Table 3.5)**. Results reported in **Figures 3.18 (A) 1 week control (B) 1 week (C) 4 week (D) 16 week and (E) 33 week** indicated no evidence of inflammation or toxicity associated with PBG-2 copolymer. Some rabbit eyes exhibited mild inflammation which may be injection procedure associated lens trauma. Based on these findings, it appears that the test articles are well tolerated by the rabbit eyes, without evidence of overt inflammation. Moreover, histopathological evidence of tissue damage indicated excellent biocompatibility of PBG copolymer. However, changes associated with injection procedure are relatively common and may cause most of the inflammatory and tissue damage observed in histology study.

Table 3.5 Histology study of PBG-2 copolymer in New Zealand white rabbit

Rabbit Number	Treatment	Euthanasia
No. 10	IVT saline	1 week
No. 12	IVT PB Gel	1 week
No. 21	IVT PB Gel	4 weeks
No. 19	IVT PB Gel	16 weeks
No. 20	IVT PB Gel	33 weeks

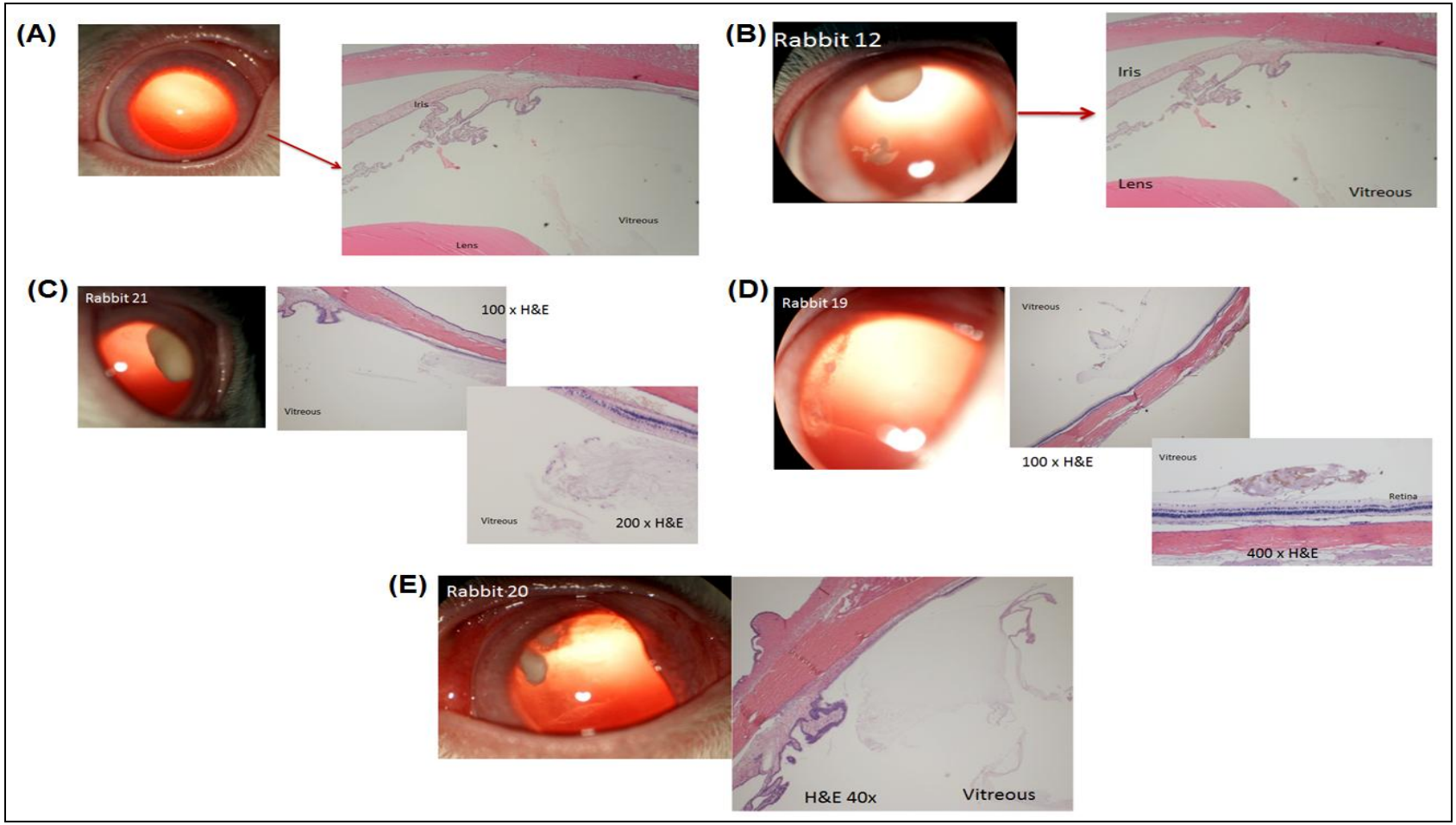

Figure 3.18 Ocular histopathology after intravitreal injection of PBG-2 using light microscopy after (A) 1 week Control; (B) 1 week; (C) 4 week (D) 16 week (E) 33 week

Conclusion

Compositions of PLA-PCL-PEG-PCL-PLA and PEG-PCL-PLA-PCL-PEG block copolymers were successfully synthesized and evaluated for their utility as injectable *in situ* hydrogel forming depot for controlled ocular delivery of macromolecules. Sol-gel transition and rheology revealed that PBG-2 block arrangements were easy to handle at room temperature and easy to administer through small gauge needle. *In vitro* cell cytotoxicity studies confirmed that PBG copolymers were superior biomaterials for ocular delivery. PBG copolymers also exhibited sustained release and the release pattern was dependent on the hydrophobicity and hydrophilicity of the PBG copolymers. It is anticipated that much longer release can be obtained by altering block composition or change in hydrophobicity and/or hydrophilicity of the gelling polymer. *In vitro* release pattern were in conjunction with approved facts that amorphous and hydrophilic polymer degrade fast. CD spectroscopy results revealed that no changes in the secondary structure of IgG. *In vivo* assessment of PBG-2 copolymer confirmed that it was well tolerated in the rabbit eyes studied up to 33 weeks. These outcomes clearly suggested that PBG based delivery systems may serve as a promising platform not only for back of the eye complications but also for the treatment of anterior segment diseases.

CHAPTER 4

COMPOSITE NANOFORMULATION FOR LONG TERM OCULAR DELIVERY OF MACROMOLECULES: EFFECT OF MOLECULAR WEIGHT ON DRUG RELEASE

Rationale

Normal aging process of the eye is characterized by a continuous loss of photoreceptor (PR), Bruch's membrane thickening, choroid thinning, scleral stiffening, vitreous degradation, and accumulation of debris. Among the posterior segment diseases diabetic retinopathy, macular edema, and macular degeneration are the leading causes of age-related vision loss. It represents 14% of the total causes of blindness globally (175) (176). Macular degeneration ensures when a small area in the retina (macula) deteriorates. It develops with age; hence it is referred as age-related macular degeneration (AMD). It is a degenerative process that damages the retinal pigment epithelium (RPE) and PR (1). With progression, AMD can be classified into the dry and wet forms. This classification is based on the absence or presence of vascular growth progression from the choroidal side toward the retina. It is subdivided into non-neovascular (NNV) and neovascular (NV) AMD. NNV is known as dry AMD and NV is called wet-AMD (177). In wet-AMD, new blood vessels from the choroid may leak, leading to macular edema. If left untreated, the progression may cause a centrally blinding disciform scar. Multiple factors such as oxidative stress, lipid metabolism, immune system activation, and angiogenesis play a key role in AMD pathogenesis (8).

Over the past decade, significant progress has been made in the treatment of AMD owing to an increased understanding of the mechanisms of ocular angiogenesis.

Several factors are associated with ocular angiogenesis, with vascular endothelial growth factor (VEGF) playing a central role (11). VEGF-A is a 46 kDa glycoprotein produced by ocular cells in response to oxidative stress. VEGF-A is the most potent mediator of both retinal and choroidal angiogenesis (178), (12). It stimulates endothelial cell growth, promotes vascular permeability and induces dissociation of tight junction components. In wet-AMD, a high level of VEGF is present below the RPE cell layer and around PR. VEGF inhibition via intraocular anti-VEGF to prevent the formation of new blood vessels represents the cornerstone of wet-AMD therapies (12). Recombinant humanized anti-VEGF antibody fragments or soluble receptor decoys (e.g. ranibizumab: Lucentis®; Genentech/Roche), pegaptanib (Macugen®), aflibercept (Eylea®; Regeneron Pharmaceuticals), and bevacizumab (off label drug: Avastin®; Genentech/Roche), are currently Food and Drug Administration (FDA) approved therapies for wet-AMD (1). Current treatments for posterior eye diseases suffer from various challenges including frequent intraocular injections, related adverse effects, and high cost of the treatment. Because of several anatomical/physiological barriers present in the eye, drug delivery to the posterior ocular segment is significantly impaired (48). However, the application of nanotechnology has been shown improvement in ocular drug delivery and offers numerous treatment options (2).

Various FDA approved biodegradable polymers such as polycaprolactone (PCL), polylactic acid (PLA), polyglycolic acid (PGA) and polyethylene glycol (PEG) have been extensively investigated for controlled delivery of macromolecules as matrices of NP formulations (154) (90). Several investigators have applied block copolymers such as polylactide-co-glycolide (PLGA) (179), PEG-PLGA (180), PCL-PEG-PCL (181), for the

development of controlled release of macromolecules or biologics (protein, peptide, antibody, Fab, Fc fragments) formulations. As a result, there is a need to develop biocompatible polymeric system which provides controlled release of macromolecule drugs for longer periods of time. In order to overcome this problem, various sequences of block copolymers can be tailor-made by considering physical chemical properties of FDA approved polymers. Among those, PEG provides hydrophilicity to copolymer which helps to degrade the matrix. PCL is another polymer which possesses crystallinity and hydrophobic in nature. This enhances the drug entrapment efficiency. PLA and PGA are other polymers; more hydrophilic relative to PCL. This polymer contributes to rapid degradation (182), (183). Based on the properties of these polymers, various tailor made combinations on the basis of different MW, ratios and arrangements can be designed to achieve a particular release rate. Moreover, block copolymers are amphiphilic in nature rendering these materials suitable for macromolecule delivery.

Therefore, the objective of this work is to synthesize the pentablock (PB) copolymers of a unique ratios and MWs consisting each block (PEG, PLA and PCL) for controlled long term delivery of macromolecules for the treatment of AMD. In this study, PB copolymers have been synthesized by sequential ring-opening bulk copolymerization method to achieve the long term release of lysozyme (14.3 kDa; Lyz), IgG-Fab (50 kDa; Fab) and IgG (150 kDA). The hypothesis of this project is centered on the release of the macromolecules encapsulated in NPs based on different molecular weight. The study has been designed to examine the effect of hydrodynamic diameter of molecules on the *in vitro* drug release profile as a function of MWs of macromolecule drugs. NPs have been characterized for particle size, PDI, entrapment efficiency, drug loading and *in vitro*

release profiles. Furthermore, in order to minimize burst release and to achieve continuous zero-order drug release, the experiments designed towards a novel composite formulation comprising drug loaded NPs suspended in thermosensitive gelling aqueous solutions. In addition, biocompatibility studies have been performed in order to ensure the safety of PB copolymers.

Materials and methods

Materials

Poly (ethylene glycol) (PEG, 4 kDa), methoxy-PEG (550 Da), stannous octoate, ε-caprolactone, poly (vinyl alcohol) (PVA), lipopolysaccharide, and *Micrococcus luteus* were procured from Sigma-Aldarich (St. Louis, MO). L-lactide and hexamethylenediisocynate (HMDI) were purchased from Acros organics (Morris Plains, NJ). Micro-BCA^{TM} assay kit was obtained from Fisher scientific Inc., (Rockford, IL). Mouse tumor necrosis factor alpha (TNF-α), Interleukin 6 (IL-6), Interleukin 1 beta (IL-1β), and enzyme-linked immunosorbent assay (ELISA) kit were purchased from e-Bioscience Inc., (San Diego, CA). All other reagents used in this study were of analytical grade.

Methods

Synthesis of PB copolymers

PB copolymers i.e, poly(caprolactone)-poly(lactic acid)-poly(ethylene glycol)-poly(lactic acid)- poly(caprolactone) (PCL-PLA-PEG-PLA-PCL i.e., PB-A and PB-B) and poly(ethylene glycol) -poly(caprolactone) -poly(lactic acid) -poly(caprolactone)-

poly(ethylene glycol) (PEG-PCL-PLA-PCL-PEG i.e., PBG-2) were synthesized by ring-opening bulk polymerization method (154), (90). PB-A copolymer was synthesized by two steps sequential ring-opening polymerization for NP preparation. PEG (4 kDa) was utilized as macroinitiator and stannous octoate served as catalyst. In the first step, triblock (TB) copolymer PLA-PEG-PLA (**Figure 4.1**, step 1) was synthesized by polymerization of PLA at two open hydroxyl ends of PEG. Lactic acid and stannous octoate (0.5% w/w) were added to anhydrous PEG with temperature raised to 150°C. After 24 h the reaction mixture was dissolved in dichloromethane (DCM) followed by precipitation in cold petroleum ether. The precipitated TB copolymers were filtered and dried overnight by using high speed under vacuum at room temperature. In a second step, PLA-PEG-PLA (TB) copolymers were added to ε-caprolactone to prepare PB-A and PB-B (**Figure 4.1**, step 2). TB copolymer and e-caprolactone were placed in round bottom flask under inert condition and temperature was raised to 150°C. To this reaction mixture, stannous octoate (0.5% w/w) was added and the reaction was allowed to run for 24 h. Subsequently, PB copolymer was purified by cold ether precipitation method. The product was dried under vacuum and stored at -20°C until further use.

The thermosensitive gelling polymer (PBG-2) was synthesized by ring-opening bulk copolymerization as described previously in chapter 3, **Figure 3.2.**

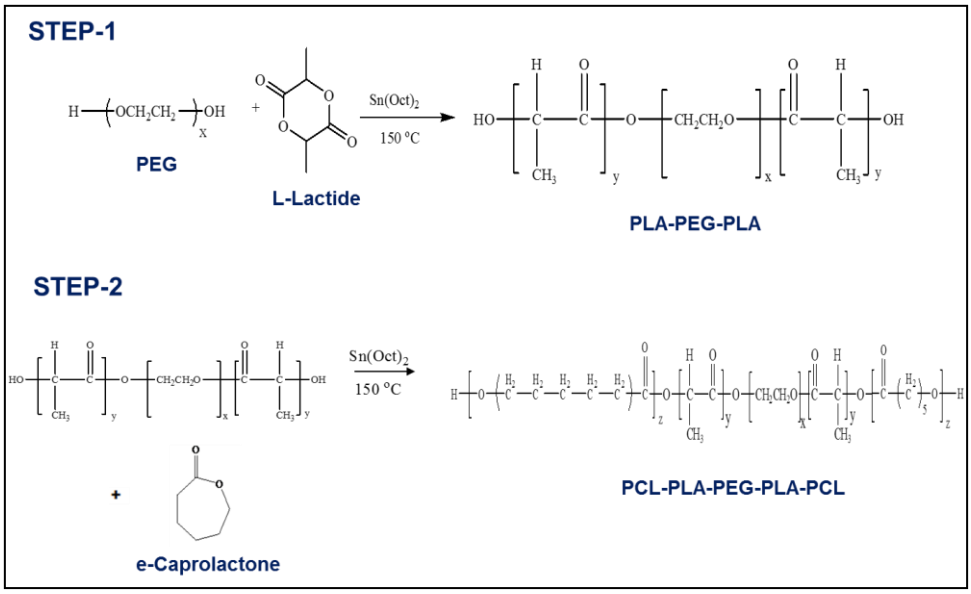

Figure 4.1 Synthesis scheme for PB-A and PB-B (PCL-PLA-PEG-PLA-PCL) copolymer

Characterization of PB copolymers

The copolymers were characterized for MW and purity by ^{1}H NMR spectroscopy and crystallinity by XRD analysis.

Proton nuclear magnetic resonance (^{1}H-NMR) spectroscopy

^{1}H-NMR spectra of TB and PB copolymers were acquired on a 400 MHz NMR instrument (Varian Inc., Palo Alto, CA). The chemical shift values were reported as δ in parts per million (ppm). NMR samples were prepared by dissolving each copolymer in deuterated chloroform in a 5-mm outer diameter NMR tubes (Wilmad-Lab Glass, Vineland, NJ).

X-ray diffraction (PXRD) analysis

The crystallinity of PB copolymers was determined by XRD analysis with Rigaku MiniFlex automated X-ray diffractometer (Rigaku, The Woodland, TX). It was equipped

with Ni-filtered Cu-Kα radiation (30 kV and 15 mA). The analysis was performed at room temperature at a scanning rate of 5°/min.

Phase transition (gelation) study of PBG-2 thermosensitive gelling copolymer

The sol-gel transition behavior of PBG-2 copolymer was examined by test tube inverting method as mentioned in chapter-3, **Figure 3.5**.

In Vitro biocompatibility studies

Mouse macrophage cells (RAW-264.7) cells were maintained according to ATCC guidelines at 37°C, 5% CO2 and 95% humidified atmosphere for 48 h. PB copolymers (PB-A, PB-B, and PBG-2) were dissolved in ACN at a concentration of 25 mg/mL. Two hundred microliters of this solution were aliquoted in 48-well cell culture plates and incubated for overnight under UV lights (laminar flow). The process continued with the ACN evaporation and sterilization of resulting polymer film. After the sterilization, RAW-264.7 cells (5.0×10^4) were seeded in each well of the cell culture plate and incubated for 24 h at 37°C and 5% CO2. After completion of the incubation period, cell supernatants were analyzed for the presence of cytokines i.e., TNF-α, IL-6 and IL-1β. Lipopolysaccharide (LPS) was selected as positive control whereas, cells without any treatment were considered as negative control. Cytokines level (in pg/mL) was measured by ELISA method according to manufacturer's protocol (e-Biosciences, San Diego, CA). Standard calibration curves for TNF-α, IL-6 and IL-1β were prepared in the concentration ranges of 10-750 pg/mL, 5-500 pg/mL and 10-500 pg/mL, respectively (154).

Preparation of NPs

Lyz, Fab and IgG-encapsulated NPs were prepared by water in oil in water ($W_1/O/W_2$) double emulsion solvent evaporation method using PB-A and PB-B copolymers (154), (90). Briefly, Fab containing aqueous solution (W_1 phase) was emulsified in the organic phase (dichloromethane: DCM) comprising PB-A or PB-B copolymer by drop-wise addition to the aqueous phase containing 2% w/v polyvinyl alcohol (PVA). This was subjected to probe sonication for 30 sec at 2W output to form a W_1/O primary emulsion. The resulting primary emulsion was then added drop-wise to 5 ml of 2% w/v PVA solution (W_2 phase) under constant sonication for 60 sec at 2W output to prepare a $W_1/O/W_2$ double emulsion. To avoid the excessive heating and any possible degradation of macromolecule, emulsion preparation was carried out in ice-bath. The double emulsion was stirred at room temperature for 30 min followed by evaporation of DCM under vacuum using a rotatory evaporator to formulate the NPs. The emulsion containing NPs was centrifuged for 30 min at 20,000 rpm and 4°C followed by two washing cycles with distilled deionized water (DDW). The Lyz-loaded PB-A based NPs and IgG loaded PB-B based NPs were formulated according to the similar protocol. Finally, the Lyz, Fab and IgG-loaded NPs were freeze-dried in the presence of 5% w/w mannitol (as a cryoprotectant) and stored at -20°C until further use.

Characterization of NPs

Particle size and PDI

Freeze-dried NPs were dispersed in DDW (1 mg/mL) and analyzed for size and distribution. Particle size was determined by Zetasizer (Zetasizer Nano ZS, Malvern

Instruments Ltd, Worcestershire, UK) at 90° scattering angel. All the NP samples were analyzed in triplicate.

Percent entrapment efficiency (EE %) and drug loading (DL %)

Lyz, Fab and IgG encapsulated freeze-dried NPs were examined for their entrapment EE and DL by estimating the amount of protein in the supernatant obtained from NPs preparation. Micro BCA^{TM} protein estimation kit was employed for the estimation of total protein. The samples were analyzed by a DTX 800 Multimode microplate reader (Beckman Coulter, Brea, CA). The standard curves of respective macromolecules (Lyz, Fab and IgG) ranging from 3.125 to 200 µg/ml were prepared in DDW. The following equations 1 and 2 were applied for the calculation of EE (%) and DL (%).

$$\% \text{ Encapsulation efficiency} = \frac{(\text{Initial amount of drug} - \text{Amount of drug in supernatant})}{\text{Initial amount of drug}} * 100 \quad \ldots \text{Eq. 4.1}$$

$$\% \text{ Drug loading} = \frac{\text{Amount of drug in nanoparticle}}{\text{Total amount of drug and polymer}} * 100 \quad \ldots \text{Eq. 4.2}$$

In vitro release studies

The PB copolymer based NPs were characterized for their ability to release the Lyz, Fab and IgG from native NPs and NPs suspended in thermosensitive gelling copolymer (composite nanosystem). In order to conduct the *in vitro* drug release studies, 1 mg of each of Lyz, Fab and IgG equivalent freeze-dried NPs was suspended in 1 ml of Phosphate Buffer Saline (PBS; pH 7.4). The resulting NP suspension was then incubated in a water bath equilibrated at 37°C. At predefined time intervals, the suspension was centrifuged at 12,000 rpm for 30 min. Two hundred microliters of supernatant was

collected and replaced with the same volume of PBS. NPs were then resuspended and the release study was continued at 37°C. In a second set (composite nanosystem) of *in vitro* release studies, 1 mg equivalent of Lyz, Fab and IgG containing NPs was suspended in 100 µl of an aqueous solution of thermosensitive gelling copolymer (PB-C; 15 wt%). The resulting suspension was incubated in an Eppendorf tube at 37°C for 30 min. Once the gel was formed, an aliquot (1 ml) of PBS (pre-incubated at 37°C) was slowly added. At predetermined time intervals, 200 µl of supernatant was collected and replaced with the same volume of fresh PBS (pre-incubated at 37°C). The drug release samples were analyzed by Micro BCA^{TM} assay for total protein content according to the supplier's instructions (Fisher scientific, Rockford, IL). *In vitro* release experiments were performed in triplicate (n = 3) and expressed as percent cumulative drug release with time.

Release kinetics

In order to delineate the release kinetics mechanisms of Lyz, Fab and IgG from NPs and composite nanosystem, release data were fitted to first-order, Higuchi, Hixon Crowell, and Korsmeyer-Peppas models as given by Eqs. (3), (4), (5), and (6), respectively.

$$\log Q_t = \log Q_0 + K_1 t/2.303 \quad \text{...Eq. 4.3}$$

$$Q_t = K_H t^{0.5} \quad \text{…Eq. 4.4}$$

$$(Q_0^{1/3} - Q_t^{1/3} = K_{hc} t) \quad \text{…Eq. 4.5}$$

$$Q_t/Q_\infty = kt^n \quad \text{…Eq. 4.6}$$

In these Equations, Q_t is the amount of drug released at time *t*, Q_0 is the initial amount of drug in solution, K_1 is first order release constant, K_H is the Higuchi release rate constant, K_{hc} is Hixon Crowell release rate constant, Q_t/Q_∞ is the fraction of drug

released at time t, Q_∞ is the total amount of drug released, and k is a kinetic constant. The constant n is the release exponent explaining the drug release mechanisms and classified as Fickian diffusion ($n \leq 0.5$), case-II transport ($n = 1$), anomalous transport ($0.5 < n < 1$), and super case-II transport ($n > 1$) (184).

Estimation of enzymatic activity of lysozyme

The enzymatic activity of Lyz in the released samples was estimated by comparing with freshly prepared Lyz solutions and/or control samples. The controls were prepared with Lyz solution incubated at 37°C in PBS (pH 7.4). These solutions were parallel to the *in vitro* release study from composite nanosystem. In order to determine the enzymatic activity of Lyz, a stock solution of *Micrococcus luteus* (0.01% w/v) was prepared with phosphate buffer (66 mM, pH 6.15) and diluted to achieve the absorbance between 0.2 - 0.6 at 450 nm. One hundred microliters of samples, standards, and controls were mixed with 2.5 ml of *Micrococcus luteus* suspension. The absorbance was measured at 450 nm over a period of 4 min at room temperature. Data were plotted for absorbance against time and slope was calculated to quantify the amount of Lyz in enzyme unit (EU). The EU units of Lyz (active) per mg of protein were calculated from the following equations 4.7 and 4.8 (185).

$$\text{Units of Lyz in one ml of sample} = \frac{(\Delta A\ 450\text{nm/min Test} - \Delta A\ 450\text{nm/min Blank})\,(df)}{(0.001)\,(0.1)} \quad \text{Eq. 4.7}$$

$$\frac{\text{Units of Lyz}}{\text{mg of sample}} = \frac{\text{Units of Lyz in one ml of sample}}{\text{mg of Lyz in one ml sample}} \quad \ldots\text{Eq. 4.8}$$

As per the definition of Lyz, one EU of enzyme is able to produce ΔAbs_{450nm} of 0.001 per minute at pH 6.15 and 25°C utilizing *Micrococcus luteus* suspension. The number 0.1 represented the volume of release samples, standards, or controls and *df* depicts the dilution factor. The biological activity observed for the release samples were compared with the respective controls at the same time points.

Results and discussion

Synthesis and characterization of PB copolymers

PB-A, PB-B and PBG-2 (Chapter 3; **Figure** 3.2) were successfully synthesized by ring-opening bulk copolymerization of ε-caprolactone, and L-lactide. In the first step, TB copolymers were synthesized, purified and characterized as mentioned in the method section. The resulting TB A and B copolymers were composed of a PEG central block bearing two PLA sequences at both ends. Purified TB-A and TB-B copolymers were then utilized for the synthesis of the respective PB copolymers A and B respectively.

Purity and molecular weight (Mn) of PB copolymers were calculated by ^{1}H-NMR spectroscopy. As showed in **Figure 4.2**, typical ^{1}H-NMR signal of a sharp peak at 3.65 δ ppm could be attributed to methylene protons (−CH2CH2O−) of PEG in TB-A copolymer (**Figure 4.2A**). PB-A was observed at 1.40, 1.65, 2.30 and 4.06 δ ppm representing the methylene (–CH_2–) protons of - $(CH_2)_5$-, -OCO-CH_2-, and -CH_2OOC- of PCL units, respectively, (**Figure 4.2B**). Typical signals at 1.50 (-CH_3) and 5.17 (-CH) ppm were assigned to PLA blocks. Figure 3C represents ^{1}H-NMR spectra of PBG-2

copolymers (thermosensitive gel) represented in chapter 3; **Figure 3.3B**. Molecular weight (Mn) of PB copolymers was very similar to theoretical MWs (**Table 4.1**).

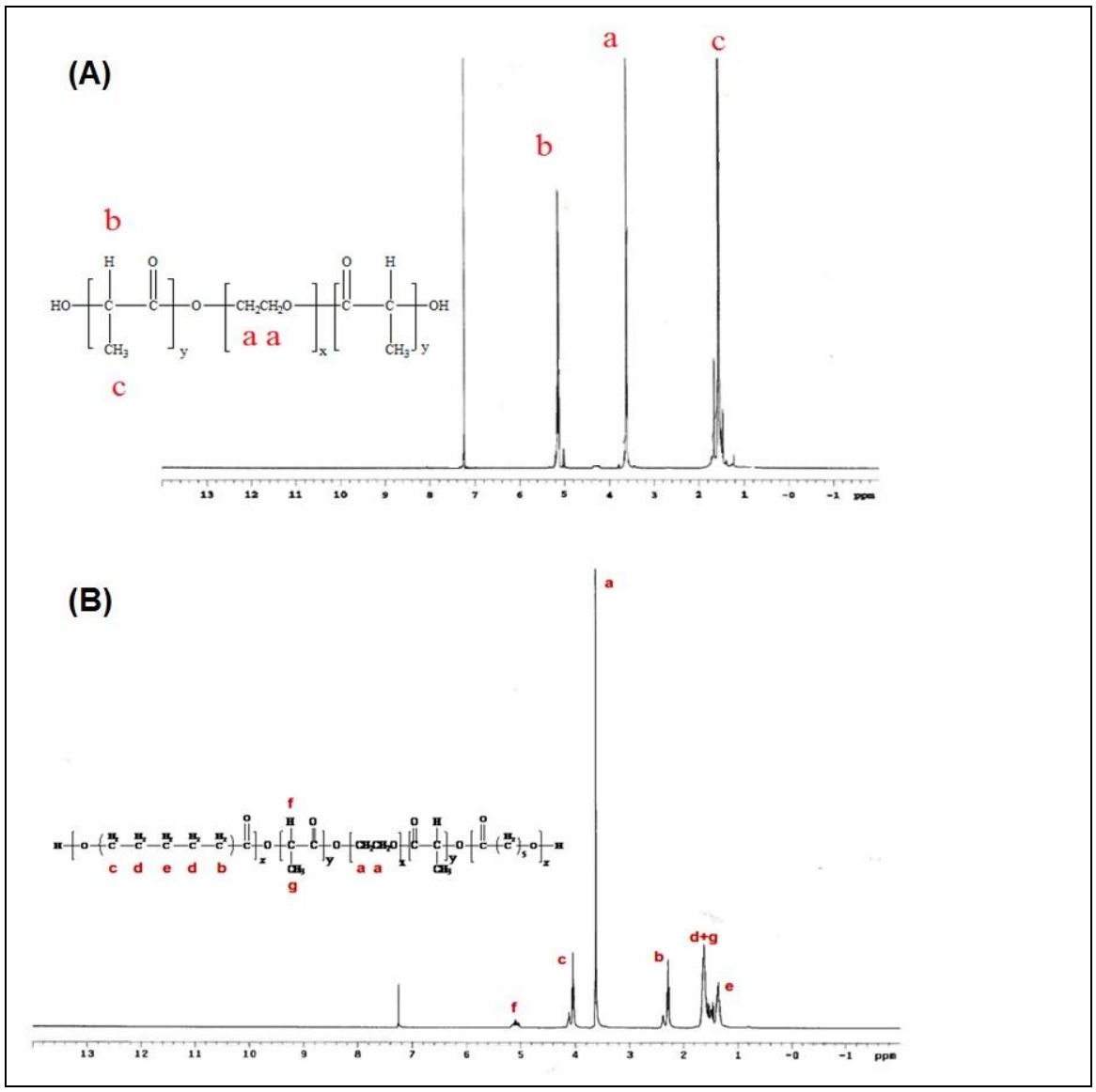

Figure 4.2 ^{1}H-Nuclear Magnetic Resonance (^{1}H-NMR) spectrogram of (A) TB-A and PB-A in $CDCl_3$

Table 4.1 Characterization of PB copolymers

Code	Structure	Total *Mn*[a] (theoretical)	Total *Mn*[b] (calculated)
PB-A	PCL_{7000}-PLA_{3000}-PEG_{4000}-PLA_{3000}-PCL_{7000}	22000	21034
PB-B	PCL_{7000}-PLA_{6000}-PEG_{4000}-PLA_{6000}-PCL_{7000}	30000	27653

a Theoretical value, calculated according to the feed ratio.
b Calculated from 1H NMR

Interestingly, TB-1 and TB-2 (PLA-PEG-PLA) copolymer exhibited a crystalline peak at 2θ = 16°, 19°, and 23° but, in PB-A and PB-B crystalline peaks of PCL shifted to 2θ = 20.5° and 2θ = 21.5° represented in **Figures 4.3 A and 4.3 B,** respectively. XRD patterns of TB-A and TB-B indicated that PLA blocks retained their crystalline structure. Conjugation of PCL blocks at the terminals of TB-A and TB-B copolymers exhibited shift in the intensity of the crystalline peak showing the semi-crystalline structures of PB-A and PB-B copolymers. Thus, the crystallinity of copolymers was easily controlled by the arrangement of polymer blocks in structural backbone. PBG-2 (Chapter 3; Figure) copolymer was devoid of any crystalline peak suggesting its amorphous nature. Previously published reports (186) suggested that a decrease in crystallinity enhanced the degradation of block copolymers.

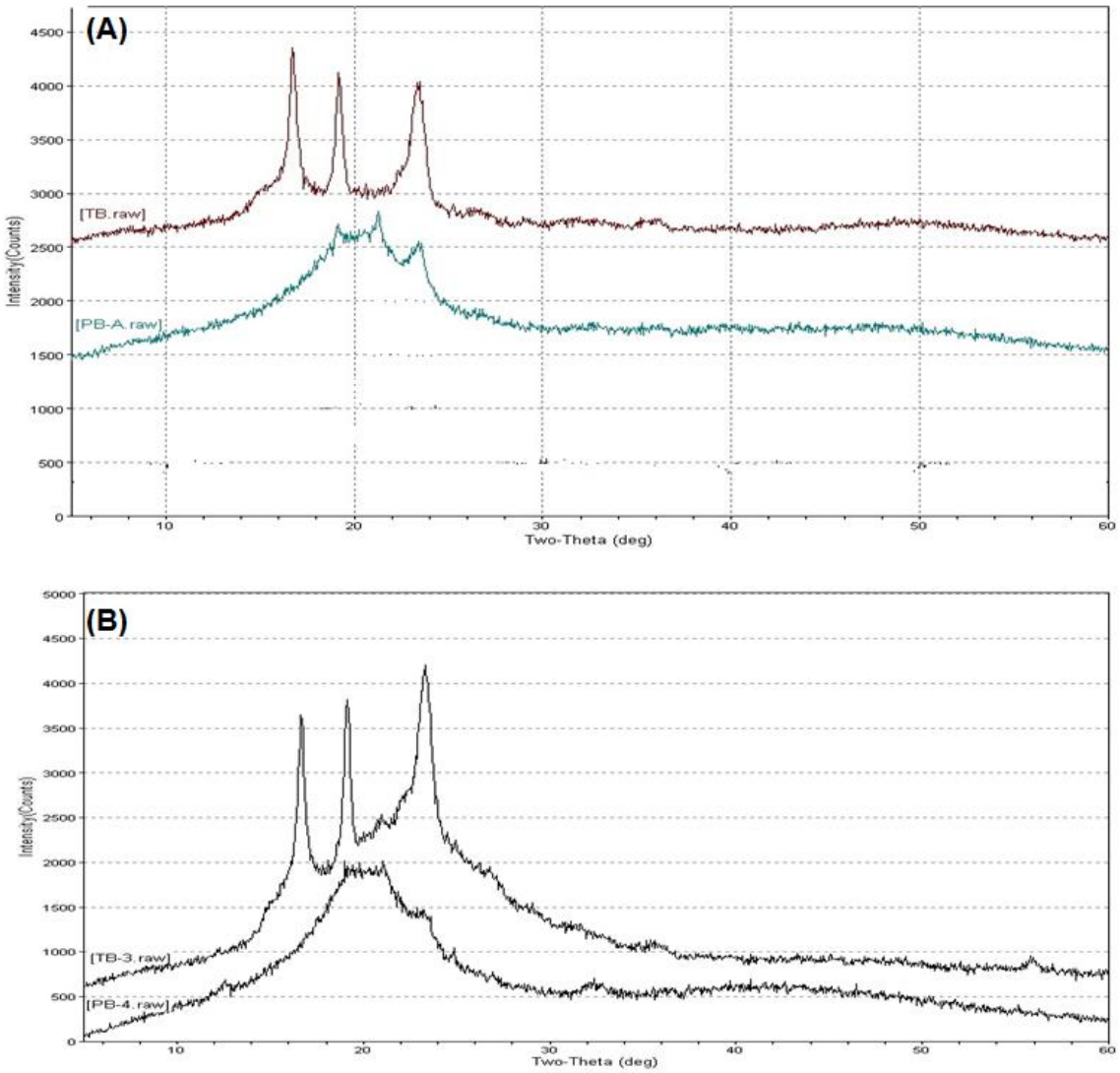

Figure 4.3 X-Ray diffraction analyses of (A) TB-A and PB-A (B) TB- B and PB-B

Phase transition (gelation) of PBG-2 thermosensitive gel

The thermosensitive gelling copolymers were amphiphilic in nature, containing hydrophilic block (PEG) and hydrophobic block(s) of PCL and/or PLA. The aqueous solution of PB-C was observed clear due to the self-assembly of polymeric chains into micellar structure which showed aggregation upon increasing the temperature and resulted in the gel formation. However, upper gel-sol conversion was due to an increased molecular motion of the hydrophobic chain of PCL and PLA. The aqueous solution of PB copolymers exhibited a sol-gel transition response upon increasing the temperature in the concentration range of 10wt-30wt%. The phase diagram (Chapter 3; **Figure 3.5**) revealed the critical gel concentration (CGC) from the solution to gel state conversion at 37°C.

***In vitro* biocompatibility studies**

The release of various cytokines releases such as TNF-α, IL-6 and IL-1β in culture supernatant following 24 h exposure to PB-A, PB-B and PB-C copolymers were examined. The samples were analyzed via sandwich ELISA method. Results depicted in **Figure 4.4** indicated the release of TNF-α (~200 pg/ml) in both groups, i.e., PB-A, PB-B and PB-C. However, the values were comparable to the negative control (cells without treatment) with no significant differences. Similarly, a negligible release of IL-6 and IL-1β was observed, suggesting that these copolymers are safe for use.

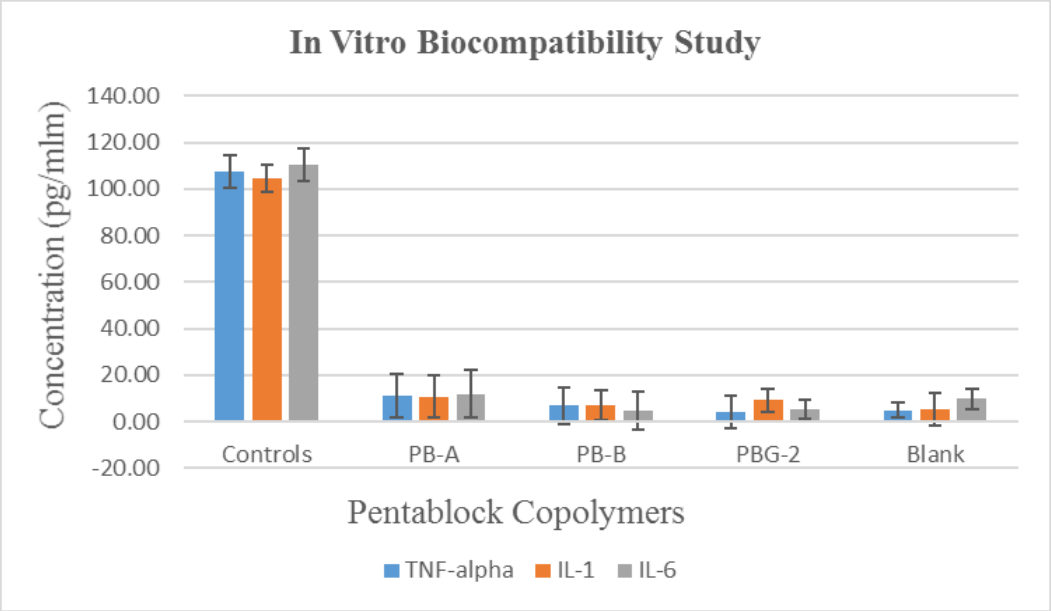

Figure 4.4 *In vitro* biocompatibility of PB-A, PB-B and PBG-2 copolymers on RAW 264.7 cells estimating the levels of TNF-α, IL-6 and IL-1β in the supernatants of PB copolymers. Results are given as mean ± SD, n = 5.

Characterization of NPs

Particle size and PDI

Lyz, Fab and IgG were encapsulated in PB-A and/or PB-B copolymers by $W_1/O/W_2$ double emulsion solvent evaporation method. NPs are ranging in diameter from 200-250 nm **(Table 4.2)**. Unimodal size distribution with narrow PDI was observed. These results suggested that the hydrodynamic diameter of macromolecules had no significant effect on the particle size distribution of NPs.

Entrapment efficiency (EE) and drug loading (DL)

As presented in **Table 4.2**, the EE of Lyz, and Fab in PB-A NPs were ~42% and ~45%, respectively. The low EE of NPs may be due to hydrophilicity of macromolecules

escaping from primary emulsion phase to the large volume of the external phase. However NPs prepared from PB-B copolymer exhibited a slightly higher EE ~49% for Fab. This could be due to the reason that the high hydrophobicity of PB-B copolymer relative to PB-A may have produced a rapid polymer precipitation to form the NPs during the solvent evaporation step and provided a slightly higher EE. It is also plausible that EE and DL were affected by the increased ratio of lactide during the NP preparation. The hydrophobic segment of PLA-PCL chain and the hydrophilic drug were associated with the PEG core which reduced the escape to the outer aqueous phase. Also, the EE and DL of IgG (molecular weight ~150 kDa) encapsulated in PB-B NPs was calculated to determine the effect of molecular weight in EE and DL of PB copolymers. Results showed that due to the high molecular weight and hydrophobicity of PB-B, it was able to encapsulate (~51% w/w) the high molecular weight macromolecule (Table 4.2). Overall, the application of high molecular weight of PB copolymers ensured a higher EE and DL of large molecules encapsulated in NPs.

Table 4.2 Characterization of Lyz, Fab and IgG loaded NPs

PB Copolymers	**Large molecule**	**Particle size (nm)**	**Poly-dispersity index**	**Entrapment efficiency (% w/w) (n=3)**	**Loading (% w/w) (n=3)**
PB-A	Lysozyme (15 kDa)	221.4	0.392	42.85 ± 1.57	6.31 ± 0.79
	IgG-Fab (50 kDa)	266.1	0.432	45.41 ± 1.30	5.46 ± 0.51
PB-B	IgG-Fab (50 kDa)	238.5	0.398	49.28 ± 1.86	11.28 ±1.13
	IgG (150 kDa)	201.8	0.360	51.19 ± 1.52	9.69 ± 0.46

In vitro release studies

In vitro release profile of different MW of macromolecules Lyz (14.5 kDa), Fab (50 kDa) and IgG (150 kDa) were evaluated for both formulations; (A) PB-A and PB-B based NPs and (B) PB-A and PB-B NPs embedded in 15 wt% thermosensitive gelling copolymer (PBG-2).vBoth PB-A NPs formulations of Lyz and Fab demonstrated biphasic release profile i.e., initial burst release followed by sustained release as described in **figures 4.5 and 4.6** respectively. Lyz exhibited significantly higher burst release (~21%) relative to Fab (~19%). It may be due to the fact that NPs have a certain amount of surface adsorbed drug, resulting into burst effect during the initial time period. Approximately, 80% of cumulative drug release was found in ~13 and ~35 days from Lyz and Fab PB-A NPs respectively. Therefore, to overcome this problem, hydrogels have been utilized to develop a formulation which can eliminate or minimize burst effect and offer zero-order drug release throughout the release period.

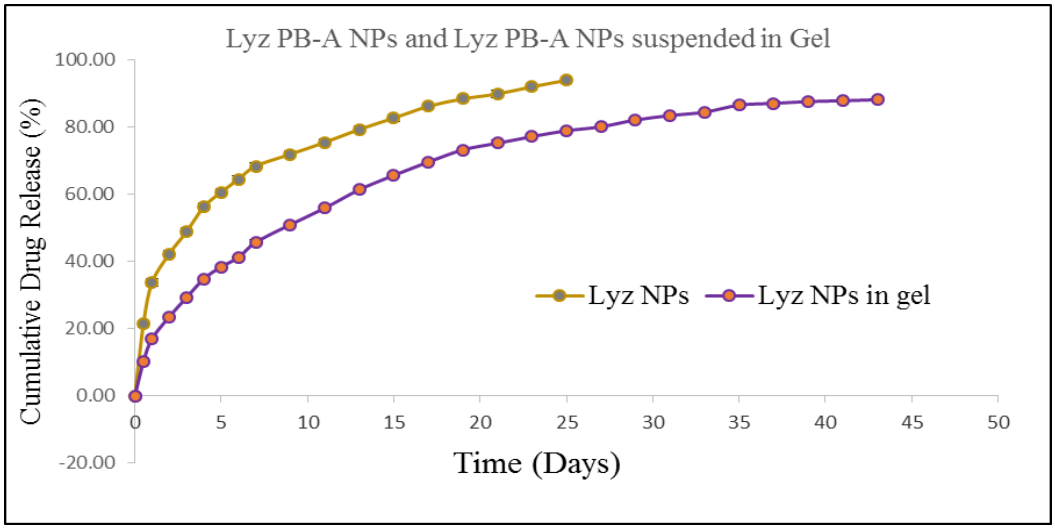

Figure 4.5 *In vitro* release of Lyz encapsulated in PB-A NPs and Lyz encapsulated in PB-A NPs suspended in PB-C thermosensitive gels (Composite nanoformulation). Results are given as mean ± SD, n = 3.

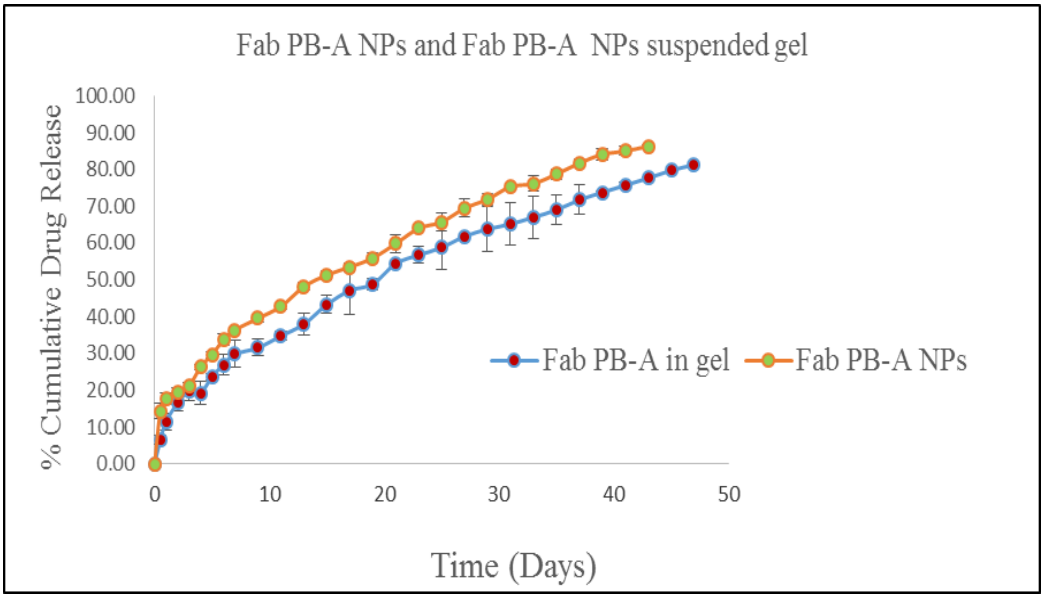

Figure 4.6 *In vitro* release of Fab encapsulated in PB-A NPs and Fab encapsulated in PB-A NPs suspended in PB-C thermosensitive gels (Composite nanoformulation). Results are given as mean ± SD, n = 3

Lyz and Fab encapsulated PB-A NPs were suspended in an aqueous solution of thermosensitive gelling polymer (PBG-2) termed as composite nanoformulation. Aqueous solution of PBG-2 copolymer remains in liquid state around room temperature but immediately transition from solution to hydrogel at the physiological temperature of 37°C (sol-gel transition) entrapping NPs throughout the polymeric matrix. From composite nanoformulation, 80% cumulative release of Lyz was for ~27 days whereas Fab prolonged the release for ~49 days from PB-A NPs as illustrated in **figures 4.5 and 4.6** respectively. Such behavior is a result of NPs suspended into the gel matrix which served an additional diffusion barrier due to surface adsorbed drug. It also resulted in a zero-order release pattern of the encapsulated drug throughout the release period. The enzymatic activity of Lyz was analyzed by the lysozyme assay kit. The integrity or

stability of the protein molecules was not addressed in this work and an assessment of the compatibility of the polymers with the macromolecule remains to be elucidated in future studies.

In addition, the effects of the MW of the PB copolymers (PB-A and PB-B) on Fab have been studied. Composite nanoformulation of Fab prepared from PB-A and PB-B copolymer demonstrated biphasic release. However, sustained release was observed from both of formulations as illustrated in **figure 4.7**. Although PB-A copolymer promises longer duration relative to PB-B but composite formulation of PB-B shows faster release compared to PB-A. It might be due to the high drug loading because of higher MW of the PB copolymer in addition to the reduced crystallinity of PB-B compared to PB-A.

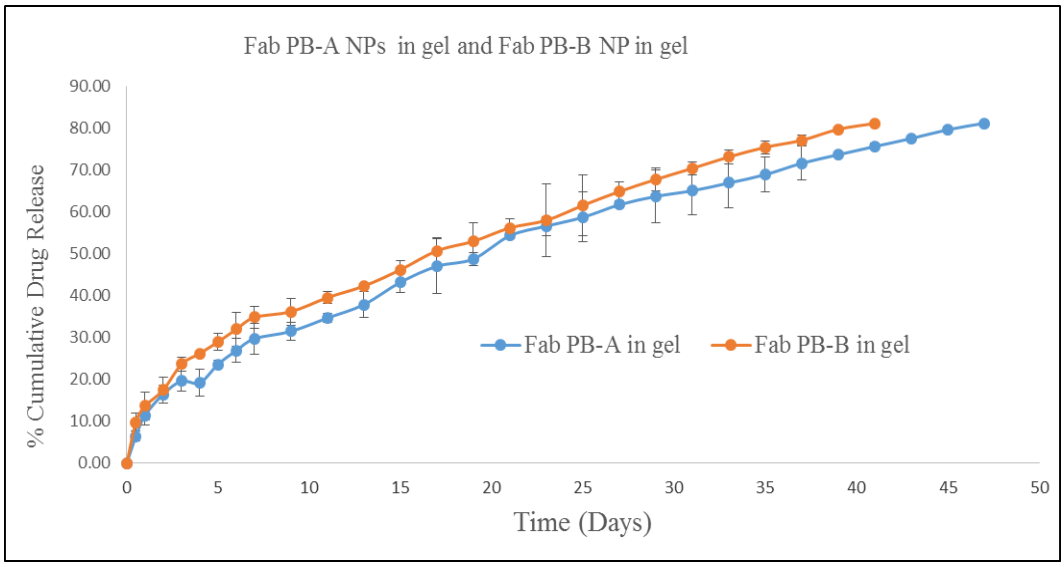

Figure 4.7 *In vitro* release (n=3) of Fab-encapsulated in PB-A NPs and PB-B NPs suspended in PBG-2 thermosensitive gels (Composite nanoformulation). Results are given as mean ± SD, n = 3.

Further, higher MW of PB copolymer (PB-B) was used to prepare NPs with Fab and IgG. *In vitro* release profile of both NPs formulations of Fab **(Fig. 4.8)** and IgG **(Fig. 4.9)** showed similar profiles as mentioned above. Fab (~21% w/w) and IgG (~18% w/w) exhibited higher burst release from the NPs alone. Similarly, composite nanoformulation minimizes the burst release (~9.78% w/w) and (~8.21% w/w) for Fab and IgG as described in **figures 4.8 and 4.9** respectively. IgG composite nanoformulation sustained release for more than 8 weeks with high MW PB-B.

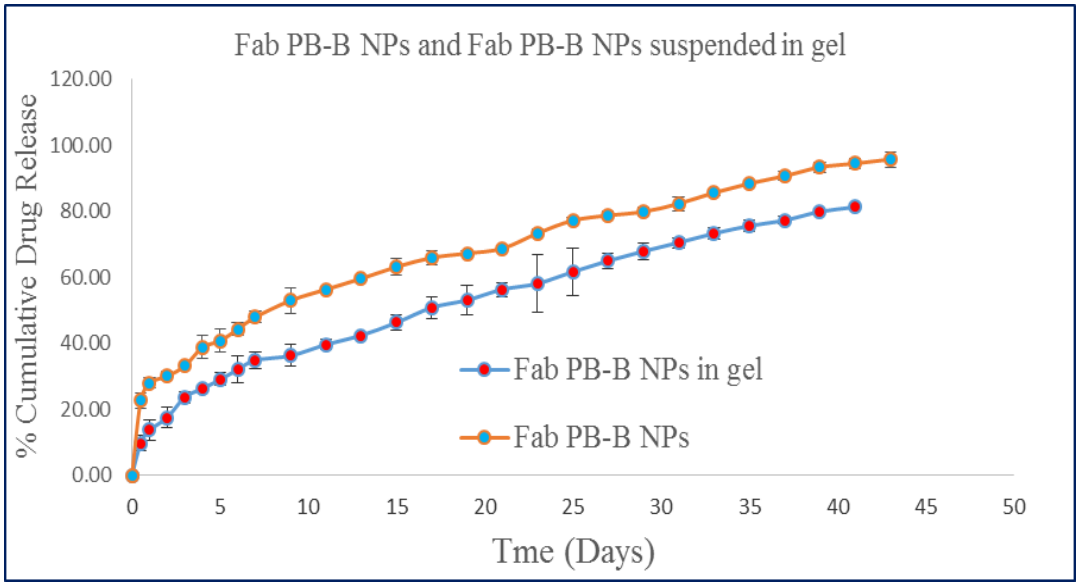

Figure 4.8 *In vitro* release of Fab encapsulated in PB-B NPs and Fab encapsulated in PB-B NPs suspended in in PBG-2 thermosensitive gels (Composite nanoformulation).

Results are given as mean ± SD, n = 3

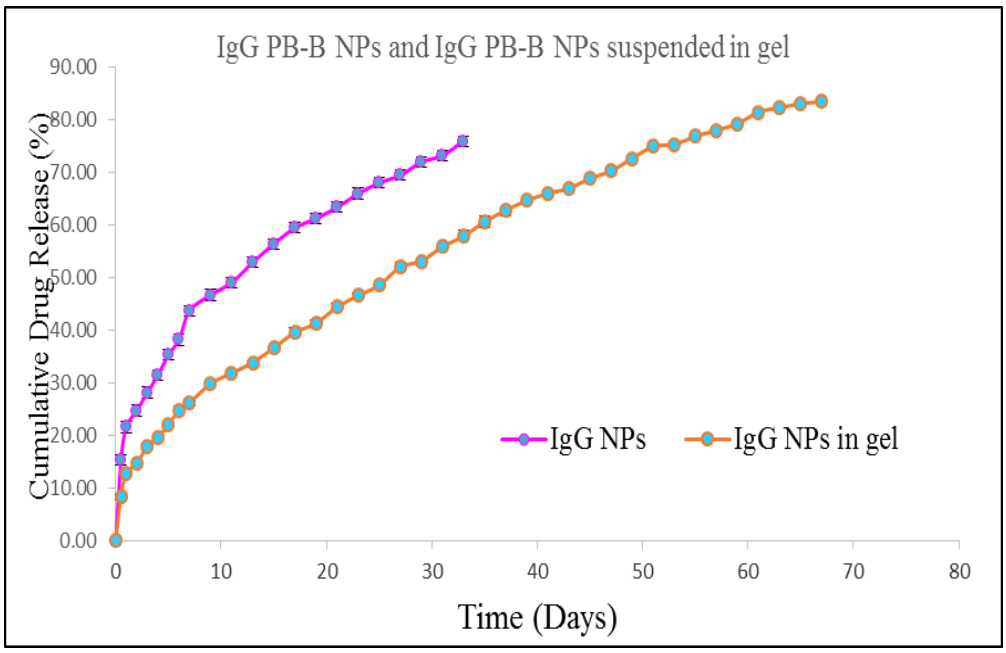

Figure 4.9 *In vitro* release of (n=3) IgG encapsulated in PB-B NPs and IgG encapsulated in PB-B NPs suspended in in PBG-2 thermosensitive gels (Composite nanoformulation). Results are given as mean ± SD, n = 3.

In vitro release profiles of Lyz and Fab from PB-A copolymer and Fab and IgG from PB-B copolymer suggest that the hydrodynamic diameter of macromolecules may exert effect on drug release pattern as depicted in **figures 4.10 and 4.11** respectively. The results suggest higher burst release and shorter release duration for Fab relative to IgG from their respective NPs. Lyz has smaller hydrodynamic diameter compared to Fab which may lead to rapid diffusion through both polymeric matrices of NP and from composite nanoformulation. **Figure 4.12** represents the comparative release pattern of all the composite nanoformulations studied in this work.

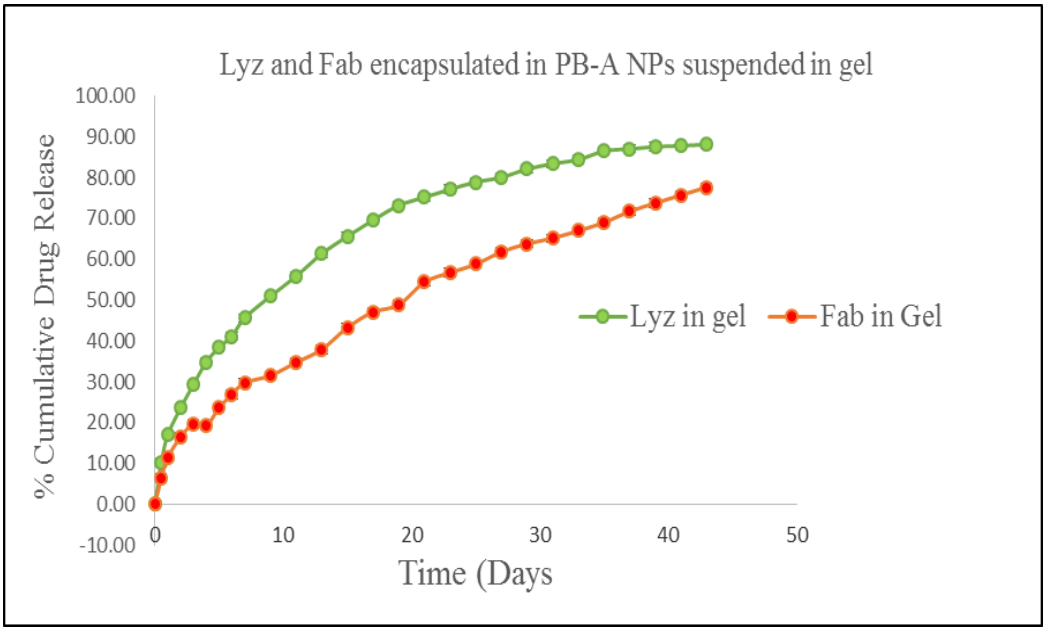

Figure 4.10 *In vitro* release (n=3) of Lyz and Fab-encapsulated in PB-A NPs suspended in in PBG-2 thermosensitive gels (Composite nanoformulation). Results are given as mean ± SD, n = 3.

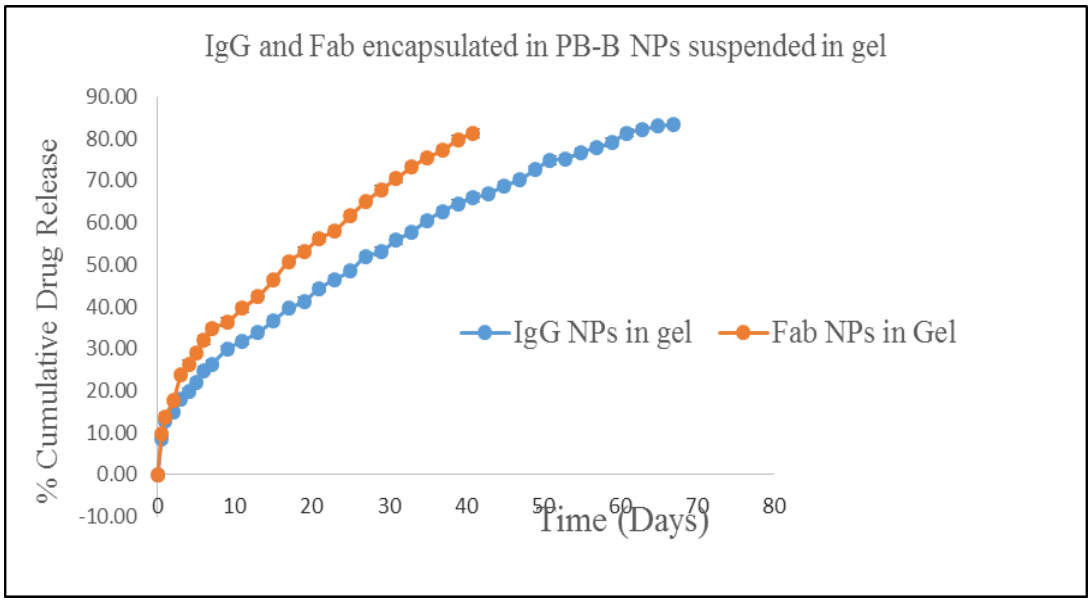

Figure 4.11 *In vitro* release (n=3) of Fab and IgG-encapsulated in PB-B NPs suspended in in PBG-2 thermosensitive gels (Composite nanoformulation). Results are given as mean ± SD, n = 3.

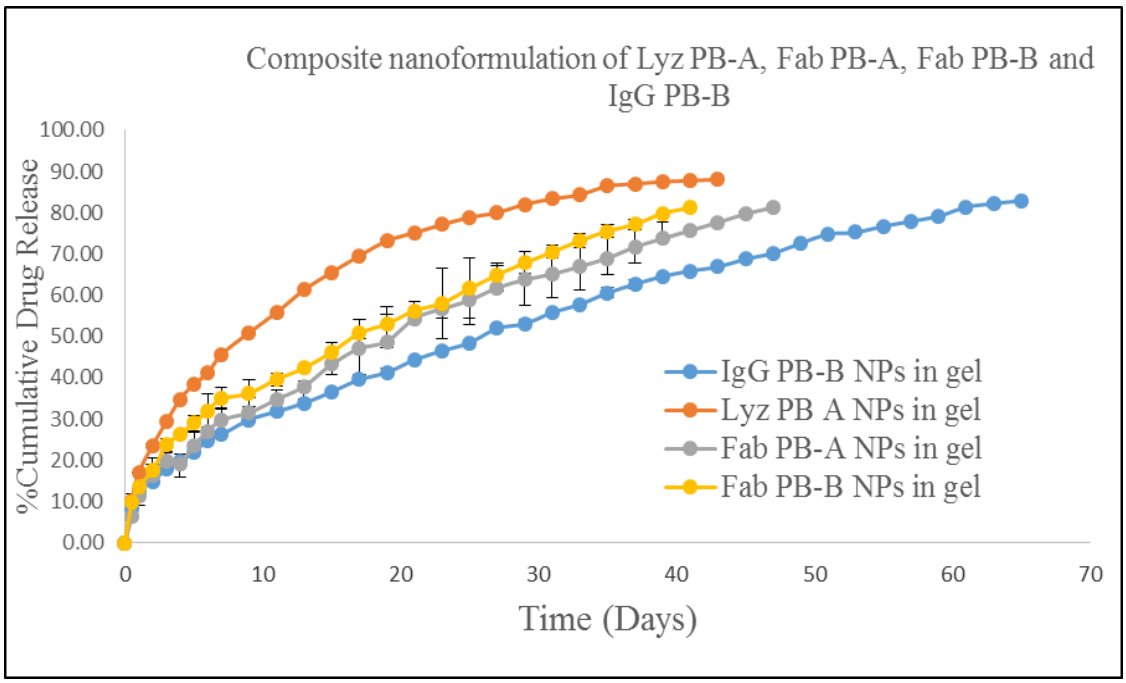

Figure 4.12 *In vitro* release (n=3) of Lyz PB-A, Fab PB-A, Fab PB-B and IgG PB-B NPs suspended in in PBG-2 thermosensitive gels (Composite nanoformulation). Results are given as mean ± SD, n = 3.

Release kinetics

In order to evaluate the release mechanisms of NPs, *in vitro* drug release data were fitted in First-order, Higuchi, Hixson-Crowell, and Korsmeyer-Peppas kinetic models. Results presented in **Table 4.3** indicated that Korsmeyer-Peppas was the best fit model for all the formulations with R^2 values ranging between 0.985-0.998. Moreover, *n* values in Korsmeyer-Peppas model for the release of Lyz, Fab and IgG from NPs were below 0.40 indicating the diffusion controlled release pattern. Interestingly, n values for composite nanosystem (NPs suspended in thermossensitive gel) of Lyz (0.402), Fab from PB-A (0.549), Fab from PB-B (0.582) and IgG (0.541) were suggested an anomalous diffusion controlled release mechanism. Hence, the release of macromolecules from composite nanosystem was controlled by diffusion as well as degradation of copolymer.

Table 4.3: Coefficient of determination (R^2) for various kinetic models for *in vitro* release of Lyz, Fab and IgG from composite nanoformulation

Block copolymers	**Korsmeyer-Peppas**		**Higuchi**	**First-Order**	**Hixon Crowell**	**Best fit model**
	R^2	n	R^2	R^2	R^2	
Lyz NPs PB-A	0.991	0.314	0.867	0.883	0.797	Korsmeyer-Peppas
Lyz NPs PB-A suspended in thermosensitive gel	0.985	0.402	0.961	0.947	0.883	Korsmeyer-Peppas
Fab NPs PB-A	0.996	0.492	0.996	0.945	0.911	Korsmeyer-Peppas
Fab NPs PB-A suspended in thermosensitive gel	0.997	0.582	0.988	0.972	0.995	Korsmeyer-Peppas
Fab NPs PB-B	0.994	0.974	0.951	0.866	0.794	Korsmeyer-Peppas
Fab NPs PB-B suspended in thermos-sensitive gel	0.990	0.569	0.983	0.959	0. 947	Korsmeyer-Peppas
IgG NPs PB-B	0.998	0.388	0.965	0.863	0.781	Korsmeyer-Peppas
IgG NPs PB-B suspended in thermosensitive gel	0.998	0.541	0.995	0.980	0.955	Korsmeyer-Peppas

Enzymatic activity of lysozyme

The biological activity of Lyz in the released samples taken at different time points was displayed in **Table 4.4**. It was observed that the enzyme activity in the released samples diminished with time due to the reason that macromolecules remained in the release medium for a long time interval. In addition, hydrophobic residues caused the protein adsorption on polymer surface that resulted in the loss of biological activity of the entrapped protein. A decrease in enzymatic activity can be attributed to storage conditions which may not be the expected case under *in vivo* conditions. It is anticipated that during the NP preparation ($W_1/O/W_2$ double emulsion), PEG (hydrophilic block) may have oriented at aqueous-organic interface. Hence, PEG may have reduced the interaction of Lyz with the hydrophobic polymer segments (PCL and PLA) which avoided the denaturation of large molecules. Therefore, it was concluded that enzyme activity of the entrapped Lyz was lower due to longer exposure in the release medium.

Table 4.4 Enzymatic activity of lysozyme estimated in the released samples (n=3)

Time (days)	**Specific enzyme activity (U/mg) x 10^3**	
	Release samples	**Controls**
1	50.3 ± 1.9	55.1 ± 3.2
7	41.2 ± 4.5	48.3 ± 3.8
14	33.6 ± 4.1	40.2 ± 4.3
21	24.5 ± 2.7	31.7 ± 3.8

Conclusion

The presented study discussed the synthesis and characterization of PB copolymers for the preparation of the composite nanosystem to achieve a controlled and long-term drug release profile of macromolecules. In order to eliminate the burst release phase, a novel composite nanosystem comprised of Lyz, Fab and IgG-encapsulated PB-A and/or PB-B NPs suspended in PB-C thermosensitive gel was successfully formulated. It was observed that the hydrodynamic diameter of macromolecules exerted its effects on drug release. The peppas model was the best fit model, suggesting that the release rate was controlled by diffusion and degradation of copolymers.

Results confirmed that the PB copolymer based composite delivery system are able to minimize the side effects associated with repeated every month intravitreal injections by lowering the injection frequency. In addition, the synthesized PB copolymers are biocompatible in nature and can be considered excellent biomaterials for ocular delivery. The enzyme activity of Lyz was observed up to three weeks. The integrity or stability of the protein molecule was not addressed in this work and an assessment of the compatibility of the polymers with the macromolecule remains to be elucidated in the future studies. However, the nanoformulations were optimized to achieve a high drug loading. This was essential so that a small volume of intravitreal injection containing a higher dose can be injected. This was also targeted in order to achieve a long-term delivery up to 3-6 months with an amount release of 2-10 µg/day. Overall, the outcomes from this study clearly suggested that the PB copolymers based control drug delivery system may serve as a promising platform not only for the back of the eye complications.

CHAPTER 5 [89]

COMPOSITE NANOFORMULATION FOR LONG TERM OCULAR DELIVERY OF IGG-FAB AND RANIBIZUMAB

Rationale

The back of the eye diseases such as macular edema (ME), diabetic macular edema (DME), diabetic retinopathy (DR) and age related macular degeneration (AMD) result in functional deficits and huge global costs. These diseases are major concerns for elderly patients and involve several side effects.(20) AMD is a major cause of central vision loss affecting the *retinal pigment epithelium* (*RPE*), Bruch's membrane, and choriocapillaris in the macular region of the neural retina. The disease is typically manifested in two forms; dry and wet AMD and is responsible for more than 80% of cases of severe visual loss and impairment (187). The hallmark of wet AMD is the formation of new anomalous blood vessels that typically arise from the choroidal vasculature that grow into the sub-retinal space. These neovascular vessels commonly hemorrhage and ultimately compromise vision (188). The degenerating tissues begin to release angiogenic growth factors that bind to specific receptors located on endothelial cells of preexisting blood vessels (189).

Vascular endothelial growth factor (VEGF) is a rate-limiting factor in angiogenesis and responsible for the growth of blood vessels. VEGF is associated with various pathophysiological processes affecting the eye including AMD and other retinal diseases such as DME, DR, retinal vein occlusion and vitreous hemorrhage. Elevated VEGF levels have been reported in AMD and DME patients (190). Similarly, VEGF is a

key mediator of blood-retinal barrier breakdown that leads to fluid leakage and the development of macular edema. Therefore, it is hypothesized that alternative or adjunct therapies using VEGF inhibitors (anti-VEGF) could be beneficial in reversing vision loss from DME and AMD (42). VEGF may also stimulate release of inflammatory cytokines, which can further reinforce the inflammation cycles and angiogenesis.

Currently, the first line therapies for these diseases include the intravitreal (IVT) injection of FDA approved anti-VEGF agents such as bevacizumab (Avastin), ranibizumab (Lucentis), and aflibercept (Eylea) (191). Although, beavcizumab a FDA approved drug is used only off label for back of the eye diseases. In general, IVT injection is the most common and effective route for delivery of anti-VEGF therapeutics as it can provide and maintain a high concentration of the therapeutic agents near the target tissues (RPE, Bruch's membrane). However, one of the major disadvantages of IVT injection is its poor patient compliance due to discomfort and inconvenience associated with frequent injections (192). Clinical trials for anti-VEGF agents further supported the need of frequent injections (monthly) for Lucentis (193), Avastin (194), and Eylea (188). This can further increase the cost of the therapy. Pharmacokinetic studies (195) suggested very short half-lives, of anti-angiogenic proteins in vitreous humor after IVT injections (9.82 days for bevacizumab(196), 10 days for ranibizumab in human subjects (197), and 5-6 days for aflibercept) (191). Retinal penetration of anti-VEGF agents after IVT administration has also been reported (198). Therefore, frequent IVT injections are required to inhibit capillary growth and leakage to maintain the clear vision. However, frequent IVT injection is not well tolerated by patients and

accompanied by numerous side effects such as endophthalmitis, retinal hemorrhage, and retinal detachment (199).

Several biodegradable polymeric nanoformulations have been extensively investigated for controlled delivery of protein therapeutics. Biodegradable polymers such as polycaprolactone (PCL), polylactic acid (PLA), polyglycolic acid (PGA), poly lactide-co-glycolide (PLGA), and polyethylene glycol (PEG) have been comprehensively studied for the preparation of protein encapsulated NPs (200), (201). Recently, many investigators have applied several block copolymers such as PLGA-PEG-PLGA, PEG-PCL-PEG, PLGA (202), and PEG-PLA (203) for the development of sustained release protein formulations. However, some reports indicated that protein/peptide molecules suffer from rapid loss of biological activity during formulation preparation, storage and/or release. Acylation with polymer degradation products (lactic acid and glycolic acid) (204, 205) further accelerates the hydrolysis of macromolecules due to lower pH induced by polymer degradation products. One of the possible causes for the loss of activity and/or irreversible aggregation of protein therapeutics is caused by the presence of hydrophobic interfaces in PLA, PGA, and PLGA based delivery systems. It is noteworthy that changes in protein/peptide structure, either physically or chemically, may cause immunogenicity and toxicity issues (182). As a result, there is an urgency to develop a biocompatible and biodegradable polymeric system which can provide sustained release of macromolecule therapeutics at near zero-order rate for longer durations without compromising the stability and functional activity of macromolecules.

Based on the above mentioned facts, the objective of this work is to synthesize a novel tailor-made PB copolymer based composite nanoformulation for the controlled and

sustained delivery of protein therapeutics for the treatment of the back of the eye diseases. Here, the composite nanoformulations were anticipated to minimize the burst release of macromolecule therapeutics to achieve a continuous zero-order drug release for longer duration.

Materials and methods

Materials

Poly (ethylene glycol) (PEG, 4 kDa), methoxy-PEG (550 Da), stannous octoate, ε-caprolactone, poly (vinyl alcohol) (PVA), lipopolysaccharide were procured from Sigma-Aldarich (St. Louis, MO). L-lactide and hexamethylene diisocynate (HMDI) were purchased from Acros organics (Morris Plains, NJ). Micro-BCA^{TM} assay kit was obtained from Fisher Scientific Inc., (Rockford, IL). Mouse TNF-α, IL-6 and IL-1β ELISA kits were obtained from e-Bioscience Inc. (San Diego, CA). Lactate dehydrogenase (LDH) estimation assay and CellTiter 96® AQueous non-radioactive cell proliferation assay (MTS) kits were obtained from Takara Bio Inc., (Otsu, Japan) and Promega Corp., (Madison, WI), respectively. RAW 264.7 cells were obtained from the American Type Culture Collection (ATCC, Manassas, VA) and TrypLE™ Express was from Invitrogen, Carlsbad, CA. All other reagents utilized in this study were of analytical grade and used as obtained from suppliers.

Methods

Synthesis of PB Copolymers

Novel PB copolymers, poly(caprolactone)-poly(lactic acid)-poly(ethylene glycol)-poly(lactic acid)-poly(caprolactone) (PCL-PLA-PEG-PLA-PCL i.e., PB-1) and methoxy-poly(ethylene glycol)-poly(caprolactone)-poly(lactic acid)-poly(caprolactone)-poly(ethylene glycol)-methoxy (mPEG-PCL-PLA-PCL-PEGm i.e., PB-2) were synthesized by ring-opening bulk polymerization method.(183, 206) PB copolymer for the preparation of NPs i.e., PB-1 was synthesized in two steps by sequential ring-opening polymerization reaction **(Figure 5.1)**. PEG (4 kDa) was utilized as macroinitiator and stannous octoate as catalyst. In the first step, triblock (TB) copolymer PLA-PEG-PLA (Figure 1, Step 1) was synthesized by polymerization of L-lactide on two open hydroxyl ends of PEG. L-lactide and stannous octoate (0.5% w/w) were added to anhydrous PEG and temperature was raised to 130°C. After 24 h, reaction mixture was dissolved in dichloromethane (DCM) followed by precipitation in cold petroleum ether. The precipitated polymer was filtered and dried under vacuum at room temperature for 24 h.

In the second step, PLA-PEG-PLA (TB copolymer) was reacted with ε-Caprolactone to synthesize the PB-1 copolymer (Figure 1, Step 2). Briefly, TB copolymer and ε-Caprolactone were added and the temperature was raised to 130°C under inert atmosphere. To the above mixture, stannous octoate (0.5% w/w) was added and the reaction was continued for 24 h. PB copolymer was then purified by cold ether precipitation method as described in the first step. The final PB-1 copolymer product was dried under vacuum and stored at -20°C until further use.

To synthesize the thermosensitive gelling copolymer (PB-2) (mPEG-PCL-PLA-PCL-PEGm), intermediate copolymer (mPEG-PCL-PLA) was synthesized by ring-opening bulk copolymerization as described in chapter-3. ε-Caprolactone was polymerized at the hydroxyl terminal of mPEG (550 Da) followed by second polymerization with L-lactide. The resulting intermediate copolymer was coupled using HMDI as a linker. The coupling reaction was continued for 8 h at 70°C. The synthesized PB-2 copolymers was purified by cold ether precipitation followed by drying under vacuum and stored at -20°C until further uses. A reaction scheme was illustrated in **Figure 5.2.**

Characterization of TB and PB copolymers

Proton nuclear magnetic resonance (^{1}H-NMR) spectroscopy

The ^{1}H-NMR spectra of TB and PB copolymers were acquired on a 400 MHz NMR instrument (Varian Inc., Palo Alto, CA). The chemical shift values were reported as δ in parts per million (ppm). The NMR samples were prepared by dissolving each copolymer in deuterated chloroform in a 5-mm outer diameter NMR tubes (Wilmad-Lab Glass, Vineland, NJ).

Gel permeation chromatography (GPC) analysis

The purity, MWs and PDI of PB copolymers were confirmed by GPC analysis. Polymeric samples were analyzed with a Waters 410 refractive index detector (Waters, Milford, MA). Briefly, samples were prepared by dissolving 5 mg of polymeric material in tetrahydrofuran (THF) whereas, THF was utilized as eluting agent at the flow rate of 1

mL/min. Separation was carried out on Styragel HR-3 column (Waters, Milford, MA). Polystyrene samples with narrow MW distribution were considered as standards.

Fourier transform infrared (FT-IR) spectroscopy

The FT-IR analysis of TB and PB copolymers was performed using Nicolet iS10 Spectrometer (Thermo Scientific, West Palm Beach, FL). The instrument was controlled by OMNIC™ Spectra™ software. The analysis was performed at 600 to 4000 cm^{-1} wave numbers. The spectra were automatically corrected with a linear baseline. No specific sample preparation method was used before the analysis.

X-ray diffraction (XRD) analysis

To analyze the crystallinity of copolymers, XRD analysis was performed using Rigaku MiniFlex automated X-ray diffractometer (Rigaku, The Woodland, TX) equipped with Ni-filtered Cu-Kα radiation (30 kV and 15 mA). The analysis was performed at room temperature at the scanning rate of 5°/min.

Phase transition (gelation) Study of PB-2 thermosensitive gelling copolymer

The sol-gel transition behavior of PB-2 copolymer was examined by test tube inverting method. The copolymer was dissolved in phosphate buffer saline (PBS, pH 7.4) at different concentrations ranging from 15-30wt% and incubated for 12 h at 4°C. Afterwards, 1 ml of PB-2 copolymer solution was taken in 4 ml glass vial with an inner diameter of 12 mm and placed in a water bath. The temperature of the water bath was raised slowly from 10 to 60°C at the rate of 1°C increment/min. The gel formation was observed visually by inverting the glass vials. A physical state of flow was characterized as sol phase whereas, a state of no flow was considered as gel phase.

In Vitro cytotoxicity of PB copolymers

Cytotoxic effects of PB copolymers on corneal and retinal cell lines were analyzed using Lactate Dehydrogenase *(*LDH) and cell viability (MTS) assays according to the supplier's instructions. The Human Corneal Epithelial (HCEC) cells were cultured were cultured at 37°C, humidified 5% CO_2/95% air atmosphere in a culture medium containing DMEM/F-12 supplemented with 10% (*v*/*v*) FBS (heat inactivated), 15 mM HEPES, 22 mM $NaHCO_3$, 100 mg of penicillin and streptomycin each, 5 μg/mL insulin, and 10 ng/mL of human epidermal growth factor following a previously published protocol.(207, 208) Cells of passage numbers between 20 and 22 were utilized for all the experiments.

The Retinal Pigment Epithelium (D407) cells were grown at 37°C, humidified 5% CO_2/95% air atmosphere in a culture medium containing DMEM supplemented with 10% (*v*/*v*) FBS (heat inactivated), 29 mM $NaHCO_3$, 20 mM HEPES, 100 mg of penicillin and streptomycin each, and 1% nonessential amino acids at pH 7.4. Cells of passage numbers between 67 and 70 were employed for all the experiments.(207) The growth medium was changed every other day. Both HCEC and D407 cells were cultured in a flask, harvested at 80–90% confluency with TrypLE™ Express (a superior replacement for trypsin).

LDH (cytotoxicity) assay

LDH assay was performed using previously published protocol with some minor modifications.(209, 210) Briefly, 100 μL of 1, 5 and 20 mg/mL of PB copolymers (PB-1 and PB-2) dissolved in acetonitrile (ACN) were aliquoted in 96-well plate. Plates were exposed overnight under UV light (laminar flow) for polymer sterilization as well as

evaporation of ACN. HCEC and D407 cells at the density of 1.0 x 10^4 were seeded in each well and incubated at 37°C, 5% CO_2 in humidified atmosphere for 48 h. After completion of incubation period, cell supernatants were analyzed for quantification of LDH using LDH assay kit as per supplier instructions. Absorbance of each well was measured at 450 nm using a DTX 800 multimode microplate reader (Beckman Coulter, Brea, CA). The LDH release (%) was calculated according to Eq. 5.1 and more than 10% of LDH release was considered as cytotoxic.

$$LDH\ release(\%) = \frac{Abs.of Sample - Abs.of negative control}{Abs.of positive control - Abs.of negative control} * 100 \qquad \ldots \text{Eq (5.1)}$$

MTS (cell viability) assay

Safety of PB copolymers was further established by performing *in vitro* cell viability (MTS) assay. The MTS (3-(4, 5-dimethylthiazol-2-yl)-2, 5-diphenyltetrazolium bromide) tetrazolium reduction) assay was performed according to a previously reported protocol with minor modifications.(209) As described earlier, PB copolymer solutions at the concentration of 1, 5 and 20 mg/mL were prepared, aliquoted and sterilized. After the sterilization, D4O7 and HCEC cells were seeded in 96-well plate at the cell density of 1.0 x 10^4, and incubated at 37°C and 5% CO_2 in humidified atmosphere for 48 h. At the end of incubation period, cell culture medium was aspirated and cells were incubated for 4 h (37°C and 5% CO_2) in the presence of 100 µL of serum free medium containing 20 µL of MTS solution. Absorbance of each well was measured at 450 nm using the above microplate reader. The percent cell viability was calculated according to Eq. 5.2 and PB

copolymers exhibiting more than 90% of cell viability were considered non-toxic and suitable for ocular applications.

$$Cell\ viability(\%) = \frac{Abs.of Sample - Abs.of negative control}{Abs.of positive control - Abs.of negative control} * 100 \qquad \ldots Eq\ (5.2)$$

In Vitro biocompatibility studies

Mouse macrophage (RAW-264.7) cells were maintained according to ATCC guidelines at 37°C, 5% CO2 and 95% humidity. Cells were plated in 96-well plates at a density of 1.0 x 10^4cells/well. Macrophage cells were grown in a similar way as explained for D407 and HCEC cells and utilized for further studies. PB copolymers were dissolved in ACN at the concentration of 1, 5, 10 and 20 mg/mL. Two hundred microliters of this solution were aliquoted in each well of 48-well cell culture plates and incubated for overnight under UV lights (laminar flow) for ACN evaporation and sterilization of resulting polymer film. After the sterilization, RAW-264.7 cells (5.0 x 10^4) were seeded in each well of cell culture plate and incubated for 24 h at 37°C and 5% CO_2. Cell supernatants were analyzed for the presence of cytokines i.e., TNF-α, IL-6 and IL-1β. Lipopolysaccharide (LPS) was used as positive control whereas, cells without any treatment were considered as negative control. Cytokines levels (in pg/mL) were measured by ELISA method according to manufacturer's (e-Biosciences, San Diego, CA) instructions. Standard calibration curves for TNF-α, IL-6 and IL-1β were prepared in the concentration range of 10-750 pg/mL, 5-500 pg/mL and 10-500 pg/mL, respectively.

Formulation of PB-1 copolymer based NPs (PB-1 NPs)

IgG-Fab loaded PB-1 NPs were prepared by water in oil in water ($W_1/O/W_2$) double emulsion solvent evaporation method. Briefly, IgG-Fab containing aqueous solution (W_1 phase) was emulsified in organic phase (DCM) comprising PB copolymers using probe sonication to form a W_1/O primary emulsion. The primary emulsion was further emulsified in aqueous phase containing 2% polyvinyl alcohol (PVA) using probe sonication to prepare a $W_1/O/W_2$ double emulsion. The resulting double emulsion was diluted with 2% PVA (W_3) under continuous stirring. Organic phase (DCM) was then evaporated under vacuum using a rotatory evaporator (BUCHI Labortechnik AG, Flawil, Switzerland). The NPs were separated by ultracentrifugation at 20,000 rpm for 30 min at 4°C. The NPs were washed twice with distilled deionized water (DDW), and centrifuged to remove the traces of PVA and unentrapped IgG-Fab. The purified NPs were freeze-dried with mannitol (3% w/v) and stored at -20°C until further uses. Similarly, Ranibizumab encapsulated NPs were prepared using above mentioned method.

Physicochemical characterization of PB-1 NPs

Size distribution analysis

The PB-1 NPs were analyzed for their particle mean diameter (PMD: in nm) and size distribution by Nanoparticle Tracking Analysis (NTA) using a Nanosight LM10 instrument (Nanosight, Salisbury, UK). To determine the particle size distribution of NPs in different media (PBS, DMEM without and with serum, RAW without and with serum), NPs samples at the concentration of 1 mg/mL were incubated at 37°C. The samples were analyzed at 0 h, 4 h, day 1, day 2, day 3, day 7, and day 10, at ambient temperature (22-

23°C) conditions using NTA analysis software. Basically, NTA determines the particle diffusion coefficient D_t by measuring the Brownian motion movement of the particle and then this employs the Stokes-Einstein equation (Eq. 5.3) to determine the particle size distribution in each sample (211).

$$D_t = \frac{TK_B}{3\pi\eta d} \quad \ldots \text{Eq (5.3)}$$

Here, T is the sample temperature, K_B is the Boltzmann's constant, and η is the solvent viscosity. Using D_t, the sphere-equivalent hydrodynamic diameter (d) of the particles was determined using Eq. 5.3.

Percent entrapment efficiency (%EE) and drug loading (%DL)

The %EE was estimated by the amount of protein in the supernatants obtained from NP preparation. Micro BCA™ protein estimation kit (Thermo scientific, IL) was employed for the estimation of total protein content. To analyze the %DL, 2 mg equivalent protein-loaded NPs were dissolved in 200 µL of dimethyl sulphoxide (DMSO). The resulting solution was analyzed by UV absorbance spectroscopy. Standard curve of IgG-Fab and Ranibizumab ranging from 31.25 to 2000 µg/mL was prepared in DMSO. The Eq. (5.4) and (5.5) were utilized for the calculation of %EE and %DL respectively.

$$\% \text{ Encapsulation efficiency} = \frac{(\text{Initial amount of drug} - \text{Amount of drug in supernatant})}{\text{Initial amount of drug}} * 100 \quad \ldots \text{Eq. 5.4}$$

$$\% \text{ Drug loading} = \frac{\text{Amount of drug in nanoparticle}}{\text{Total amount of drug and polymer}} * 100 \quad \ldots \text{Eq. 5.5}$$

In vitro drug release profile and kinetics of composite nanoformulations

In order to analyze the *in vitro* drug release profile of NPs, 1 mg of IgG-Fab equivalent freeze-dried NPs were suspended in 100 µL of aqueous solution of thermosensitive gelling polymer (PB-2) (15wt% and 20wt%). The resulting suspension was incubated at 37°C for 30 min. Once gel was formed, an aliquot (1 mL) of PBS (pre-incubated at 37°C) was added slowly. At predetermined time intervals, 200 µL of clear supernatant was collected and replaced with same volume of fresh PBS (preincubated at 37°C). Release samples were analyzed by Micro BCA^{TM} assay for total protein content. *In vitro* release data were expressed as cumulative drug released (%) with time. Similarly, 1 mg equivalent Ranibizumab equivalent freeze-dried NPs were suspended in 100 µL of aqueous solution of thermosensitive gelling polymer (PB-2) (15wt%, 17 wt%, and 20wt%) and *in vitro* drug release profile was determined by above mentioned protocol.

The drug release kinetics of IgG-Fab and Ranibizumab loaded NPs was analyzed by using zero order, first order, Higuchi, and Korsmeyer-Peppas models as given by Eq. (5.6), (5.7), (5.8) and (5.9), respectively(96, 212).

$$Q_t = Q_0 + K_0 t \quad \text{…Eq (5.6)}$$

$$\log Q_t = \log Q_0 + K_1 t/2.303 \quad \text{…Eq (5.7)}$$

$$Q_t = K_H t^{0.5} \quad \text{…Eq (5.8)}$$

$$\log Q_t/Q_\infty = n \log t + \log k \quad \text{…Eq (5.9)}$$

In these Equations, Q_t is the amount of drug released at time *t*, Q_0 is initial amount of drug in solution, K_0 is zero order release constant, K_1 is first order release constant, K_H is Higuchi dissolution constant, Q_t/Q_∞ is the fraction of drug released at time *t*, Q_∞ is the total amount of drug released, *k* is a kinetic constant and *n* is the exponent explaining the drug release mechanisms.(212) The exponent *n* is classified as Fickian diffusion ($n \leq 0.5$).

Evaluation of Anti-VEGF activity of ranibizumab released from composite nanoformulation

At predetermined time points, release samples were withdrawn and replaced with similar amount of PBS buffer to continue *in vitro* release study. Concentration of released drug in supernatant was estimated using micro BCA assay. After protein estimation, the released samples were subjected for indirect ELISA assay. For this Samples and standards were diluted to achieve 20ng/mL, 10ng/mL and 5ng/mL protein concentration. An indirect ELISA assay, developed and validated in our lab, was used for estimating anti-VEGF activity of ranibizumab from the released sample. Briefly, wells of flat-bottomed microtiter plates were coated with 100 µL of 0.5µg/mL VEGF in 50 mM carbonate buffer (pH 9.6) and incubated overnight at 4°C. Then, wells were washed with washing buffer (0.05% Tween 20 in PBS) and blocked with 1% BSA in PBS for 2 h at room temperature by gentle shaking. Serial dilutions of reference ranibizumab and samples were plated at 100 µL per well and incubated for 2 h at room temperature. Following incubation, wells were washed and incubated with secondary antibody solution (1:8000 dilutions in 1% BSA in PBS) for 45 min at room temperature. Finally,

100 µL of color developing agent was added to each well for the enzymatic reaction to occur. Color was allowed to develop, and the absorbance was measured at 450 nm. Subsequent to each incubation, plates were washed 3 times with 200 µL of a washing solution (0.05% Tween 20 in PBS).

Results and discussion

Synthesis and characterization of PB copolymers

PB copolymers (PB-1 and PB-2) were successfully synthesized by ring-opening bulk copolymerization of ε-Caprolactone, and L-lactide as given in **Figure 5.1 and 5.2,** respectively. The characterization of synthesized PB copolymer was performed as explained below.

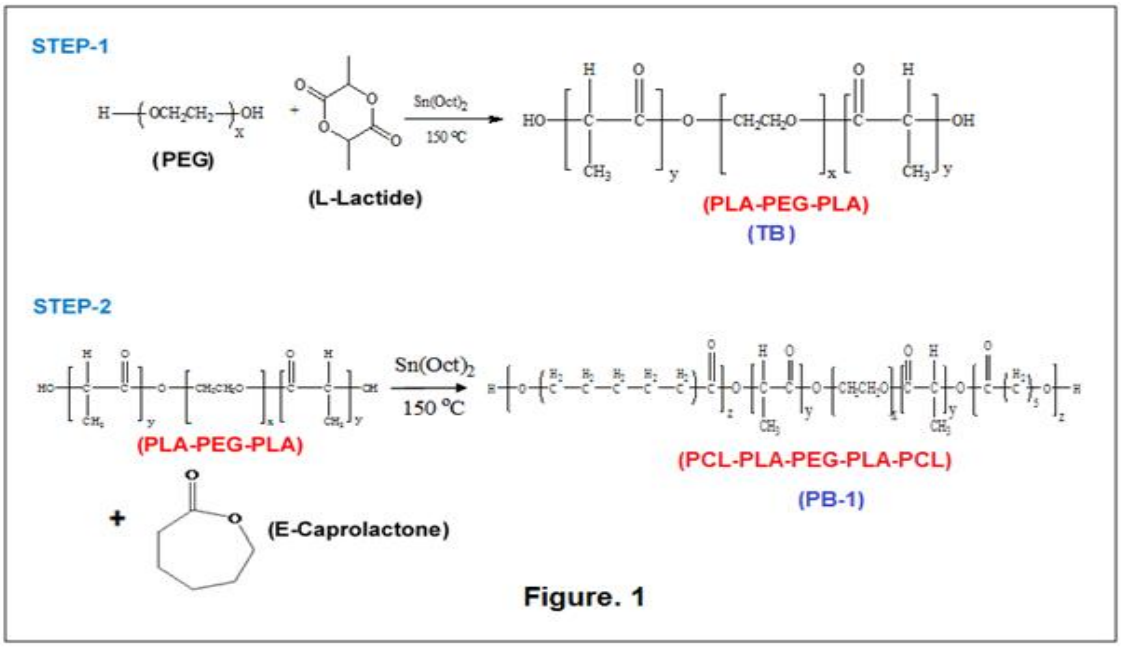

Figure 5.1 Reaction scheme for the synthesis of PB-1 (PCL-PLA-PEG-PLA-PCL) copolymer (Reproduced from Ref. 89).

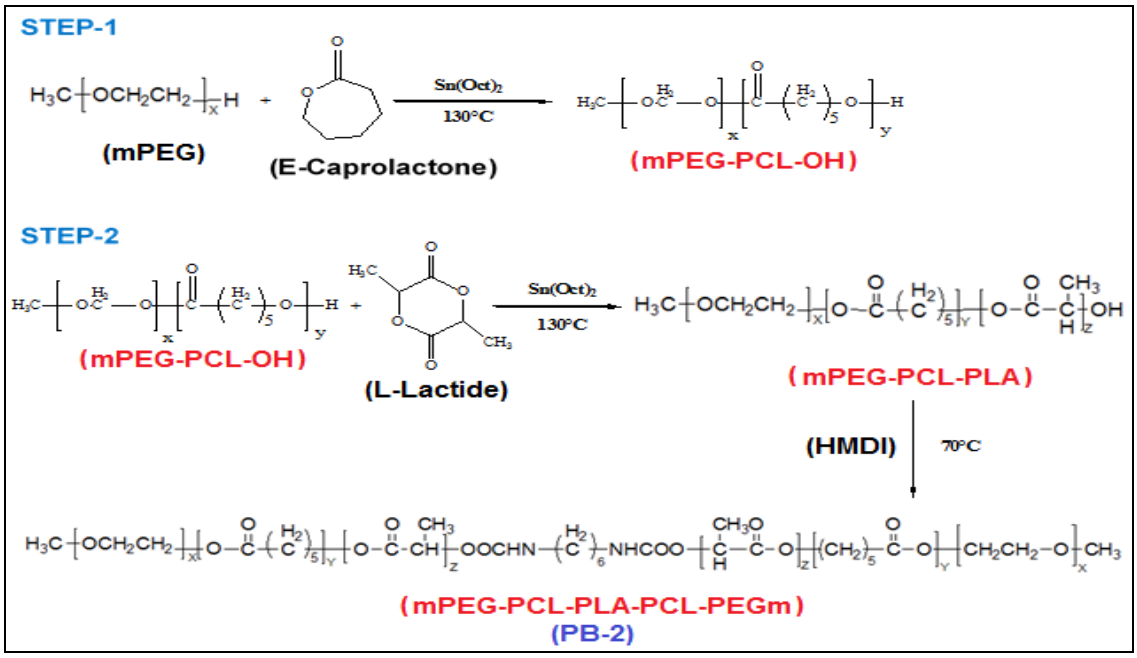

Figure 5.2 Reaction scheme for the synthesis of thermosensitive copolymer PB-2 (mPEG-PCL-PLA-PCL-PEGm). (Reproduced from Ref. 89).

The purity and molecular weight (Mn) of PB copolymers were calculated by ^{1}H-NMR spectroscopy **(Figures 5.3)**. The ^{1}H-NMR spectra of TB copolymer was given in Figure 3A. The typical ^{1}H-NMR characteristic peaks of PB-1 were observed at 1.40, 1.65, 2.30 and 4.06 δ ppm represented the methylene (–CH_2–) protons of -$(CH_2)_5$-, -OCO-CH_2-, and -CH_2OOC- of PCL units, respectively, (Figure 3B). A sharp peak at 3.65 δ ppm was attributed to methylene protons (-CH_2CH_2O-) of PEG. Typical signals at 1.50 (-CH_3) and 5.17 (-CH-) ppm were assigned for PLA blocks. Figure 3C of ^{1}H-NMR spectra of PB-2 copolymers (thermosensitive gel), depicted peaks a, b and c as methylene protons of the PCL block, while peaks e and f represent methyl and -CH- groups of PLA block, respectively. The ratio of mPEG and ε-Caprolactone was computed through proton

integration ratio of $–CH_2–$ proton peak at 3.65 (d) and 2.3 (c), respectively, and for L-lactide it was computed through –CH– proton peak at 5.10 (f).

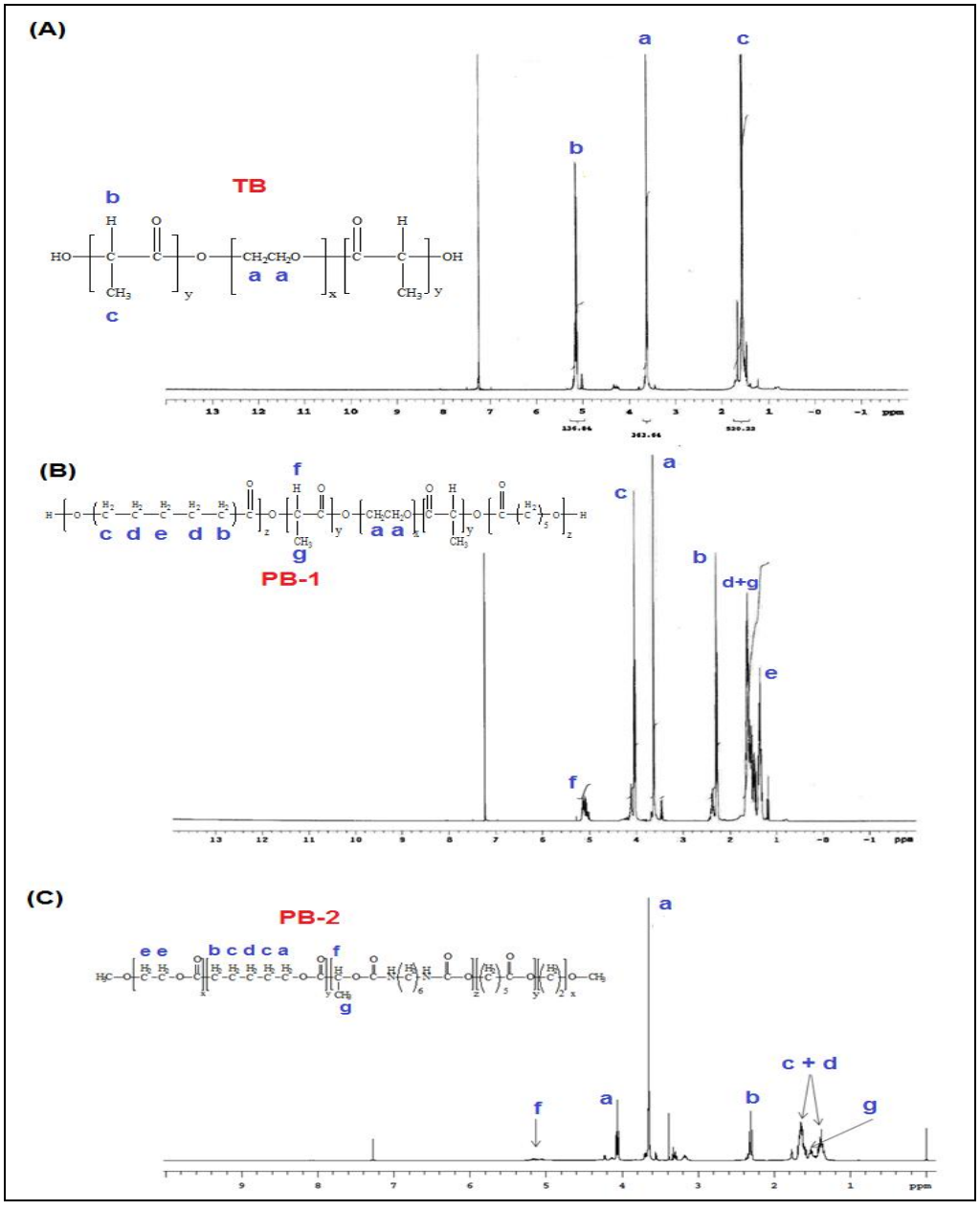

Figure 5.3 ^{1}H-NMR spectra of: (A) TB (PLA-PEG-PLA); (B) PB-1 (PCL-PLA-PEG-PLA-PCL); and (C) PB-2 (mPEG-PCL-PLA-PCL-PEGm) copolymers (Reproduced from Ref. 89).

The molecular weights (Mw and Mn) and PDI of copolymers was determined by GPC analysis **(Figure 5.4)**. A single peak of each polymer was observed describing unimodal MW distribution and absence of any other homo-copolymer block such as PEG, PCL or PLA. Moreover, MWs were very close to the feed ratio. The low PDI values of < 1.5 described the narrow distribution of MWs calculated by ^{1}H-NMR and GPC analyses (**Table 5.1).**

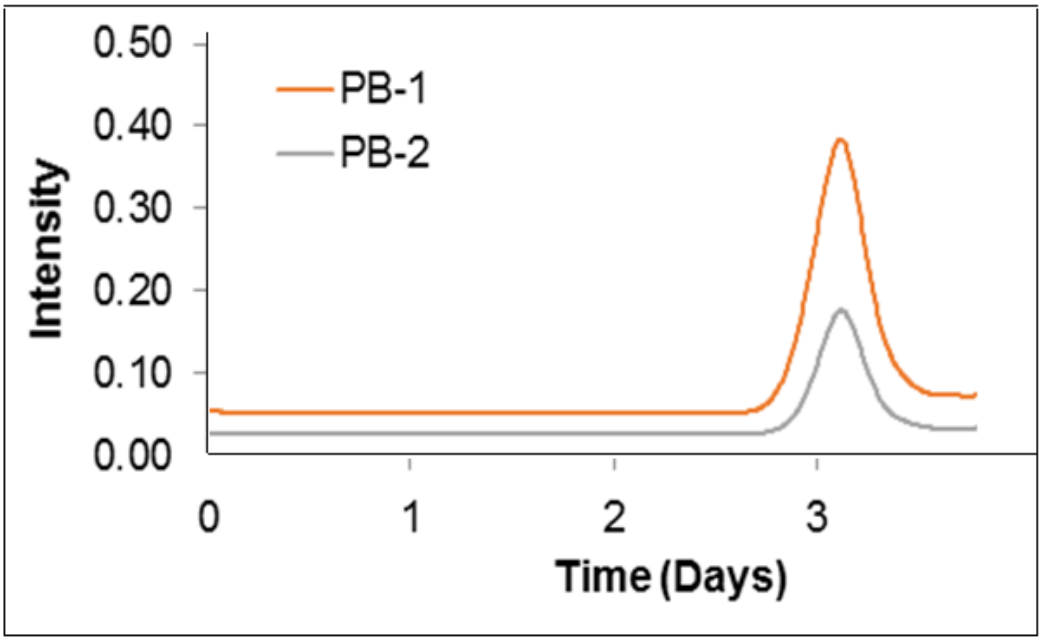

Figure 5.4 GPC chromatograms for PB-1 (PCL-PLA-PEG- PLA-PCL) and PB-2 (mPEG-PCL-PLA-PCL-PEGm) copolymer (Reproduced from Ref. 89).

Table 5.1 PB copolymer utilized for the preparation of composite nanoformulation (PB-1 NPs suspended in the thermosensitive gelling copolymer PB-2).

Name	**Structure**	**Total Mn[a] (theoretical)**	**Total Mn[b] (calculated)**	**Total Mn[c] (calculated)**	**Mw[c] (GPC)**	**PDI[c]**
PB-1	PCL_{10000}-PLA_{6000}-PEG_{4000}-PLA_{6000}-PCL_{10000}	36,000	32,400	39,425	38,232	1.39
PB-2	PEG_{550}-PCL_{825}-PLA_{550}-PCL_{825}-PEG_{550}	3,300	3,255	4,390	6,082	1.41

[a] Theoretical value, calculated according to the feed ratio. [b] Calculated from ^{1}H-NMR.

[c] Determined by GPC analysis.

The FT-IR spectra for the TB, PB-1, and PB-2 copolymers were presented in **Figure 5.5**. The C-H stretching band of PEG was observed at ~2876 cm^{-1} in TB copolymer (Figure 5.5A). However, the C-H stretching bands of PCL were observed at ~2942 cm^{-1} in PB-1 (Figure 5.5B) and PB-2 (Figure 5.5C) copolymers. The strong band in the region around 1730-1750 cm^{-1} was due to the stretching bands of the carbonyl groups present in the PLA, PCL, and PEG monomers. Overall, the FTIR spectra confirmed the functional groups of TB and PB copolymers.

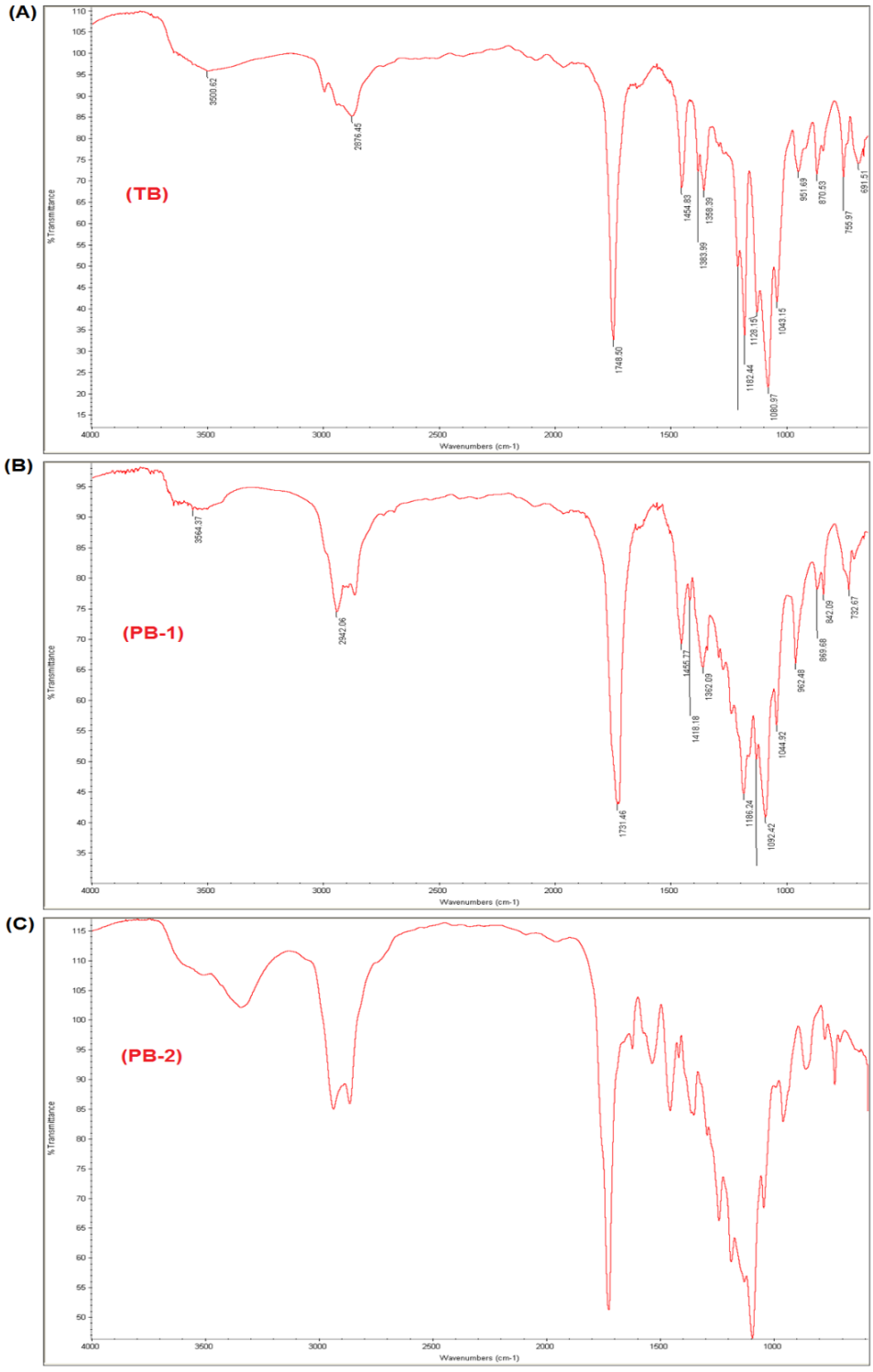

Figure 5.5 FT-IR spectra of: (A) TB (PLA-PEG-PLA); (B) PB-1 (PCL-PLA-PEG-PLA-PCL); and (C) PB-2 (mPEG-PCL-PLA-PCL-PEGm) copolymers (Reproduced from Ref. 89).

In order to assess the crystallinity and phase composition, the PB copolymers were analyzed for their XRD patterns (Figure 5.6). Interestingly, TB (PLA-PEG-PLA) copolymer exhibited a crystalline peak at 2θ = 16° and 19° but, in PB-1 crystalline peaks of PCL shifted to 2θ = 21.5°. A peak at 2θ = 24° was observed in both PB-1 and PB-2 copolymers. XRD patterns of TB and PB-1 indicated that PLA blocks retained their semi-crystalline structure even after covalent conjugation with the PCL blocks. Conjugation of PCL blocks at the terminals of TB copolymers exhibited shift in the intensity of the crystalline peak indicated the semi-crystalline structures of PB-1. Thus, the crystallinity of copolymers was easily controlled by the arrangement of polymer blocks in structural backbone. PB-2 **(Figure 5.6)** copolymer was devoid of any crystalline peak suggested its amorphous nature. Previously published reports(186) showed that a decrease in crystallinity significantly enhanced the degradation of block copolymers.

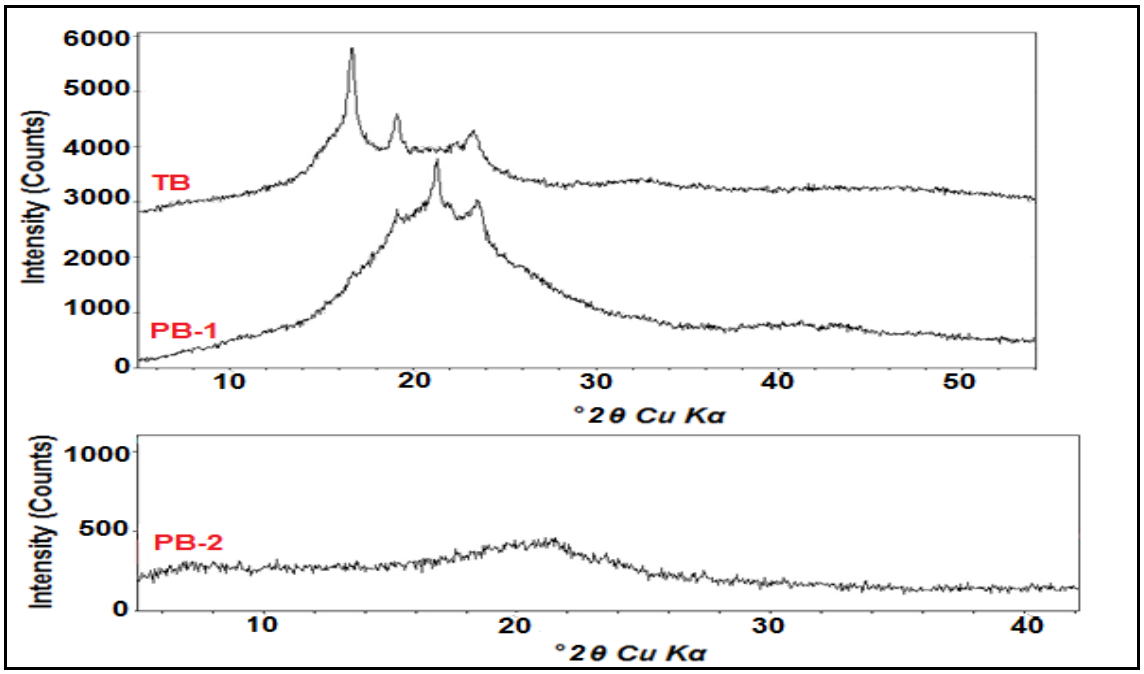

Figure 5.6 XRD patterns of TB (PLA-PEG-PLA), PB-1(PCL-PLA-PEG-PLA-PCL) and PB-2 (mPEG-PCL-PLA-PCL-PEGm) copolymers (Reproduced from Ref. 89).

Phase transition (gelation) of PB-2 thermosensitive gel

The thermosensitive gelling copolymers was amphiphilic in nature containing hydrophilic block (PEG) and hydrophobic block(s) of PCL and/or PLA. The aqueous solution of PB-2 was observed clear due to self-assembly of polymeric chains into micellar structure which showed aggregation upon increasing the temperature and resulted in the gel formation. However, upper gel-sol conversion was due to increased molecular motion of the hydrophobic chain of PCL and PLA. The aqueous solution of PB copolymers exhibited a sol-gel transition response upon increasing the temperature in a concentration range of 15wt%. The phase diagram (Figure 5.7) revealed the critical gel concentration (CGC) from the solution to gel state conversion at 37°C.

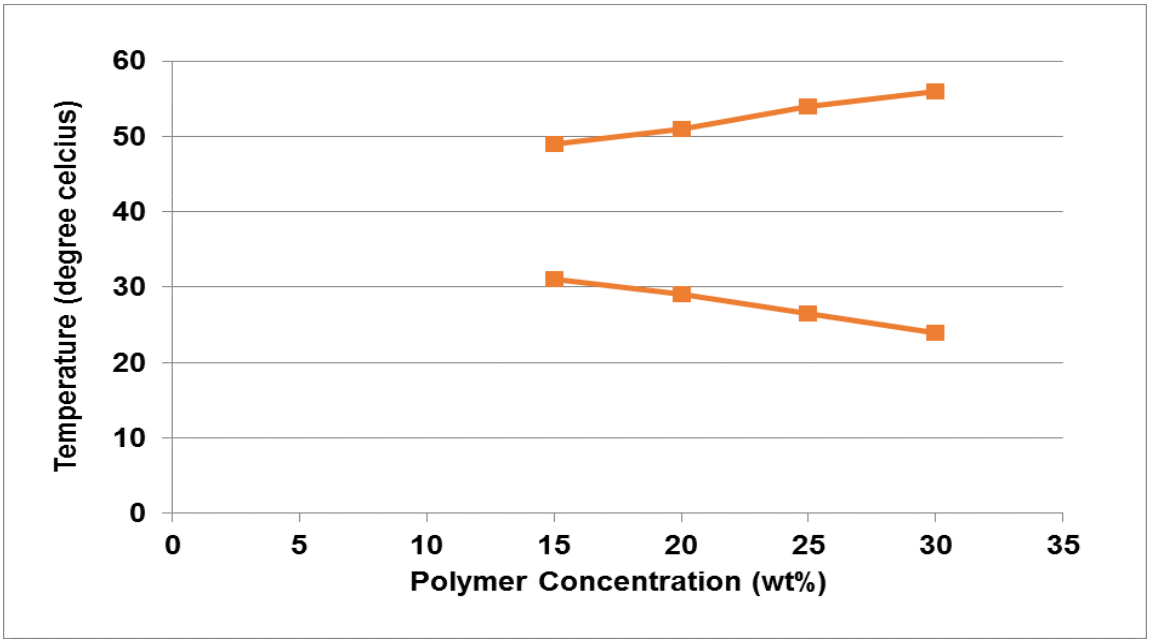

Figure 5.7 Phase transition (gelation) of thermosensitive gelling copolymer PB-2 (mPEG-PCL-PLA-PCL-PEGm) (Reproduced from Ref. 89).

In vitro cytotoxicity studies

LDH assay

In order to investigate the toxicity of PB copolymers with biological system, ocular cell lines (HCEC and D407 cells) were treated with 1, 5, 20 mg/mL of PB-1 and PB-2 for 48 h. LDH is a cytoplasmic enzyme, secreted in cell culture medium following cell-membrane damage. Less than 10% of LDH release was observed after 48 h exposure indicated a negligible toxicity with HCEC (Figure 5.8A) and D407 (Figure 5.8B) cell lines. Noticeably, results were comparable with negative controls whereas, significant differences were observed compared to the positive control (Triton-X). Triton X is one of the most widely used nonionic surfactants to analyze the cell cytotoxicity and viability. The toxicity of Triton-X arises because of the disrupting action of its polar head group on the hydrogen bonding present within the cell's lipid bilayer leading to a disruption of cellular structure.

MTS assay

To further confirm the cytotoxicity of PB copolymers, MTS cell viability assay was performed using a similar protocol as described above. In MTS assay, only metabolically active cells converted the tetrazolium compound to a formazan product. Hence, the concentrations of formazan products provided a direct estimation of cell viability. Results in Figure 5.9A and 5.9B demonstrated more than 90% cell viability for HCEC and D407 cell lines, respectively, after 48 h exposure to copolymer materials. The results suggested an excellent safety profile of block copolymers for ocular applications. No significant difference in the cell viability of copolymers was observed compared to the negative control. However, no toxicity was found with the *in vitro* cell-based (LDH

and MTS) assays as cultured cells can only address the ocular toxicity to certain extent especially when the exposure time was shorter (in a couple of hours only), and further *in vivo* evaluation will be needed.

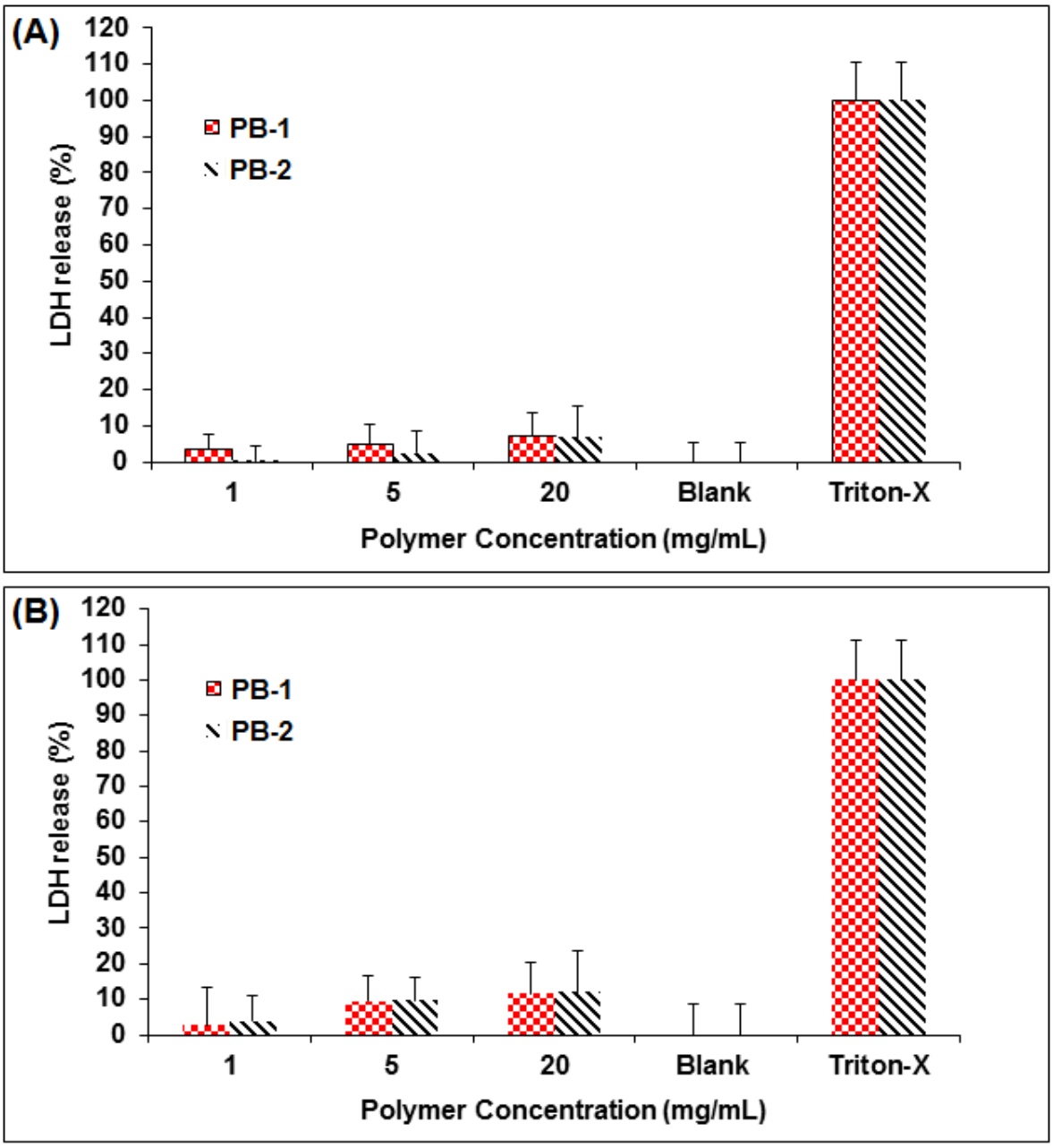

Figure 5.8 *In vitro* cytotoxicity (LDH) assay of PB-1 and PB-2 copolymers at different concentrations on: (A) HCEC cells, and (B) D4O7 cells. Results are given as mean ± SD, n = 3 (Reproduced from Ref. 89).

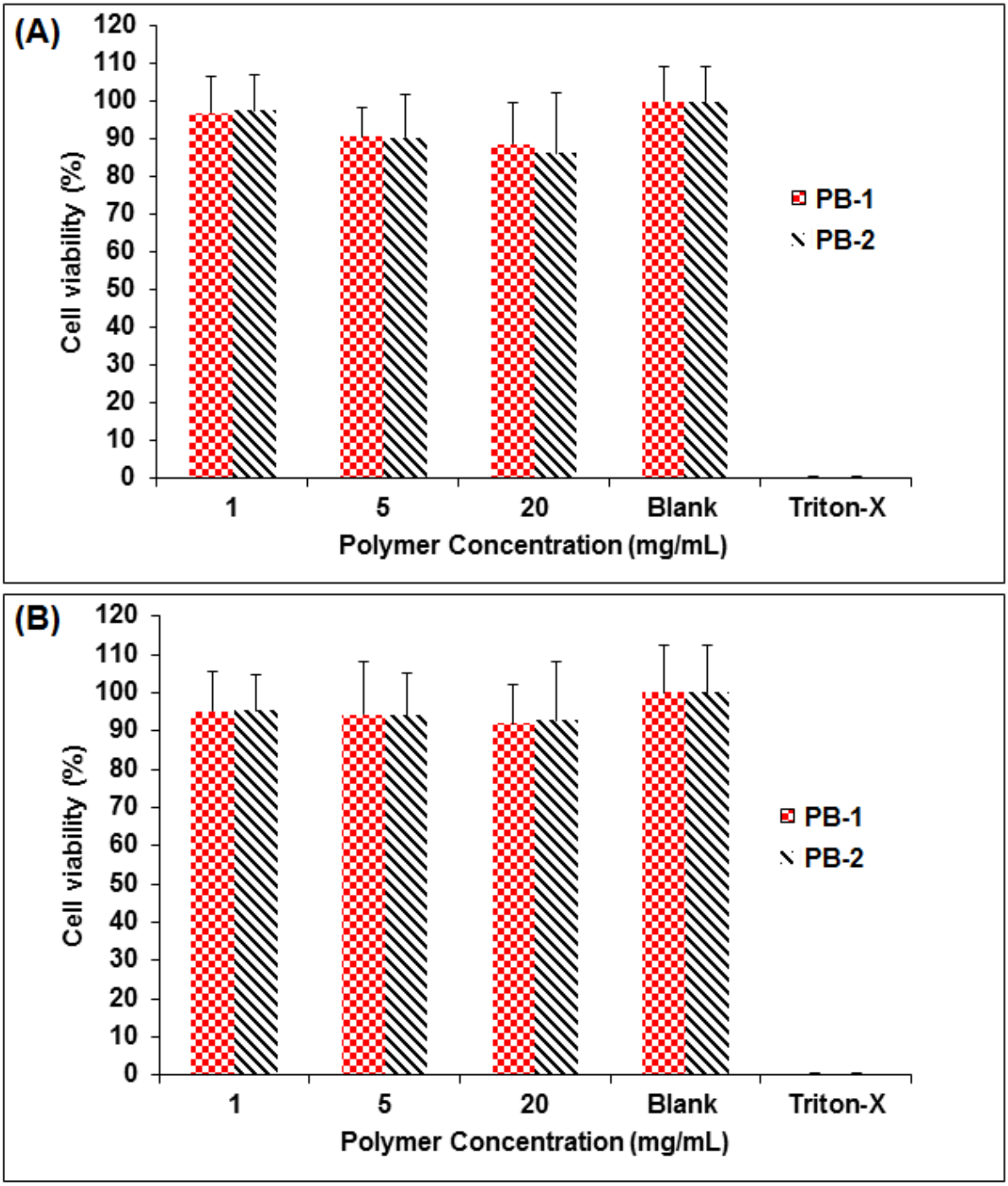

Figure 5.9 *In vitro* cell viability (MTS) assay of PB-1 and PB-2 copolymers at different concentrations on: (A) HCEC cells, and (B) D4O7 cell. Results are given as mean ± SD, n = 3 (Reproduced from Ref. 89).

In Vitro biocompatibility studies

Many investigators have utilized the *in vitro* cell culture model using RAW-264.7 cells for the estimation of biocompatibility of polymeric materials intended for human applications. In this study, we examined the cytokines (TNF-α, IL-6 and IL-1β) release in culture supernatant following 24 h exposure to PB-1 and PB-2 copolymers. Samples were analyzed via a sandwich ELISA assay. Results depicted in Figure 5.10A and 5.10B indicated that there was no significant release of TNF-α, IL-6 and IL-1β in both groups i.e., PB-1 and PB-2 compared to the negative control (cells without treatment). These results suggested that PB copolymers are safe for their clinical applications in humans.

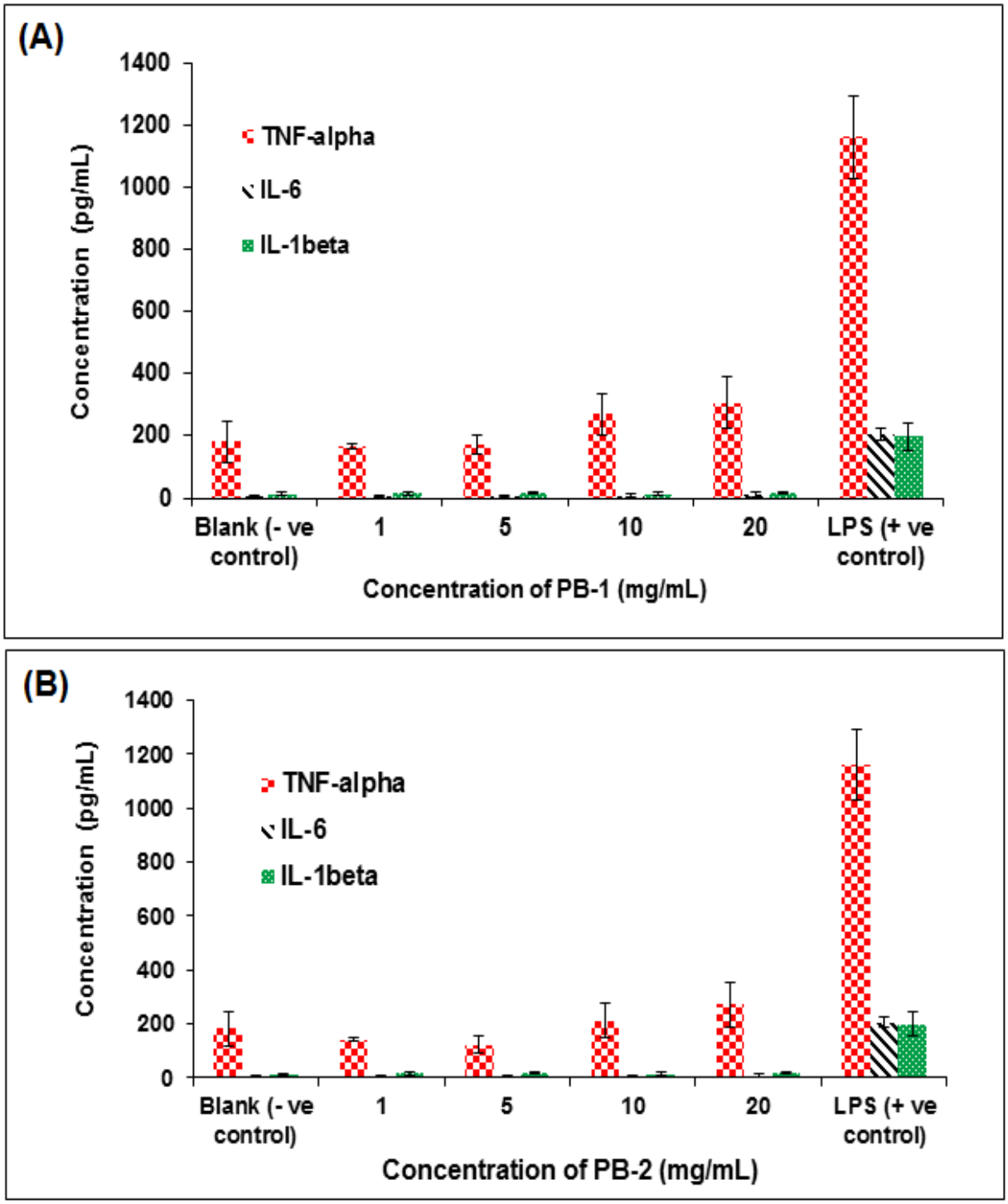

Figure 5.10 *In vitro* release of TNF-α, IL-6, and IL-1β from RAW 264.7 cells on exposure to: (A) PB-1, and (B) PB-2 copolymers. Results are given as mean ± SD, n = 3 (Reproduced from Ref. Ref. 89).

Formulation and characterization of PB-1 NPs

Size distribution analysis

IgG-Fab encapsulated PB-1 NPs were prepared by $W_1/O/W_2$ double emulsion solvent evaporation method. The mean particle size distribution of NPs in PBS was found in the range of ~150 nm **(Figure 5.11A)** and was consistent throughout the study in different media analyzed up to 10 days **(Figure 5.11B)**. These results confirmed the higher stability of NPs in different media. The NPs particle size distribution graphs were provided in PBS (Figure 5.11A & 5.11B), DMEM-with serum (Figure 5.11C & 5.11D), RAW-with serum (Figure 5.11E & 5.11F), DMEM-without serum (Figure 5.11G & 5.11H), RAW-without serum (Figure 5.11I & 5.11J), analyzed at 0 day and 10 days, respectively.

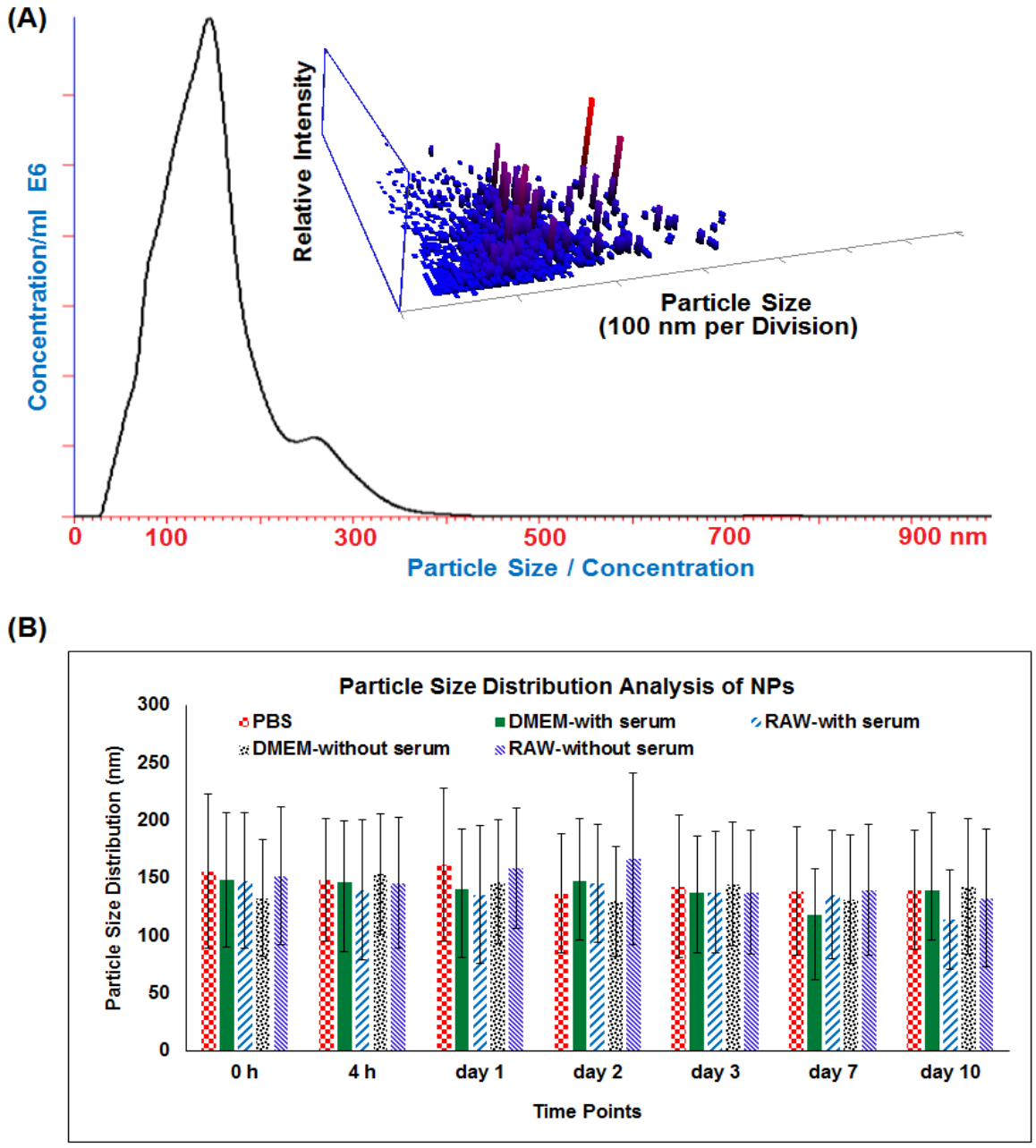

Figure 5.11 (A) Particle size distribution graph of PB-1 NPs in PBS. (B) Particle size distribution of PB-1 NPs in PBS, DMEM-with serum, RAW-with serum, DMEM-without serum, RAW-without serum, at 0 hr, 4 hr, day 1, day 2, day 3, day 7, and day 10, analyzed by NTA measurements. Results are given as mean ± SD, n = 3 (Reproduced from Ref. 89).

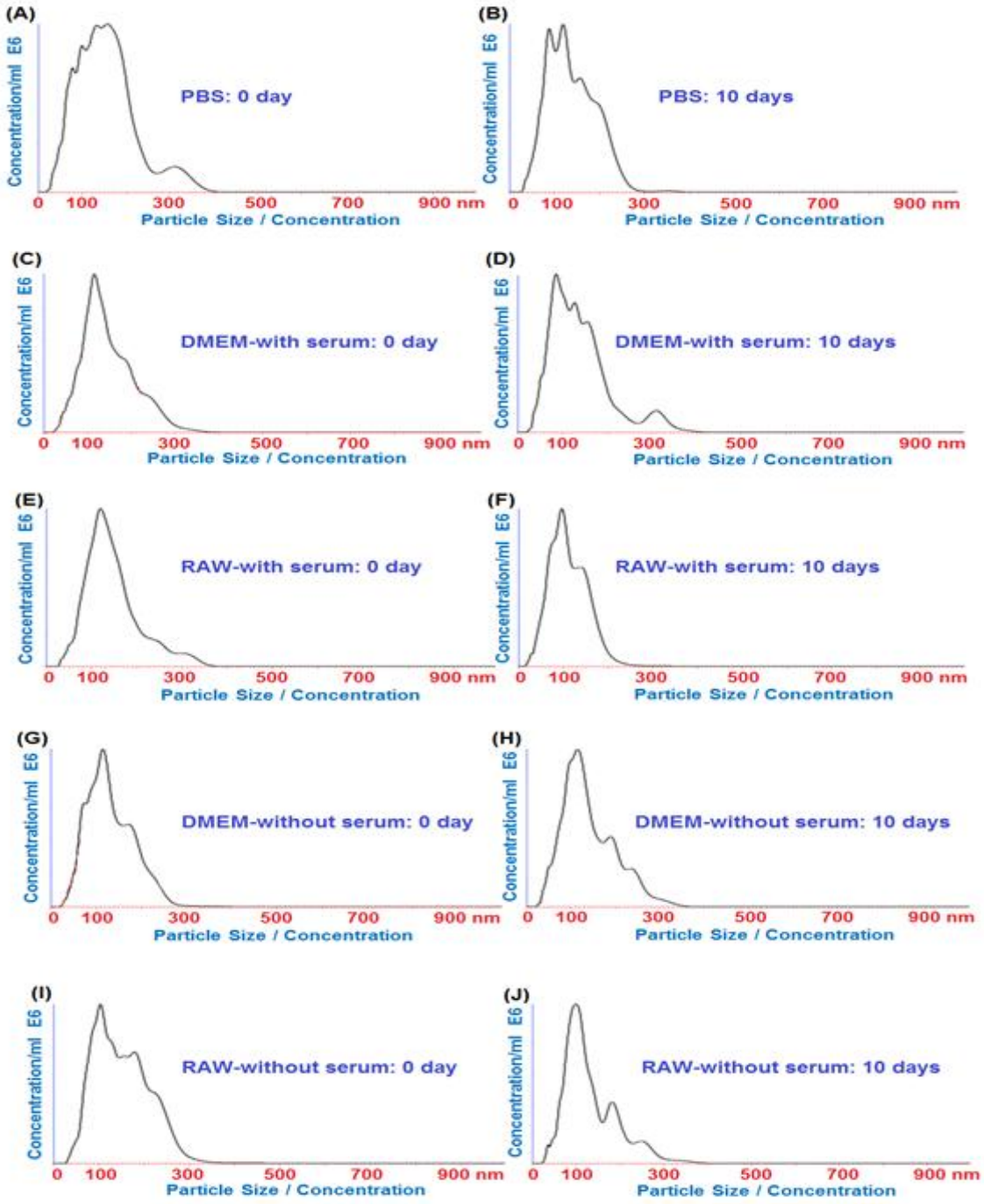

Figure 5.12 PB-1 NPs particle size distribution graphs in: PBS (A & B), DMEM-with serum (C & D), RAW-with serum (E & F), DMEM-without serum (G & H), RAW-without serum (I & J), at 0 day and 10 days, respectively, analyzed by NTA measurements (Reproduced from Ref. 89).

% EE and % DL

The %EE and %DL for IgG-Fab encapsulated in PB-1 copolymers were 66.64% ± 1.75 and 18.17% ± 0.39, respectively, (n = 3). Similarly, %EE and %DL for Ranibizumab encapsulated in PB-1 copolymers were 61.45% ± 2.89 and 16.99% ± 0.66, respectively, (n = 3). PB-1 NPs demonstrated a higher %DL relative to previously published results(182) which may be attributed to relatively high hydrophobicity of PB-1 copolymer synthesized in this study. During the solvent evaporation step, high hydrophobicity of PB-1 copolymer may allow more rapid polymer precipitation to form the NPs. This has been prevented the diffusion of IgG-Fab in external aqueous (W_2) phase. The lower volume of phase ratios (W_1, W_2 and O) compared to previously published method(182) diminished the protein partitioning in aqueous phase, thus, improved the drug loading efficiency In addition, reduction in organic phase volume had raised the polymer concentration that led to rapid polymer precipitation and thus, NP formation.

***In vitro* drug release profile and kinetics of composite nanoformulations of IgGFab**

The composite nanoformulations comprised of IgG-Fab-loaded (1 mg IgG-Fab equivalent) PB-1 NPs were suspended in thermo-sensitive gelling copolymer (PB-2) (15wt% and 20wt% gelling solution) and evaluated for the release profile. The solution then brought to 37°C which immediately transitioned the solution to solid hydrogel entrapping NPs throughout the polymeric matrix. The aqueous solution of PB-2 copolymer remained in a liquid state at room temperature but immediately transformed to hydrogel at physiological temperature of 37°C (sol-gel transition).

As depicted in **Figure 5.13**, burst release of IgG-Fab from composite nanoformulation was negligible relative to the burst release observed from PB-1 NPs alone (Data not shown here).(182) Moreover, with NPs alone, the release profile reached to > 90 % compared to composite nanoformulations (~20% with 20wt%, and ~40% with 15wt %) in ~35 days. In this study, the composite nanoformulation of IgG-Fab exhibited negligible burst release followed by a zero-order release as analyzed up to 80 days. This behavior may be due to the fact that when the NPs were suspended into the gel matrix, the matrix served as an additional diffusion barrier for the surface adsorbed drug. It also led to a zero-order release pattern of the encapsulated drug throughout the release period. The integrity or stability of the protein molecule was not addressed here and an assessment of the compatibility of the polymers with the protein is remains to be elucidated in future studies.

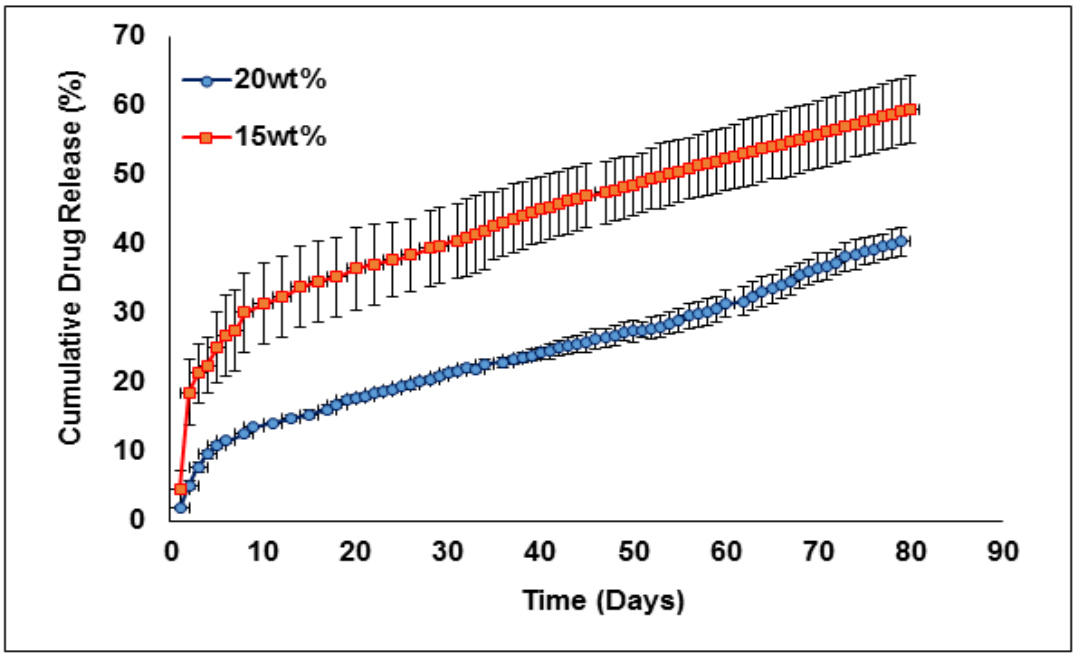

Figure 5.13 *In vitro* release of IgG-Fab from composite nanoformulation (15 wt% and 20 wt%). Results are given as mean ± SD, n = 3 (Reproduced from Ref. 89).

The release on day-1 was followed to be 4.6%, and 1.8% w/w for 15wt%, and 20wt%, PB-2 gel, respectively. PB-1 copolymer maintained ~4 µg/day for more than 2 months in both the gel concentrations of 15wt% and 20wt%. Theoretically, for 15wt% gel ~430 µg of drug remained in formulation after 80 days with projected release for an additional 120 days. For 20wt% gel, ~600 µg of drug remained in formulation after 80 days. Therefore, it can be projected that release could be sustained for additional 150 days. The wt% of gelling copolymer had a significant effect on the initial burst release and higher the gel concentration, minimal burst release was observed. Overall, the release profile was slower with 20wt % gel compare to 15wt % gel.

The drug release kinetics from the PB-1 Fab NPs in thermosensitive gels (15wt %) and (20wt %) was analyzed using various *in vitro* kinetic models. The parameters obtained were given in **Table 5.2**. Based on the r^2 values observed, 15wt% and 20wt% composite nanoformulations followed the Peppas model. To determine the drug release mechanism, the Korsmeyer-Peppas model was further applied. It was observed that the drug release from 15wt% composite nanoformulation occurred through Fickian diffusion *($n < 0.5$),* whereas, 20wt% composite nanoformulation followed anomalous (non-Fickian) transport (diffusion and erosion controlled release) mechanism since $0.5 < n < 1$.

Table 5.2 *In vitro* IgG-Fab release kinetic models of composite nanoformulation (PB-1 NPs suspended in the thermosensitive gelling copolymer PB-2).

Composite nanoformulations	**Zero order release model**	**First order release model**	**Higuchi release model**	**Korsmeyer-Peppas model**
	r^{2} [a]	r^{2} [a]	r^{2} [a]	r^{2} [a], (exponent *n*)
PB-1 NPs suspended in thermosensitive gels PB-2 (15wt %)	0.939	0.967	0.987	0.993, (0.351)
PB-1 NPs suspended in thermosensitive gels PB-2 (20wt %)	0.986	0.988	0.984	0.989, (0.609)

[a] Correlation coefficient.

In vitro drug release profile of composite nanoformulations of ranibizumab

In vitro release studies were performed by suspending 1 mg equivalent ranibizumab equivalent NPs prepared from PB-I in 100 µL solution with 15 wt%, 17 wt% and 20 wt% gelling polymer. The release study was performed as described earlier. The steady state sustained release was observed with zero order as shown in **Figure 5.14.** The release was found to be 7%, 4.51%, and 2.52% for 15 wt%, 17 wt% and 20 wt%, respectively for day 1. PB-I copolymer maintains ~ 4 µg/day for more than 2 months with

all three studies. For 15 wt% gel ~350 µg of drug remained in formulation after 84 days with release rate, release that can be sustained for 106 days. For 17 wt% gel ~ 460 µg of drug is remaining in formulation after 74 days and release is sustained for ~215 days more. For 20 wt% gel, ~ 480 µg of drug is remaining in formulation after 74 days and release is sustained for further 221 days. Wt% of gelling polymer had effect on release rate. Higher the concentration of gel, minimal burst release was observed. (Release kinetics of ranibizumab not shown here).

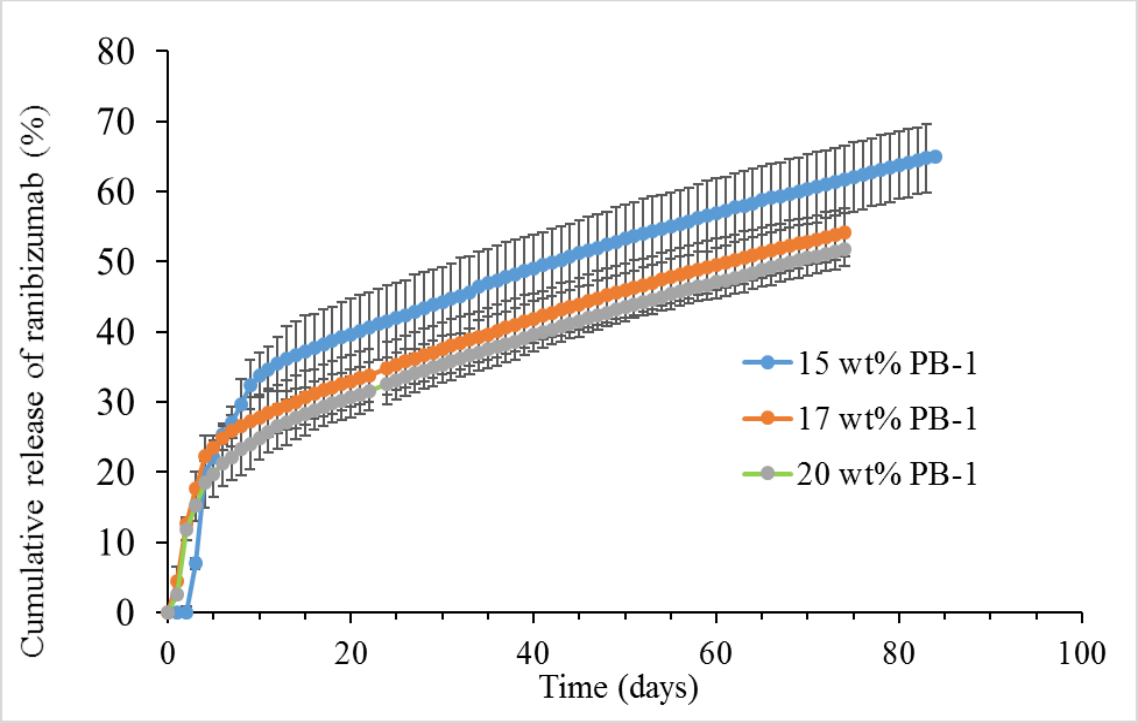

Figure 5.14 *In vitro* release of ranibizumab from NPs prepared with PB-1 suspended in gelling polymer of different wt %. Results are given as mean ± SD, n = 3.

Evaluation of anti-VEGF activity of ranibizumab released from composite nanoformulation

Indirect ELISA was used to examine anti-VEGF activity of ranibizumab following release from composite nanoformulation. Results of anti-VEGF activity are given in **Table 5.3,** results are given as mean ± SD, n = 3. Ranibizumab released from composite nanoformulation retained its VEGF binding activity. Results of both the studies clearly indicate that ranibizumab was stable thorough out the process of NP preparation. The plausible explanation is that drug remains inside the PEG core by less exposing the drug at the oil/aqueous interphase provided shielding effect to ranibizumab against sonication. It is plausible that PB copolymer possess lower mass of lactic acid and no glycolic acid block which produce very low amounts of lactic acid, thereby eliminating or reducing the possibilities of protein degradation.

Table 5.3 Anti-VEGF activity form released sample

Days	**Concentration (µg/mL)**	
	Micro BCA	Indirect ELISA
1	25.25 ± 4.81	20.1 ± 5.29
7	9.98 ± 1.89	8.1 ± 2.63
15	5.72 ± 0.71	4.88 ± 2.56
30	4.31 ± 0.82	4.54 ±2.07

Conclusion

This study discussed the synthesis and characterization of novel PB copolymers for the formulation of NPs and thermosensitive gelling copolymer to achieve the long term, zero order release of both Fab fragments of similar MW. A novel composite nanoformulation comprised of IgG Fab and Ranibizumab-loaded PB-1 NPs suspended in PB-2 thermosensitive gelling copolymer was successfully formulated and characterized. IgG-Fab and Ranibizumab encapsulated NPs suspended in thermosensitive gelling copolymer demonstrated a continuous zero-order release, thus avoiding the potential toxicity in the target tissues due to burst release effect. The synthesized PB copolymers were non-cytotoxic and biocompatible in nature attributes to superior biomaterials for ocular delivery. The NPs possess higher stability in the cell culture (DMEM and RAW with and without serum) and PBS medium. In addition, indirect ELISA confirmed retention of physical stability, VEGF binding activity and antigen binding capacity of ranibizumab. Such a copolymer based delivery system can minimize the side effects associated with frequent IVT injections. These outcomes clearly suggested that a PB copolymer based controlled drug delivery system developed here may serve as a promising platform for back of the eye complications.

CHAPTER 6

SUMMARY AND RECOMMENDATIONS

Summary

Developing a nanoformulation to provide a long term release of macromolecules for back of the eye diseases is a challenging task. The ideal characteristics to obtain such formulation are; (a) minimal burst effect and biphasic drug release profile (b) high drug loading in a small injection volume (≤ 100 μL) (c) syringibility: easy to administer through 27G needle, (d) ensure a higher stability of macromolecules, (e) provide controlled/sustained drug release profile throughout the release period at least for 4-6 months, and (f) the time required for the biodegradation of formulation should not be more than 1.5 times the drug release profile. Considering the above objectives, the rationale behind developing a novel biodegradable and biocompatible PB copolymer based biomaterial was to achieve controlled drug delivery over a period of several weeks from a single IVT injection.

In chapter 1, a brief overview of back of the eye diseases and available treatment was provided. Ocular drug delivery to back of the eye, ocular barrier, routes of administration has also been highlighted. A concise discussion on FDA approved polyester biodegradable polymer was provided that has been utilized to improve ophthalmic drug delivery. Nanotechnology based drug delivery systems for the posterior segment of eye diseases with their advantages and limitations are discussed. Moreover, the ideal characteristics, therapeutic potential, advantage and limitations of macromolecule for ocular drug delivery have been summarized.

In chapter 2, the objective and rationale of developing NPs and composite nanoformulations have been discussed. In order to achieve the aforementioned goal, biodegradable and biocompatible PB copolymers for thermosensitive gel and NPs have been synthesized. PB copolymers are composed of FDA approved polymeric blocks such as PEG, PCL, and PLA/PGA. Each block plays an important role such as presence of PEG helps to improve stability of NPs by reducing NP aggregation. PCL is a slow degrading semi-crystalline polymer which improves the loading of large molecules in NPs and sustains the drug release for a longer duration. It is important to synchronize polymer degradation profiles with the drug release in order to avoid accumulation of the formulation in the limited vitreous cavity. Previous reports suggested that poor degradation of the PCL is attributed to its crystalline nature; hence reduction in the crystallinity of PCL may improve its hydrolytic and enzymatic degradation. Covalent conjugation of PCL to PLA chains can reduce crystallinity resulting in faster degradation of PCL. In addition, to minimize the burst effect and to extend the duration of drug release; a composite nanoformulation approach has been introduced.

In chapter 3, synthesis and characterization of PBG-1 (PLA-PCL-PEG-PCL-PLA) and PBG-2 (PEG-PCL-PLA-PCL-PEG) copolymer based thermosensitive gelling polymers have been discussed. Arrangement of polymer blocks exhibited significant effect on the sol-gel transition curve and kinematic viscosity of respective aqueous solutions. PBG-2 copolymer demonstrated noticeably lower kinematic viscosity of aqueous solution at 25°C than PBG-1 copolymers. Cell viability and biocompatibility studies suggested that PCL, PLA and PEG based block copolymers were compatible with D407 ocular cell lines. Octreotide, IgGFab, IgGFab' and IgG-loaded PBG-1 and PBG-2

thermosensitive gels exhibited sustained release profile. The release profile was depended on the hydrophilic and hydrophobic nature of the gelling polymer in addition to the MW of the macromolecules. Results of release kinetics modeling suggested that the Korsmeyer-Peppas model was best fitted and the exponent values (n value) were ranging from 0.272-0.386, indicating diffusion controlled release of macromolecules. It is anticipated that a further longer release profile can be obtained by altering block composition or change in hydrophobicity and/or hydrophilicity of the gelling polymer. The drug release pattern was in conjunction with approved facts that amorphous and hydrophilic polymers degrade fast. CD spectroscopy results revealed no changes in secondary structure of IgG. Further, the degradation of hydrophilic gelling PBG-2 copolymers was performed at four different conditions. The gelling polymer was degraded at a faster rate initially, due to its amorphous and hydrophilic nature. The rate of degradation was faster in borate buffer (pH 9.0) incubated at 37°C. Accelerated conditions such as pH 9.0 (37°C) and high temperature (40°C) exhibited MW loss of ~45% and ~40% w/w, respectively, which were significantly higher compared to the MW loss observed under the normal conditions (pH 7.4, 37°C) i.e., ~35% w/w. No significant effect of enzymes was observed on polymer degradation. Approximately 50% MW loss was noticed in 5 days and a similar degradation pattern was observed under all four conditions. After the initial hydrolytic degradation of mPEG, PCL was exposed at the terminal. Therefore, the degradation was slower and the MW was fairly constant till 45 days of analysis. The *in vivo* assessment of PBG-2 provided a safe environment and was well tolerated in the rabbit eyes analyzed up to 33 weeks. Over all, a biocompatible and biodegradable polymeric gel formulation was developed to sustain the drug release

profile. However, thermogelling system exhibited the sustained drug release upto only ~20 days, which was shorter than the desired target profile (4-6 months). Moreover, it also demonstrated a significant burst drug release effect.

In chapter 4, a composite nanoformulation has been designed to study the effect the *in vitro* release of macromolecule [(Lyz (14 kDa), Fab (48kDa) and IgG (150 kDa)] encapsulated PB-NPs suspended in PBG thermosensitive gelling polymer. The dual approach had successfully diminished the burst release effect and exhibited nearly zero-order release throughout the release period. This behavior may be due to the fact that when NPs were suspended in a gel matrix, entangled polymer chains of thermosensitive gel may have served as an additional diffusion barrier for the surface adsorbed drug. The polymer matrix had prevented the dumping of surface adsorbed dose, thus eliminating burst drug release effect and avoiding any possibility of dose dependent toxicity. A series of PB copolymers from low to high MWs have been synthesized and evaluated for the preparation of NPs. PB copolymers were successfully synthesized by ring-opening bulk polymerization reaction and characterized by ^{1}H-NMR, gel permeation chromatography (GPC) and X-ray diffraction (XRD) spectroscopy analyses. IgG, IgG-Fab and Lysozyme-loaded PB-NPs were studied to analyze the effects of MW, polymer composition on various formulation parameters such as %EE, %DL and *in vitro* drug release profile. Results demonstrated that crystallinity of PB copolymers was easily modulated by altering the ratio of PLA/PCL. Moreover, MW, crystallinity and copolymer composition exhibited significant effect on EE, DL and *in vitro* release profile. The PB copolymers composed of high MW demonstrated a high EE (~63%), and DL (~8%) with sustained drug release profile up to ~60 days which was significantly higher than PBG copolymers

(Chapter-3). It may be possible that IgG-Fab, IgG and catalase have very less diffusivity through polymer matrix owing to large MW and hence their release was mainly controlled by degradation of polymers. Enzymatic activity of released Lyz from PB-NPs and control was compared upto one month. The enzyme activity in the released samples diminished with time. *In vitro* cell culture study on macrophage cell lines (RAW-264.7) established a higher biocompatibility of PB copolymers for ocular applications. It was hypothesized that the *in vitro* release of macromolecules with similar MWs behaves very identical in the same polymer matrix. Although, several positive results were observed, a poor DL has been observed in this study. Therefore, the objective of the next study was to optimize several formulation parameters to achieve a high drug loading. In addition, the effect of *in vitro* release of similar MW of macromolecules was investigated.

In chapter 5, high MW hydrophobic PB copolymers to sustain the drug release for a significantly longer duration have been synthesized. Hydrophobic PB copolymers were synthesized with high MW of PLA and PCL but keeping the MW of the PEG similar. The NP preparation method was successfully optimized with respect to polymer hydrophobicity, drug to polymer ratio, and phase volumes to achieve a high DL. With optimized NP preparation methods, more than 15% w/w of loading for IgG-Fab and ranibizumab in PB NPs was achieved. PB NPs encapsulating IgG-Fab and ranibizumab were also evaluated for their sustain release behavior. The NPs depicted negligible burst release phase. According to our results, proteins with similar MWs behave very similar during NP preparation with same PB copolymers. Hence, they exhibited very similar %EE, %DL and *in vitro* release profile. IgG-Fab and Ranibizumab encapsulated NPs suspended in thermosensitive gelling copolymer demonstrated a continuous zero-order

release, thus avoiding the potential toxicity in the target tissues. In addition, indirect ELISA method confirmed retention of physical stability, VEGF binding activity and antigen binding capacity of ranibizumab. Such a copolymer based delivery system can minimize the side effects associated with frequent IVT injections. Moreover, cell viability, cytotoxicity and biocompatibility studies revealed non-toxic and biocompatible nature of PB copolymers. As per the result obtained and with the projected release profiles for IgG-Fab, and ranibizumab, a sustain drug release for more than 6 months can be achieved from these novel systems. In summary, the composite formulation approach can serve as a delivery platform of siRNA, peptides, proteins and antibodies in the treatment of ocular diseases. This technology is limited to ocular applications but may also be used for any chronic diseases where sustained delivery of macromolecules is required.

Recommendations

Despite being successful in attempting high drug loading and long term release, these polymeric systems were not useful to release the desired amount of drug for a long period of time. The target drug dose of 4µg/day was observed up to 11 weeks of analysis however, after that the release amount was decreased and reached to a level of ~3.5µg/day in 12 weeks of analysis. Therefore, there is a need to develop the formulations that can provide the desired amount of drug release per day for a longer period (targeted for 3-6 months). According to the results observed, the release of IgG-Fab and ranibizumab from the composite nanoformulations was mainly governed by the degradation of polymers. Hence, it is hypothesized that by improving the hydrolytic

degradation of PB copolymers, a higher rate of macromolecule release can be achieved. This can be obtained by changing the order of block copolymers to random block arrangements or tetrablock copolymer.

The PB copolymer (PCL-PLA-PEG-PLA-PCL) investigated in this work showed reduced crystallinity; however, there was a reduction in the amount of drug release in the later phase. It may be plausible due to the fact that the polymer degrades rapidly due to the amorphous nature of PB copolymer. It was anticipated that after the degradation of the terminal flank i.e. PCL, PB copolymer may generate the TB copolymer (PLA-PEG-PLA) which may be slow in degradation resulting in the slower release. Therefore, newer arrangements of the block copolymers i.e. random block or tetrablock copolymers may be useful for further study. It is anticipated that new arrangement polymer degrades rapidly while leaving a small fragment comprised of homopolymers (PCL or PEG), or diblock copolymers (PCL-PLA or PLA-PEG). In addition, it is of prime importance to investigate the stability of proteins in presence of excipients such as sugars (sucrose, trehalose, and glucose), tweens and other supplemental additives such as retinol.

It has been well documented that the proteins at elevated concentration in aqueous solution undergoes irreversible aggregation (formation of trimers and tetramers) resulting in degradation. Hence, many of the in situ gel systems with high loading have reported incomplete release of protein *in vitro*. Therefore, to develop the next generation delivery systems for macromolecules, it is obvious to understand the interaction of protein molecules with polymer surfaces, protein-excipient interaction/compatibility and *in vitro -in vivo* correlation of released profile to understand the complete release.

HIP complexation is another approach may be useful to enhance the encapsulation of various macromolecules and to develop sustained release delivery systems using PB copolymers. It was well documented that freeze dried protein may be generated using HIP complexation approach without aggregation. HIP complexation can be tailored by changing several parameters such as size, structure, pKa, pH of complexation, ion pairing agents and number of charges of protein/peptides. HIP complexation may protect macromolecule against stress conditions such as presence of organic solvents, sonication and may improve protein stability during formulation and storage.

PART II: DEXAMETHASONE NANOPARTICLE TO DEVELOP AN *IN VITRO* MODEL FOR GLAUCOMA

CHAPTER 7

INTRODUCTION

Statement of problem

Glaucoma is a leading cause of blindness and visual impairment worldwide. It is a group of progressive optic neuropathies and characterized by the degeneration of retinal ganglion cells related to the level of intraocular pressure and other factors (213). Several types of glaucoma have been broadly classified as acute and chronic, secondary and primary. In general, glaucoma in humans is classified into three major types: Primary Open Angle Glaucoma (POAG), Primary Angle Closure Glaucoma (PACG), and Primary Congenital Glaucoma (PCG) and POAG being the most common type (214). Although, the common pathway of tissue damage in all three types of glaucoma is the axonal damage that manifests as optic nerve atrophy, causing progressive visual field defects that eventually lead to blindness. Elevated intraocular pressure (IOP) is a common thread that connects most forms of glaucoma and is a major risk factor for the disease. IOP is a function of aqueous humor moving into and out of the eye. Elevated IOP in glaucoma is a result of disease in the primary efflux route, the conventional outflow pathway, affecting the proper drainage of aqueous humor (215). The research in the field of glaucoma is substantial, may be because of the fact that the pathophysiologic mechanisms causing the disease are not completely understood (216).

Controlling IOP in glaucoma patients is important because large clinical trials involving tens of thousands of patients repeatedly demonstrate that significant, sustained IOP reduction slows or halts vision loss. Unfortunately, current daily medical treatments

do not target the diseased conventional pathway and do not lower IOP sufficiently in most people with glaucoma. Therefore, finding new, more effective ways to medically control IOP by targeting the conventional pathway is a central hypothesis of this project. Using cellular and organ-based model systems, this study seeks to identify and validate novel drug targets in the conventional outflow pathway such that novel treatment of ocular hypertension and glaucoma can be developed.

To understand the mechanism of glaucoma, a wide variety of agents such as Ginkgo biloba extract (217), topical corticosteroids (218), dexamethasone (DEX) (219), intracameral injection of polystyrene microbeads (220), and benzalkonium chloride (221) have been employed to achieve acute and short-term IOP elevation. However, IOP elevation was poorly controlled and frequently led to a loss of vision. Several researchers have attempted to develop the in vivo (222), ex vivo (223), and *in vitro* glaucoma models (224). A wide variety of animal models including monkeys, dogs, cats, and rodents have been used to study glaucoma (222), (225). These animal models not only helped to identify targets for therapeutic drugs, but also improved the understanding of the causes and progression of glaucoma. Due to their inherent advantages, rodent animals, including mice and rats, have been widely applied as models to study various aspects of glaucoma and to evaluate possible novel therapies (226). Although these models have provided valuable information about the disease, there is still no ideal model available for studying glaucoma due to its complexity. Moreover, *ex vivo* models (227) are limited by the absence of survival factors supplied by blood or axonal transport, in addition to the incubation period is time limited (225).

In comparison with *in vivo* and *ex vivo* models, *in vitro* cell-based models (228), (224) offer the advantages of being simple, quick to construct, relatively inexpensive, and reproducible. In addition, it is easy to maintain the environment of *in vitro* cell-based models, small volumes of samples required, control on experimental settings, and reduction of the number of animals in *in vivo* studies. Therefore, use of *in vitro* models for the study of glaucoma opened the possibility of a better understanding of cellular and molecular mechanisms that may contribute to disease onset and progression. These models can be used in a wide variety from of cell cultures (cell lines) to more complex models such as tissue cultures. The opportunity to investigate whole tissue cultures poses clear advantages compared to a monolayer of cultured cells, allowing the study of cell-to-cell interactions and maintaining an anatomical structure. Therefore, there is a need to develop an *in vitro* model that can be advanced to develop glaucoma animal model based on the experimental needs.

Glucocorticoids (GC) have been a mainstay of therapy in reducing systemic and ocular inflammation. GC-induced ocular hypertension (due to the steroid response) has long been associated with the pathophysiology of glaucoma (229). Several clinical observations suggested that there is a link between GCs and glaucoma (230). A subset of the general population (steroid responders) experiences a significant elevation of IOP in response to GC administration. Extended periods of steroid-induced ocular hypertension resulted in glaucomatous optic atrophy and visual field loss that persist after the drug therapy is discontinued and the IOP has returned to normal. With the extensive clinical use of GCs for the treatment of various ocular diseases, GC-related ocular hypertension has attracted much attention. GCs cause a plethora of changes to the trabecular meshwork

(TM) including cytoskeletal, cell junction, extracellular, and functional changes (231). GCs alter the expression of several genes in the TM, likely responsible in impairing the outflow facility and elevating the IOP.

TM is porous connective tissue with complex 3D structure (232). Resident TM cells are responsible for maintaining its unique architecture and extracellular matrix (ECM) constituents (233). ECM is a dynamic structure composed of a number of different matrix proteins those are constantly remodeled by a new deposition and proteolysis (234). Three secreted ECM-related proteins: matrix metalloproteinase-2 (MMP-2); myocilin (MYOC); and fibronectin whose expression is altered by dexamethasone (DEX: a GC) have shown to play important roles in ECM formation and remodeling (235). Morphological examination of the TM in patients having GC-induced glaucoma shows an increased deposition of extracellular materials, specifically ECM content in the juxtacanalicular tissue. It has been proposed that reduction in MMP activity led to enhancing deposition of ECM material in the TM and thus induces an elevated juxtacanalicular outflow resistance (234). Other common features of GC treated eyes are MYOC induction, cytoskeletal rearrangement, which all may contribute to increased outflow resistance. Recently, it was noted that both humans and mice on prolonged GC treatment display increased deposition of basement membrane materials below the inner wall of Schlemm's canal (SC), possibly contributing to increased barrier function resulted in fluid flow resistance (236). The function of MYOC is unknown, however mutations in MYOC are a cause of hereditary open-angle glaucoma with ocular hypertension (237). Overall, an exact pathogenesis of glaucoma is not known, and current therapeutic options are not sufficient to prevent or recover vision loss in glaucoma patients.

Animal models are essential to elucidate the natural course of the glaucoma and to develop novel therapeutic approaches. However, glaucoma has a complicated pathogenesis that is far from being completely understood (45). Since the mechanisms of glaucoma differ among animal models, data obtained from a particular model should not be generalized and should be interpreted within the context of that model. Therefore, the selection of *in vitro* or *in vivo* models should be based on experimental needs and the hypothesis being tested. Experimentally, induced *in vivo* models have the advantage of studying certain changes in glaucoma in a living animal. However, the duration of IOP elevation in these models is transient without sequential treatments. In addition, precise control over IOP is difficult, and the timing of induction and progression of glaucoma is often unpredictable. Also, *in vivo* experiments include the involvement of undefined and uncontrollable factors. All these limitations associated with *in vivo* models have encouraged development and validation of *in vitro* models derived from human primary and immortalized cells.

Rationale of investigation

Based on the above stated problems of *in vivo* animal models, it was made clear that the exploitation of an appropriate *in vitro* model is crucial for the development of new approaches to overcome ocular barriers. *In vitro* models can be used to evaluate combinations of several experimental parameters; those are often not achievable with animal models. In addition to being much less complexed than animal models, *in vitro* models offer the advantage of having controlled experimental conditions, clarifying

individual cell responses to stress and allowing preliminary targeting of a specific cell type or pathway involved in the progression of glaucoma. Due to the lack of model systems to study glaucoma, the use of cultured TM cells provides means to evaluate their biological properties when challenged with conditions linked to glaucoma (233), (238). TM of the eye that is composed of cells and matrix is thought to regulate aqueous humor outflow to control IOP (239). TM and aqueous humor outflow pathway has a wide anatomical variation from one species to another; however, TM of humans, rat and mouse all contain extracellular meshwork organized into a network of beams covered with endothelial cells. Human TM (HTM) cells are usually obtained from whole donor eyes or from corneal buttons and ideally, one would like to compare HTM cells from glaucomatous tissue to normal HTM cells. Aspects of the different HTM *in vitro* models can be combined and developed to create more accurate representations of TM cell behavior *in vivo*. Ultimately, a more complete understanding of the cellular properties of HTM cells will provide new treatment options for glaucoma.

In order to understand the pathophysiology of glaucoma, HTM cell lines can be selected to develop an *in vitro* model of ocular hypertension. To elevate and maintain the IOP, a long-term release of GC drug is required which should be biocompatible to HTM cell lines. DEX is one of the effective GC that has been widely indicated in the clinical practice of ophthalmology. With the development of nanotechnology, slow, sustained, and controlled-release of DEX could be achieved. Polymeric nanocarriers such as nanoparticles (NPs) of biodegradable materials are useful in the development of such kind of delivery systems. FDA approved biodegradable polymers such as polycaprolactone (PCL), polylactic acid (PLA), polyglycolic acid (PGA), polyethylene

glycol (PEG) and poly lactide-co-glycolide (PLGA) have been comprehensively studied for the development of sustained release formulations of the GC.

Objective

The objective of this study is to design the optimized block copolymer based delivery system to provide long-term delivery of DEX with minimal burst release effect. In this approach, the *in vitro* drug release profile was optimized by adjusting the block length, arrangement and ratios of the PCL/PLA/PGA with PEG. These arrangements may be further optimized by changing the MW of each polymeric block. The PB copolymer displayed a unique block arrangement, ratio and MW, which can significantly influence the drug release profile of hydrophobic molecules. Considering these facts, a PB copolymer (PGA-PCL-PEG-PCL-PGA) has been synthesized to encapsulate DEX in PB based NPs. The purpose of the present study is to examine the long-term DEX release profile of PB copolymer based NPs in physiological solution and culture media. In addition, the activity and safety over time in ocular cell culture were examined using primary cultures of HTM cells. Current study investigated the possible association between MYOC expression and the steroid response on HTM cell. This approach will be followed to generate an animal model for GC induced ocular hypertension in a glaucoma model. The above mentioned hypothesis was studied with the aim of ‘development and characterization of PB copolymer based NP formulations of GC model drug (DEX) to develop a glaucoma model’. This aim is experimentally performed by the following methods.

(A) Synthesis and characterization of PB copolymers: Novel PB copolymer [PGA-PCL-PEG-PCL-PGA] was synthesized in two steps by sequential ring-opening polymerization reaction. The synthesized PB copolymers were characterized for their MW, PDI, and purity by (^{1}H) nuclear magnetic resonance (^{1}H-NMR) spectroscopy, gel permeation chromatography (GPC), and powder X-ray diffraction (PXRD).

(B) **Development, and optimization, and characterization of DEX loaded PB-NPs**: DEX-loaded PB copolymer NPs were prepared by oil in water (O/W) single emulsion solvent evaporation method. DEX-encapsulate PB-NPs were optimized to achieve a high entrapment efficiency and drug loading.

(C) Cytotoxicity evaluation of PB copolymers and PB-NPs: The cytotoxic effects of PB copolymers and PB-NPs on corneal, conjunctival and retinal cell lines, cell cytotoxicity (Lactate Dehydrogenase: LDH) and cell viability (MTT) assays were performed.

(D) C**haracterization of DEX loaded PB-NPs**: NPs were analyzed for their particle mean diameter and size distribution by Nanoparticle Tracking Analysis (NTA). The EE (%) and DL (%) of NPs were estimated by the ultra-fast liquid chromatography (UFLC) assay. The UFLC assay was used for quantitative estimation of *in vitro* drug release of DEX from NPs.

(E) Cytotoxicity evaluation of NPs in HTM cell line by WST-1 and LDH assays.

(F) MYOC level estimation: The long-term secretion of MYOC from HTM cells triggered from nanoformulation was analyzed by Western Blot analysis**.**

(G) *In vivo* study: IOP measurement and histology study in C57BL/6 (C57) mice model using DEX-PB-NPs to examine the changes in the tissue morphology of the eye.

CHAPTER 8

PENTABLOCK COPOLYMER BASED DEXAMETHASONE NANOFORMULATIONS ELEVATE MYOC: *IN VITRO* LIBERATION, ACTIVITY AND SAFETY IN HUMAN TRABECULAR MESHWORK CELLS AND MICE MODEL [240]

Rationale

Glucocorticoids (GCs) have been a mainstay of therapy in reducing systemic and ocular inflammation since 1950s (241). However, GC uses often induces ocular hypertension, optic nerve head damage, and visual field defects if left untreated. Elevation of intraocular pressure (IOP) usually occurs weeks to months after GC administration, and happens in ~40% of patients without glaucoma, called "steroid responder". Glaucoma, a group of diseases characterized by progressive optic nerve degeneration resulting in visual field loss and irreversible blindness, is a leading cause of permanent vision loss worldwide. The death of retinal ganglion cells (RGCs) is a major element in the pathophysiology of these diseases, relating to the level of IOP and other factors. The exact mechanism for the GC-induced IOP elevation is uncertain, but due to its time course likely involves at least two cellular processes in the resistance-generation region of the conventional outflow pathway: increased barrier function at the inner wall of Schlemm's canal (SC) and alterations in cell contractility and extracellular matrix (ECM) turnover in the trabecular meshwork (TM). Morphological examination of the TM in patients having GC-induced glaucoma shows increased deposition of extracellular materials, specifically, increased ECM content in the juxtacanalicular tissue (cribriform

region). Moreover, GC treatment results in decreased intra-trabecular spaces as a result of increased collagen, fibronectin and elastin deposition and an imbalance in ECM enzymes. Other common features of GC treated eyes are myocilin (MYOC) induction, cytoskeletal rearrangement, which all may contribute to increased outflow resistance.

Recently, it was noted that both humans and mice on prolonged corticosteroid treatment display increased deposition of basement membrane materials below the inner wall of SC, possibly contributing to increased barrier function. This was modeled *in vitro* by Alvarado showing that Dexamethasone (DEX) increased the junction complexes in both SC and TM cells, which resulted in increased transendothelial fluid flow resistance. TM is a porous connective tissue with complex three-dimensional structure. The resident TM cells are responsible for maintenance of its unique architecture and their ECM constituents. The ECM is a dynamic structure composed of a number of different matrix proteins that is constantly remodeled by new deposition and proteolysis. In the current study, we focused on MYOC whose expression is altered by DEX and shown to play important roles in ECM formation in normal physiological processes. The function of MYOC is unknown, however, mutations in MYOC is a cause of hereditary open-angle glaucoma with ocular hypertension. Since exact pathogenesis of glaucoma is not known, and current therapeutic options are not sufficient to prevent or recover vision loss in glaucoma patients. Functional, repeatable, and easy-to-use *in vitro* and animal models are therefore needed. Because of their inherent advantages, rodent animals, including mice and rats, have been widely developed as models to study various aspects of glaucoma and to evaluate possible novel therapies. However, no single model has been shown to

emulate all aspects of glaucoma to understand its pathology and physiological mechanism.

Nanocarriers offer several benefits in ocular drug delivery (1, 242). DEX, one of the most effective GCs, has been widely indicated in the clinical practice of ophthalmology as an anti-inflammatory and immunosuppressive agent. It can be administrated via topical, periocular (i.e. subconjunctival) or intraocular (i.e. intravitreal) routes. Topical DEX has proven efficacious for the management of postoperative inflammation in the anterior segment after cataract surgery, treatment of anterior uveitis (iritis) and dry-eye disease symptoms (243-245). Intravitreal administration of DEX has been effective in the treatment of macular edema following retinal vein occlusion, diabetic macular edema (246-248), and non-infectious uveitis (249), particularly when other therapeutic agents have failed to provide treatment benefits. However, DEX has a short half-life (250), and requires multiple applications. As a consequence, technologies that achieve slow, sustained, and controlled-release of DEX may prevent frequent administrations or multiple invasive treatments (251, 252). In this regard, FDA approved biodegradable polymers such as polycaprolactone (PCL), polylactic acid (PLA), polyglycolic acid (PGA) polyethylene glycol (PEG) and poly lactide-co-glycolide (PLGA) have been comprehensively studied for the sustained delivery of the corticosteroid (253, 254). These polymers have been widely tested, preparing various diblock (DB) (255), and triblock (TB) copolymers (255) for drug delivery technologies.

Investigators have applied various block copolymers combinations such as PLGA-PEG-PLGA (256), PEG-PLA-PEG (257, 258), for the development of sustained release formulations. Several of these polymers are incorporated in microparticle (259),

NP (254), and liposomal preparations (260) for long term release. Recently, the FDA has approved a DEX intravitreal implant for the treatment of macular edema following retinal vein occlusion, diabetic macular edema, or non-infectious uveitis (249, 261). Several attempts have been made to overcome initial burst release by using DB or TB copolymers. It has been observed that lipophilic drugs can be trapped in the hydrophobic core of the NPs causing no or limited release in later time intervals. Therefore, there is an unmet need of designing the optimized block copolymer based delivery system to provide continuous delivery of corticosteroids for longer duration with minimal burst release.

In this regard, PB copolymers have been designed in this study to overcome the limitation of the burst release associated with the NP and to provide long term delivery of therapeutic molecules (90, 154). In this approach, the *in vitro* drug release profile was optimized by adjusting the block length, arrangement and ratio of the PCL/PLA/PGA with PEG. The arrangements may be further optimized by changing the MW of each polymeric block. Considering these facts, we have developed a novel PB copolymer (PGA-PCL-PEG-PCL-PGA) to encapsulate DEX in PB-NPs attempting to achieve long term delivery. The PB copolymer displays unique block arrangement, ratio and MW, which can influence drug release profile of hydrophobic molecules. The purpose of the present study is to examine the DEX release profile of PB copolymer in physiological solution and culture media. In addition, the activity and safety over time in ocular cell culture were examined using primary cultures of HTM cells. This approach will be followed to generate an animal model for corticosteroid induced ocular hypertension.

Materials and Methods

Materials

Poly (ethylene glycol) (PEG 1 kDa), poly (vinyl alcohol) (PVA), and DEX were obtained from Sigma Aldrich, USA. The ε-caprolactone, glycolide and L-lactide were procured from Acros Organics, USA. Stannous octoate, HPLC solvents and other reagents utilized in this study were of analytical grade.

Methods

Synthesis of PB copolymers

Novel PB copolymer, (PGA-PCL-PEG-PCL-PGA) was synthesized in two steps by sequential ring-opening polymerization reaction (90). PEG (1 kDa) was utilized as the macroinitiator and stannous octoate act as the catalyst. In the first step, triblock (TB) copolymer PCL-PEG-PCL was synthesized by polymerization of ε-caprolactone on two open hydroxyl ends of PEG. E-caprolactone and stannous octoate (0.5% w/w) were added to anhydrous PEG and temperature was raised to 130°C. After 24 h, the reaction mixture was dissolved in methylene chloride followed by precipitation in cold ether. Purified TB copolymer was then used for the preparation of the PB copolymer. Stannous octoate (0.5% w/w) was added as a catalyst in the reaction mixture containing a predetermined quantity of the TB copolymer. The synthesis of PB copolymer was carried out at 130°C for 24 h under inert atmosphere. After 24 h, the reaction mixture was dissolved in methylene chloride followed by precipitation in cold petroleum ether. The purified PB copolymer was vacuum-dried and stored at -20°C until further analysis.

Reaction schemes for the synthesis of TB and PB copolymers were depicted in **Figures 8.1A** and **8.1B**, respectively.

Characterization of copolymers

The synthesized TB and PB copolymers were characterized for their MW, PDI, and purity by ^{1}H-NMR spectroscopy, GPC, and PXRD. The structures and MWs of copolymers (TB and PB) are described in **Table-8.1.**

^{1}H-NMR spectroscopy

^{1}H-NMR spectra of TB and PB copolymers were acquired on a 400 MHz NMR instrument (Varian Inc., Palo Alto, CA, USA). The chemical shift (δ) values were reported in parts per million (ppm). NMR samples were prepared by dissolving TB and PB copolymers in deuterated chloroform in a 5-mm outer diameter NMR tubes (Wilmad-LabGlass, Vineland, NJ, USA).

GPC analysis

The purity, MW and PDI of TB and PB copolymers were further analyzed by GPC analysis. Polymer samples were analyzed with Waters 410 refractive in DEX detector (Waters, Milford, MA, USA). Briefly, samples were prepared by dissolving 1 mg of copolymers in tetrahydrofuran (THF) (THF was utilized as eluting agent at the flow rate of 1 mL/min). Separation was carried out on Styragel HR-3 column (Waters, Milford, MA, USA). The internal and external temperatures of the SEC column was maintained at 35°C using Waters column heater module controlled by 410 RI detector. The data were acquired and processed with Waters Millenium^{32} software (version 3.2). A calibration curve was prepared by using Dextran SEC standards (Polymer Standards

Service-USA, Amherst, MA, USA) in the MW range of 5.2 to 410 kDa. A volume of 200 µL was injected into the SEC system in each analysis.

PXRD analysis

To analyze the crystallinity of copolymers, PXRD analysis was performed using RigakuMiniFlex automated X-ray diffractometer (Rigaku, The Woodland, TX, USA) equipped with Ni-filtered Cu-Kα radiation (30 kV and 15 mA). The analysis was performed at room temperature at the scanning rate of 5°/min.

Formulation of PB copolymer based DEX NPs (DEX-PB-NPs)

DEX-loaded PB copolymer NPs were prepared by oil in water (O/W) single emulsion solvent evaporation method. Briefly, DEX (5 mg) and PB copolymer (25 mg) were dissolved in methylene chloride copolymers to make the organic phase. The aqueous phase was comprised of 5 mL of 2% PVA. The O/W emulsion was formed using probe sonication. The organic phase was then evaporated by stirring the emulsion overnight. NPs were separated by ultracentrifugation at 20,000 rpm for 45 min at 4°C. NPs were washed twice with distilled deionized water (DDW), and centrifuged to remove traces of PVA and unentrapped DEX. The purified NPs were freeze-dried with mannitol as a cryoprotectant and stored at -20°C until further uses.

Physicochemical characterization of NPs

Size distribution measurements

DEX-PB-NPs were analyzed for their particle mean diameter: nm, and size distribution by Nanoparticle Tracking Analysis (NTA) using a Nanosight LM10

instrument (Nanosight, Salisbury, UK). Freeze dried DEX-PB-NPs (1 mg/mL) suspended in DDW were subjected to particle size analysis at room temperature and 90° scattering angel. All the samples were analyzed in triplicate (n=3).

Entrapment efficiency (EE) and drug loading (DL)

The EE (%) and DL (%) were estimated by the ultra-fast liquid chromatography (UFLC) assay for the amount of DEX in the supernatants obtained from the NP preparation. Equations 8.1 and 8.2 were utilized for the calculation of EE (%) and DL (%), respectively.

$$\% \text{ Encapsulation efficiency} = \frac{(\text{Initial amount of drug} - \text{Amount of drug in supernatant})}{\text{Initial amount of drug}} * 100 \quad \ldots \text{Eq. 8.1}$$

$$\% \text{ Drug loading} = \frac{\text{Amount of drug in nanoparticle}}{\text{Total amount of drug and polymer}} * 100 \quad \ldots \text{Eq. 8.2}$$

***In vitro* drug release profile of DEX-NPs**

To analyze the *in vitro* drug release profile, 1 mg of DEX equivalent freeze-dried NPs were suspended in a dialysis tube. DEX-loaded NPs were suspended in 25 mL of phosphate buffer saline (PBS) pH - 7.4 at 37°C. The tube containing dialysis bag was placed in a water bath at 37°C (GFL 3032 Shaker, LABOTEC, Germany). At predetermined time intervals, 1 mL of clear supernatant was collected and replaced with same volume of fresh PBS (preincubated at 37°C). Drug concentrations were measured by UFLC analysis. All experiments were conducted in triplicate (n = 3). *In vitro* release data were expressed as cumulative drug released (%) with time.

Ultra-fast liquid chromatography (UFLC) assay

Reversed phase UFLC assay was employed to analyze the entrapment efficiency, drug loading and *in vitro* release profile of DEX-PB-NPs. A Shimadzu UFLC system (Shimadzu Scientific Instruments, Columbia, MD, USA) coupled with pumps (LC-20AT), degasser (DGU-20A3R), DAD detector (SPD-20AV) and autosampler (SIL-20AHT) was used. A Phenomenax column (Phenomenex C18 kinetex column (100×4.6 mm, 5 mm) was used at total flow rate of 0.5 mL/min. An isocratic elution method was employed for separation with mobile Phase A (water with 0.1% formic acid) at 60% and mobile phase B (ACN with 0.1% formic acid) at 40% were ran for 8 min. Concentration of DEX standards ranged from 250 ug/mL to 0.488 ug/mL prepared in the mobile phase. All solvent fractions were in %v/v ratio. Injection volume of 30 uL was used for each analysis and the DAD detector was set at 254 nm for quantification.

***In vitro* tolerability studies of PB copolymer and PB-NPs**

To analyze the cytotoxic effects of PB copolymers on corneal, conjunctival and retinal cell lines, cell cytotoxicity (Lactate Dehydrogenase: LDH) and cell viability (MTT) assays were performed according to the supplier's instructions. SV-40 (Human Corneal Epithelial transfected with a recombinant SV40-adenovirus vector Cell), CCL20.2 (Human Conjunctival Epithelial Cell/ Chang's Conjunctival Cell Line) and D407 (Human Retinal Pigment Epithelium Cell) cells are immortalized and can be sub-cultured many times, while maintaining their physiological properties. SV40 cells were cultured in DMEM/F-12 medium supplemented with 15% (v/v) heat-inactivated fetal bovine serum (FBS), 22 mM $NaHCO_3$, 15 mM HEPES and 5 mg/L insulin, 10 μg/L

human epidermal growth factor, 100 mg penicillin, and 100 mg streptomycin each. The cells were incubated at 37°C, 5% CO_2, and 98% humidity. CCL20.2 cells were maintained in a cell culture flask containing Minimum Essential Medium (MEM), Earle's Balanced Salt Solution (BSS) medium supplemented with 10% FBS, 100 U/L of penicillin, 100 mg/L of streptomycin, sodium bicarbonate (2.2 mg/mL), and 2 mM l-glutamine. D407 cells were grown at 37°C, humidified 5% CO_2/95% air atmosphere in a DMEM culture medium supplemented with 10% (v/v) FBS (heat inactivated), 29 mM $NaHCO_3$, 20 mM HEPES, 100 mg of penicillin and streptomycin each, and 1% nonessential amino acids at pH 7.4. The cells were harvested at 80–90% confluency with TrypLE™ Express (a superior replacement for trypsin). (96, 255)

Human trabecular meshwork (HTM) cell culture

Five strains of TM cells (HTM120, 136, 126, 134 and 141) were isolated from eyes of human donors of ages11- and 3-month-old (HTM120 and 136), 88-, 51-, and 38-year old (HTM126, 134 and 141), respectively, with no documented history of eye disease. The genders for the HTM cells were HTM126, 136: females; HTM134, 141: males; HTM120: unknown, no records from the Eye Bank. Cells were isolated and characterized as previously described (262, 263). Human eye tissues were sourced ethically from Miracles in Sight (Winston Salem, NC, USA), accredited by the Eye Bank Association of America. The research uses of eye tissues were in accordance with the terms of the informed consents of the donors and/or donor family. HTM cells (passages 3-6) were seeded into 24- or 96-well culture plates in DMEM containing 10% fetal bovine serum (FBS) (Atlanta Biologicals, Atlanta, GA) until cells reached confluency. As

a differentiation step, the cells were then switched to DMEM medium containing 1% FBS for at least 7 days prior to the experiments.

Dexamethasone NP (DEX-PB-NPs) treatment

HTM cells were treated with DEX-PB-NPs (1 mg/mL) containing a total of 23 µg DEX (DEX-PB-NPs) or Con-NPs (without DEX), DEX (39.25 ng/mL) or control (Con: 0.1% ethanol) in fresh 1 mL DMEM containing 1% FBS (1% DMEM). Two days after initial treatment, cell culture supernatant was removed and replaced with fresh 1% DMEM medium containing either 0.1% ethanol vehicle or DEX (39.25 ng/mL in 0.1% ethanol). Similarly, medium in Con-NPs or DEX-PB-NPs treated wells was replaced with fresh 1% DMEM. Then, cell culture supernatant was collected and replaced with fresh 1% DMEM once/week for a total of 12 weeks for DEX-NP or Con-NP treatment wells. Other wells were replaced with fresh 1% DMEM medium containing either Con or DEX once/week. After 4 weeks, all wells were replaced with fresh 1% FBS medium once in a week for additional 8 weeks and stored at -80°C until further analysis.

Western blot analysis

Secreted MYOC levels in cell culture supernatant was detected and normalized following our previously published method (264). Briefly, cell culture supernatants were collected from wells of culture plates after 2 days of treatment, and then once/week for 12 weeks. At the end of 12 weeks, cells were harvested, and rinsed twice with cold PBS. Cells were scraped into 80 µL of lysis buffer (25% glycerol, 0.0625M Tris.HCl, 2% SDS) containing 5% beta mercaptoethanol. Cell culture media at each time point was

mixed with 4 × loading buffer (50% glycerol, 0.125M Tris.HCl, 4% SDS) containing 5% beta mercaptoethanol and boiled for 10 min before storing at -20°C. For Western blotting, 24 µL of solubilized proteins in the cell culture supernatant containing 4 × loading buffer were loaded into 8% polyacrylamide gel slabs; and 10 µL of cell lysates were loaded to 10% polyacrylamide gel slabs. The proteins were separated via SDS-PAGE. Fractionated proteins were then transferred electrophoretically to nitrocellulose membranes. Non-specific binding of antibodies to membranes containing transferred proteins was reduced by incubating with Tris-buffered saline with 0.1% Tween 20 (TBS-T) containing 5% nonfat dry milk (blocking buffer).

Rabbit polyclonal antibodies against MYOC or a mouse monoclonal antibody against beta-actin (Sigma, St. Louis, MO, USA) in blocking buffer were incubated overnight with membranes at 4°C. The next day, membranes were first washed in TBS-T (3 times for 10 minutes) and then were incubated in blocking buffer containing horseradish peroxidase-conjugated secondary antibodies (Jackson ImmunoResearch Laboratories, Inc., West Grove, PA, USA) for 1 hour. After incubation, membranes were washed with TBS-T. Protein-antibody complexes were visualized using a chemiluminescent HRP antibody detection reagent spray (HyGLO; Denville Scientific, Inc., Metuchen, NJ, USA) and exposure to x-ray film (Phonix Research Company, Candler, NC, USA). The protein abundance in each band was quantified by densitometry using ImageJ image analysis software (GeneSnap/GeneTools; Syngene, Frederick, MD, USA).

Cell cytotoxicity (LDH) assay

The LDH assay was performed using supplier's instructions. Briefly, 5, 25 and 50 mg/mL of PB copolymer were dissolved in acetonitrile (ACN) and 100 µL was aliquoted in each well of the 96-well plate. Plates were exposed overnight under UV light (laminar flow) for polymer sterilization as well as evaporation of ACN. Similarly, 5, 25 and 50 mg/mL of PB-NP was dispersed in culture media and filtered through 0.22 µM filter. One hundred microliter of this solution was added to the 96-well cell culture plate. D407, SV-40 and CCL.20.2 cells at the density of 1.0 x 10^4 were seeded in each well and incubated at 37°C, 5% CO_2 in humidified atmosphere for 48 h. After completion of the incubation period, cell supernatants were analyzed for the quantification of LDH release using LDH assay kit (Takara Bio Inc., Otsu, Japan). Absorbance of each well was measured at 450 nm using a DTX 800 multimode microplate reader (Beckman Coulter, Brea, CA). The LDH release (%) was calculated according to Eq. 8.3 and more than 10% of LDH release was considered as cytotoxic.

$$LDH\ release(\%) = \frac{Abs.of Sample - Abs.of negativecontrol}{Abs.of positivecontrol - Abs.of negativecontr} \quad \ldots \text{Eq. 8.3}$$

To test the cytotoxicity in HTM cells, three strains of confluent HTM cells (HTM141, HTM126 and HTM136) kept in 1% DMEM media for 1 week were treated with Con vehicle (0.1% ethanol), DEX (39.25 ng/mL in 0.1% ethanol), Con-NPs (1 mg/mL) or DEX-PB-NPs (1 mg/mL) in 1% DMEM media. The treatment protocol was the same as for collecting media for MYOC analysis as explained before. At the end of 12 weeks of incubation, cytotoxicity was determined by measuring LDH release from

cells using LDH assay kit (Roche, Indianapolis, IN, USA). Briefly, the supernatant was carefully removed, centrifuged, and transferred to a 96-well plate. The cells were lysed and then transferred to a 96-well plate. A reaction mixture consisting of catalyst/dye combination was prepared, and 100 µL was added directly to each of 100 µL of the cell supernatant, cell lysates, plain media and lysate solution. After incubation at 25°C for 30 min, absorbance was measured using a spectrophotometer at 490 nm with a reference wavelength at 690 nm. Released LDH in the cell supernatant was calculated by subtraction of media background and then normalized by total LDH in cell lysates from each treatment group.

Cell viability assay

The safety and biocompatibility of PB copolymers was further established by performing an *in vitro* cell viability assay (MTS; (3-(4, 5-dimethylthiazol-2-yl)-2, 5-diphenyltetrazolium bromide) tetrazolium reduction) (Promega Corp., Madison, WI, USA), according to suppliers instructions. PB copolymer solutions at the concentration of 5, 25 and 50 mg/mL in ACN were prepared, aliquoted and sterilized. Following sterilization, D407, SV-40 and CCL20.2 cells were seeded in each well of 96-well plate at a cell density of 1.0×10^4, and incubated at 37°C and 5% CO_2 in humidified atmosphere for 48 h. Similarly, 5, 25 and 50 mg/mL of PB-NP solution were prepared in culture media and filtered through 0.22 µM filter. From this, 100 µL was added to the 96-well plate. At the end of incubation period, cell culture medium was aspirated and cells were incubated for 4 h (37°C and 5% CO_2) in the presence of 100 µL of serum free medium containing 20 µL of MTS solution. The fluorescence intensity was measured at

the excitation and emission wavelengths of 560 nm and 590 nm, respectively, using the above microplate reader. Percent cell viability was calculated using Eq. 8.4. The PB copolymers exhibiting more than 90% of cell viability were considered suitable for ocular applications.

$$Cell\ viability(\%) = \frac{Abs.of\ Sample - Abs.of\ negative control}{Abs.of\ positive control - Abs.of\ negative control} * 100 \quad \ldots \text{Eq. 8.4}$$

To test the cell viability of HTM cells with DEX, Con-NPs or DEX-PB-NPs, a colorimetric assay was performed based on the cleavage of the tetrazolium salt WST-1 (4-[3-(4-lodophenyl)-2-(4-nitrophenyl)-2H-5-tetrazolio]-1.3-benzene disulfonate) by mitochondrial dehydrogenases in viable cells (Roche, Mannheim, Germany). Twelve weeks after the initial treatment, WST-1 solution (10µL/well) was added to each well containing 100 µL of cell culture supernatant. Cells were further incubated for 30 min at 37°C. The plate was read on a spectrophotometer at 440 nm with a reference wavelength of 690 nm.

Extraction method of DEX from cell culture media

Cell culture medium samples were analyzed using an UFLC method as described earlier. Sample preparation was carried out using liquid–liquid extraction technique. Hydrocortisone, a corticosteroid, similar in structure to DEX was employed as an internal standard. Briefly, samples were thawed at room temperature and 50 µL of internal standard was added to the samples (300 µL). The solutions were vortexed for 30 sec, 100 µL of ACN was added, and vortexed again for 30 sec to deactivate the serum proteins

and enzymes. Each sample was mixed with 300 µL of organic solvent and vortexed again for another 2.5 min to allow equilibration between the phases. For efficient separation of the aqueous and organic layers, samples were extracted twice and centrifuged at 10,000 rpm for 7 min. Aliquots (500 µL) were collected and dried under reduced pressure for 45 min. The residue was reconstituted with 300 µL of mobile phase [ACN (40%) & water (60%)], vortexed for 30 sec and transferred into a pre-labeled UFLC autosampler vial with silanized inserts. A 30 µL of the resulting solution was injected onto the UFLC system and analyzed for DEX quantification.

Statistical analysis

The experimental values were generally presented as mean ± standard deviation (SD) of triplicate determinations (n = 3). Mann–Whitney U test was used to analyze statistical significant difference between groups. A *P* value of ≤ 0.05 was considered statistically significant.

In vivo* study *in C57BL/6 mice

Mice were handled in accordance with animal care and use guidelines of Duke University and in compliance with the ARVO Statement for the Use of Animals in Ophthalmic and Vision Research. C57BL/6 mice were from the Jackson Laboratory (Bar Harbor, Maine, USA), bred/housed in clear cages and kept in housing rooms at 21 °C with a 12 h: 12 h light-dark cycle. Mice were examined at ages between 3 and 4 months old. There were 7 mice (14 eyes) in the ghost group and 6 mice (12 eyes) in the DEX treated group. DEX-PB-NPs or Con-NPs were diluted in PBS at concentrations of 0.5

mg/µL, vortexed for 10 min and then sonicated for 10 min. Mice were anesthetized with Ketamine/Xylazine 100mg/10mg/kg. IOPs were measured right after mice stop moving. NPs (20 µL from 1mg/mL containing ~23ug of DEX or no DEX) were slowly injected into superior subconjunctival fornix on both eyes using 30-gauge needle with a Hamilton glass microsyringes (50 µL volume; Hamilton Company, Reno, NV, USA). After withdrawing the needle, antibiotic ointment was applied to the eyes and mice were recovered on the warm pad.

Intraocular pressure (IOP) measurement

IOP was measured in both eyes for control and treated groups (Group # 1, 1A, 2, 3 and 4). The mice were anesthetized with ketamine (60 mg/kg) and xylazine (6 mg/kg). IOP was immediately measured just as the mice stopped moving (light sleep) using rebound tonometry (TonoLab) between 10am to 1pm (265). Each IOP recorded was the average of six measurements, giving a total of 36 rebounds from the same eye. Post-treatment and pre-treatment IOPs were measured during the same time of the day.

Histology Study in C57BL/6 mice

Mice were euthanized at the predefined time intervals by decapitalization under anesthesia condition following the approved animal study protocol. Immediately after euthanasia, eyes were enucleated and processed for histopathology. Following eye removal, carcasses were discarded without necropsy. Three weeks after DEX-PB-NPs/Con-NPs injection in both eyes, eyes were collected and immerse fixed in 4% paraformaldehyde, and kept at 4 °C overnight. The eyes were then bisected and the

posterior segments and lenses were removed. The anterior segments were cut into four quadrants and each quadrant was embedded into Epon (Electron Microscopy Sciences, ON, Canada). The blocks were cut into 0.5 µm semi-thin sections and stained with 1% methylene Blue. The images were captured digitally using light microscopy.

Results and Discussion

Synthesis of PB copolymer

PB copolymer designed for the preparation of NPs was successfully synthesized by ring-opening bulk copolymerization as represented in **Figure 8.1A and 8.1B**.

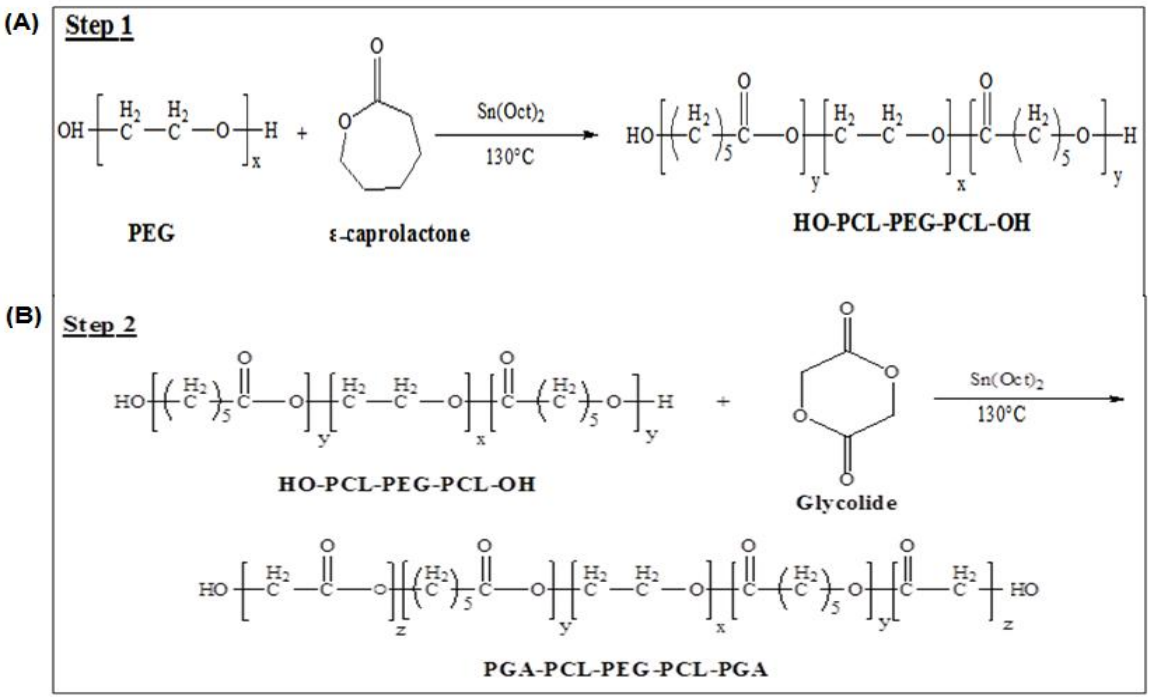

Figure 8.1 Synthesis scheme for (A) triblock (TB: PCL-PEG-PCL) copolymer and (B) pentablock (PB: PGA-PCL-PEG-PCL-PGA) copolymer by ring opening bulk copolymerization method. (Reproduced from Ref. 240).

Characterization of PB Copolymer

A typical ^{1}H-NMR peaks comprised of glycolic acid which displayed a series of singlets between 4.6 to 4.9 ppm confirming the methylene protons of PGA block as depicted in **Figure 8.2**. The MWs of copolymers were calculated from the integration values of ^{1}H-NMR peaks of individual blocks. Moreover, absence of any additional peaks in ^{1}H-NMR spectrum confirmed the purity of PB copolymers. The MWs calculated from ^{1}H-NMR are reported in **Table 8.1.**

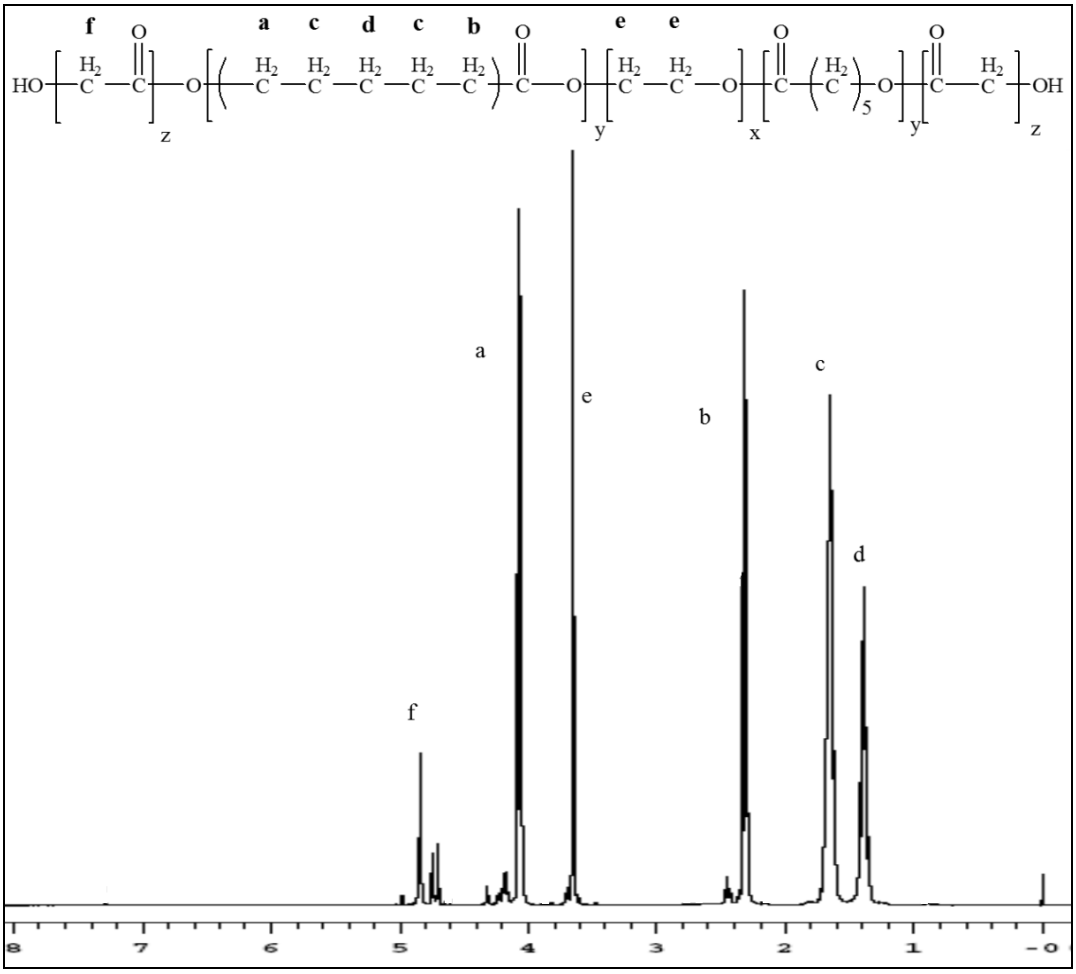

Figure 8.2 Characterizations of pentablock (PB) copolymer by proton nuclear magnetic resonance spectra (^{1}H NMR) spectroscopy. (Reproduced from Ref. 240).

Table 8.1 Characterization of triblock and PB copolymers

Co-polymers	**Structure**	**Total Mn[a] (theoretical)**	**Total Mn[b] (calculated)**	**Total Mn[c] (calculated)**	**Mw[c] (GPC)**	**PDI[c]**
TB	PCL_{7000}-PEG_{1000}-PCL_{7000}	15000	14278	12289	17562	1.83
PB	PGA_{3000}-PCL_{7000}-PEG_{1000}-PCL_{7000}-PGA_{3000}	21000	20264	17952	23158	1.36

a: Theoretical value, calculated according to the feed ratio.

b: Calculated from ^{1}H-NMR.

c: Determined by GPC analysis.

The purity, molecular weights (Mn and Mw) and PDI were further evaluated by GPC and represented in **Figure 8.3**. The PDI values of PB copolymers were below 1.5 suggesting a narrow distribution of MWs. Moreover, PB copolymers depicted a single peak in GPC chromatogram indicating mono distribution of MW. Calculated MWs appear to be very similar to the theoretical MWs obtained from feed ratio. Therefore, theoretical MWs were considered instead of calculated MWs subsequently.

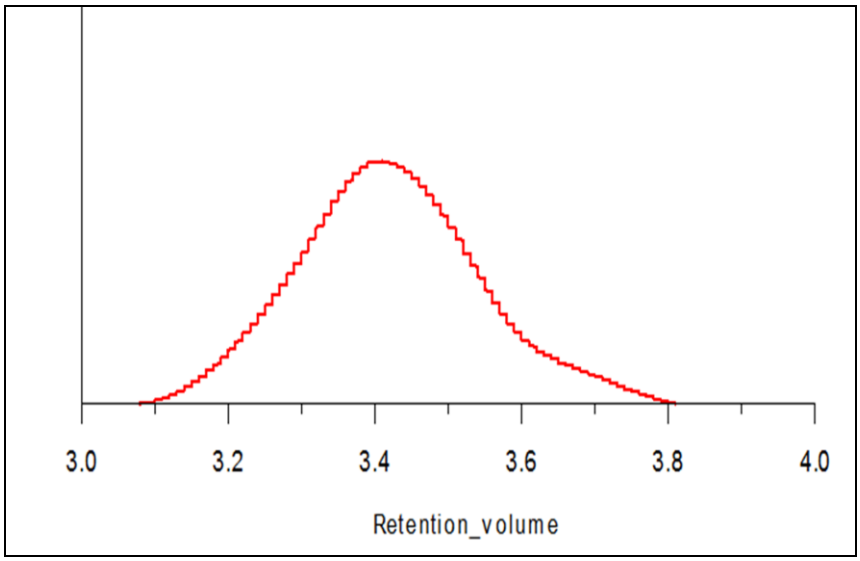

Figure 8.3 Gel permeation chromatograms (GPC) of pentablock (PB) copolymer depict a single peak indicating mono distribution of MW. (Reproduced from Ref. 240).

XRD spectra revealed the crystallinity of block copolymers as represented in **Figure 8.4**. Interestingly, TB and PB copolymers exhibited crystalline peaks of PCL at 2θ = 21.5° and 23.9°. XRD patterns of TB and PB indicated that PCL blocks have retained semi-crystalline structure even after covalent conjugation with PGA blocks. Conjugation of PGA blocks at the terminals of TB copolymers slightly affected the intensity of crystalline peak. Previously published reports suggested that decrease in crystallinity significantly enhances the degradation of block copolymers (183). Hence, it is anticipated that PB copolymer can display a slower rate of degradation due to its semi-crystalline nature.

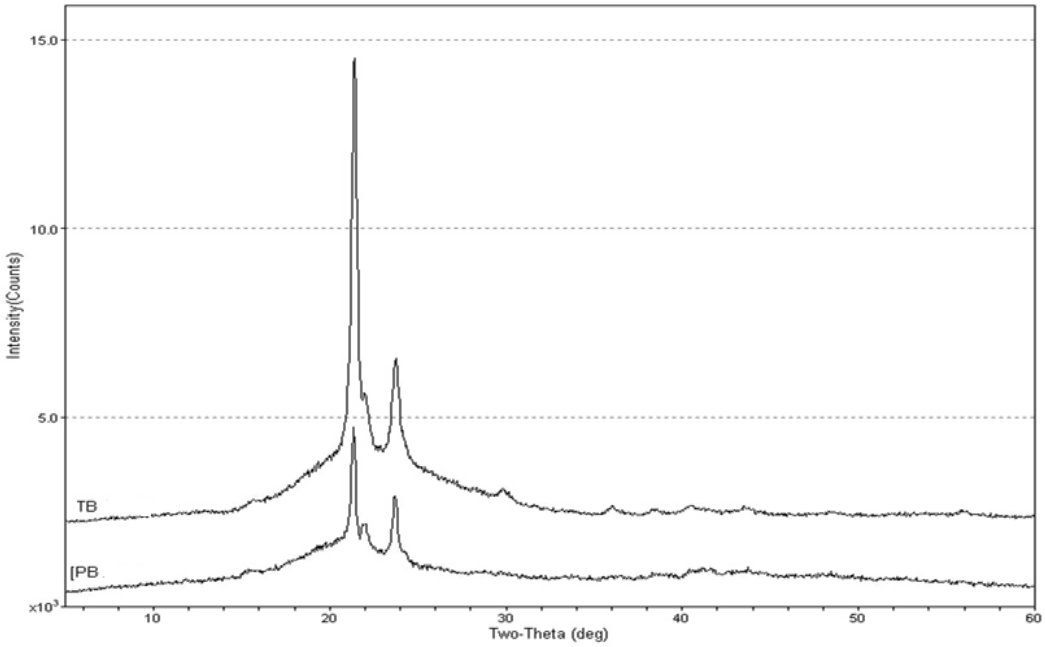

Figure 8.4 X-ray diffraction patterns (XRD) of triblock (TB) and PB copolymers.

(Reproduced from Ref. 240).

Formulation and Characterization of DEX-PB-NPs

Particle size

The particle size of NPs was found to be 109 ± 3.77 (n = 3) as analyzed by nanoparticle tracking analysis (NTA) reported in **Figure 8.5.**

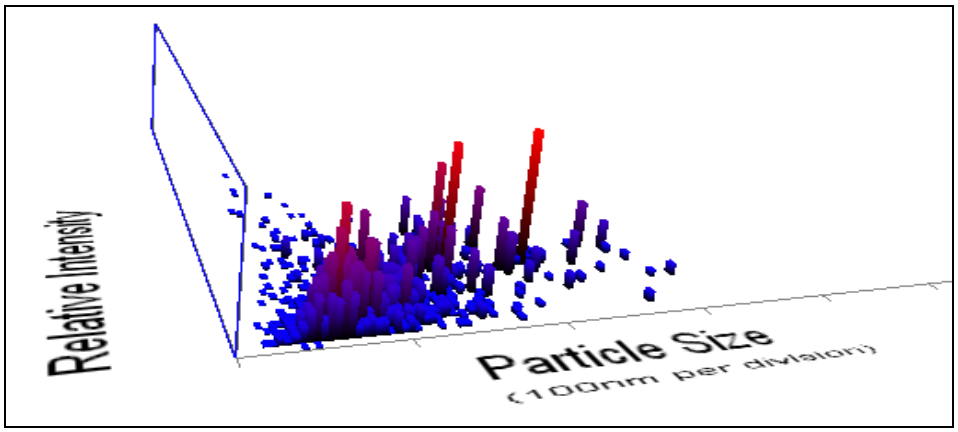

Figure 8.5 Particle size distributions of DEX-PB-NPs by Nanoparticle Tracking Analysis.

(Reproduced from Ref. 240).

Entrapment efficiency (EE %) and drug loading (DL %)

The percent EE and DL was calculated as 63.23 (±2.31) and 10.53 (±0.38) respectively, (n = 3).

***In vitro* DEX release study**

The release study was performed by suspending 1 mg of DEX equivalent PB-NPs in PBS at 37°C and sampling from dialysis chamber. Burst release (20%) was observed for the first two days possibly due to the release of surface bound drug of NPs. Cumulative %DEX released *vs.* time profile was illustrated in **Figure 8.6**. DEX release from the PB-NPs was continuous over three months. About 50% of DEX was released within six weeks which appeared to be responsible for interactions with PGA chains resulting in relatively faster release pattern. A bi-phasic release pattern of DEX was evidented from NPs with initial burst release, followed by a sustained release phase. DEX demonstrated slow release rate from NP because of the hydrophobicity and low crystallinity of PB copolymer. Hence, PB copolymer based NPs were considered to be more effective relative to existing PLGA and other polymers based systems. The advantages associated with this sustained release formulation (DEX loaded NPs) offered a higher drug residence at the site of absorption.

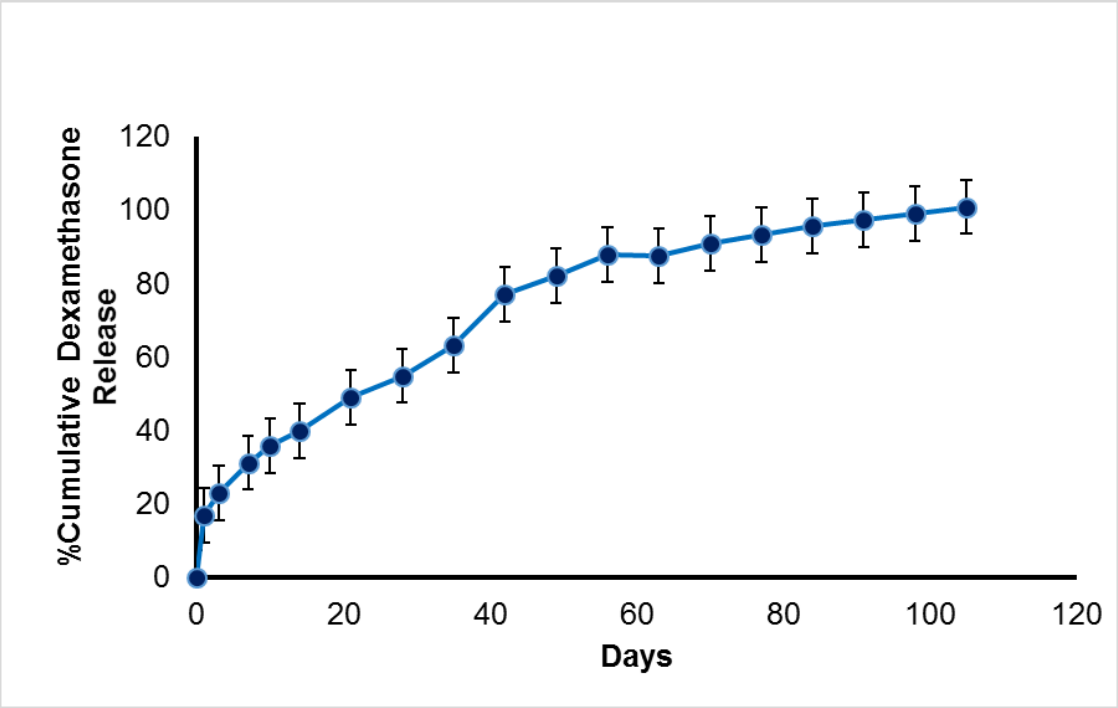

Figure 8.6 *In vitro* release of Dexamethasone (DEX) from DEX-PB-NPs. Results are given as mean ± SD, n = 3. (Reproduced from Ref. 240).

***In vitro* tolerability of PB copolymer and PB-NP on ocular cells**

In order to investigate the toxicity of PB copolymer and PB-NPs with biological system, transformed ocular cell lines (SV-40, CCL.20.2 and D407 cells) were treated with 5, 25 and 50 mg/mL of PB copolymer and PB-NPs for 48 h (**Figures 8.7**). Primary cultures of HTM cells were treated with 1 mg/mL of PB copolymer and DEX-PB-NPs for 12 weeks (Figure 8.8 A). LDH is a cytoplasmic enzyme, secreted in cell culture medium following cell-membrane damage. Estimation of LDH concentration in culture supernatant was used to provide PB copolymer toxicity information. Less than 10% of LDH release was observed after 48 h and 12 weeks exposure indicated a negligible toxicity. Noticeably, results were comparable with negative controls.

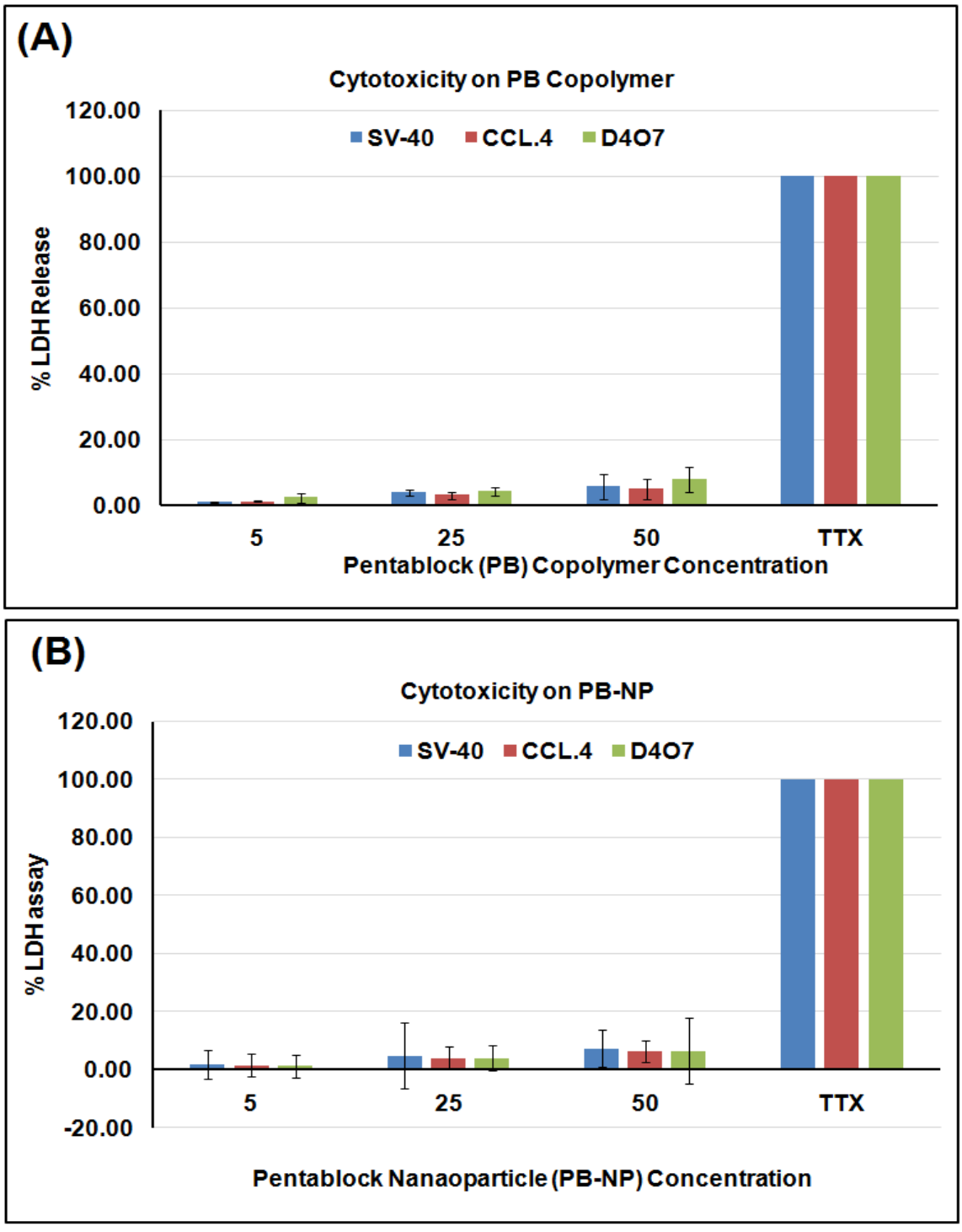

Figure 8.7 *In vitro* cytotoxicity assay (LDH) of: (A) pentablock (PB) copolymers; (B) Blank PB-NPs at different concentrations on D407, SV-40, and CCL20.2 cells. Results are given as mean ± SD, n = 5. (Reproduced from Ref. 240).

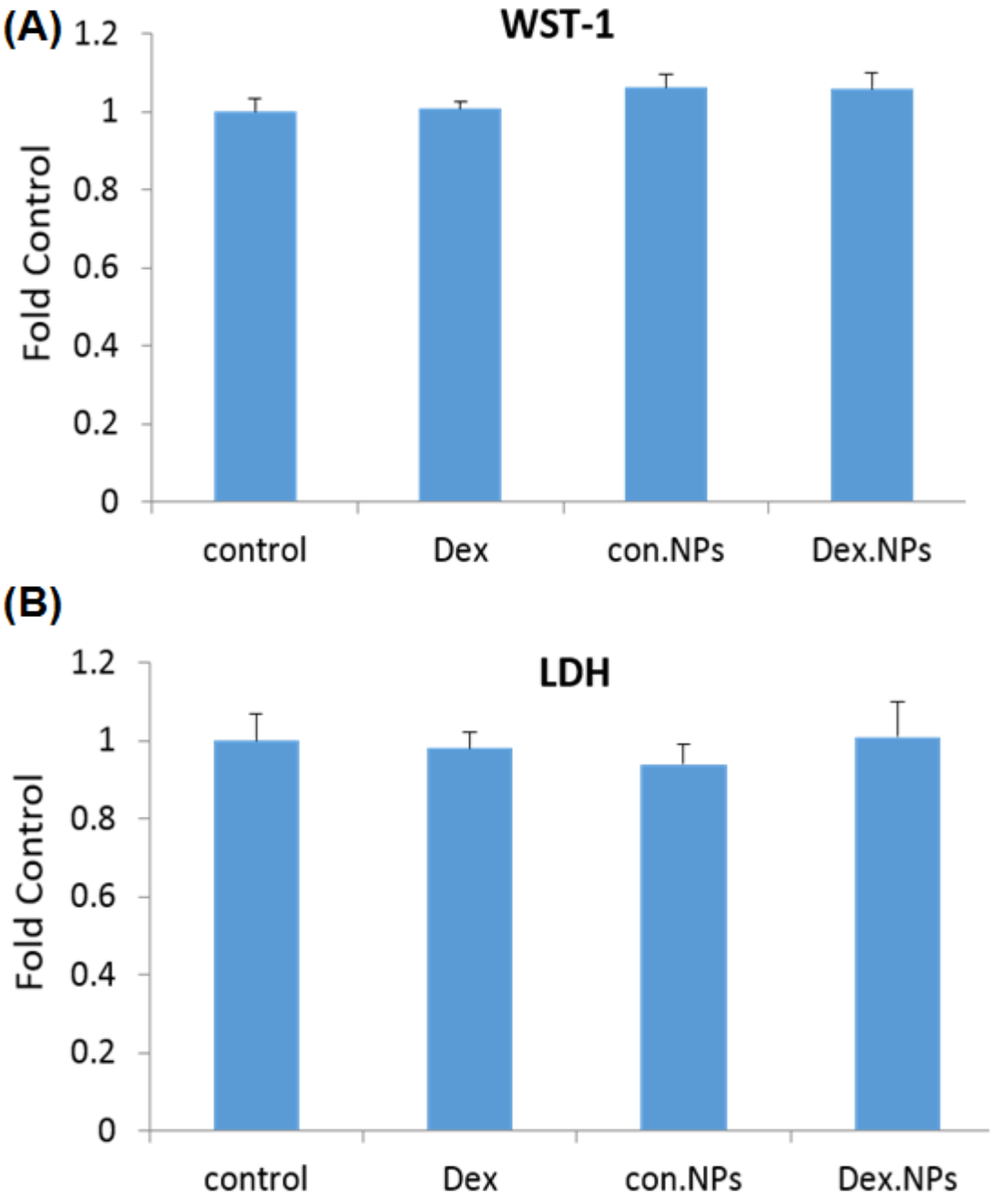

Figure 8.8 Effect of DEX-PB-NP on HTM cytotoxicity over time. Confluent HTM cells were treated with a single application of con-NPs or DEX-PB-NPs (1 mg/mL). Cell viability was determined by (A) WST-1 and cytotoxicity was examined by (B) LDH release after 12 weeks. (Reproduced from Ref. 240).

To further confirm the cytotoxicity of copolymers, MTS or WST-1 cell viability assays were performed. The WST-1 assay is a rapid and sensitive colorimetric assay based on the cleavage of the tetrazolium salt WST-1 (4-[3-(4-Iodophenyl)-2-(4-nitrophenyl)-2H-5-tetrazolio]-1.3-benzene disulfonate) by mitochondrial dehydrogenases in viable cells (Roche, Mannheim, Germany). In MTS assay, only metabolically active cells convert tetrazolium compound to formazan. Hence, the concentrations of formazan products provide a direct estimation of the cell viability. Results in **Figure 8.9** demonstrated that we observed more than 90% cell viability (for all the cell lines) after 48 hours and 12 weeks exposure to PB copolymer and PB-NPs (**Figure 8.8 B**). This suggested an excellent safety profile of PB copolymer and nanoformulation for ocular applications.

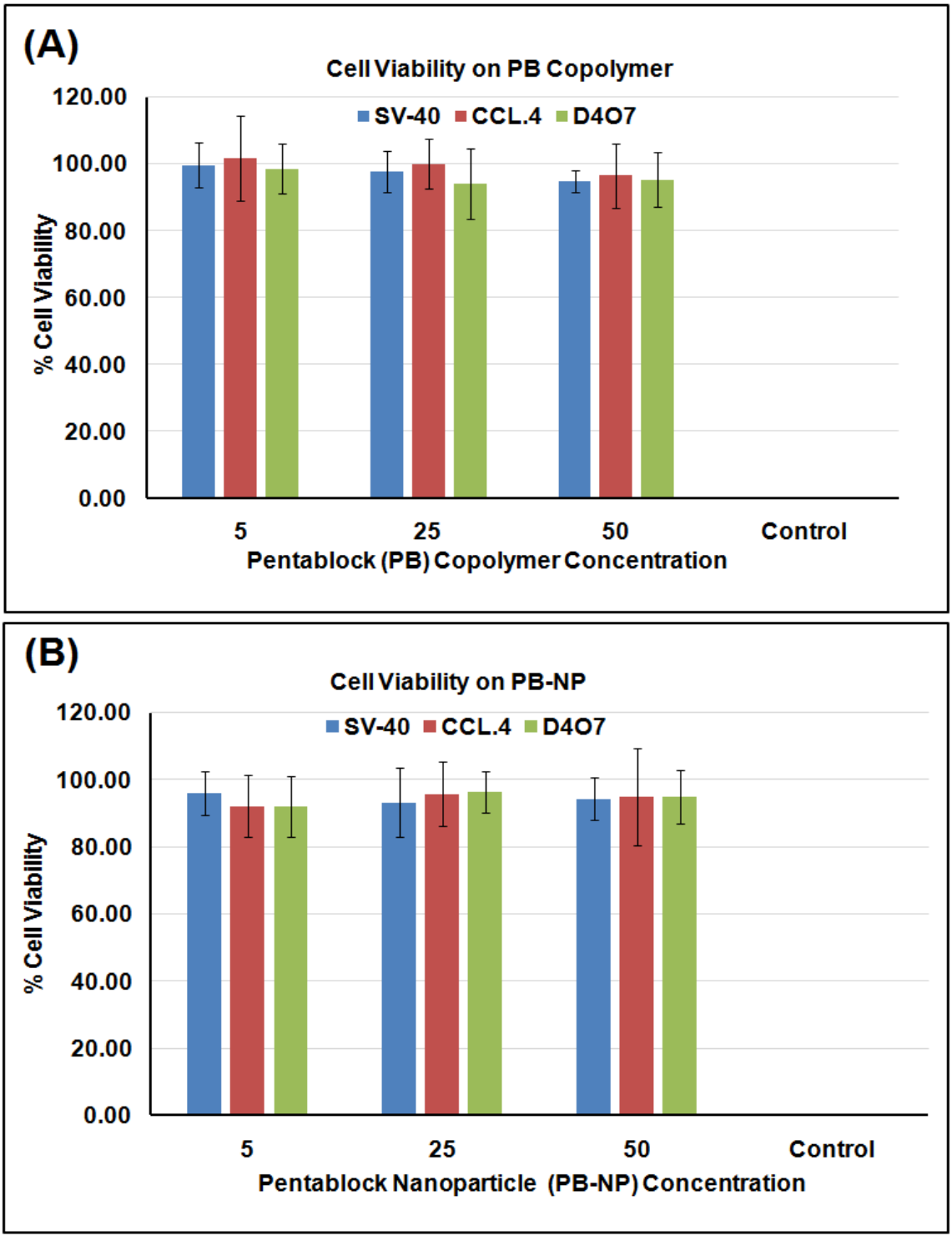

Figure 8.9 *In vitro* cell viability assay (MTS) of: (A) PB copolymers; (B) blank PB-NPs at different concentrations on D407, SV-40, and CCL20.2 cells. Results are given as mean ± SD, n = 5. (Reproduced from Ref. 240).

MYOC secretion from cultured HTM cells

The expression and secretion of MYOC from primary cultures of TM cells was robustly enhanced following DEX treatment (264, 266-270). Previous studies (264) suggested that MYOC was continually upregulated following prolonged 4 weeks DEX treatment and its expression declines over time in the absence of DEX. Thus, the secretion of MYOC can be used as a surrogate read out of biological activity of DEX released from DEX-PB-NPs. A single application of DEX-PB-NPs (1 mg/mL) or control NPs were given to HTM cells. Cell culture supernatant was collected and replaced with fresh 1% DMEM once/week for 12 weeks. DEX or Con vehicle serves as controls to compare MYOC secretion levels by Western blot, being applied once/week for 4 weeks, and then switched to fresh 1% DMEM media for the last 8 weeks. Four HTM cell strains showed similar MYOC secretion patterns, having robust responses for the entire monitoring period **(Figure 8.10)**. In contrast, one cell strain only responded over a few weeks **(Figure 8.11)**.

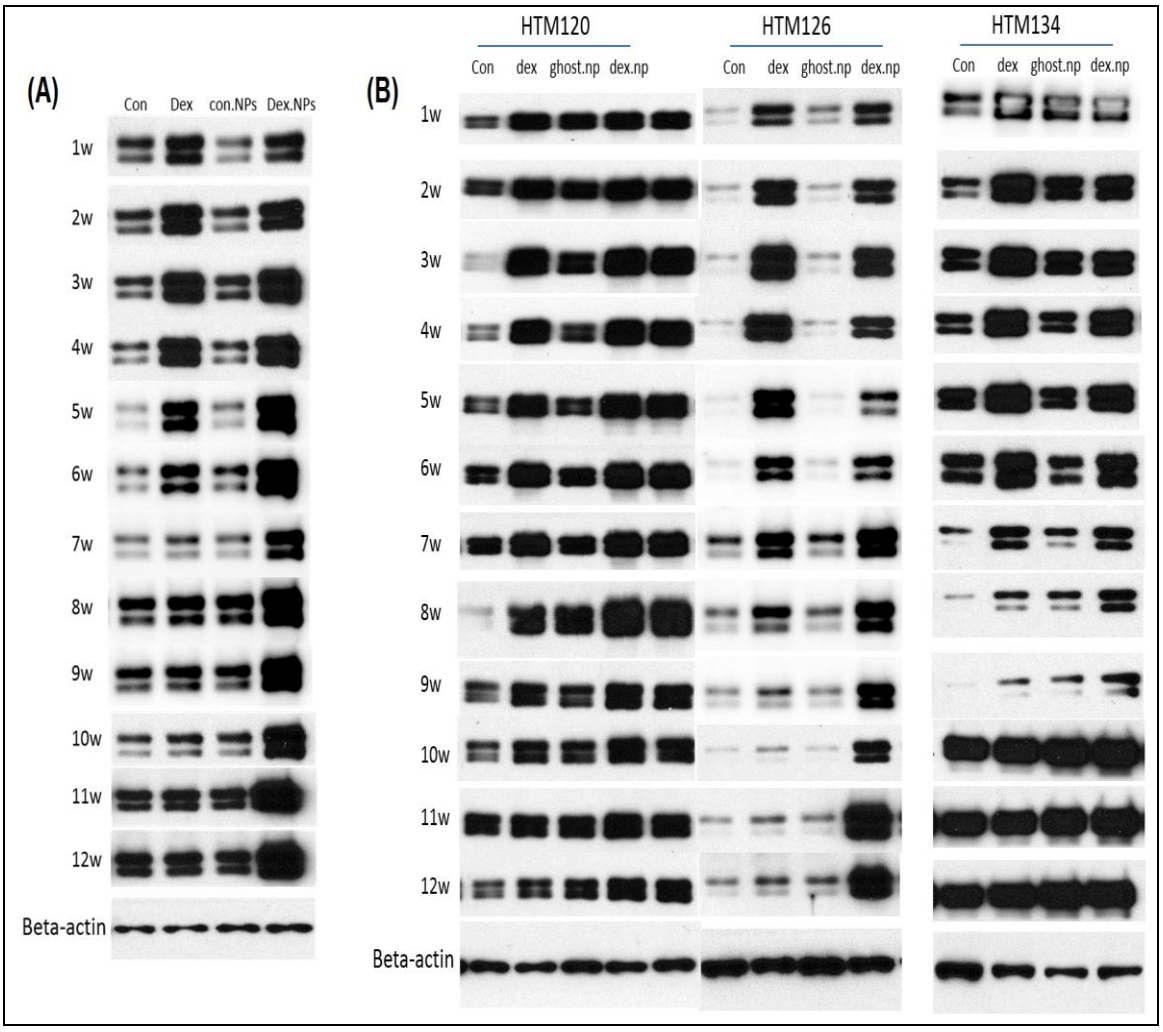

Figure 8.10 DEX-PB-NPs induced prolonged myocilin (MYOC) secretion from cultured HTM cells. Representative WB images showed MYOC secretion over time in response to DEX (39.25 ng/mL), Con-NPs and DEX-PB-NPs treatment. Cells were exposed to NP preparations for entire 12 week period, while only exposed to DEX for the first 4 weeks. Rows 1 to 12 show MYOC protein levels from week 1 to 12. Last row shows beta-actin from the same cells collected at end of 12 week period. Four HTM cell strains (A) HTM 136 (B) HTM 120, HTM 126, HTM 134, showed similar MYOC secretion pattern.

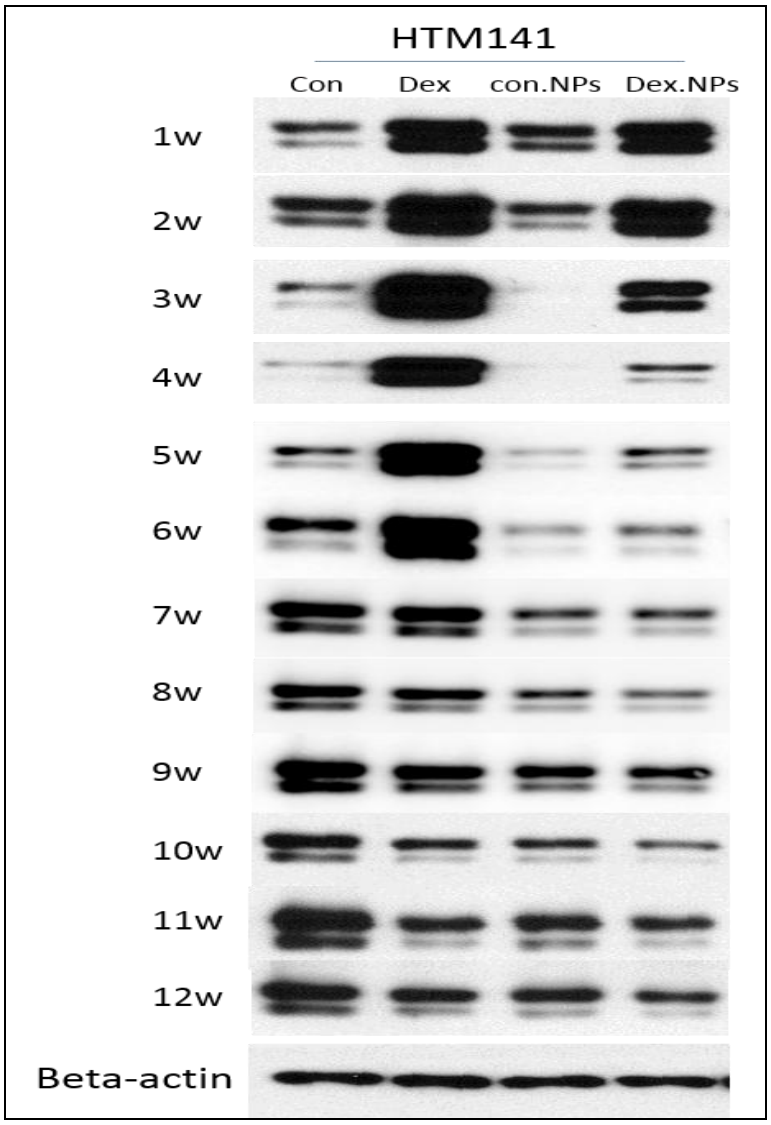

Figure 8.11 Unique myocilin (MYOC) secretion pattern observed in a single cell strain. Confluent HTM141 cells were treated with single application of Con-NPs or DEX-PB-NPs (1 mg/mL) and exposed for 12 weeks. Dex (39.25 ng/mL) treatment was repeated once/week for four weeks and then withdrawn. Cell culture media was collected and replaced with fresh 1% FBS media once/week for 12 weeks. Rows 1 to 12 show MYOC protein levels by Western blot from week 1 to 12. Last row shows beta-actin from the same cells collected at end of 12 weeks. (Reproduced from Ref. 240).

Quantitation of WB data from 5 HTM cell strains **(Figure 8.12)** showed that MYOC levels was increased 5.2 ± 1.3, 7.4 ± 4.3, and 2.8 ± 1.1 fold at 4, 8, and 12 weeks in presence of DEX-PB-NPs compared to 9.2 ± 3.8, 2.2 ± 0.5, and 1.5 ± 0.3 fold at 4, 8, and 12 weeks in control DEX treatment group. There were significant differences at early time points when DEX group is compared to the Control group (*). The DEX-PB-NP group was compared to ghost-NP group (#) using Mann-Whitney U Test. They did not reach statistical significant difference at later time points in DEX-PB-NPs compared to ghost-NP, primarily due to the unresponsiveness of on one cell strain HTM141(out of five cell strains) at later time points. The control data were consistent with our previous results (264) where MYOC from cells treated with DEX were significantly up-regulated (>4-fold) within the first 6 weeks and then gradually returned to near baseline levels at the end of 6 weeks. Based on the decline in MYOC levels after withdrawal of DEX from control wells, the data suggested that DEX-PB-NPs released the biologically active DEX for at least 10 weeks. Interestingly, the first measurement of MYOC levels in Con-NPs-treated groups at week 1 showed 4-fold increase, then dramatically dropped back to near control levels by 2 weeks, where it remained. By comparison, MYOC levels in vehicle treated control wells remained unchanged.

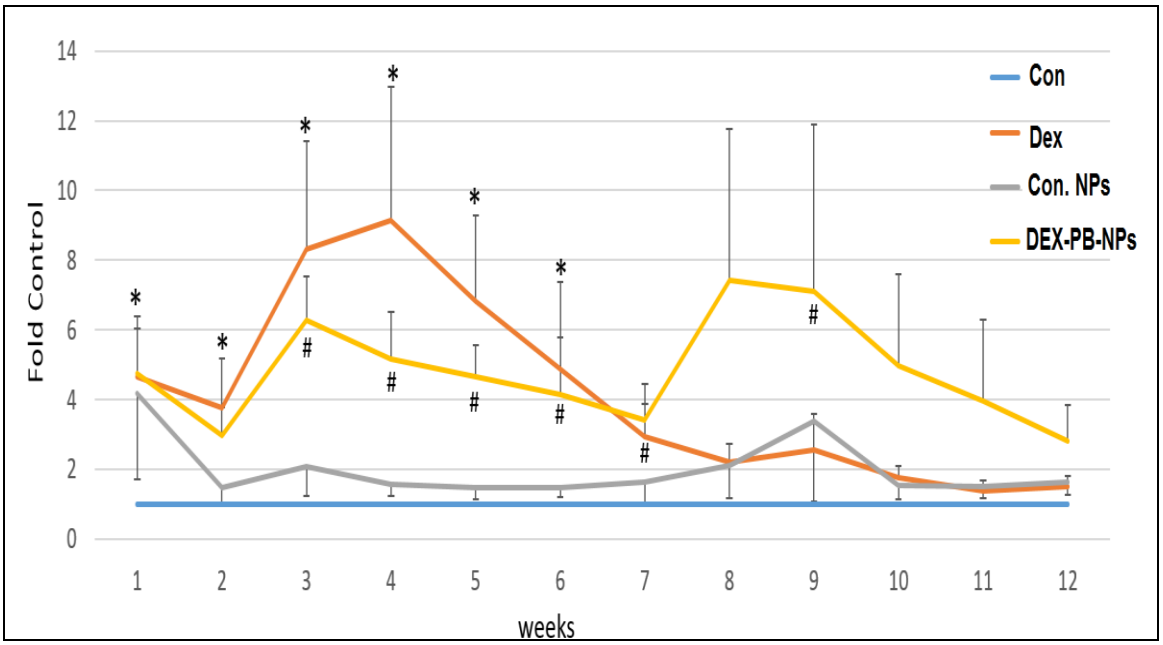

Figure 8.12 Quantification of myocilin (MYOC) secretion in response to Dexamethasone (DEX)-loaded nanoparticles (NPs) over time from HTM cells. MYOC Western blot images from all five HTM cell strains treated with DEX-NPs, Con NPs or DEX (39.25 ng/mL) for 12 time points for each strain were digitized and quantified using ImageJ software whereby the band intensities were normalized by beta-actin level observed for each individual cell strain. Cells were exposed to NP preparations for entire 12 weeks, while cells were only exposed to DEX for first four weeks. The relative MYOC secretion levels from DEX, Con-NPs and DEX-PB-NPs were compared to their individual controls at each time point. The combined data represent mean ± SE, N = 5. Symbols (* and $^{\#}$) indicates the significant differences compared to the Control group and ghost-NP group, respectively, using Mann-Whitney U Test. (Reproduced from Ref. 240).

Modification of HTM cell morphology by the PB polymer

Although not showing any signs of cytotoxicity, we did observe that HTM cells changed morphology in the presence of either NP alone or DEX-PB-NP, becoming more elongated **(Figure 8.13),** possibly due to phagocytosis of NPs. A change in morphology was observed as early as 6 weeks and continued upto the last observation at 12 weeks. Interestingly, morphology alterations did not appear to change the MYOC secretion response to DEX released from PB-NPs. In contrast, cells treated with DEX looked similar to vehicle control treated cells during the 4 weeks of treatment, compared to 12 weeks of Con-NPs. Regardless, changes in morphology were observed in cells treated with Con-NPs alone, suggesting that DEX was not responsible for morphological alterations.

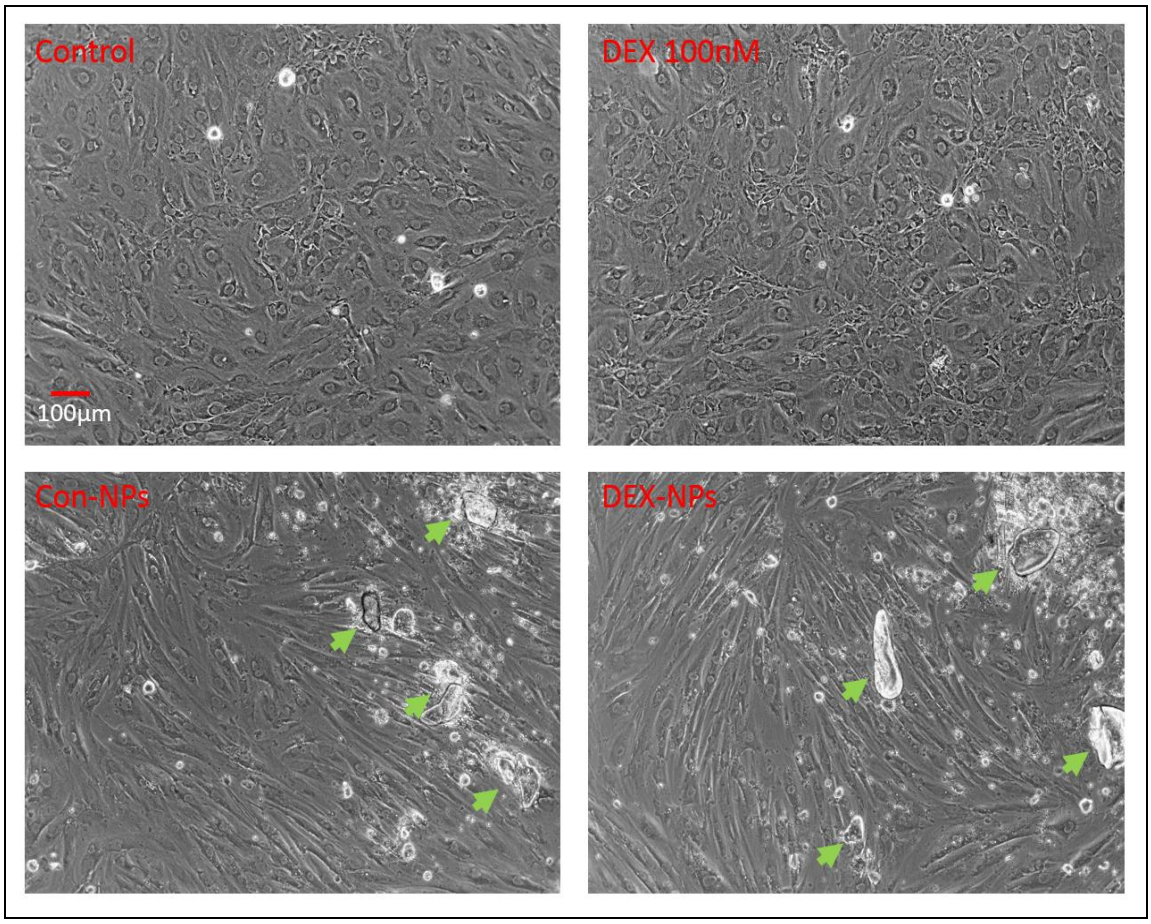

Figure 8.13 Modifications of HTM cells morphology by Con-NPs and DEX-PB-NPs but not by Dexamethasone (DEX). Confluent HTM cells were treated with single application of Con-NPs or DEX-PB-NPs (1 mg/mL) for entire 12 week observation period. In contrast, DEX (39.25 ng/mL) treatment was repeated once/week for four weeks. At the end of 12 weeks, cell morphology from each treatment was recorded under phase/contrast light microscope with 10 × magnifications. N = 5. Arrows indicate aggregated polymers. (Reproduced from Ref. 240).

Extraction of DEX from cell culture media

The culture media from the different cell strains of HTM cells was thawed and collected from cells exposed to DEX-PB-NPs once a week. DEX was extracted from the

collected media to determine the amount of DEX released from the NPs. The extraction efficiency was found to be > 90% for both DEX and HC. Interestingly, the amount of DEX released from all three strains was almost equal and detectable for 12 weeks.

Elevation of IOP by DEX-PB-NPs

IOP data were collected before and twice/week after DEX-PB-NPs or Con-NPs injection. As shown in **figure 8.14**, IOP was clearly elevated in DEX-PB-NPs treatment group, but not in Con-NPs group. By comparing between the two groups, significant IOP elevation observed for 8 days to 3 weeks after initial NPs injection. If IOP was compared to pre-injection, significant elevation started as early as 4 days post-injection in DEX-PB-NPs group and reached significantly different at all the time points.

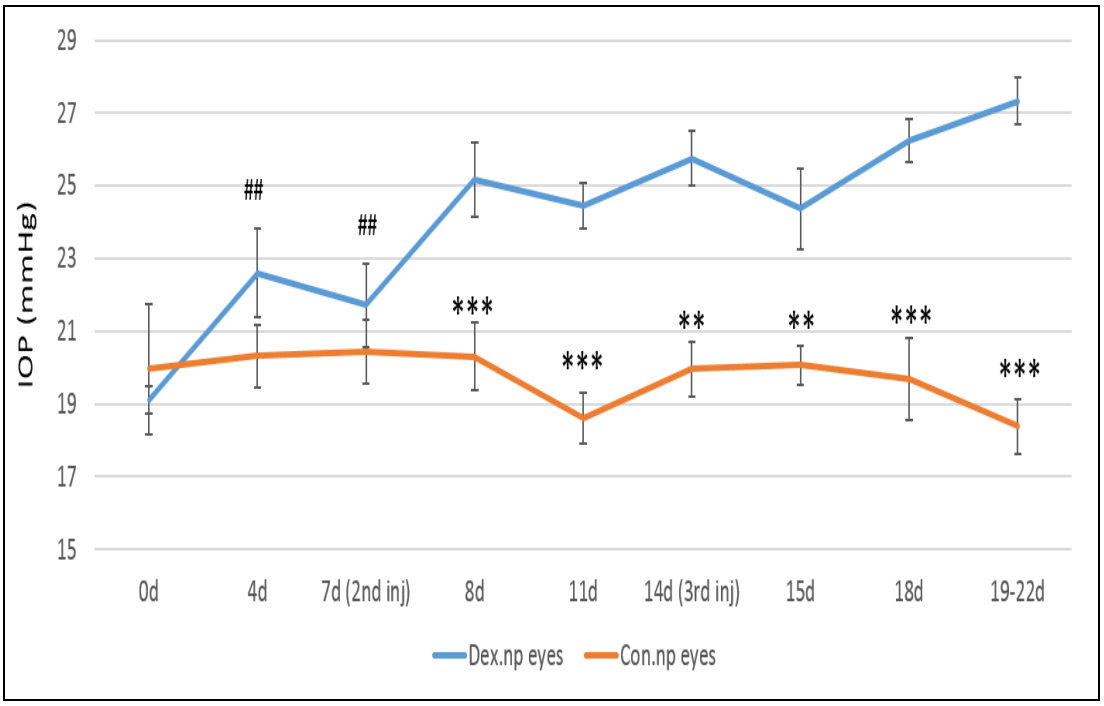

Figure 8.14 Elevation in intraocular pressure (IOP) by DEX-PB-NPs treatment group, compared to Con-NPs.

***In vivo* histology on C57BL/6 (C57) mice**

Histology analysis showed that neither DEX-PB-NPs nor Con-NPs modified gross outflowed tissues morphology after 3 weeks of initial DEX-NPs or Con-NPs injection as shown in **Figure 8.15.** The outflow tissues (TM, SC) did not show any abnormal phenomenon in gross morphology.

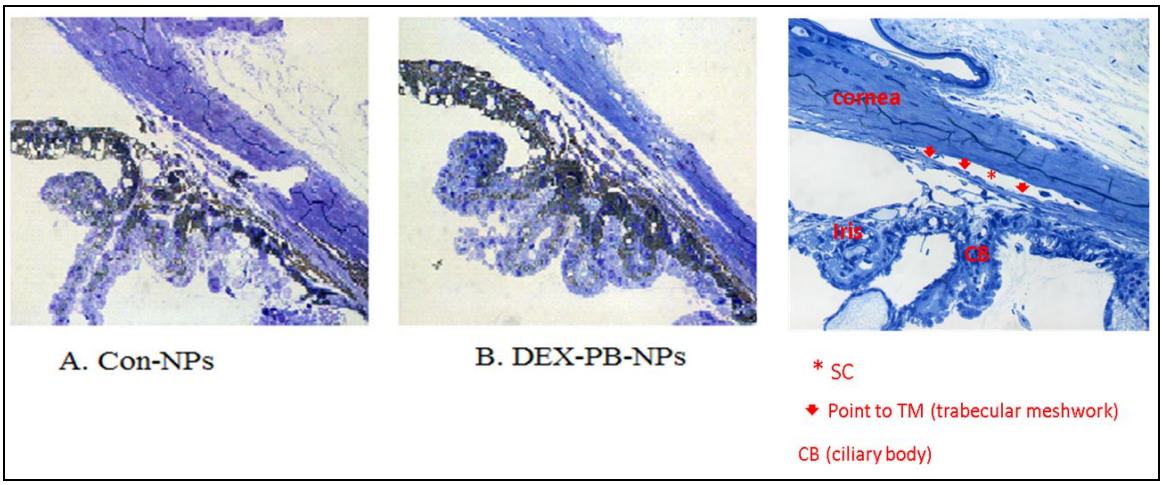

Figure 8.15 Ocular tissue morphology of DEX-PB-NPs and Con-NPs after subconjunctival injection

Conclusion

In the current study, a novel PB-NP loaded with DEX was developed to obtain a long-term slow release of DEX. The longer DEX release from the PB-NP was observed due to the high MW of the PB copolymer which required longer time for degradation. The activity of DEX-loaded PB copolymers on MYOC secretion was examined by the *in vitro* cell culture system using HTM cells. With a single application of the DEX-PB-NPs to cultured HTM cells, the robust upregulation of MYOC secretion by HTM cells was detected and maintained for more than 12 weeks. Consistent with a previous study, HTM cells from different donors can vary in response to DEX treatment (264). Out of five HTM cell strains studied, four of them showed consistent MYOC increase over the first 6 weeks (4 weeks of treatment). The level of MYOC in the media from these four cell strains decreased afterwards, but was still significantly higher than control levels after the 7 weeks. Only one cell strain (HTM141) showed an increase in MYOC secretion in response to DEX-PB-NPs for only three weeks before equal to or below control levels for the remainder of the study. The varied response to polymer treatments in different cell strains indicated that the polymers should be examined on various strains from multiple donors before it is studied *in vivo*.

The individual response to DEX treatment in the clinic varies; about 40% of non-glaucoma individuals are steroids responders. The exact mechanism for the steroids-induced IOP elevation is uncertain, but due to its time course likely involves at least two cellular processes in the resistance-generation region of the conventional outflow pathway: increased barrier function at the inner wall of SC and/or alterations in cell contractility and/or ECM turnover in the TM [33]. Resident TM cells are responsible for

maintenance of its unique architecture and their ECM constituents. The differential response of individual HTM cell strains to DEX and DEX-PB-NPs treatment in our study may have partially explained the important role of TM cells in steroids-induced ocular hypertension. For these reasons, it was important that multiple cell strains were tested.

Although, the PB copolymers didn't display any sign of cytotoxicity to HTM cells in this long-term study, it did modify the HTM cells morphology. HTM cell elongation was present in all strains following Con-NPs and DEX-PB-NPs treatments. Morphological modification of HTM cells by polymers may have accompanied functional changes that could not be measured in the present study, but needs further investigation. In addition, MYOC elevation was also observed in three HTM cell strains with Con-NPs treatment during the first week of the treatment. Therefore, the safety of copolymers must be ascertained further. This study provided the evidences that the *in vitro* system is a valuable tool for testing safety as well as the biological effects on steroids release from the polymers.

Although, the *in vitro* release conditions were somewhat different compared to DEX release study with HTM cell strains, an approximately equal amounts of DEX release was observed into the culture media. Under both *in vitro* conditions, DEX was released for a longer period of time. Although slow and long-term (>1 month) DEX release was detected in the current study, early burst release phenomenon still occurred with PB copolymers. This may limit the PB copolymers applications in some of the *in vivo* studies, especially in clinic. Our next goal is to develop the PB copolymers with different MWs, ratios, and arrangements so that the therapeutic agents could be released in more controlled zero-rate release fashion without initial burst release effect. At the

same time the PB copolymers must be biocompatible, biodegradable and should not modify the cellular functions and morphology.

In this project, DEX-induced ocular hypertension in mice was investigated. Within 1 week of DEX-PB-NPs, IOP became elevated by 2 to 3mm Hg, and IOP elevation was sustained throughout the entire 3- to 4-weeks duration of the study, which showed the promising use of DEX-PB-NPs. However, no single model has been shown to recapitulate all aspects of glaucoma, and each rodent model has particular advantages and disadvantages that make it suited to answer specific research questions. With several new developments in biotechnology, basic science research tools, and better understanding of the pathogenesis of glaucoma, more and better animal glaucoma models would be developed, helping to better treat the disease.

CHAPTER 9

SUMMARY AND FUTURE PROSPECTIVE

Summary

In chapter 8, PB copolymer (PGA-PCL-PEG-PCL-PGA) was synthesized in two steps by sequential ring-opening bulk copolymerization reaction. The PB copolymer was characterized by NMR, GPC and XRD. ^{1}H-NMR peaks comprised of glycolic acid displayed a series of singlets between 4.6 to 4.9 ppm confirming methylene protons of PGA block. PB copolymers depicted a single peak in GPC chromatogram indicating mono distribution of MW with PDI <1.5. XRD patterns of copolymer indicated that PCL blocks have retained semi-crystalline structure even after covalent conjugation with PGA blocks. DEX-loaded PB copolymer base NPs were prepared by oil in water (O/W) single emulsion solvent evaporation method. The percent EE and DL was determined as 63.23 ±2.31 and 10.53±0.38 %w/w (n = 3), respectively. The particle size of NPs was found to be 109 ± 3.77 nm, analyzed by NTA measurements. A long term DEX release from the PB-NPs was observed for over three months. A biphasic release pattern of DEX was evident from NPs with an initial burst release followed by a sustained release phase. Cytotoxic effects of PB copolymers on corneal (SV-40), conjunctival (CCL20.2), retinal (D407), and HTM cells indicated a negligible toxicity. In addition, more than 90% cell viability (for all the cell lines) after 48 hours and 12 weeks of exposure of HTM cells to PB copolymer and PB-NPs suggested their excellent safety profiles.

To study MYOC elevation, five strains of TM cells (HTM120/136/126/134/141) were isolated from eyes of human donors of ages11- and 3-month-old (HTM120/136),

88-, 51-, and 38-year old (HTM126/134/141), respectively and treated with DEX-PB-NPs. The expression and secretion of MYOC from primary cultures of TM cells was robustly enhanced following DEX treatment and quantitatively analyzed by Western Blot. Based on the decline in MYOC levels after withdrawal of DEX from control wells, the data suggested that DEX-PB-NPs released the DEX for at least 10 weeks. Interestingly, MYOC levels in Con-NPs-treated groups at week one showed a 4-fold increase, and then dramatically dropped back to near control levels by 2 weeks. The MYOC levels in vehicle treated control wells remain unchanged. The C57BL/6 mice were selected to develop *in vivo* model for glaucoma. After subcutaneous injection, IOP level became elevated by 2 to 3 mm and sustained throughout the entire 3- to 4-week duration of the study. *In vivo histology* was performed in the presence of control and DEX-PB-NP on the ocular tissues. The outflow tissues (TM, SC) did not show any abnormal phenomenon in gross morphology in the presence of DEX-PB-NPs and Con-NPs, analyzed after 3 weeks of injection.

Future prospective

The ocular hypertension related to GC induced glaucoma using primary cultures of HTM cells has been investigated. Activity and safety of DEX-PB-NPs over time with HTM was excellent. Therefore, the developed system is found to be a valuable and novel tool for determining the safety and effects of steroids released from polymeric NPs. Although, the PB copolymer did not show any sign of cytotoxicity to HTM cells in this long-term study, it did modify the HTM cell morphology. HTM cell elongation was present in all cell strains after both Con-NPs and DEX-PB-NPs treatment. Morphological

modification of HTM cells by the copolymers may accompany functional changes those were not measured in the present study, but needs further investigation. Moreover, in future, the synthesis of PB copolymers with different MWs, ratios and arrangements will be studied to obtain a controlled zero-order drug release rate with minimal initial burst effect. In addition, several HTM cell strains will be analyzed from different donors. Currently, the pathogenesis of TM dysfunction, on primary cultures of HTM cells are under investigation. Further, this model will be evaluated for new ocular therapies aimed at lowering intra-ocular pressure in humans. Moreover, the IOP-lowering capabilities of novel rho kinase inhibitor (netarsudil), beta-blockers (timolol), Prostaglandin analogs (latanoprost), Alpha-adrenergic agent (brimonidine) and carbonic anhydrase inhibitors (dorzolamide) will be studied in a mouse model. Overall, this approach will be followed to generate an animal model for GC induced ocular hypertension and to evaluate the IOP-lowering capabilities of several class of glaucoma drugs.

REFERENCES

1. Agrahari V, Agrahari V, Mandal A, Pal D, Mitra AK. How are we improving the delivery to back of the eye? Advances and challenges of novel therapeutic approaches. Expert Opin Drug Deliv. 2016:1-17. doi: 10.1080/17425247.2017.1272569.
2. Agrahari V, Agrahari V, Mitra AK. Nanocarrier fabrication and macromolecule drug delivery: challenges and opportunities. Ther Deliv. 2016;7(4):257-78. doi: 10.4155/tde-2015-0012.
3. Wong WL, Su X, Li X, Cheung CM, Klein R, Cheng CY, et al. Global prevalence of age-related macular degeneration and disease burden projection for 2020 and 2040: a systematic review and meta-analysis. Lancet Glob Health. 2014;2(2):e106-16. doi: 10.1016/S2214-109X(13)70145-1.
4. Agarwal A, Rhoades WR, Hanout M, Soliman MK, Sarwar S, Sadiq MA, et al. Management of neovascular age-related macular degeneration: current state-of-the-art care for optimizing visual outcomes and therapies in development. Clin Ophthalmol. 2015;9:1001-15. doi: 10.2147/OPTH.S74959.
5. Volz C, Pauly D. Antibody therapies and their challenges in the treatment of age-related macular degeneration. Eur J Pharm Biopharm. 2015;95(Pt B):158-72. doi: 10.1016/j.ejpb.2015.02.020.
6. Nazari H, Zhang L, Zhu D, Chader GJ, Falabella P, Stefanini F, et al. Stem cell based therapies for age-related macular degeneration: The promises and the challenges. Prog Retin Eye Res. 2015;48:1-39. doi: 10.1016/j.preteyeres.2015.06.004.
7. Ambati J, Atkinson JP, Gelfand BD. Immunology of age-related macular degeneration. Nat Rev Immunol. 2013;13(6):438-51. doi: 10.1038/nri3459.
8. Shaw PX, Stiles T, Douglas C, Ho D, Fan W, Du H, et al. Oxidative stress, innate immunity, and age-related macular degeneration. AIMS Mol Sci. 2016;3(2):196-221. doi: 10.3934/molsci.2016.2.196.
9. Bertolotti E, Neri A, Camparini M, Macaluso C, Marigo V. Stem cells as source for retinal pigment epithelium transplantation. Prog Retin Eye Res. 2014;42:130-44. doi: 10.1016/j.preteyeres.2014.06.002.
10. Zhu Y, Carido M, Meinhardt A, Kurth T, Karl MO, Ader M, et al. Three-dimensional neuroepithelial culture from human embryonic stem cells and its use for quantitative conversion to retinal pigment epithelium. PLoS One. 2013;8(1):e54552. doi: 10.1371/journal.pone.0054552.
11. Smith AG, Kaiser PK. Emerging treatments for wet age-related macular degeneration. Expert Opin Emerg Drugs. 2014;19(1):157-64. doi: 10.1517/14728214.2014.884559.
12. Ozkiris A. Anti-VEGF agents for age-related macular degeneration. Expert Opin Ther Pat. 2010;20(1):103-18. doi: 10.1517/13543770902762885.
13. Age-Related Eye Disease Study Research G. A randomized, placebo-controlled, clinical trial of high-dose supplementation with vitamins C and E, beta carotene, and zinc for age-related macular degeneration and vision loss: AREDS report no. 8. Arch Ophthalmol. 2001;119(10):1417-36.
14. Kawczyk-Krupka A, Bugaj AM, Potempa M, Wasilewska K, Latos W, Sieron A. Vascular-targeted photodynamic therapy in the treatment of neovascular age-related

macular degeneration: Clinical perspectives. Photodiagnosis Photodyn Ther. 2015;12(2):161-75. doi: 10.1016/j.pdpdt.2015.03.007.
15. Rishi E, Rishi P, Sharma V, Koundanya V, Athanikar R. Long-term outcomes of combination photodynamic therapy with ranibizumab or bevacizumab for treatment of wet age-related macular degeneration. Oman J Ophthalmol. 2016;9(2):87-92. doi: 10.4103/0974-620X.184511.
16. Yang S, Zhao J, Sun X. Resistance to anti-VEGF therapy in neovascular age-related macular degeneration: a comprehensive review. Drug Des Devel Ther. 2016;10:1857-67. doi: 10.2147/DDDT.S97653.
17. Villegas VM, Aranguren LA, Kovach JL, Schwartz SG, Flynn HW, Jr. Current advances in the treatment of neovascular age-related macular degeneration. Expert Opin Drug Deliv. 2016:1-10. doi: 10.1080/17425247.2016.1213240.
18. Amadio M, Govoni S, Pascale A. Targeting VEGF in eye neovascularization: What's new?: A comprehensive review on current therapies and oligonucleotide-based interventions under development. Pharmacol Res. 2016;103:253-69. doi: 10.1016/j.phrs.2015.11.027.
19. Kompella UB, Amrite AC, Pacha Ravi R, Durazo SA. Nanomedicines for back of the eye drug delivery, gene delivery, and imaging. Prog Retin Eye Res. 2013;36:172-98. doi: 10.1016/j.preteyeres.2013.04.001.
20. Kaur IP, Kakkar S. Nanotherapy for posterior eye diseases. J Control Release. 2014;193:100-12. doi: 10.1016/j.jconrel.2014.05.031.
21. Eandi CM, Alovisi C, De Sanctis U, Grignolo FM. Treatment for neovascular age related macular degeneration: The state of the art. Eur J Pharmacol. 2016. doi: 10.1016/j.ejphar.2016.03.002.
22. Zhou B, Wang B. Pegaptanib for the treatment of age-related macular degeneration. Exp Eye Res. 2006;83(3):615-9. doi: 10.1016/j.exer.2006.02.010.
23. Lu X, Sun X. Profile of conbercept in the treatment of neovascular age-related macular degeneration. Drug Des Devel Ther. 2015;9:2311-20. doi: 10.2147/DDDT.S67536.
24. Holz FG, Dugel PU, Weissgerber G, Hamilton R, Silva R, Bandello F, et al. Single-Chain Antibody Fragment VEGF Inhibitor RTH258 for Neovascular Age-Related Macular Degeneration: A Randomized Controlled Study. Ophthalmology. 2016;123(5):1080-9. doi: 10.1016/j.ophtha.2015.12.030.
25. Souied EH, Devin F, Mauget-Faysse M, Kolar P, Wolf-Schnurrbusch U, Framme C, et al. Treatment of exudative age-related macular degeneration with a designed ankyrin repeat protein that binds vascular endothelial growth factor: a phase I/II study. Am J Ophthalmol. 2014;158(4):724-32 e2. doi: 10.1016/j.ajo.2014.05.037.
26. Kim J, Kim TE, Kim JA, Yun JH, Sohn S, Shim SR, et al. Intravitreal tanibirumab, a fully human monoclonal antibody against vascular endothelial growth factor receptor 2, partially suppresses and regresses laser-induced choroidal neovascularization in a rat model. J Ocul Pharmacol Ther. 2014;30(10):847-53. doi: 10.1089/jop.2014.0021.
27. Lee SH. Tanibirumab (TTAC-0001): a fully human monoclonal antibody targets vascular endothelial growth factor receptor 2 (VEGFR-2). Arch Pharm Res. 2011;34(8):1223-6. doi: 10.1007/s12272-011-0821-9.

28. Cade WT. Diabetes-related microvascular and macrovascular diseases in the physical therapy setting. Phys Ther. 2008;88(11):1322-35. doi: 10.2522/ptj.20080008.
29. Stitt AW, Curtis TM, Chen M, Medina RJ, McKay GJ, Jenkins A, et al. The progress in understanding and treatment of diabetic retinopathy. Prog Retin Eye Res. 2016;51:156-86. doi: 10.1016/j.preteyeres.2015.08.001.
30. Hendrick AM, Gibson MV, Kulshreshtha A. Diabetic Retinopathy. Prim Care. 2015;42(3):451-64. doi: 10.1016/j.pop.2015.05.005.
31. Tarr JM, Kaul K, Chopra M, Kohner EM, Chibber R. Pathophysiology of diabetic retinopathy. ISRN Ophthalmol. 2013;2013:343560. doi: 10.1155/2013/343560.
32. Rosberger DF. Diabetic retinopathy: current concepts and emerging therapy. Endocrinol Metab Clin North Am. 2013;42(4):721-45. doi: 10.1016/j.ecl.2013.08.001.
33. Das A, McGuire PG, Monickaraj F. Novel pharmacotherapies in diabetic retinopathy: Current status and what's in the horizon? Indian J Ophthalmol. 2016;64(1):4-13. doi: 10.4103/0301-4738.178154.
34. Das A, Stroud S, Mehta A, Rangasamy S. New treatments for diabetic retinopathy. Diabetes Obes Metab. 2015;17(3):219-30. doi: 10.1111/dom.12384.
35. Vaziri K, Schwartz SG, Relhan N, Kishor KS, Flynn HW, Jr. New Therapeutic Approaches in Diabetic Retinopathy. Rev Diabet Stud. 2015;12(1-2):196-210. doi: 10.1900/RDS.2015.12.196.
36. Amoaku WM, Saker S, Stewart EA. A review of therapies for diabetic macular oedema and rationale for combination therapy. Eye (Lond). 2015;29(9):1115-30. doi: 10.1038/eye.2015.110.
37. Das A. Diabetic Retinopathy: Battling the Global Epidemic. Invest Ophthalmol Vis Sci. 2016;57(15):6669-82. doi: 10.1167/iovs.16-21031.
38. Arevalo JF. Diabetic macular edema: changing treatment paradigms. Curr Opin Ophthalmol. 2014;25(6):502-7. doi: 10.1097/ICU.0000000000000102.
39. Lally DR, Shah CP, Heier JS. Vascular endothelial growth factor and diabetic macular edema. Surv Ophthalmol. 2016;61(6):759-68. doi: 10.1016/j.survophthal.2016.03.010.
40. Colucciello M. Current intravitreal pharmacologic therapies for diabetic macular edema. Postgrad Med. 2015;127(6):640-53. doi: 10.1080/00325481.2015.1052523.
41. Ramakrishnan S, Anand V, Roy S. Vascular endothelial growth factor signaling in hypoxia and inflammation. J Neuroimmune Pharmacol. 2014;9(2):142-60. doi: 10.1007/s11481-014-9531-7.
42. Stefanini FR, Badaro E, Falabella P, Koss M, Farah ME, Maia M. Anti-VEGF for the management of diabetic macular edema. J Immunol Res. 2014;2014:632307. doi: 10.1155/2014/632307.
43. Pescosolido N, Pranno F, Buomprisco G. Intravitreal injections and diabetic macular edema: actual and new therapeutic options. Curr Diabetes Rev. 2013;9(6):491-8.
44. Greco A, Rizzo MI, De Virgilio A, Gallo A, Fusconi M, de Vincentiis M. Emerging Concepts in Glaucoma and Review of the Literature. Am J Med. 2016;129(9):1000 e7- e13. doi: 10.1016/j.amjmed.2016.03.038.
45. Conlon R, Saheb H, Ahmed, II. Glaucoma treatment trends: a review. Can J Ophthalmol. 2017;52(1):114-24. doi: 10.1016/j.jcjo.2016.07.013.
46. Weinreb RN, Aung T, Medeiros FA. The pathophysiology and treatment of glaucoma: a review. JAMA. 2014;311(18):1901-11. doi: 10.1001/jama.2014.3192.

47. Schehlein EM, Novack GD, Robin AL. New classes of glaucoma medications. Curr Opin Ophthalmol. 2017;28(2):161-8. doi: 10.1097/ICU.0000000000000346.
48. Agrahari V, Mandal A, Agrahari V, Trinh HM, Joseph M, Ray A, et al. A comprehensive insight on ocular pharmacokinetics. Drug Deliv Transl Res. 2016;6(6):735-54. doi: 10.1007/s13346-016-0339-2.
49. Eljarrat-Binstock E, Pe'er J, Domb AJ. New techniques for drug delivery to the posterior eye segment. Pharm Res. 2010;27(4):530-43. doi: 10.1007/s11095-009-0042-9.
50. Patel A, Cholkar K, Agrahari V, Mitra AK. Ocular drug delivery systems: An overview. World J Pharmacol. 2013;2(2):47-64. doi: 10.5497/wjp.v2.i2.47.
51. Boddu SH, Gupta H, Patel S. Drug delivery to the back of the eye following topical administration: an update on research and patenting activity. Recent Pat Drug Deliv Formul. 2014;8(1):27-36.
52. Gurman P, Miranda OR, Clayton K, Rosen Y, Elman NM. Clinical applications of biomedical microdevices for controlled drug delivery. Mayo Clin Proc. 2015;90(1):93-108. doi: 10.1016/j.mayocp.2014.10.003.
53. Bruno BJ, Miller GD, Lim CS. Basics and recent advances in peptide and protein drug delivery. Ther Deliv. 2013;4(11):1443-67. doi: 10.4155/tde.13.104.
54. Pinholt C, Hartvig RA, Medlicott NJ, Jorgensen L. The importance of interfaces in protein drug delivery - why is protein adsorption of interest in pharmaceutical formulations? Expert Opin Drug Deliv. 2011;8(7):949-64. doi: 10.1517/17425247.2011.577062.
55. Nicolas J, Mura S, Brambilla D, Mackiewicz N, Couvreur P. Design, functionalization strategies and biomedical applications of targeted biodegradable/biocompatible polymer-based nanocarriers for drug delivery. Chem Soc Rev. 2013;42(3):1147-235. doi: 10.1039/c2cs35265f.
56. Demetzos C, Pippa N. Advanced drug delivery nanosystems (aDDnSs): a mini-review. Drug Deliv. 2014;21(4):250-7. doi: 10.3109/10717544.2013.844745.
57. Kim JK, Kim HJ, Chung JY, Lee JH, Young SB, Kim YH. Natural and synthetic biomaterials for controlled drug delivery. Arch Pharm Res. 2014;37(1):60-8. doi: 10.1007/s12272-013-0280-6.
58. Danhier F, Ansorena E, Silva JM, Coco R, Le Breton A, Preat V. PLGA-based nanoparticles: an overview of biomedical applications. J Control Release. 2012;161(2):505-22. doi: 10.1016/j.jconrel.2012.01.043.
59. Kapoor DN, Bhatia A, Kaur R, Sharma R, Kaur G, Dhawan S. PLGA: a unique polymer for drug delivery. Ther Deliv. 2015;6(1):41-58. doi: 10.4155/tde.14.91.
60. Pillai CK, Sharma CP. Review paper: absorbable polymeric surgical sutures: chemistry, production, properties, biodegradability, and performance. J Biomater Appl. 2010;25(4):291-366. doi: 10.1177/0885328210384890.
61. Farah S, Anderson DG, Langer R. Physical and mechanical properties of PLA, and their functions in widespread applications - A comprehensive review. Adv Drug Deliv Rev. 2016;107:367-92. doi: 10.1016/j.addr.2016.06.012.
62. Xu Y, Kim CS, Saylor DM, Koo D. Polymer degradation and drug delivery in PLGA-based drug-polymer applications: A review of experiments and theories. J Biomed Mater Res B Appl Biomater. 2016. doi: 10.1002/jbm.b.33648.

63. Yasukawa T, Ogura Y, Sakurai E, Tabata Y, Kimura H. Intraocular sustained drug delivery using implantable polymeric devices. Adv Drug Deliv Rev. 2005;57(14):2033-46. doi: 10.1016/j.addr.2005.09.005.
64. Hines DJ, Kaplan DL. Poly(lactic-co-glycolic) acid-controlled-release systems: experimental and modeling insights. Crit Rev Ther Drug Carrier Syst. 2013;30(3):257-76.
65. Makadia HK, Siegel SJ. Poly lactic-co-glycolic acid (plga) as biodegradable controlled drug delivery carrier. Polymers (Basel). 2011;3(3):1377-97. doi: 10.3390/polym3031377.
66. Labet M, Thielemans W. Synthesis of polycaprolactone: a review. Chem Soc Rev. 2009;38(12):3484-504. doi: 10.1039/b820162p.
67. Kamaly N, Yameen B, Wu J, Farokhzad OC. Degradable controlled-release polymers and polymeric nanoparticles: mechanisms of controlling drug release. Chem Rev. 2016;116(4):2602-63. doi: 10.1021/acs.chemrev.5b00346.
68. Dash TK, Konkimalla VB. Polymeric modification and its implication in drug delivery: poly-epsilon-caprolactone (PCL) as a model polymer. Mol Pharm. 2012;9(9):2365-79. doi: 10.1021/mp3001952.
69. Sahoo SK, Dilnawaz F, Krishnakumar S. Nanotechnology in ocular drug delivery. Drug Discov Today. 2008;13(3-4):144-51. doi: 10.1016/j.drudis.2007.10.021.
70. Meng J, Agrahari V, Youm I. Advances in Targeted drug delivery approaches for the central nervous system tumors: the inspiration of nanobiotechnology. J Neuroimmune Pharmacol. 2016. doi: 10.1007/s11481-016-9698-1.
71. Diebold Y, Calonge M. Applications of nanoparticles in ophthalmology. Prog Retin Eye Res. 2010;29(6):596-609. doi: 10.1016/j.preteyeres.2010.08.002.
72. Nagarwal RC, Kant S, Singh PN, Maiti P, Pandit JK. Polymeric nanoparticulate system: a potential approach for ocular drug delivery. J Control Release. 2009;136(1):2-13. doi: 10.1016/j.jconrel.2008.12.018.
73. Bochot A, Fattal E. Liposomes for intravitreal drug delivery: a state of the art. J Control Release. 2012;161(2):628-34. doi: 10.1016/j.jconrel.2012.01.019.
74. Akbarzadeh A, Rezaei-Sadabady R, Davaran S, Joo SW, Zarghami N, Hanifehpour Y, et al. Liposome: classification, preparation, and applications. Nanoscale Res Lett. 2013;8(1):102. doi: 10.1186/1556-276X-8-102.
75. Herrero-Vanrell R, Bravo-Osuna I, Andres-Guerrero V, Vicario-de-la-Torre M, Molina-Martinez IT. The potential of using biodegradable microspheres in retinal diseases and other intraocular pathologies. Prog Retin Eye Res. 2014;42:27-43. doi: 10.1016/j.preteyeres.2014.04.002.
76. Kim YC, Chiang B, Wu X, Prausnitz MR. Ocular delivery of macromolecules. J Control Release. 2014;190:172-81. doi: 10.1016/j.jconrel.2014.06.043.
77. Lu Y, Park K. Polymeric micelles and alternative nanonized delivery vehicles for poorly soluble drugs. Int J Pharm. 2013;453(1):198-214. doi: 10.1016/j.ijpharm.2012.08.042.
78. Vaishya RD, Khurana V, Patel S, Mitra AK. Controlled ocular drug delivery with nanomicelles. Wiley Interdiscip Rev Nanomed Nanobiotechnol. 2014;6(5):422-37. doi: 10.1002/wnan.1272.

79. Cholkar K, Patel A, Vadlapudi AD, Mitra AK. Novel Nanomicellar formulation approaches for anterior and posterior segment ocular drug delivery. Recent Pat Nanomed. 2012;2(2):82-95. doi: 10.2174/1877912311202020082.
80. Rodriguez Villanueva J, Navarro MG, Rodriguez Villanueva L. Dendrimers as a promising tool in ocular therapeutics: Latest advances and perspectives. Int J Pharm. 2016;511(1):359-66. doi: 10.1016/j.ijpharm.2016.07.031.
81. Kambhampati SP, Kannan RM. Dendrimer nanoparticles for ocular drug delivery. J Ocul Pharmacol Ther. 2013;29(2):151-65. doi: 10.1089/jop.2012.0232.
82. Coursey TG, Henriksson JT, Marcano DC, Shin CS, Isenhart LC, Ahmed F, et al. Dexamethasone nanowafer as an effective therapy for dry eye disease. J Control Release. 2015;213:168-74. doi: 10.1016/j.jconrel.2015.07.007.
83. Yuan X, Marcano DC, Shin CS, Hua X, Isenhart LC, Pflugfelder SC, et al. Ocular drug delivery nanowafer with enhanced therapeutic efficacy. ACS Nano. 2015;9(2):1749-58. doi: 10.1021/nn506599f.
84. Sharma OP, Patel V, Mehta T. Nanocrystal for ocular drug delivery: hope or hype. Drug Deliv Transl Res. 2016;6(4):399-413. doi: 10.1007/s13346-016-0292-0.
85. Gupta S, Samanta MK, Raichur AM. Dual-drug delivery system based on in situ gel-forming nanosuspension of forskolin to enhance antiglaucoma efficacy. AAPS PharmSciTech. 2010;11(1):322-35. doi: 10.1208/s12249-010-9388-x.
86. Tuomela A, Liu P, Puranen J, Ronkko S, Laaksonen T, Kalesnykas G, et al. Brinzolamide nanocrystal formulations for ophthalmic delivery: reduction of elevated intraocular pressure in vivo. Int J Pharm. 2014;467(1-2):34-41. doi: 10.1016/j.ijpharm.2014.03.048.
87. Peptu CA, Popa M, Savin C, Popa RF, Ochiuz L. Modern drug delivery systems for targeting the posterior segment of the eye. Curr Pharm Des. 2015;21(42):6055-69.
88. Buwalda SJ, Boere KW, Dijkstra PJ, Feijen J, Vermonden T, Hennink WE. Hydrogels in a historical perspective: from simple networks to smart materials. J Control Release. 2014;190:254-73. doi: 10.1016/j.jconrel.2014.03.052.
89. Agrahari V, Agrahari V, Hung WT, Christenson LK, Mitra AK. Composite nanoformulation therapeutics for long-term ocular delivery of macromolecules. Mol Pharm. 2016. doi: 10.1021/acs.molpharmaceut.5b00828.
90. Patel SP, Vaishya R, Patel A, Agrahari V, Pal D, Mitra AK. Optimization of novel pentablock copolymer based composite formulation for sustained delivery of peptide/protein in the treatment of ocular diseases. J Microencapsul. 2016;33(2):103-13. doi: 10.3109/02652048.2015.1134685.
91. Yasin MN, Svirskis D, Seyfoddin A, Rupenthal ID. Implants for drug delivery to the posterior segment of the eye: a focus on stimuli-responsive and tunable release systems. J Control Release. 2014;196:208-21. doi: 10.1016/j.jconrel.2014.09.030.
92. Lee SS, Hughes P, Ross AD, Robinson MR. Biodegradable implants for sustained drug release in the eye. Pharm Res. 2010;27(10):2043-53. doi: 10.1007/s11095-010-0159-x.
93. Bourges JL, Bloquel C, Thomas A, Froussart F, Bochot A, Azan F, et al. Intraocular implants for extended drug delivery: therapeutic applications. Adv Drug Deliv Rev. 2006;58(11):1182-202. doi: 10.1016/j.addr.2006.07.026.
94. Mura S, Nicolas J, Couvreur P. Stimuli-responsive nanocarriers for drug delivery. Nat Mater. 2013;12(11):991-1003. doi: 10.1038/nmat3776.

95. Mahlumba P, Choonara YE, Kumar P, du Toit LC, Pillay V. Stimuli-responsive polymeric systems for controlled protein and peptide delivery: future implications for ocular delivery. Molecules. 2016;21(8). doi: 10.3390/molecules21081002.
96. Agrahari V, Zhang C, Zhang T, Li W, Gounev TK, Oyler NA, et al. Hyaluronidase-sensitive nanoparticle templates for triggered release of HIV/AIDS microbicide in vitro. AAPS J. 2014;16(2):181-93. doi: 10.1208/s12248-013-9546-7.
97. Porta IBM, Eckstein C, Xifre-Perez E, Formentin P, Ferre-Borrull J, Marsal LF. Sustained, Controlled and stimuli-responsive drug release systems based on nanoporous anodic alumina with layer-by-layer polyelectrolyte. Nanoscale Res Lett. 2016;11(1):372. doi: 10.1186/s11671-016-1585-4.
98. Zhang T, Zhang C, Agrahari V, Murowchick JB, Oyler NA, Youan BB. Spray drying tenofovir loaded mucoadhesive and pH-sensitive microspheres intended for HIV prevention. Antiviral Res. 2013;97(3):334-46. doi: 10.1016/j.antiviral.2012.12.019.
99. Christie JG, Kompella UB. Ophthalmic light sensitive nanocarrier systems. Drug Discov Today. 2008;13(3-4):124-34. doi: 10.1016/j.drudis.2007.12.005.
100. Huu VA, Luo J, Zhu J, Zhu J, Patel S, Boone A, et al. Light-responsive nanoparticle depot to control release of a small molecule angiogenesis inhibitor in the posterior segment of the eye. J Control Release. 2015;200:71-7. doi: 10.1016/j.jconrel.2015.01.001.
101. Tyagi P, Barros M, Stansbury JW, Kompella UB. Light-activated, in situ forming gel for sustained suprachoroidal delivery of bevacizumab. Mol Pharm. 2013;10(8):2858-67. doi: 10.1021/mp300716t.
102. Matanovic MR, Kristl J, Grabnar PA. Thermoresponsive polymers: insights into decisive hydrogel characteristics, mechanisms of gelation, and promising biomedical applications. Int J Pharm. 2014;472(1-2):262-75. doi: 10.1016/j.ijpharm.2014.06.029.
103. Xie B, Jin L, Luo Z, Yu J, Shi S, Zhang Z, et al. An injectable thermosensitive polymeric hydrogel for sustained release of Avastin(R) to treat posterior segment disease. Int J Pharm. 2015;490(1-2):375-83. doi: 10.1016/j.ijpharm.2015.05.071.
104. Huang D, Wang L, Dong Y, Pan X, Li G, Wu C. A novel technology using transscleral ultrasound to deliver protein loaded nanoparticles. Eur J Pharm Biopharm. 2014;88(1):104-15. doi: 10.1016/j.ejpb.2014.04.011.
105. Zderic V, Vaezy S, Martin RW, Clark JI. Ocular drug delivery using 20-kHz ultrasound. Ultrasound Med Biol. 2002;28(6):823-9.
106. Lafond M, Aptel F, Mestas JL, Lafon C. Ultrasound-mediated ocular delivery of therapeutic agents: a review. Expert Opin Drug Deliv. 2016:1-12. doi: 10.1080/17425247.2016.1198766.
107. Burke CW, Alexander Et, Timbie K, Kilbanov AL, Price RJ. Ultrasound-activated agents comprised of 5FU-bearing nanoparticles bonded to microbubbles inhibit solid tumor growth and improve survival. Mol Ther. 2014;22(2):321-8. doi: 10.1038/mt.2013.259.
108. Nabili M, Shenoy A, Chawla S, Mahesh S, Liu J, Geist C, et al. Ultrasound-enhanced ocular delivery of dexamethasone sodium phosphate: an in vivo study. J Ther Ultrasound. 2014;2:6. doi: 10.1186/2050-5736-2-6.
109. Lo R, Li PY, Saati S, Agrawal R, Humayun MS, Meng E. A refillable microfabricated drug delivery device for treatment of ocular diseases. Lab Chip. 2008;8(7):1027-30. doi: 10.1039/b804690e.

110. Meng E, Hoang T. MEMS-enabled implantable drug infusion pumps for laboratory animal research, preclinical, and clinical applications. Adv Drug Deliv Rev. 2012;64(14):1628-38. doi: 10.1016/j.addr.2012.08.006.
111. Pirmoradi FN, Jackson JK, Burt HM, Chiao M. On-demand controlled release of docetaxel from a battery-less MEMS drug delivery device. Lab Chip. 2011;11(16):2744-52. doi: 10.1039/c1lc20134d.
112. Takashima Y, Tsuchiya T, Igarashi Y, Kanazawa T, Okada H, Urtti A. [Non-invasive ophthalmic liposomes for nucleic acid delivery to posterior segment of eye]. Yakugaku Zasshi. 2012;132(12):1365-70.
113. Davis BM, Normando EM, Guo L, Turner LA, Nizari S, O'Shea P, et al. Topical delivery of Avastin to the posterior segment of the eye in vivo using annexin A5-associated liposomes. Small. 2014;10(8):1575-84. doi: 10.1002/smll.201303433.
114. Honda M, Asai T, Umemoto T, Araki Y, Oku N, Tanaka M. Suppression of choroidal neovascularization by intravitreal injection of liposomal SU5416. Arch Ophthalmol. 2011;129(3):317-21. doi: 10.1001/archophthalmol.2011.12.
115. Abrishami M, Zarei-Ghanavati S, Soroush D, Rouhbakhsh M, Jaafari MR, Malaekeh-Nikouei B. Preparation, characterization, and in vivo evaluation of nanoliposomes-encapsulated bevacizumab (avastin) for intravitreal administration. Retina. 2009;29(5):699-703. doi: 10.1097/IAE.0b013e3181a2f42a.
116. Elsaid N, Jackson TL, Elsaid Z, Alqathama A, Somavarapu S. PLGA Microparticles Entrapping Chitosan-Based Nanoparticles for the Ocular Delivery of Ranibizumab. Mol Pharm. 2016. doi: 10.1021/acs.molpharmaceut.6b00335.
117. Hirani A, Grover A, Lee YW, Pathak Y, Sutariya V. Triamcinolone acetonide nanoparticles incorporated in thermoreversible gels for age-related macular degeneration. Pharm Dev Technol. 2016;21(1):61-7. doi: 10.3109/10837450.2014.965326.
118. Suen WL, Chau Y. Specific uptake of folate-decorated triamcinolone-encapsulating nanoparticles by retinal pigment epithelium cells enhances and prolongs antiangiogenic activity. J Control Release. 2013;167(1):21-8. doi: 10.1016/j.jconrel.2013.01.004.
119. Varshochian R, Riazi-Esfahani M, Jeddi-Tehrani M, Mahmoudi AR, Aghazadeh S, Mahbod M, et al. Albuminated PLGA nanoparticles containing bevacizumab intended for ocular neovascularization treatment. J Biomed Mater Res A. 2015;103(10):3148-56. doi: 10.1002/jbm.a.35446.
120. Manickavasagam D, Wehrung D, Chamsaz EA, Sanders M, Bouhenni R, Crish SD, et al. Assessment of alkoxylphenacyl-based polycarbonates as a potential platform for controlled delivery of a model anti-glaucoma drug. Eur J Pharm Biopharm. 2016. doi: 10.1016/j.ejpb.2016.06.012.
121. Ying L, Tahara K, Takeuchi H. Drug delivery to the ocular posterior segment using lipid emulsion via eye drop administration: effect of emulsion formulations and surface modification. Int J Pharm. 2013;453(2):329-35. doi: 10.1016/j.ijpharm.2013.06.024.
122. Zhang L, Si T, Fischer AJ, Letson A, Yuan S, Roberts CJ, et al. Coaxial electrospray of ranibizumab-loaded microparticles for sustained release of anti-vegf therapies. PLoS One. 2015;10(8):e0135608. doi: 10.1371/journal.pone.0135608.
123. Yandrapu SK, Upadhyay AK, Petrash JM, Kompella UB. Nanoparticles in porous microparticles prepared by supercritical infusion and pressure quench technology for

sustained delivery of bevacizumab. Mol Pharm. 2013;10(12):4676-86. doi: 10.1021/mp400487f.
124. Ye Z, Ji YL, Ma X, Wen JG, Wei W, Huang SM. Pharmacokinetics and distributions of bevacizumab by intravitreal injection of bevacizumab-PLGA microspheres in rabbits. Int J Ophthalmol. 2015;8(4):653-8. doi: 10.3980/j.issn.2222-3959.2015.04.02.
125. Osswald CR, Kang-Mieler JJ. Controlled and extended release of a model protein from a microsphere-hydrogel drug delivery system. Ann Biomed Eng. 2015;43(11):2609-17. doi: 10.1007/s10439-015-1314-7.
126. Patel S, Garapati C, Chowdhury P, Gupta H, Nesamony J, Nauli S, et al. Development and evaluation of dexamethasone nanomicelles with potential for treating posterior uveitis after topical application. J Ocul Pharmacol Ther. 2015;31(4):215-27. doi: 10.1089/jop.2014.0152.
127. Ma F, Nan K, Lee S, Beadle JR, Hou H, Freeman WR, et al. Micelle formulation of hexadecyloxypropyl-cidofovir (HDP-CDV) as an intravitreal long-lasting delivery system. Eur J Pharm Biopharm. 2015;89:271-9. doi: 10.1016/j.ejpb.2014.12.010.
128. Yavuz B, Pehlivan SB, Vural I, Unlu N. In Vitro/in vivo evaluation of dexamethasone--pamam dendrimer complexes for retinal drug delivery. J Pharm Sci. 2015;104(11):3814-23. doi: 10.1002/jps.24588.
129. Holden CA, Tyagi P, Thakur A, Kadam R, Jadhav G, Kompella UB, et al. Polyamidoamine dendrimer hydrogel for enhanced delivery of antiglaucoma drugs. Nanomedicine. 2012;8(5):776-83. doi: 10.1016/j.nano.2011.08.018.
130. Wu X, Yu G, Luo C, Maeda A, Zhang N, Sun D, et al. Synthesis and evaluation of a nanoglobular dendrimer 5-aminosalicylic Acid conjugate with a hydrolyzable schiff base spacer for treating retinal degeneration. ACS Nano. 2014;8(1):153-61. doi: 10.1021/nn4054107.
131. Xu X, Weng Y, Xu L, Chen H. Sustained release of Avastin(R) from polysaccharides cross-linked hydrogels for ocular drug delivery. Int J Biol Macromol. 2013;60:272-6. doi: 10.1016/j.ijbiomac.2013.05.034.
132. Rauck BM, Friberg TR, Medina Mendez CA, Park D, Shah V, Bilonick RA, et al. Biocompatible reverse thermal gel sustains the release of intravitreal bevacizumab in vivo. Invest Ophthalmol Vis Sci. 2014;55(1):469-76. doi: 10.1167/iovs.13-13120.
133. Wang CH, Hwang YS, Chiang PR, Shen CR, Hong WH, Hsiue GH. Extended release of bevacizumab by thermosensitive biodegradable and biocompatible hydrogel. Biomacromolecules. 2012;13(1):40-8. doi: 10.1021/bm2009558.
134. Yu Y, Lau LC, Lo AC, Chau Y. Injectable Chemically Crosslinked Hydrogel for the Controlled Release of Bevacizumab in Vitreous: A 6-Month In Vivo Study. Transl Vis Sci Technol. 2015;4(2):5. doi: 10.1167/tvst.4.2.5.
135. Ibraheem D, Elaissari A, Fessi H. Administration strategies for proteins and peptides. Int. J of Pharm. 2014;477(1-2):578-89. doi: DOI 10.1016/j.ijpharm.2014.10.059.
136. Martins S, Sarmento B, Ferreira DC, Souto EB. Lipid-based colloidal carriers for peptide and protein delivery--liposomes versus lipid nanoparticles. Int J Nanomedicine. 2007;2(4):595-607.
137. Schwendener RA. Liposomes as vaccine delivery systems: a review of the recent advances. Ther Adv Vaccines. 2014;2(6):159-82. doi: 10.1177/2051013614541440.

138. Leader B, Baca QJ, Golan DE. Protein therapeutics: a summary and pharmacological classification. Nat Rev Drug Discov. 2008;7(1):21-39. doi: 10.1038/nrd2399.
139. El Sanharawi M, Kowalczuk L, Touchard E, Omri S, de Kozak Y, Behar-Cohen F. Protein delivery for retinal diseases: from basic considerations to clinical applications. Prog Retin Eye Res. 2010;29(6):443-65. doi: 10.1016/j.preteyeres.2010.04.001.
140. Tah V, Orlans HO, Hyer J, Casswell E, Din N, Sri Shanmuganathan V, et al. Anti-VEGF therapy and the retina: an update. J Ophthalmol. 2015;2015:627674. doi: 10.1155/2015/627674.
141. Zhang Y, Han Q, Ru Y, Bo Q, Wei RH. Anti-VEGF treatment for myopic choroid neovascularization: from molecular characterization to update on clinical application. Drug Des Devel Ther. 2015;9:3413-21. doi: 10.2147/DDDT.S87920.
142. Azanza Perea JR, Garcia Layana A. [Ranibizumab versus bevacizumab. Pharmacological considerations]. Arch Soc Esp Oftalmol. 2012;87 Suppl 1:3-9. doi: 10.1016/S0365-6691(12)70046-1.
143. Blick SK, Keating GM, Wagstaff AJ. Ranibizumab. Drugs. 2007;67(8):1199-206; discussion 207-9.
144. Ferrara N, Damico L, Shams N, Lowman H, Kim R. Development of ranibizumab, an anti-vascular endothelial growth factor antigen binding fragment, as therapy for neovascular age-related macular degeneration. Retina. 2006;26(8):859-70. doi: 10.1097/01.iae.0000242842.14624.e7.
145. Thomas M, Mousa SS, Mousa SA. Comparative effectiveness of aflibercept for the treatment of patients with neovascular age-related macular degeneration. Clin Ophthalmol. 2013;7:495-501. doi: 10.2147/OPTH.S29974.
146. Sarwar S, Clearfield E, Soliman MK, Sadiq MA, Baldwin AJ, Hanout M, et al. Aflibercept for neovascular age-related macular degeneration. Cochrane Database Syst Rev. 2016;2:CD011346. doi: 10.1002/14651858.CD011346.pub2.
147. Solomon SD, Lindsley K, Vedula SS, Krzystolik MG, Hawkins BS. Anti-vascular endothelial growth factor for neovascular age-related macular degeneration. Cochrane Database Syst Rev. 2014;(8):CD005139. doi: 10.1002/14651858.CD005139.pub3.
148. Chang JH, Garg NK, Lunde E, Han KY, Jain S, Azar DT. Corneal neovascularization: an anti-VEGF therapy review. Surv Ophthalmol. 2012;57(5):415-29. doi: 10.1016/j.survophthal.2012.01.007.
149. Ba J, Peng RS, Xu D, Li YH, Shi H, Wang Q, et al. Intravitreal anti-VEGF injections for treating wet age-related macular degeneration: a systematic review and meta-analysis. Drug Des Devel Ther. 2015;9:5397-405. doi: 10.2147/DDDT.S86269.
150. Pavot V, Berthet M, Resseguier J, Legaz S, Handke N, Gilbert SC, et al. Poly(lactic acid) and poly(lactic-co-glycolic acid) particles as versatile carrier platforms for vaccine delivery. Nanomedicine (Lond). 2014;9(17):2703-18. doi: 10.2217/nnm.14.156.
151. Kang J, Lambert O, Ausborn M, Schwendeman SP. Stability of proteins encapsulated in injectable and biodegradable poly(lactide-co-glycolide)-glucose millicylinders. Int J Pharm. 2008;357(1-2):235-43. doi: 10.1016/j.ijpharm.2008.02.004.
152. Vaishya R, Khurana V, Patel S, Mitra AK. Long-term delivery of protein therapeutics. Expert Opin Drug Deliv. 2015;12(3):415-40. doi: 10.1517/17425247.2015.961420.

153. Vaishya R, Mitra AK. Future of sustained protein delivery. Ther Deliv. 2014;5(11):1171-4. doi: 10.4155/tde.14.86.
154. Agrahari V, Agrahari V, Hung WT, Christenson LK, Mitra AK. Composite nanoformulation therapeutics for long-term ocular delivery of macromolecules. Mol Pharm. 2016;13(9):2912-22. doi: 10.1021/acs.molpharmaceut.5b00828.
155. Patel SP, Vaishya R, Pal D, Mitra AK. Novel pentablock copolymer-based nanoparticulate systems for sustained protein delivery. AAPS PharmSciTech. 2015;16(2):327-43. doi: 10.1208/s12249-014-0196-6.
156. Mishra GP, Tamboli V, Mitra AK. Effect of hydrophobic and hydrophilic additives on sol-gel transition and release behavior of timolol maleate from polycaprolactone-based hydrogel. Colloid Polym Sci. 2011;289(14):1553-62. doi: 10.1007/s00396-011-2476-y.
157. Gao P, Nie X, Zou M, Shi Y, Cheng G. Recent advances in materials for extended-release antibiotic delivery system. J Antibiot (Tokyo). 2011;64(9):625-34. doi: 10.1038/ja.2011.58.
158. Mitragotri S, Burke PA, Langer R. Overcoming the challenges in administering biopharmaceuticals: formulation and delivery strategies. Nat Rev Drug Discov. 2014;13(9):655-72. doi: 10.1038/nrd4363.
159. Radhakrishnan K, Sonali N, Moreno M, Nirmal J, Fernandez AA, Venkatraman S, et al. Protein delivery to the back of the eye: barriers, carriers and stability of anti-VEGF proteins. Drug Discov Today. 2017;22(2):416-23. doi: 10.1016/j.drudis.2016.10.015.
160. Penedones A, Mendes D, Alves C, Batel Marques F. Safety monitoring of ophthalmic biologics: a systematic review of pre- and postmarketing safety data. J Ocul Pharmacol Ther. 2014;30(9):729-51. doi: 10.1089/jop.2013.0206.
161. Schwartz SG, Scott IU, Flynn HW, Jr., Stewart MW. Drug delivery techniques for treating age-related macular degeneration. Expert Opin Drug Deliv. 2014;11(1):61-8. doi: 10.1517/17425247.2013.859135.
162. Gao Y, Sun Y, Ren F, Gao S. PLGA-PEG-PLGA hydrogel for ocular drug delivery of dexamethasone acetate. Drug Dev Ind Pharm. 2010;36(10):1131-8. doi: 10.3109/03639041003680826.
163. Luo Z, Jin L, Xu L, Zhang ZL, Yu J, Shi S, et al. Thermosensitive PEG-PCL-PEG (PECE) hydrogel as an in situ gelling system for ocular drug delivery of diclofenac sodium. Drug Deliv. 2016;23(1):63-8. doi: 10.3109/10717544.2014.903535.
164. Yin H, Gong C, Shi S, Liu X, Wei Y, Qian Z. Toxicity evaluation of biodegradable and thermosensitive PEG-PCL-PEG hydrogel as a potential in situ sustained ophthalmic drug delivery system. J Biomed Mater Res B Appl Biomater. 2010;92(1):129-37. doi: 10.1002/jbm.b.31498.
165. Rafat M, Cleroux CA, Fong WG, Baker AN, Leonard BC, O'Connor MD, et al. PEG-PLA microparticles for encapsulation and delivery of Tat-EGFP to retinal cells. Biomaterials. 2010;31(12):3414-21. doi: 10.1016/j.biomaterials.2010.01.031.
166. Wadhwa S, Paliwal R, Paliwal SR, Vyas SP. Nanocarriers in ocular drug delivery: an update review. Curr Pharm Des. 2009;15(23):2724-50.
167. Li X, Zhang Z, Chen H. Development and evaluation of fast forming nano-composite hydrogel for ocular delivery of diclofenac. Int J Pharm. 2013;448(1):96-100. doi: 10.1016/j.ijpharm.2013.03.024.

168. Taich P, Moretton MA, Del Sole MJ, Winter U, Bernabeu E, Croxatto JO, et al. Sustained-release hydrogels of topotecan for retinoblastoma. Colloids Surf B Biointerfaces. 2016;146:624-31. doi: 10.1016/j.colsurfb.2016.07.001.
169. Gombotz WR, Pettit DK. Biodegradable polymers for protein and peptide drug delivery. Bioconjug Chem. 1995;6(4):332-51.
170. Marin E, Briceno MI, Caballero-George C. Critical evaluation of biodegradable polymers used in nanodrugs. Int J Nanomedicine. 2013;8:3071-90. doi: 10.2147/IJN.S47186.
171. Gopferich A. Mechanisms of polymer degradation and erosion. Biomaterials. 1996;17(2):103-14.
172. Lu L, Peter SJ, Lyman MD, Lai HL, Leite SM, Tamada JA, et al. In vitro and in vivo degradation of porous poly(DL-lactic-co-glycolic acid) foams. Biomaterials. 2000;21(18):1837-45. doi: S0142961200000478.
173. Qiao M, Chen D, Ma X, Hu H. Sustained release of bee venom peptide from biodegradable thermosensitive PLGA-PEG-PLGA triblock copolymer-based hydrogels in vitro. Pharmazie. 2006;61(3):199-202.
174. Jeong B, Bae YH, Kim SW. Drug release from biodegradable injectable thermosensitive hydrogel of PEG-PLGA-PEG triblock copolymers. J Control Release. 2000;63(1-2):155-63.
175. Kang-Mieler JJ, Osswald CR, Mieler WF. Advances in ocular drug delivery: emphasis on the posterior segment. Expert opinion on drug delivery. 2014;11(10):1647-60. doi: 10.1517/17425247.2014.935338.
176. Delplace V, Payne S, Shoichet M. Delivery strategies for treatment of age-related ocular diseases: From a biological understanding to biomaterial solutions. J of control release. 2015;219:652-68. doi: 10.1016/j.jconrel.2015.09.065.
177. Jager RD, Mieler WF, Miller JW. Age-related macular degeneration. The New England j. of med. 2008;358(24):2606-17. doi: 10.1056/NEJMra0801537.
178. Park YG, Rhu HW, Kang S, Roh YJ. New approach of Anti-VEGF agents for age-related macular degeneration. J of ophthalmology. 2012;2012:637316. doi: 10.1155/2012/637316.
179. Fonte P, Araujo F, Seabra V, Reis S, van de Weert M, Sarmento B. Co-encapsulation of lyoprotectants improves the stability of protein-loaded PLGA nanoparticles upon lyophilization. Int. j of pharm. 2015;496(2):850-62. doi: 10.1016/j.ijpharm.2015.10.032.
180. Karve S, Werner ME, Cummings ND, Sukumar R, Wang EC, Zhang YA, et al. Formulation of diblock polymeric nanoparticles through nanoprecipitation technique. Journal of visualized experiments : JoVE. 2011;(55). doi: 10.3791/3398.
181. Gou M, Gong C, Zhang J, Wang X, Wang X, Gu Y, et al. Polymeric matrix for drug delivery: honokiol-loaded PCL-PEG-PCL nanoparticles in PEG-PCL-PEG thermosensitive hydrogel. J of biomed. mat research Part A. 2010;93(1):219-26. doi: 10.1002/jbm.a.32546.
182. Patel SP, Vaishya R, Mishra GP, Tamboli V, Pal D, Mitra AK. Tailor-made pentablock copolymer based formulation for sustained ocular delivery of protein therapeutics. J Drug Deliv. 2014;2014:401747. doi: 10.1155/2014/401747.
183. Tamboli V, Mishra GP, Mitra AK. Novel pentablock copolymer (PLA-PCL-PEG-PCL-PLA) based nanoparticles for controlled drug delivery: Effect of copolymer

compositions on the crystallinity of copolymers and in vitro drug release profile from nanoparticles. Colloid Poly Sci. 2013;291(5):1235-45. doi: 10.1007/s00396-012-2854-0.
184. Yang X, Shah SJ, Wang Z, Agrahari V, Pal D, Mitra AK. Nanoparticle-based topical ophthalmic formulation for sustained release of stereoisomeric dipeptide prodrugs of ganciclovir. Drug delivery. 2016;23(7):2399-409. doi: 10.3109/10717544.2014.996833.
185. Tang Y, Singh J. Biodegradable and biocompatible thermosensitive polymer based injectable implant for controlled release of protein. International journal of pharmaceutics. 2009;365(1-2):34-43. doi: 10.1016/j.ijpharm.2008.08.018.
186. Lam CX, Savalani MM, Teoh SH, Hutmacher DW. Dynamics of in vitro polymer degradation of polycaprolactone-based scaffolds: accelerated versus simulated physiological conditions. Biomedical materials. 2008;3(3):034108. doi: 10.1088/1748-6041/3/3/034108.
187. Delplace V, Payne S, Shoichet M. Delivery strategies for treatment of age-related ocular diseases: From a biological understanding to biomaterial solutions. J of control release. 2015. doi: 10.1016/j.jconrel.2015.09.065.
188. Ohr M, Kaiser PK. Aflibercept in wet age-related macular degeneration: a perspective review. Therapeutic advances in chronic disease. 2012;3(4):153-61. doi: 10.1177/2040622312446007.
189. Kovach JL, Schwartz SG, Flynn HW, Jr., Scott IU. Anti-VEGF treatment strategies for wet AMD. J of ophthalmology. 2012;2012:786870. doi: 10.1155/2012/786870.
190. Campa C, Harding SP. Anti-VEGF compounds in the treatment of neovascular age related macular degeneration. Current drug targets. 2011;12(2):173-81.
191. Avery RL, Castellarin AA, Steinle NC, Dhoot DS, Pieramici DJ, See R, et al. Systemic pharmacokinetics following intravitreal injections of ranibizumab, bevacizumab or aflibercept in patients with neovascular AMD. The British j of ophthal. 2014;98(12):1636-41. doi: 10.1136/bjophthalmol-2014-305252.
192. Thakur SS, Barnett NL, Donaldson MJ, Parekh HS. Intravitreal drug delivery in retinal disease: are we out of our depth? Expert opin on drug deliv. 2014;11(10):1575-90. doi: 10.1517/17425247.2014.927864.
193. Schmidt-Erfurth U, Eldem B, Guymer R, Korobelnik JF, Schlingemann RO, Axer-Siegel R, et al. Efficacy and safety of monthly versus quarterly ranibizumab treatment in neovascular age-related macular degeneration: the EXCITE study. Ophthalmology. 2011;118(5):831-9. doi: 10.1016/j.ophtha.2010.09.004.
194. Malgorzata W, Diana D, Agnieszka B, Zofia M. Bevacizumab intravitreal injections in the treatment of diabetic macular oedema. Klinika oczna. 2013;115(1):15-9.
195. Stewart MW, Rosenfeld PJ, Penha FM, Wang F, Yehoshua Z, Bueno-Lopez E, et al. Pharmacokinetic rationale for dosing every 2 weeks versus 4 weeks with intravitreal ranibizumab, bevacizumab, and aflibercept (vascular endothelial growth factor Trap-eye). Retina. 2012;32(3):434-57. doi: 10.1097/IAE.0B013E31822C290F.
196. Bakri SJ, Snyder MR, Reid JM, Pulido JS, Singh RJ. Pharmacokinetics of Intravitreal Bevacizumab (Avastin). Ophthalmology. 2007 May;114(5):855-9.
197. Lowe J, Araujo J, Yang J, Reich M, Oldendorp A, Shiu V, et al. Ranibizumab inhibits multiple forms of biologically active vascular endothelial growth factor in vitro and in vivo. Exp eye res. 2007;85(4):425-30. doi: 10.1016/j.exer.2007.05.008.

198. Keane PA, Sadda SR. Development of Anti-VEGF Therapies for Intraocular Use: A Guide for Clinicians. J of ophthal. 2012;2012:483034. doi: 10.1155/2012/483034.
199. Sampat KM, Garg SJ. Complications of intravitreal injections. Current opinion in ophthalmology. 2010;21(3):178-83. doi: 10.1097/ICU.0b013e328338679a.
200. Pescina S, Sonvico F, Santi P, Nicoli S. Therapeutics and carriers: the dual role of proteins in nanoparticles for ocular delivery. Current topics in medicinal chemistry. 2015;15(4):369-85.
201. Shmueli RB, Ohnaka M, Miki A, Pandey NB, Lima e Silva R, Koskimaki JE, et al. Long-term suppression of ocular neovascularization by intraocular injection of biodegradable polymeric particles containing a serpin-derived peptide. Biomaterials. 2013;34(30):7544-51. doi: 10.1016/j.biomaterials.2013.06.044.
202. Bilati U, Allemann E, Doelker E. Poly(D,L-lactide-co-glycolide) protein-loaded nanoparticles prepared by the double emulsion method--processing and formulation issues for enhanced entrapment efficiency. J Microencapsul. 2005;22(2):205-14. doi: U45T0787RXG48086 [pii] 10.1080/02652040400026442.

203. Lee SH, Zhang Z, Feng SS. Nanoparticles of poly(lactide)-tocopheryl polyethylene glycol succinate (PLA-TPGS) copolymers for protein drug delivery. Biomaterials. 2007;28(11):2041-50. doi: S0142-9612(07)00004-X [pii] 10.1016/j.biomaterials.2007.01.003.

204. Vaishya RD, Mandal A, Gokulgandhi M, Patel S, Mitra AK. Reversible hydrophobic ion-paring complex strategy to minimize acylation of octreotide during long-term delivery from PLGA microparticles. Int. j of pharm. 2015;489(1-2):237-45. doi: 10.1016/j.ijpharm.2015.04.075.
205. Zhang Y, Schwendeman SP. Minimizing acylation of peptides in PLGA microspheres. Journal of controlled release : official journal of the Controlled Release Society. 2012;162(1):119-26. doi: 10.1016/j.jconrel.2012.04.022.
206. Khurana V, Patel S, Agrahari V, Pal D and Mitra A. Novel pentablock copolymer based nanoparticles containing pazopanib: a potential therapy for ocular neovascularization. Recent Pat. on Nanomed. 2014;4(1):12.
207. Vadlapudi AD, Vadlapatla RK, Pal D, Mitra AK. Functional and molecular aspects of biotin uptake via SMVT in human corneal epithelial (HCEC) and retinal pigment epithelial (D407) cells. The AAPS journal. 2012;14(4):832-42. doi: 10.1208/s12248-012-9399-5.
208. Khurana V, Vadlapudi AD, Vadlapatla RK, Pal D, Mitra AK. Functional characterization and molecular identification of vitamin C transporter (SVCT2) in human corneal epithelial (HCEC) and retinal pigment epithelial (D407) cells. Current eye res. 2015;40(5):457-69. doi: 10.3109/02713683.2014.935443.
209. Youm I, Agrahari V, Murowchick JB, Youan BB. Uptake and cytotoxicity of docetaxel-loaded hyaluronic acid-grafted oily core nanocapsules in MDA-MB 231 cancer cells. Pharm res. 2014;31(9):2439-52. doi: 10.1007/s11095-014-1339-x.
210. Meng J, Zhang T, Agrahari V, Ezoulin MJ, Youan BB. Comparative biophysical properties of tenofovir-loaded, thiolated and nonthiolated chitosan nanoparticles intended for HIV prevention. Nanomed. 2014;9(11):1595-612. doi: 10.2217/nnm.13.136.

211. Filipe V, Hawe A, Jiskoot W. Critical evaluation of nanoparticle tracking analysis (NTA) by NanoSight for the measurement of nanoparticles and protein aggregates. Pharm res. 2010;27(5):796-810. doi: 10.1007/s11095-010-0073-2.
212. Costa P, Sousa Lobo JM. Modeling and comparison of dissolution profiles. Eur J Pharm Sci. 2001;13(2):123-33.
213. Vianna JR, Chauhan BC. How to detect progression in glaucoma. Prog Brain Res. 2015;221:135-58. doi: 10.1016/bs.pbr.2015.04.011.
214. Gupta D, Chen PP. Glaucoma. Am Fam Physician. 2016;93(8):668-74.
215. Clement CI, Bhartiya S, Shaarawy T. New perspectives on target intraocular pressure. Surv Ophthalmol. 2014;59(6):615-26. doi: 10.1016/j.survophthal.2014.04.001.
216. Tamm ER, Braunger BM, Fuchshofer R. Intraocular pressure and the mechanisms involved in resistance of the aqueous humor flow in the trabecular meshwork outflow pathways. Prog Mol Biol Transl Sci. 2015;134:301-14. doi: 10.1016/bs.pmbts.2015.06.007.
217. Jia LY, Sun L, Fan DS, Lam DS, Pang CP, Yam GH. Effect of topical Ginkgo biloba extract on steroid-induced changes in the trabecular meshwork and intraocular pressure. Arch Ophthalmol. 2008;126(12):1700-6. doi: 10.1001/archophthalmol.2008.512.
218. Qin Y, Lam S, Yam GH, Choy KW, Liu DT, Chiu TY, et al. A rabbit model of age-dependant ocular hypertensive response to topical corticosteroids. Acta Ophthalmol. 2012;90(6):559-63. doi: 10.1111/j.1755-3768.2010.02016.x.
219. Whitlock NA, McKnight B, Corcoran KN, Rodriguez LA, Rice DS. Increased intraocular pressure in mice treated with dexamethasone. Invest Ophthalmol Vis Sci. 2010;51(12):6496-503. doi: 10.1167/iovs.10-5430.
220. Matsumoto Y, Kanamori A, Nakamura M, Negi A. Rat chronic glaucoma model induced by intracameral injection of microbeads suspended in sodium sulfate-sodium hyaluronate. Jpn J Ophthalmol. 2014;58(3):290-7. doi: 10.1007/s10384-014-0311-y.
221. Baudouin C, Denoyer A, Desbenoit N, Hamm G, Grise A. In vitro and in vivo experimental studies on trabecular meshwork degeneration induced by benzalkonium chloride (an American Ophthalmological Society thesis). Trans Am Ophthalmol Soc. 2012;110:40-63.
222. Overby DR, Clark AF. Animal models of glucocorticoid-induced glaucoma. Exp Eye Res. 2015;141:15-22. doi: 10.1016/j.exer.2015.06.002.
223. Mao W, Tovar-Vidales T, Yorio T, Wordinger RJ, Clark AF. Perfusion-cultured bovine anterior segments as an ex vivo model for studying glucocorticoid-induced ocular hypertension and glaucoma. Invest Ophthalmol Vis Sci. 2011;52(11):8068-75. doi: 10.1167/iovs.11-8133.
224. Aires ID, Ambrosio AF, Santiago AR. Modeling human glaucoma: lessons from the in vitro models. Ophthalmic Res. 2017;57(2):77-86. doi: 10.1159/000448480.
225. Ishikawa M, Yoshitomi T, Zorumski CF, Izumi Y. Experimentally induced mammalian models of glaucoma. Biomed Res Int. 2015;2015:281214. doi: 10.1155/2015/281214.
226. Pang IH, Wang WH, Clark AF. Acute effects of glaucoma medications on rat intraocular pressure. Exp Eye Res. 2005;80(2):207-14. doi: 10.1016/j.exer.2004.09.001.

227. Ishikawa M, Yoshitomi T, Zorumski CF, Izumi Y. Neurosteroids are endogenous neuroprotectants in an ex vivo glaucoma model. Invest Ophthalmol Vis Sci. 2014;55(12):8531-41. doi: 10.1167/iovs.14-15624.
228. Shafaie S, Hutter V, Cook MT, Brown MB, Chau DY. In Vitro cell models for ophthalmic drug development applications. Biores Open Access. 2016;5(1):94-108. doi: 10.1089/biores.2016.0008.
229. Li G, Cui G, Dismuke WM, Navarro I, Perkumas K, Woodward DF, et al. Differential response and withdrawal profile of glucocorticoid-treated human trabecular meshwork cells. Exp Eye Res. 2017;155:38-46. doi: 10.1016/j.exer.2016.12.002.
230. Tan JC, Peters DM, Kaufman PL. Recent developments in understanding the pathophysiology of elevated intraocular pressure. Curr Opin Ophthalmol. 2006;17(2):168-74. doi: 10.1097/01.icu.0000193079.55240.18.
231. Wordinger RJ, Clark AF. Effects of glucocorticoids on the trabecular meshwork: towards a better understanding of glaucoma. Prog Retin Eye Res. 1999;18(5):629-67.
232. Gasiorowski JZ, Russell P. Biological properties of trabecular meshwork cells. Exp Eye Res. 2009;88(4):671-5. doi: 10.1016/j.exer.2008.08.006.
233. Vranka JA, Kelley MJ, Acott TS, Keller KE. Extracellular matrix in the trabecular meshwork: intraocular pressure regulation and dysregulation in glaucoma. Exp Eye Res. 2015;133:112-25. doi: 10.1016/j.exer.2014.07.014.
234. Pattabiraman PP, Toris CB. The exit strategy: Pharmacological modulation of extracellular matrix production and deposition for better aqueous humor drainage. Eur J Pharmacol. 2016;787:32-42. doi: 10.1016/j.ejphar.2016.04.048.
235. Raghunathan VK, Morgan JT, Park SA, Weber D, Phinney BS, Murphy CJ, et al. Dexamethasone stiffens trabecular meshwork, trabecular meshwork cells, and matrix. Invest Ophthalmol Vis Sci. 2015;56(8):4447-59. doi: 10.1167/iovs.15-16739.
236. Stamer WD, Braakman ST, Zhou EH, Ethier CR, Fredberg JJ, Overby DR, et al. Biomechanics of Schlemm's canal endothelium and intraocular pressure reduction. Prog Retin Eye Res. 2015;44:86-98. doi: 10.1016/j.preteyeres.2014.08.002.
237. Menaa F, Braghini CA, Vasconcellos JP, Menaa B, Costa VP, Figueiredo ES, et al. Keeping an eye on myocilin: a complex molecule associated with primary open-angle glaucoma susceptibility. Molecules. 2011;16(7):5402-21. doi: 10.3390/molecules16075402.
238. Sacca SC, Pulliero A, Izzotti A. The dysfunction of the trabecular meshwork during glaucoma course. J Cell Physiol. 2015;230(3):510-25. doi: 10.1002/jcp.24826.
239. Roy Chowdhury U, Hann CR, Stamer WD, Fautsch MP. Aqueous humor outflow: dynamics and disease. Invest Ophthalmol Vis Sci. 2015;56(5):2993-3003. doi: 10.1167/iovs.15-16744.
240. Agrahari V, Li G, Agrahari V, Navarro I, Perkumas K, Mandal A, et al. Pentablock copolymer dexamethasone nanoformulations elevate MYOC: in vitro liberation, activity and safety in human trabecular meshwork cells. Nanomedicine (Lond). 2017;12(16):1911-26. doi: 10.2217/nnm-2017-0140.
241. Lerman S. Steroid Therapy and Secondary Glaucoma. Am J Ophthalmol. 1963;56:31-3.
242. Joseph RR, Venkatraman SS. Drug delivery to the eye: what benefits do nanocarriers offer? Nanomedicine (Lond). 2017;12(6):683-702. doi: 10.2217/nnm-2016-0379.

243. Bian F, Pelegrino FS, Henriksson JT, Pflugfelder SC, Volpe EA, Li DQ, et al. Differential effects of dexamethasone and doxycycline on inflammation and mmp production in murine alkali-burned corneas associated with dry eye. Ocul Surf. 2016;14(2):242-54. doi: 10.1016/j.jtos.2015.11.006.
244. Quentin CD, Behrens-Baumann W. [Double-blind study of the effectiveness of the prostaglandin synthesis inhibitor diclofenac and dexamethasone phosphate in the treatment of iritis after local administration]. Fortschr Ophthalmol. 1987;84(4):353-5.
245. Coassin M, Iovieno A, Soldani A, Cavuto S, Cimino L, Sartori A, et al. Bromfenac ophthalmic solution 0.09% as an adjunctive therapy to topical steroids after cataract surgery in pseudoexfoliation syndrome. J Cataract Refract Surg. 2016;42(8):1119-25. doi: 10.1016/j.jcrs.2016.04.031.
246. Narayanan R, Kuppermann BD. Corticosteroids and anti-complement therapy in retinal diseases. Handb Exp Pharmacol. 2016. doi: 10.1007/164_2016_22.
247. Schwartz SG, Scott IU, Stewart MW, Flynn HW, Jr. Update on corticosteroids for diabetic macular edema. Clin Ophthalmol. 2016;10:1723-30. doi: 10.2147/OPTH.S115546.
248. Haller JA, Bandello F, Belfort R, Jr., Blumenkranz MS, Gillies M, Heier J, et al. Dexamethasone intravitreal implant in patients with macular edema related to branch or central retinal vein occlusion twelve-month study results. Ophthalmology. 2011;118(12):2453-60. doi: 10.1016/j.ophtha.2011.05.014.
249. Tsang AC, Virgili G, Abtahi M, Gottlieb CC. Intravitreal dexamethasone implant for the treatment of macular edema in chronic non-infectious uveitis. Ocul Immunol Inflamm. 2016:1-8. doi: 10.3109/09273948.2016.1160130.
250. Brady ME, Sartiano GP, Rosenblum SL, Zaglama NE, Bauguess CT. The pharmacokinetics of single high doses of dexamethasone in cancer patients. Eur J Clin Pharmacol. 1987;32(6):593-6.
251. Balzus B, Feleke Sahle F, Honzke S, Gerecke C, Schumacher F, Hedtrich S, et al. Formulation and ex vivo evaluation of polymeric nanoparticles for controlled delivery of corticosteroids to the skin and the corneal epithelium. Eur J Pharm Biopharm. 2017. doi: 10.1016/j.ejpb.2017.02.001.
252. Gerecke C, Edlich A, Giulbudagian M, Schumacher F, Zhang N, Said A, et al. Biocompatibility and characterization of polyglycerol-based thermoresponsive nanogels designed as novel drug delivery systems and their intracellular localization in keratinocytes. Nanotoxicology. 2017:1-35. doi: 10.1080/17435390.2017.1292371.
253. Yang X, Trinh HM, Agrahari V, Sheng Y, Pal D, Mitra AK. Nanoparticle-based topical ophthalmic gel formulation for sustained release of hydrocortisone butyrate. AAPS PharmSciTech. 2016;17(2):294-306. doi: 10.1208/s12249-015-0354-5.
254. Boddu SH, Jwala J, Vaishya R, Earla R, Karla PK, Pal D, et al. Novel nanoparticulate gel formulations of steroids for the treatment of macular edema. J Ocul Pharmacol Ther. 2010;26(1):37-48. doi: 10.1089/jop.2009.0074.
255. Vaishya RD, Gokulgandhi M, Patel S, Minocha M, Mitra AK. Novel dexamethasone-loaded nanomicelles for the intermediate and posterior segment uveitis. AAPS PharmSciTech. 2014;15(5):1238-51. doi: 10.1208/s12249-014-0100-4.
256. Chen X, Chen J, Li B, Yang X, Zeng R, Liu Y, et al. PLGA-PEG-PLGA triblock copolymeric micelles as oral drug delivery system: In vitro drug release and in vivo

pharmacokinetics assessment. J Colloid Interface Sci. 2017;490:542-52. doi: 10.1016/j.jcis.2016.11.089.
257. Calucci L, Forte C, Buwalda SJ, Dijkstra PJ, Feijen J. Self-aggregation of gel forming PEG-PLA star block copolymers in water. Langmuir. 2010;26(15):12890-6. doi: 10.1021/la101613b.
258. Wu X, Li S, Coumes F, Darcos V, Lai Kee Him J, Bron P. Modeling and self-assembly behavior of PEG-PLA-PEG triblock copolymers in aqueous solution. Nanoscale. 2013;5(19):9010-7. doi: 10.1039/c3nr02899b.
259. Loftsson T, Hreinsdottir D, Stefansson E. Cyclodextrin microparticles for drug delivery to the posterior segment of the eye: aqueous dexamethasone eye drops. J Pharm Pharmacol. 2007;59(5):629-35. doi: 10.1211/jpp.59.5.0002.
260. Ebrahim S, Peyman GA, Lee PJ. Applications of liposomes in ophthalmology. Surv Ophthalmol. 2005;50(2):167-82. doi: 10.1016/j.survophthal.2004.12.006.
261. Sudhalkar A, Chhablani J, Vasavada A, Bhojwani D, Vasavada V, Vasavada S, et al. Intravitreal dexamethasone implant for recurrent cystoid macular edema due to Irvine-Gass syndrome: a prospective case series. Eye (Lond). 2016;30(12):1549-57. doi: 10.1038/eye.2016.205.
262. Stamer DW, Roberts BC, Epstein DL, Allingham RR. Isolation of primary open-angle glaucomatous trabecular meshwork cells from whole eye tissue. Current eye research. 2000;20(5):347-50.
263. Stamer WD, Seftor RE, Williams SK, Samaha HA, Snyder RW. Isolation and culture of human trabecular meshwork cells by extracellular matrix digestion. Current eye research. 1995;14(7):611-7.
264. Li G, Cui G, Dismuke WM, Navarro I, Perkumas K, Woodward DF, et al. Differential response and withdrawal profile of glucocorticoid-treated human trabecular meshwork cells. Exp Eye Res. 2016;155:38-46. doi: 10.1016/j.exer.2016.12.002.
265. Li G, Farsiu S, Chiu SJ, Gonzalez P, Lutjen-Drecoll E, Overby DR, et al. Pilocarpine-induced dilation of Schlemm's canal and prevention of lumen collapse at elevated intraocular pressures in living mice visualized by OCT. Invest Ophthalmol Vis Sci. 2014;55(6):3737-46. doi: 10.1167/iovs.13-13700.
266. Acott TS, Kelley MJ. Extracellular matrix in the trabecular meshwork. Exp Eye Res. 2008;86(4):543-61. doi: 10.1016/j.exer.2008.01.013.
267. Chuang TD, Pearce WJ, Khorram O. miR-29c induction contributes to downregulation of vascular extracellular matrix proteins by glucocorticoids. Am J Physiol Cell Physiol. 2015;309(2):C117-25. doi: 10.1152/ajpcell.00254.2014.
268. Nguyen TD, Chen P, Huang WD, Chen H, Johnson D, Polansky JR. Gene structure and properties of TIGR, an olfactomedin-related glycoprotein cloned from glucocorticoid-induced trabecular meshwork cells. J Biol Chem. 1998;273(11):6341-50.
269. Stamer WD, Hoffman EA, Kurali E, Krauss AH. Unique response profile of trabecular meshwork cells to the novel selective glucocorticoid receptor agonist, GW870086X. Invest Ophthalmol Vis Sci. 2013;54(3):2100-7. doi: 10.1167/iovs.12-11298.
270. Wordinger RJ, Fleenor DL, Hellberg PE, Pang IH, Tovar TO, Zode GS, et al. Effects of TGF-beta2, BMP-4, and gremlin in the trabecular meshwork: implications for glaucoma. Invest Ophthalmol Vis Sci. 2007;48(3):1191-200. doi: 10.1167/iovs.06-0296.

APPENDIX

(A) Abbreviations

(^{1}H) NMR: proton nuclear magnetic resonance

AMD: age related macular degeneration

BRB: blood retinal barrier

CD: circular dichroism spectroscopy

CGT: critical gelling temperature

CPT: critical precipitation temperature

DDW: distilled deionized water

DEX: dexamethasone

DL: drug loading

DLS: dynamic light scattering

DME: diabetic macular edema

DR: diabetic retinopathy

EE: entrapment efficiency

ELISA: enzyme linked immunosorbent assays

FT-IR: fourier-transform infrared spectroscopy

GPC: gel permeation chromatography

HTM: human trabecular meshwork cell

IOP: intraocular pressure

LDH: lactate dehydrogenase

ME: macular edema

MW: molecular weight

MYOC: myocilin

NC: nanocarrier

NNV: non-neovascular

NP: nanoparticle

NTA: nanoparticle tracking analysis

NV: neovascular

PB: pentablock

PBG: pentablock gelling polymer

PBS: phosphate buffer saline

PEG: polyethylene glycol

PDI: Poly dispersity index

PCL: polycaprolactone

PGA: polyglycolic acid

PLA: polylactic acid

PLGA: poly lactide-co-glycolide

RPE: retinal pigment epithelium

SC: schlemm's canal

TM: trabecular meshwork

UFLC: ultra-fast liquid chromatography

VEGF: vascular endothelial growth factor

XRD: X-ray diffraction analysis

(B) Permission Request

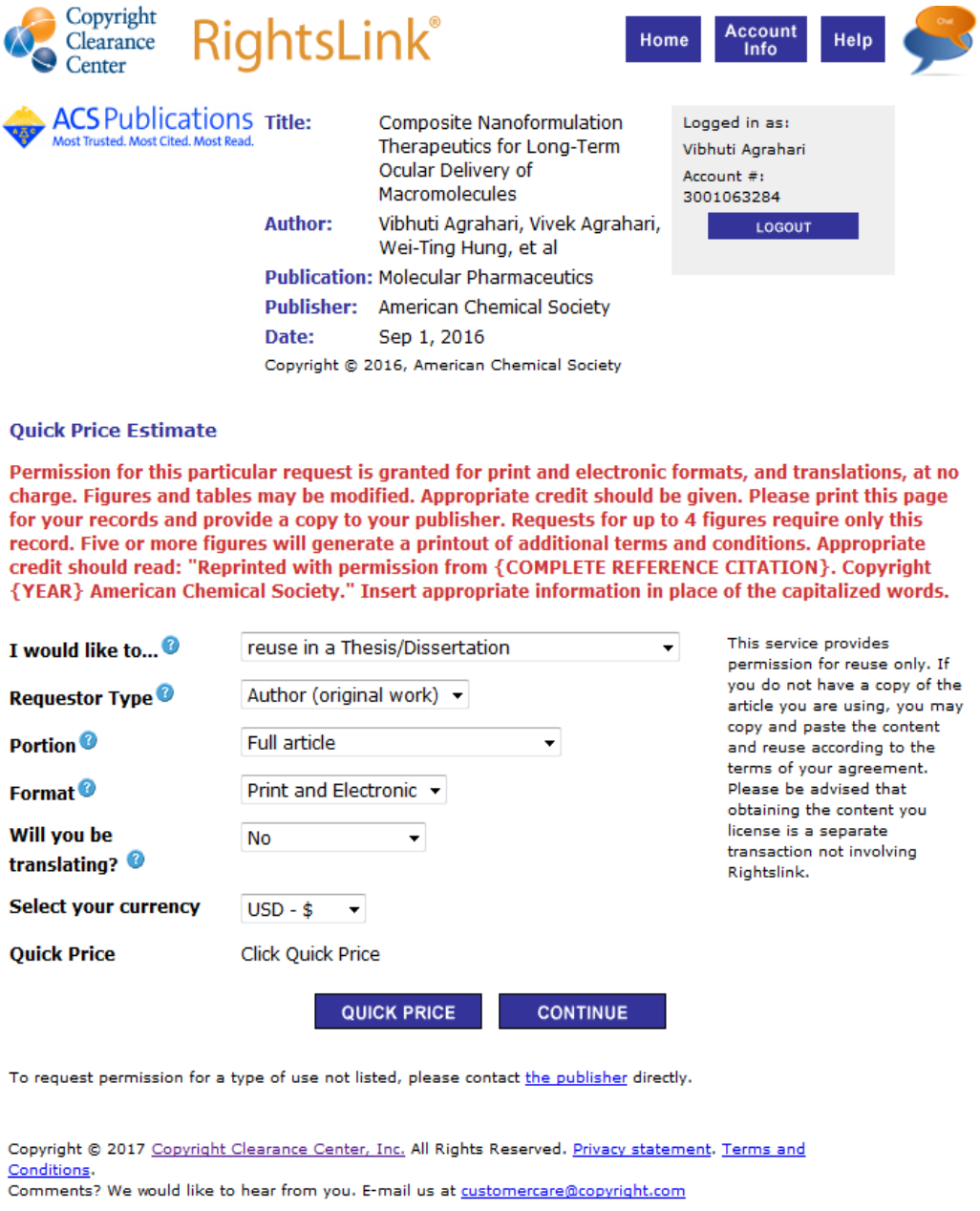

Copyright Clearance Center RightsLink®

Home | Account Info | Help

ACS Publications Most Trusted. Most Cited. Most Read.

Title: Composite Nanoformulation Therapeutics for Long-Term Ocular Delivery of Macromolecules

Author: Vibhuti Agrahari, Vivek Agrahari, Wei-Ting Hung, et al

Publication: Molecular Pharmaceutics

Publisher: American Chemical Society

Date: Sep 1, 2016

Copyright © 2016, American Chemical Society

Logged in as:
Vibhuti Agrahari
Account #:
3001063284
LOGOUT

Quick Price Estimate

Permission for this particular request is granted for print and electronic formats, and translations, at no charge. Figures and tables may be modified. Appropriate credit should be given. Please print this page for your records and provide a copy to your publisher. Requests for up to 4 figures require only this record. Five or more figures will generate a printout of additional terms and conditions. Appropriate credit should read: "Reprinted with permission from {COMPLETE REFERENCE CITATION}. Copyright {YEAR} American Chemical Society." Insert appropriate information in place of the capitalized words.

I would like to... reuse in a Thesis/Dissertation

Requestor Type Author (original work)

Portion Full article

Format Print and Electronic

Will you be translating? No

Select your currency USD - $

Quick Price Click Quick Price

QUICK PRICE CONTINUE

This service provides permission for reuse only. If you do not have a copy of the article you are using, you may copy and paste the content and reuse according to the terms of your agreement. Please be advised that obtaining the content you license is a separate transaction not involving Rightslink.

To request permission for a type of use not listed, please contact the publisher directly.

Copyright © 2017 Copyright Clearance Center, Inc. All Rights Reserved. Privacy statement. Terms and Conditions.
Comments? We would like to hear from you. E-mail us at customercare@copyright.com

Our Ref: LA/IEDD/P606

Dear Vibhuti Agrahari,

Material requested: 2 Figure – Fig1&2 from Vibhuti Agrahari, Vivek Agrahari, Abhirup Mandal, Dhananjay Pal & Ashim K. Mitra (2016): How are we improving the delivery to back of the eye? Advances and challenges of novel therapeutic approaches, Expert Opinion on Drug Delivery

Thank you for your correspondence requesting permission to reproduce the above mentioned material from our Journal in your printed thesis and to be posted in the university's repository - University of Missouri Kansas City.

We will be pleased to grant permission on the sole condition that you acknowledge the original source of publication and insert a reference to the article on the Journals website: http://www.tandfonline.com

This is the authors accepted manuscript of an article published as the version of record in Expert Opinion on Drug Delivery © 14 Dec 2016 http://tandfonline.com/10.1080/17425247.2017.1272569

This permission does not cover any third party copyrighted work which may appear in the material requested.

Please note that this license does not allow you to post our content on any third party websites or repositories.

Thank you for your interest in our Journal.

Yours sincerely

Lee-Ann

Lee-Ann Anderson – Senior Permissions & Licensing Executive, Journals

Taylor & Francis Group

3 Park Square, Milton Park, Abingdon, Oxon, OX14 4RN, UK.

Tel: +44 (0)20 7017 7932

Fax:+44 (0)20 7017 6336

Web: www.tandfonline.com

e-mail: lee-ann.anderson@tandf.co.uk

Dear Vibhuti Agrahari,

Future Medicine Ltd has approved your recent request described below. Before you can use this content, you must accept the license fee and terms set by the publisher.

Licensee:	Vibhuti Agrahari
Order Date:	Aug 8, 2017
Order Number:	501296052
Title:	Nanomedicine
Type of Use:	Thesis/Dissertation

This Agreement between Vibhuti Agrahari ("You") and Future Medicine Ltd ("Future Medicine Ltd") consists of your order details and the terms and conditions provided by Future Medicine Ltd and Copyright Clearance Center.

License number	Reference confirmation email for license number
License date	Aug, 08 2017
Licensed content publisher	Future Medicine Ltd
Licensed content title	Nanomedicine
Licensed content date	Jan 1, 2006
Type of use	Thesis/Dissertation
Requestor type	Academic institution
Format	Electronic
Portion	chapter/article
Title or numeric reference of the portion(s)	Pentablock copolymer dexamethasone nanoformulations elevate MYOC: in vitro liberation, activity and safety in human trabecular meshwork cells
Title of the article or chapter the portion is from	Pentablock copolymer dexamethasone nanoformulations elevate MYOC: in vitro liberation, activity and safety in human trabecular meshwork cells
Editor of portion(s)	N/A
Author of portion(s)	Agrahari, Vibhuti ; et al
Volume of serial or monograph	N/A
Issue, if republishing an article from a serial	N/A
Page range of portion	
Publication date of portion	Aug 1, 2017
Rights for	Main product
Duration of use	Life of current edition
Creation of copies for the disabled	no

With minor editing privileges	yes
For distribution to	Worldwide
In the following language(s)	Original language of publication
With incidental promotional use	no
Lifetime unit quantity of new product	Up to 499
Made available in the following markets	education
Specified additional information	N/A
The requesting person/organization	University of Missouri-Kansas City
Order reference number	
Author/Editor	Author
The standard identifier of New Work	No
Title of New Work	Pentablock copolymer dexamethasone nanoformulations elevate MYOC: in vitro liberation, activity and safety in human trabecular meshwork cells
Publisher of New Work	No
Expected publication date	Aug 2018
Estimated size (pages)	15
Requestor Location	Vibhuti Agrahari 2464 Charlotte Street HSb5258 KANSAS CITY, MO 64108 United States Attn: Vibhuti Agrahari
Billing Type	Invoice
Billing address	Vibhuti Agrahari 2464 Charlotte Street HSb5258 KANSAS CITY, MO 64108 United States Attn: Vibhuti Agrahari
Total (may include CCC user fee)	0.00 USD
Total	0.00 USD

VITA

Vibhuti Agrahari completed her Bachelor of Pharmacy, 2004 and Master degree in Medicinal and Pharmaceutical Chemistry from Shri G. S. Institute of Technology & Sciences, Rajiv Gandhi Proudyogiki Vishwavidyalaya (RGPV), Indore, Madhya Pradesh, India in 2008. Following completion of her degree, she joined Acropolis Institute of Pharmaceutical Education and Research, Indore, India as a lecturer.

Vibhuti Agrahari joined the interdisciplinary Ph.D. program at the University of Missouri-Kansas City (UMKC) School of Pharmacy in Spring 2012. She is completing her Ph.D. research projects under the supervision of Dr. Ashim K. Mitra where she aimed to develop composite nanoformulations for sustained ocular delivery of macromolecules and steroid induced *in vitro* model for ocular hypertension/glaucoma. Vibhuti has presented her research works at various conferences, authored several peer reviewed papers and book chapters. She has received Quality by Design and Product Performance Focus Group Award (2016), Ocular Drug Delivery Disposition Focus Group Graduate Student Poster Awards (2014 and 2015) and American Association of Indian Pharmaceutical Scientists (AAiPS) Research Award (2014) at the AAPS annual meetings. She is the recipient of the AAPS Biotechnology Graduate Student Symposium Awards (2015 and 2016) at National Biotechnology Conferences. At UMKC, Vibhuti has received several awards, including Women's Council Graduate Assistant Fund (2014, 2015, 2016, 2017), Ronald MacQuarrie Fellowship (2015), School of Graduate Studies Research Grant Proposal Award (2014 and 2015), Judith Hemberger Graduate Scholarship (2014), PFF Fellowship (2014-2016), Best Poster Award-Community of Scholar Symposium (2014), Best Speaker Award Fall 2014 seminar series; division of

pharmaceutical sciences, Best Poster Award at UMKC Research Summit (2016), Podium Presentation winner at UMKC Interdisciplinary Student Conference (2017) and Tony B. Academic Travel Award (2017) from Society of Laboratory Automation and screening (SLAS).

Vibhuti is also a playing an active role in several professional organizations. She has contributed her services as a Chair of the AAPS-UMKC Student Chapter, President of the CRS-UMKC Student Chapter and President of the Graduate Student Council in 2015-2016. She served as a secretary of the Interdisciplinary Doctoral Student Council (IDSC) Executive Board, Senator at the Student Government Association, and student representative of the Graduate Program Committee (GPC) at UMKC. Vibhuti chaired the community of scholar's symposium (2016) and co-chaired the PGSRM 2016 meeting hosted by the school of pharmacy, UMKC. She was student representative of the Student and Postdoctoral Outreach Committee (SPOD) and Ocular Drug Delivery Disposition Focus Group of the AAPS in 2014-2016. She is a member of several professional organizations such as the American Association of Pharmaceutical Scientists (AAPS), Controlled Release Society (CRS), and Association for Research in Vision and Ophthalmology (ARVO).

Vibhuti received Graduate Student Professional Leadership Program Certificate (2015) from UM system. She holds a Graduate Certificate in College Teaching and Career Preparation (December 2016), Designing Courses for Significant Learning Certificate (2016), and Effective Teaching Practices Certificate Course (2015).